

# Luminescent Organic Materials and Their Application in Solar Technologies

by

Gregory D. Gutierrez

B. A. *magna cum laude* with distinction in all subjects, Chemistry

Cornell University, 2011

Submitted to the Department of Chemistry

In Partial Fulfillment of the Requirements for the Degree of

DOCTOR OF PHILOSOPHY IN CHEMISTRY

at the

MASSACHUSETTS INSTITUTE OF TECHNOLOGY

JUNE 2016

© 2016 Massachusetts Institute of Technology. All Rights Reserved.

**Signature redacted**

Signature of Author: \_\_\_\_\_  
Department of Chemistry

**Signature redacted** May 6, 2016

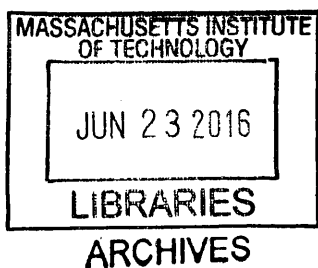
Certified by: \_\_\_\_\_  
Timothy M. Swager

John D. MacArthur Professor of Chemistry  
Thesis Supervisor

**Signature redacted,**

Accepted by: \_\_\_\_\_  
Robert W. Field

Haslam and Dewey Professor of Chemistry  
Chairman, Departmental Committee on Graduate Students



This doctoral thesis has been examined by a Committee of the Department of Chemistry as follows:

Signature redacted

Professor Jeremiah A. Johnson: \_\_\_\_\_

Chairman

Department of Chemistry

Signature redacted

Professor Timothy M. Swager: \_\_\_\_\_

Thesis Supervisor

Department of Chemistry

Signature redacted

Professor Mohammad Movassaghi: \_\_\_\_\_

Member

Department of Chemistry

*for Mom, Dad, and Julie*

# Luminescent Organic Materials and Their Application in Solar Technologies

by

Gregory D. Gutierrez

Submitted to the Department of Chemistry on May 6, 2016  
In Partial Fulfillment of the Requirements for the Degree of  
Doctor of Philosophy in Chemistry

## Abstract

In Chapter 1, we begin with a brief introduction to the principles of photoluminescence from organic materials and the luminescent solar concentrator (LSC). In Chapter 2, we describe the red phosphorescence from a class of four structurally simple benzo[2,1,3]thiadiazoles in cyclohexane. The photophysical properties of these molecules are presented along with a computational analysis of their electronic excited states. Chapter 3 discusses the development and evaluation of an efficient, low-reabsorbing luminescent solar concentrator (LSC) that employs two  $\pi$ -conjugated polymers as surrogate absorbers for a minority amount of the perylene bisimide Lumogen F Red 305. We developed a small LSC wherein a mixture of the two polymers act as both the host layer and antennae for a 1.5 wt% loading of Lumogen F Red 305. A Monte Carlo simulation predicts the LSC to possess high edge optical efficiencies and concentration factors on larger, commercially relevant scales. Efforts toward an efficient energy transfer cascade between three  $\pi$ -conjugated polymers in poly(methyl methacrylate) (PMMA) are also discussed. Chapter 4 describes an LSC that utilizes a deoxygenated liquid perfluorocarbon (PFC) as the host for a strongly fluorescent perfluoroalkylated thieno[3,4-*b*]pyrazine between two slabs of PMMA. In the event the luminophore photodegrades after prolonged exposure to sunlight, the luminescent layer can be easily replaced with new solution. Additionally, we demonstrate that the relatively low refractive indices of PFCs causes the luminophore's emission to efficiently couple into the PMMA slabs, where no reabsorption processes can undermine the efficiency of the LSC. In Chapter 5, we present progress toward iptycene-functionalized naphthazarins intended for the development of solid-state luminescent or redox-active metallopolymers.

Thesis Supervisor: Timothy M. Swager

Title: John D. MacArthur Professor of Chemistry

## Table of Contents

Title Page.....	1
Signature Page.....	2
Dedication.....	3
Abstract.....	4
Table of Contents.....	5
List of Figures.....	9
List of Schemes.....	15
List of Tables.....	16
<b>Chapter 1: Principles of Photoluminescence from Organic Molecules and an Introduction to Luminescent Solar Concentrators.....</b>	<b>17</b>
1.1. Introduction.....	18
1.2. Modes of Photoluminescence and the Jablonski Diagram.....	18
1.2.1 Photophysical Spectra and Photoluminescence Quantum Yield.....	21
1.3. Energy Transfer between Photoluminescent Molecules.....	23
1.3.1. Förster Resonance Energy Transfer.....	24
1.3.2. Electron Exchange Energy Transfer – The Dexter Mechanism.....	25
1.4 The Luminescent Solar Concentrator.....	26
1.5 References.....	31
<b>Chapter 2: Red Phosphorescence from Benzo[2,1,3]thiadiazoles at Room Temperature....</b>	<b>33</b>
2.1 Introduction.....	34
2.2 Photophysical Properties of 4,7-Dihalogenated-5,6-bis(tetradecyloxy)benzo[2,1,3]thiadiazoles in Cyclohexane.....	34

2.3 Synthesis of Thioether-functionalized Benzo[2,1,3]thiadiazoles and Their Photophysical Properties in Cyclohexane.....	39
2.4 Time-Dependent Density Functional Theory Calculations.....	42
2.5 Conclusion.....	46
2.6 Experimental Section.....	46
2.6.1 Materials and Instrumentation.....	46
2.6.2 Electronic Structure Calculations.....	48
2.6.3 Synthetic Procedures.....	48
2.7 References.....	51
<b>Appendix I for Chapter 2: <sup>1</sup>H and <sup>13</sup>C NMR Spectra.....</b>	<b>56</b>
<b>Appendix II for Chapter 2: Computational Data.....</b>	<b>64</b>
<b>Chapter 3: <math>\pi</math>-Conjugated Polymers as Surrogate Absorbers for Minority Emitters in Low-Reabsorbing Luminescent Solar Concentrators.....</b>	<b>108</b>
3.1 Introduction.....	109
3.2 Addressing the Reabsorption Problem with Amplifying $\pi$ -Conjugated Polymers.....	110
3.3 Properties of a Prototype of the Designed LSC.....	112
3.4 Monte Carlo Simulation of the Designed LSC.....	117
3.5 LSCs Utilizing Conjugated Polymers in PMMA.....	118
3.6 Conclusion.....	120
3.7 Experimental Section.....	120
3.7.1 Materials and Instrumentation.....	120
3.7.2 Thin Films of <b>P1</b> , <b>P2</b> , <b>P3</b> , and <b>Red 305</b> in PMMA and LSCs.....	123
3.7.3 Synthetic Procedures.....	124

3.7.4 Spectroscopic Ellipsometry.....	131
3.7.5 Details for Monte Carlo Simulation.....	137
3.8 References.....	139
<b>Appendix for Chapter 3: <math>^1\text{H}</math> and <math>^{13}\text{C}</math> NMR Spectra.....</b>	<b>144</b>
<b>Chapter 4: The Fluorofluorescent Solar Concentrator.....</b>	<b>158</b>
4.1 Introduction.....	159
4.2 Synthesis and Properties of a Highly Emissive Perfluoroalkylated Organic Dye.....	161
4.3 Construction and Characterization of the Fluorofluorescent Solar Concentrator.....	163
4.4 Conclusion.....	166
4.5 Experimental Section.....	167
4.5.1 Materials and Instrumentation.....	167
4.5.2 Electronic Structure Calculations.....	168
4.5.3 FSC Preparation.....	168
4.5.3 Synthetic Procedures.....	168
4.6 References.....	169
<b>Appendix for Chapter 4: <math>^{13}\text{C}</math> and <math>^{19}\text{F}</math> NMR Spectra and Photoluminescence Lifetime Data.....</b>	<b>171</b>
<b>Appendix II for Chapter 4: Computational Data.....</b>	<b>175</b>
<b>Chapter 5: Toward Naphthazarin Iptycenes as New Scaffolds for Solid-State Luminescent and Novel Redox-Active Metallopolymers.....</b>	<b>181</b>
5.1 Introduction.....	182
5.2 Iptycene-Functionalized Naphthazarin Metallopolymers.....	182
5.3 Synthetic Progress and Outlook.....	182

5.4 Experimental Section.....	185
5.4.1 Materials and Instrumentation.....	185
5.4.2 Synthetic Procedures.....	186
5.5 References.....	188
<b>Appendix for Chapter 5: <math>^1\text{H}</math> and <math>^{13}\text{C}</math> NMR Spectra.....</b>	<b>190</b>
Curriculum Vitae.....	201
Acknowledgements.....	204



## List of Figures

### Chapter 1

- Figure 1.1.** (a) Jablonski diagram for a closed-shell single organic molecule with numbered photophysical processes defined. The Jablonski diagram is simplified to conveniently depict photophysical phenomena and not representative of any specific molecule nor nuclear/electronic coordinates. (b) Electronic configurations of the ground state ( $S_0$ ) and excited singlet ( $S_n$ ) and triplet ( $T_n$ ) states. ....20
- Figure 1.2.** Absorption and emission spectra of Lumogen F Red 305 in PMMA (0.5 wt%) with spectral overlap indicated. ....23
- Figure 1.3.** Schematic illustration of FRET from a singlet excited-state donor ( $^1D^*$ ) to a closed-shell acceptor in the ground state ( $^1A$ ). The FRET efficiency  $\varepsilon$  is defined as an inset. ....24
- Figure 1.4.** Electron exchange energy transfer from a donor ( $^1D^*$ ) to a ground-state acceptor ( $^1A$ ). The rate term  $k$  is defined as an inset. ....25
- Figure 1.5.** Quenching of a triplet state to its ground state by triplet oxygen to produce singlet oxygen via electron exchange energy transfer.....26
- Figure 1.6.** Illustration of a standard single-slab LSC waveguiding the emission (red) of a luminophore to its edges via total internal reflection after absorption of sunlight (blue). The critical angle  $\theta_c$  is defined in the figure. ....28
- Figure 1.7.** (a) Cross-sectional schematics of an index-matched thin-film LSC waveguiding a luminophore's emission (red). The critical angle  $\theta_c'$  that dictates the extent of

waveguiding between layers is indicated. (b) A thin-film LSC in which  $\theta_c'$  is undefined. ....30

## Chapter 2

**Figure 2.1.** Photophysical properties of phosphorescent compounds **1-Br** and **1-I** in cyclohexane.

(a) **1-Br** and (d) **1-I** and their appearance in degassed cyclohexane under normal and UV ( $\lambda = 365$  nm) lighting. (b) Absorption spectrum and photoluminescence spectra under air and  $N_2$  gas for **1-Br** and (e) **1-I** ( $\lambda_{ex} = 370$  nm). (c) Phosphorescence excitation spectrum of **1-Br** and (f) **1-I** ( $\lambda_{em} = 575$  nm). Photoluminescence and excitation spectra were measured for 50  $\mu M$  solutions. A small peak attributed to Raman scattering ( $\lambda_{max} = 414$  nm) of the excitation beam by the solvent overlaps with the fluorescence of all phosphorescent samples presented in this study and is not considered in our analysis. ....36

**Figure 2.2.** Time-dependent photoluminescence decays of (a) **1-Br** and (b) **1-I** in cyclohexane (50  $\mu M$ ) under inert atmosphere and at room temperature. ....37

**Figure 2.3.** Absorption and emission spectra of **1-Cl** in cyclohexane. Emission spectra ( $\lambda_{ex} = 370$  nm) are reported for 50  $\mu M$  samples in aerobic and deoxygenated cyclohexane. ....39

**Figure 2.4.** (a) **2-H** in cyclohexane with its (b) absorption spectrum and photoluminescence spectra under air and  $N_2$  gas and (c) phosphorescence excitation spectra at 50  $\mu M$  and 2.6  $\mu M$  ( $\lambda_{em} = 575$  nm). (d-f) **2-Br** with its corresponding absorption/photoluminescence spectra ( $\lambda_{ex} = 370$  nm, 50  $\mu M$ ) and phosphorescence excitation spectrum ( $\lambda_{em} = 600$  nm, 50  $\mu M$ ). (g) Time-dependent photoluminescence decays for **2-H** and (h) **2-Br** in deoxygenated cyclohexane at 50  $\mu M$ . ....41

**Figure 2.5.** (a) Energy level diagrams for methoxy-functionalized derivatives **1-Cl\***, **1-Br\***, and **1-I\*** in the gas phase. (b) Kohn-Sham orbitals representing the electronic configuration descriptions of  $S_1$ ,  $T_1$ , and  $T_2$  for each calculated molecule. ....44

**Figure 2.6.** (a) Energy level diagrams for **2-H\*** and **2-Br\*** in the gas phase. (b) Kohn-Sham orbitals representing the electronic configuration description of  $S_1$ ,  $T_1$ , and  $T_2$  manifolds of **2-H\*** and (c) **2-Br\***. Indicated percentages describe the overall character for each displayed transition. ....46

### Chapter 3

**Figure 3.1.** Photoinduced migratory cascade of excitons in thin films of two  $\pi$ -conjugated polymers, **P1** (blue) and **P2** (green), to minority fluorophore **Red 305** (red) via (a) FRET and (b) electron exchange (Dexter) energy transfer. (c) Structures of **P1**, **P2**, and **Red 305**. (d) Absorption (solid) and emission (dashed) spectra of thin films of **P1** (blue) and **P2** (green) and a sample of 0.5 wt% **Red 305** in PMMA (red). Optical bandgaps were estimated from absorption onsets. ....112

**Figure 3.2.** (a) Schematic of the designed LSC (yellow layer: blend of **P1** and **P2**; red: molecule of **Red 305**) illustrating exciton diffusion from **P1** and **P2** to **Red 305**. (b) Refractive index ( $n$ ) of a film of 1:1 (by weight) **P1:P2** (thickness = 188.3 nm). ....114

**Figure 3.3.** (a) Absorption and emission ( $\lambda_{ex} = 405$  nm) spectra of **LSC1** with absorption in terms of its absorbance. (b) Absorption and excitation spectra ( $\lambda_{em} = 630$  nm) of **LSC1** normalized at  $\lambda = 564$  nm. (c) Plots of the energy transfer efficiency ( $\eta_{ET}$ ) from **P1** and **P2** to **Red 305** and estimated photoluminescence quantum yield of Red 305 ( $\Phi_{PL,R}$ ) in

**LSC1** with respect to wavelength. (d) **LSC1** under normal lighting (left) and UV radiation at  $\lambda = 365$  nm to illustrate light concentration at the edges (right). .....115

**Figure 3.4.** (a) Projected optical efficiency ( $\eta_{opt}$ ) and concentration factor with increasing geometric gain ( $G$ ) for **LSC1**. (b) Calculated loss channels (rounded) for  $G = 200$  ( $\lambda_{ex} = 405$  nm). .....118

**Figure 3.5.** Schematic for LSC exploiting the phase-separating tendency of different polymers to enable an energy transfer cascade from **P1** and **P2** to a minority emitter **P3**. The red circles represent phase-separated microdomains of three  $\pi$ -conjugated polymers. ..119

**Figure 3.6.** Photophysical properties of (a) **P3** as a thin film and (b) **LSC2**. .....120

**Figure 3.7.** The configuration used to measure the absolute quantum yield of **LSC1**. .....123

**Figure 3.8.** Ellipsometry data for the amplitude ratio  $\Psi$  (“Y”) and its model fit. ....134

**Figure 3.9.** Ellipsometry data for the phase shift  $\Delta$  (“D”) and its model fit. ....135

**Figure 3.10.** Profile of the extinction coefficient  $k$  of the analyzed blend composed of **P1** and **P2**. .....138

**Figure 3.11.** Absorption and emission spectra (logarithmic) of **LSC1** after the specified baseline correction. ....140

Chapter 4

**Figure 4.1.** Cross-sectional illustration of an LSC utilizing the emission of a luminophore (orange dots) dissolved in a liquid PFC (yellow layer) to power PV devices at the edges of two transparent plastic or glass sheets. ....160

**Figure 4.2.** Photophysical spectra and computations for compound **4.1**. (a) Absorption spectrum and photoluminescence spectra under air and nitrogen ( $\lambda_{\text{ex}} = 420$  nm). (b) Excitation spectrum of **4.1** (monitored  $\lambda_{\text{em}} = 550$  nm) with corresponding electronic transitions as suggested by TD-DFT calculations. Transition dipole moments (***D***) and Kohn-Sham molecular orbitals for  $S_1$ ,  $S_2$ , and  $S_3$  as determined by TD-DFT calculations. ....163

**Figure 4.3.** FSC1 under (a) ambient and (b) ultraviolet ( $\lambda = 365$  nm) lighting. ....164

**Figure 4.4.** Distant-dependent excitation studies of FSC1. (a) Illustration of detection method from edge of central frame. (b) Photoluminescence output as a function of the excitation distance  $d$ . (c) The same outputs presented in Figure 4.4b, but each normalized to their own data sets to depict how the emission is affected by non-radiative reabsorption by traveling directly through the luminescent solution. ....165

**Figure 4.5.** Relative edge emission output of FSC1 from the upper PMMA slabs. (a) Method of detection, as similar to Figure 4.4a. (b) Relative photoluminescence output as a function of  $d$ . (c) Photoluminescence outputs each normalized to their own maximum to illustrate that the observed edge emission is not affected by reabsorption effects with increasing  $d$ . ....166

Chapter 5

**Figure 5.1.** (a) Main-chain metallopolymers of quinizarins and (b) naphthazarins. ....182

**Figure 5.2.** (a) Naphthazarin-based iptycene metallopolymers with suggested metals for complexation. (b) Predicted orientation of iptycene wings that could preclude luminescence quenching interactions in the solid state. ....183

## List of Schemes

### Chapter 2

**Scheme 2.1.** Synthesis of chlorinated benzo[2,1,3]thiadiazole **1-Cl**. .....38

**Scheme 2.2.** Syntheses of thioether-functionalized benzo[2,1,3]thiadiazoles **2-H** (a) and **2-Br**  
(b). .....40

### Chapter 3

**Scheme 3.1.** Synthesis of *tert*-butylated pentiptycene dialkyne **1**. ..... 124

**Scheme 3.2.** Synthesis of  $\pi$ -conjugated polymers **P1** and **P2** from **1** and their respective bandgap-  
limiting co-monomers **5** and **7**. ..... 127

**Scheme 3.3.** Synthesis of **P3**. ..... 130

### Chapter 4

**Scheme 4.1.** Synthesis of perfluoroalkylated thieno[3,4-*b*]pyrazine **1**. ..... 161

### Chapter 5

**Scheme 5.1.** Synthesis toward naphthazarin pentiptycene **5**. ..... 184

**Scheme 5.2.** (a) Synthesis of **6** with oxidation occurring under acidic conditions. (b) Synthesis of  
naphthazarin triptycene **6** under mild oxidation with KO<sup>t</sup>Bu/I<sub>2</sub> from Diel-Alder  
cycloadduct **7**. ..... 185

## List of Tables

### Chapter 2

<b>Table 2.1.</b> Summary of photophysical properties of phosphorescent benzo[2,1,3]thiadiazoles in deoxygenated cyclohexane. ....	42
--	----

### Chapter 3

<b>Table 3.1.</b> Fitted parameters obtained for Equation 3.3 ( $N = 7$ ). ....	136
---	-----



## **Chapter 1**

# **Principles of Photoluminescence from Organic Molecules and an Introduction Luminescent Solar Concentrators**

## 1.1 Introduction

Materials that exhibit luminescence, the release of light in response to the absorption of non-thermal energy, have been known to humanity since antiquity. Aristotle notably documented the identities of various luminescent natural objects, including fish scales and certain species of mushrooms.<sup>1</sup> In modern times, luminescent materials have been widely employed in many technologies, from optical sensors<sup>2</sup> to biotechnology<sup>3</sup> and forensic science.<sup>4</sup>

Various forms of energy are capable of causing a material to undergo luminescence; the mechanisms by which they occur can often be explained at the molecular level. For example, many molecules display luminescence when the excitation source is an electric current (electroluminescence) and are widely studied as the primary components of light-emitting diodes (LEDs) for next-generation electronic displays.<sup>5</sup> Molecules may also take part in a chemical reaction to harness energy and produce photons as a product (chemiluminescence). This particular form of luminescence is naturally produced by *Photinus pyralis*, a firefly commonly found in North America.<sup>6</sup>

This thesis concerns the development and application of organic molecules that undergo *photoluminescence*, or luminescence resulting from the absorption of light. When absorption occurs, an electron lying in the ground state of the photoluminescent molecule is promoted to a higher-energy excited state. After a period of time known as the luminescence lifetime, this higher-energy electron will transition back to the ground state, causing the residual energy produced as a result of this relaxation to be ejected from the molecule in the form of a photon.

## 1.2 Modes of Photoluminescence and the Jablonski Diagram

After a molecule absorbs a photon with sufficient energy to promote one of its electrons to an excited state, several processes may occur prior to relaxation. Such photophysical phenomena may be conveniently described with a Jablonski diagram,<sup>7</sup> a scheme commonly employed by chemists to depict the landscape of a molecule's electronic excited states and the possible mechanisms by which photoluminescence can occur. A Jablonski diagram for a conventional, closed-shell single organic molecule is shown in Figure 1.1a. Prior to absorption, the molecule possesses a ground state in which all electrons are spin-paired (i.e. the spin multiplicity is zero). Such a configuration is termed a singlet state. The ground state is therefore the lowest energy singlet electronic state and denoted as  $S_0$  with higher-level states listed as  $S_n$ , where  $n$  is an integer greater than zero (Figure 1.1b). In the case where the excited-state electron is unpaired, the resulting electronic configuration is termed a triplet state, or  $T_n$  (i.e. the spin multiplicity is one). Additionally, the coupling of these electronic states with vibrational wavefunctions associated with relevant chemical bonds in the molecule gives rise to discrete energy levels that an electron may occupy depending on the energy of light absorbed. Thus, individual singlet and triplet manifolds are often depicted as Morse potential wells to account for these vibrational couplings.<sup>8</sup>

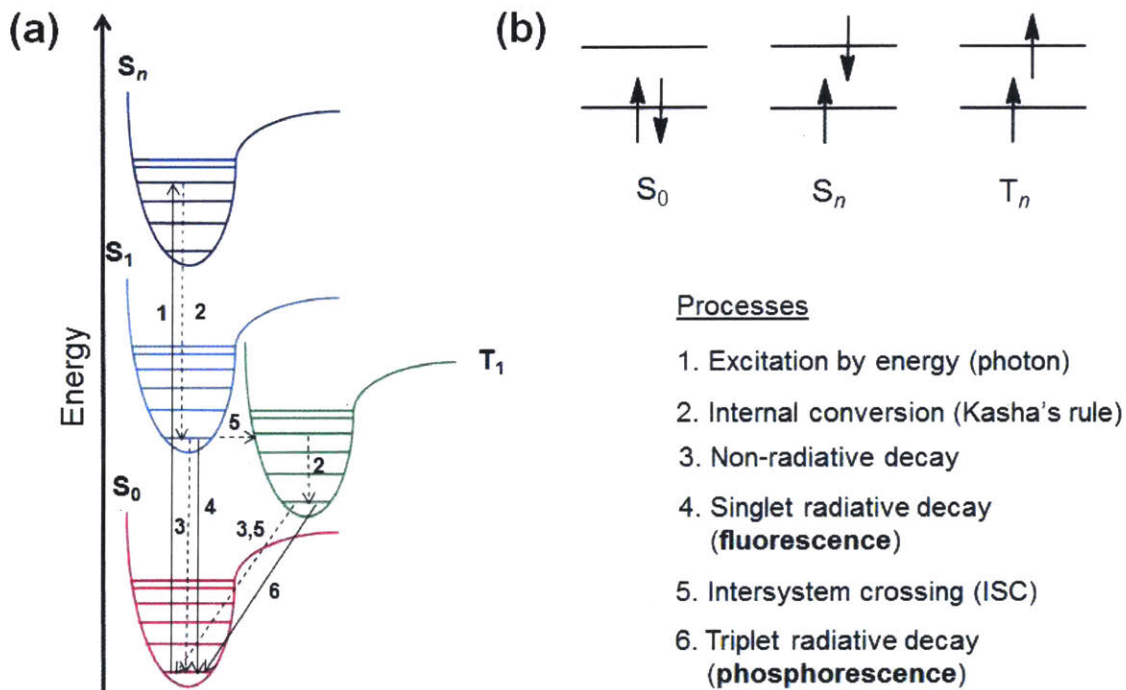


**Figure 1.1.** (a) Jablonski diagram for a closed-shell single organic molecule with numbered photophysical processes defined (lower right). The diagram is simplified to conveniently depict photophysical phenomena and not representative of any specific molecule nor nuclear/electronic coordinates. (b) Electronic configurations of the ground state ( $S_0$ ) and excited singlet ( $S_n$ ) and triplet ( $T_n$ ) states.

Once the molecule absorbs light and promotes an electron to an excited state (process 1), the molecule is converted to a higher-energy singlet state  $S_n$ . However, before photoluminescence occurs, molecules often release heat such that the excited-state electron is relaxed to the first vibrational energy level of the first excited singlet state ( $S_1$ ). This rapid non-radiative dissipation of energy, or internal conversion (IC), to  $S_1$  is also known as Kasha's rule (process 2).<sup>9</sup> After IC occurs, several routes to full electronic relaxation are possible. Another thermal dissipation event may then occur, causing the excited-state electron to fully relax to the ground state. Relaxation to

the ground state from the  $S_1$  manifold can also result in the release of energy in the form of an emitted photon, a phenomenon known as *fluorescence* (process 4). Additionally, the electron may not fully relax and instead undergo a change in its spin angular momentum to access a lower-energy triplet state, a process known as intersystem crossing (ISC, process 5). Once in the triplet manifold, the electron may undergo IC once more and then participate in ISC to relax to  $S_0$  by releasing heat (processes 3 and 5). However, this final relaxation from  $T_1$  to the ground state can still result in a photoluminescent emission specifically known as *phosphorescence* (process 6). Phosphorescent organic materials are not as common as their fluorescent counterparts due to the fact that both ISC and phosphorescence are “spin-forbidden” processes. That is, the change in spin angular momentum required to access the triplet manifold is fundamentally forbidden by quantum mechanics.

Although a spin-forbidden process, ISC may be better enabled through the inclusion of atoms considerably heavier than those typically encountered in organic molecules (e.g. carbon, nitrogen, and hydrogen). These heavy atoms, which range from transition metals (e.g. platinum,<sup>10</sup> iridium,<sup>11</sup> and osmium<sup>12</sup>) to halogens (see Chapter 2), are often capable of influencing the electronic states of a molecule to circumvent the obstacles to ISC set forth by quantum mechanics. Additionally, ISC may also be accomplished by coupling the change in the spin-angular momentum with a change in the overall orbital angular momentum associated with the transition. Examples of both strategies are discussed in detail in Chapter 2.

### *1.2.1 Photophysical Spectra and Photoluminescence Quantum Yield*

As a result of the coupling of different wavefunctions with electronic states, a molecule can absorb many wavelengths of light that can result in photoluminescence; the overall profile of absorbed photons is called the electronic absorption spectrum of the molecule. The extent by which

a molecule can absorb a photon of a specific wavelength  $\lambda$  can be quantified by its extinction coefficient (or absorptivity),  $\varepsilon$ , from Beer's Law (Equation 1.1).

$$\varepsilon = \frac{A}{lc}$$

**Equation 1.1**

$A$  is the absorbance, or a measure of how much of the light the specific sample absorbs as determined by a spectrometer,  $l$  is the path length of the analyzed sample, and  $c$  is the concentration of the sample in a diluent medium. Throughout this thesis, concentrations are defined in terms of molarity;  $\varepsilon$  is therefore expressed as a "molar absorptivity."

Fluorescence or phosphorescence may relax the molecule to different states within  $S_0$ .<sup>8</sup> The distribution of possible emitted photons consequently make up the photoluminescence spectrum, or emission spectrum, of the molecule. An example of an absorption spectrum coupled with an emission spectrum is shown for the fluorescent perylene bisimide Lumogen F Red 305 in poly(methyl methacrylate) (PMMA) in Figure 1.2. Due to the small Stokes shift, or difference between the absorption and emission maxima, of this dye, the two spectra strongly overlap, enabling Lumogen F Red 305 to readily reabsorb its own emission. Luminophore reabsorption is a central theme of this thesis and its implications regarding the applications of photoluminescence is further described in Section 1.4 and Chapters 3 and 4.

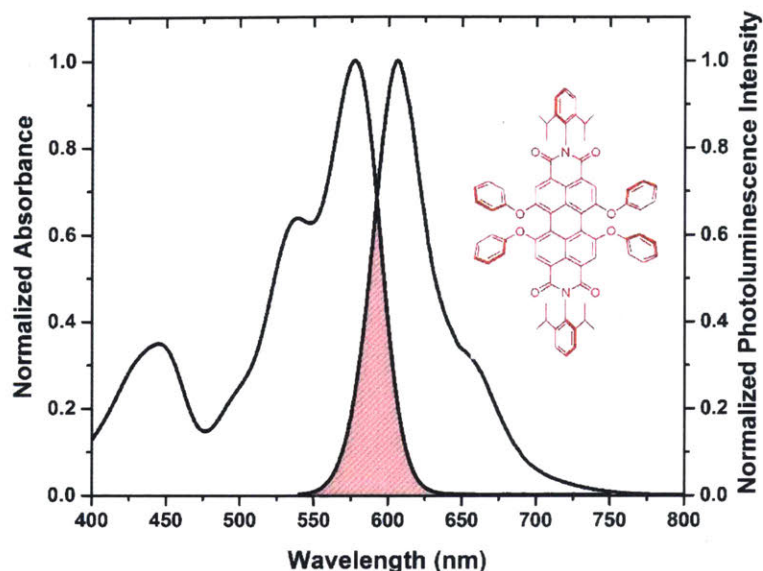


**Figure 1.2.** Absorption and emission spectra of Lumogen F Red 305 in PMMA (0.5 wt%) with spectral overlap indicated.

In addition to spectral data like those shown in Figure 1.2, a critical experimental parameter that describes the efficiency of photoluminescence from a molecule is the photoluminescence quantum yield ( $\Phi_{PL}$ ), or the probability that an absorbed photon results in an emission event. Depending on the mode of photoluminescence,  $\Phi_{PL}$  may be further categorized as a fluorescence ( $\Phi_F$ ) or phosphorescence ( $\Phi_P$ ) quantum yield. Various experimental methods to measure  $\Phi_{PL}$  are described throughout the Experimental Sections of this thesis.

### 1.3 Energy Transfer between Photoluminescent Molecules

Fluorescent and phosphorescent molecules are often capable of shuttling the energy they absorb to other photoluminescent species. This transfer of energy from donor to acceptor may occur through different mechanisms: those that concern this work, Förster resonance energy transfer and electron exchange energy transfer, are highly sensitive to the distance between donor

and acceptor. These two types of near-field excitation energy transfer are utilized to engineer a new and efficient luminescent solar concentrator (Section 1.4) that is presented in Chapter 3.

**1.3.1 Förster Resonance Energy Transfer.** Promoting or relaxing an electron to a different electronic state within a molecule can create a dipole moment associated with this transition. In 1948, Förster proposed an explanation for energy transfer that occurs through the coupling of such transition dipole moments of a donor (“D”) and acceptor (“A”) as illustrated in Figure 1.3.<sup>13</sup> The efficiency  $E$  of this mode of energy transfer, now commonly known as Förster resonance energy transfer (FRET), may be calculated as function of donor-acceptor distance  $R$  (Figure 1.3 inset).

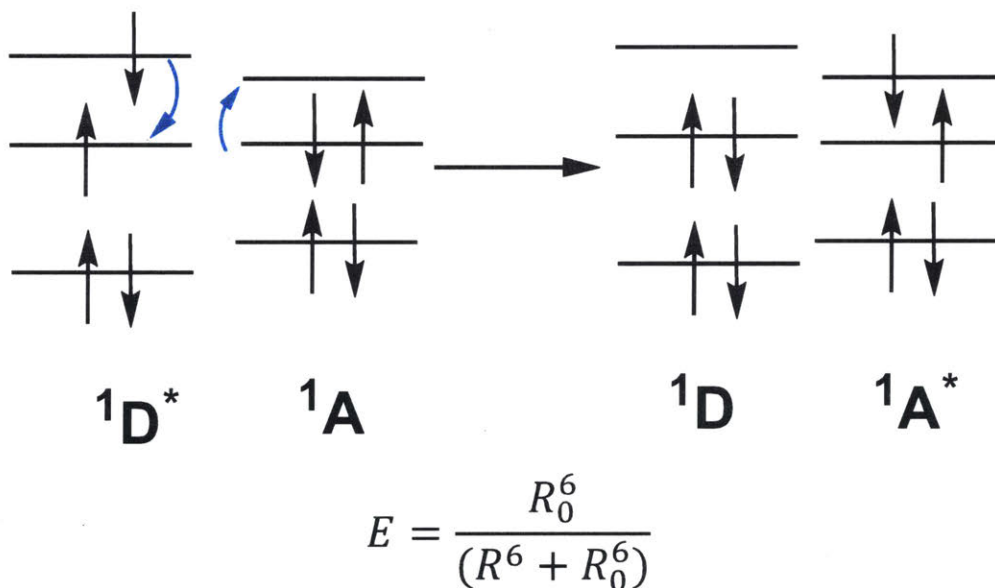


**Figure 1.3.** Schematic illustration of FRET from a singlet excited-state donor ( $^1D^*$ ) to a closed-shell acceptor in the ground state ( $^1A$ ). The FRET efficiency  $E$  is defined as an inset.

As the equation in Figure 1.3 suggests,  $E$  is inversely proportional to  $R$ . Thus, larger donor-acceptor distances result in less efficient energy transfer.  $E$  is also directly proportional to a parameter  $R_0$  that represents the distance between donor and acceptor such that  $\varepsilon = 0.5$ .  $R_0$ , also called the Förster radius.  $R_0$  is dependent on many factors, such as the photoluminescence quantum



yield of the donor, the degree of overlap of the photoluminescence spectrum of the donor and the absorption spectrum of the acceptor, and the orientation of transition dipole moments between participants.

**1.3.2 Electron Exchange Energy Transfer – The Dexter Mechanism.** Energy transfer independent of a transition dipole coupling mechanism may also occur if the donor-acceptor distance is especially small. Under this condition, energy transfer can occur through an exchange of electrons between donor and acceptor via overlap of the wavefunctions of their electronic states. Dexter formulated the rate of this electron exchange energy transfer as shown in Figure 1.4.<sup>14</sup>

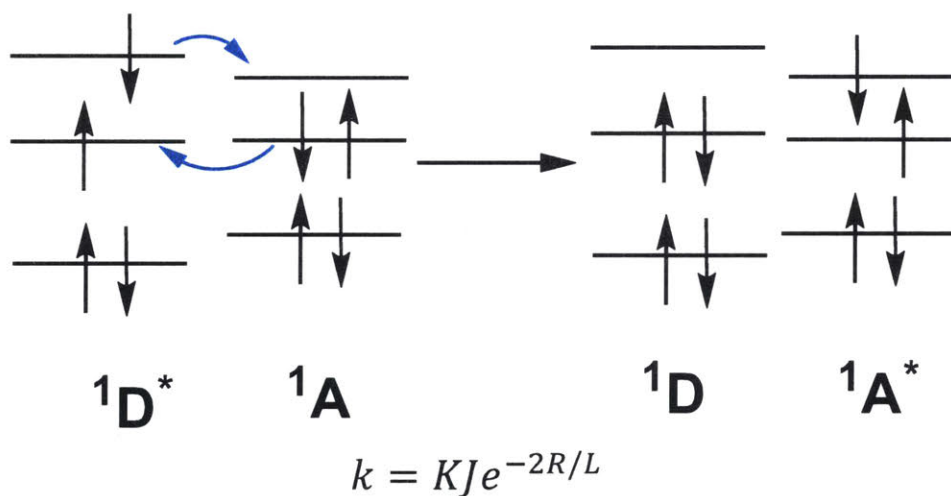


**Figure 1.4.** Electron exchange energy transfer from a donor ( $^1D^*$ ) to a ground-state acceptor ( $^1A$ ). The rate term  $k$  is defined as an inset.

In this case, the rate term  $k$  is dependent on relevant orbital-orbital interactions (quantified by  $K$ ), the spectral overlap integral between the absorption spectra of the donor and acceptor ( $J$ ), the donor-acceptor distance ( $R$ ), and the corresponding van der Waals radii between the participants ( $L$ ).  $k$  carries an exponential dependence on donor-acceptor distance and therefore decreases faster with increasing distance than if energy transfer were operating through FRET.

Molecular oxygen is also well-known for participating in electron exchange energy transfer with luminescent organic molecules.  $O_2$  is most stable in a triplet electronic configuration ( $^3O_2$ ) and particularly participates in energy transfer with luminophores with relatively long photoluminescence lifetimes to generate singlet oxygen ( $^1O_2$ ), which subsequently phosphoresces around a wavelength 1270 nm to relax back to  $^3O_2$ . As an example, Figure 1.5 illustrates how oxygen can quench a triplet state through electron exchange. Chapters 2 and 4 describe organic molecules that are sensitive to  $O_2$  and are consequently deoxygenated to improve their photoluminescence quantum yields.

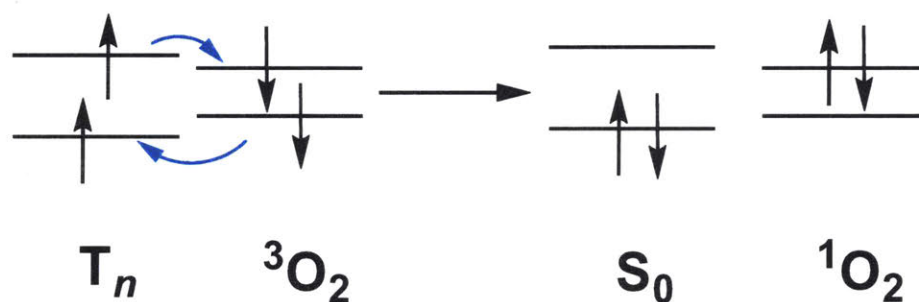


**Figure 1.5.** Quenching of a triplet state to its ground state by triplet oxygen to produce singlet oxygen via electron exchange energy transfer.

#### 1.4 The Luminescent Solar Concentrator

The technological motivation for the research presented in this thesis, particularly in Chapters 3 and 4, is the luminescent solar concentrator (LSC). The LSC is a functional window that utilizes the photoluminescence of an organic molecule or inorganic structure, hereafter collectively referred to as a luminophore, to readily integrate efficient photovoltaics (PVs) into buildings at low costs.<sup>15</sup> Examples of state-of-the-art organic luminophores used in LSCs include perylene bisimides,<sup>16</sup> benzo[2,1,3]thiadiazoles,<sup>17</sup> and cyanines.<sup>18</sup> Additionally, inorganic semiconductor

quantum dots represent a highly popular class of investigated LSC emitters that will be further discussed in Chapter 3.

LSCs are optical waveguides, or structures that confine and guide light in one or more directions. Conventional LSCs employ isotropic luminophores, or those whose photoluminescence can be released in any direction prior to waveguiding. These emitters are usually suspended within an optically transparent, dielectric slab such as PMMA. Within an LSC with refractive index  $n$  employing an isotropic luminophore, an emitted photon can be guided into modes via total internal reflection (Figure 1.6) if the photon's trajectory is at or above a critical angle  $\theta_c$  as defined in Equation 1.2,

$$\theta_c = \sin^{-1} \left( \frac{n_{air}}{n_{LSC}} \right) \approx \sin^{-1} \left( \frac{1}{n_{LSC}} \right),$$

**Equation 1.2**

where  $n_{air}$  is the refractive index of air (approximately 1) and  $n_{LSC}$  is the refractive index of the transparent slab. If photons travel along pathways that exceed  $\theta_c$ , they will not be guided by the LSC and ejected from device.

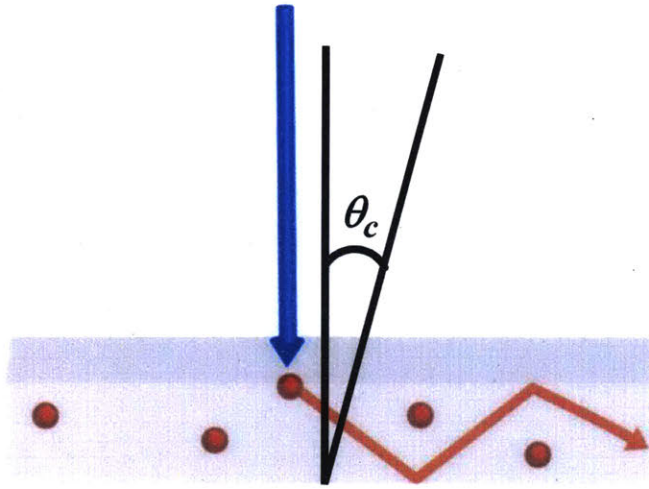


**Figure 1.6.** Illustration of a standard single-slab LSC waveguiding the emission (red) of a luminophore to its edges via total internal reflection after absorption of sunlight (blue). The critical angle  $\theta_c$  is defined in the figure.

The collective distribution of trajectories that fall below  $\theta_c$  and result in a loss of emitted photons is called the escape cone of the LSC. The maximum possible fraction of emitted light that is waveguided by the LSC is quantified by the trapping efficiency,  $\eta_t$  (Equation 1.3).<sup>19</sup>

$$\eta_t = \frac{\sqrt{n_{LSC}^2 - 1}}{n_{LSC}}$$

**Equation 1.3**

As Equation 1.3 suggests,  $\eta_t$  is dictated by the refractive index of the LSC and thus the type of material used as the transparent matrix hosting the luminophore. For example, an LSC composed of PMMA as the host slab possesses a refractive index of about 1.5 and thus a trapping efficiency of 0.75 (i.e. only 75% of the emitted light can be waveguided to the edges of the device). In practice, a trapping efficiency of 100% for typical LSCs that rely on total internal reflection is not

possible; some photoluminescence by the luminophore will leak through the escape cone due to finite values of  $n$  for conventional glass or plastic substrates.

An alternative, yet common type of LSC that concentrates emitted photons utilizes a thin luminescent film whose photoluminescence is directed into and subsequently waveguided by a thicker transparent substrate. Compared to the conventional single-slab LSC illustrated in Figure 1.6, this “thin-film LSC” (Figure 1.7) allows for the use and facile processing of unique luminescent layers on top of the blank substrate. Due to the presence of two distinct components (luminescent layer and substrate) in the LSC, the photoluminescent emission must enter the substrate at or below an additional critical angle  $\theta_c'$ , defined in Equation 1.4.

$$\theta_c' = \sin^{-1} \left( \frac{n_{sub}}{n_{film}} \right)$$

**Equation 1.4**

Here,  $n_{film}$  is the refractive index of the luminescent layer at a given wavelength of emitted light and  $n_{sub}$  is the corresponding refractive index of the substrate. As Equation 1.4 implies,  $\theta_c'$  is  $90^\circ$  when  $n_{film}$  is equal to  $n_{sub}$ . Under such an “index matching” condition, guided emitted light freely moves through both the thin luminescent layer and substrate (Figure 1.7a). As a result, the waveguide essentially behaves as a conventional single-slab LSC. Furthermore, if  $n_{film}$  is less than  $n_{sub}$ , then  $\theta_c'$  is undefined and all guided emission will be trapped within the substrate as it travels to the edges of the LSC (Figure 1.7b).<sup>20</sup> The index-matching condition is applied to the LSC presented in Chapter 3, while LSCs with undefined  $\theta_c'$  inspires the research presented in Chapter 4.

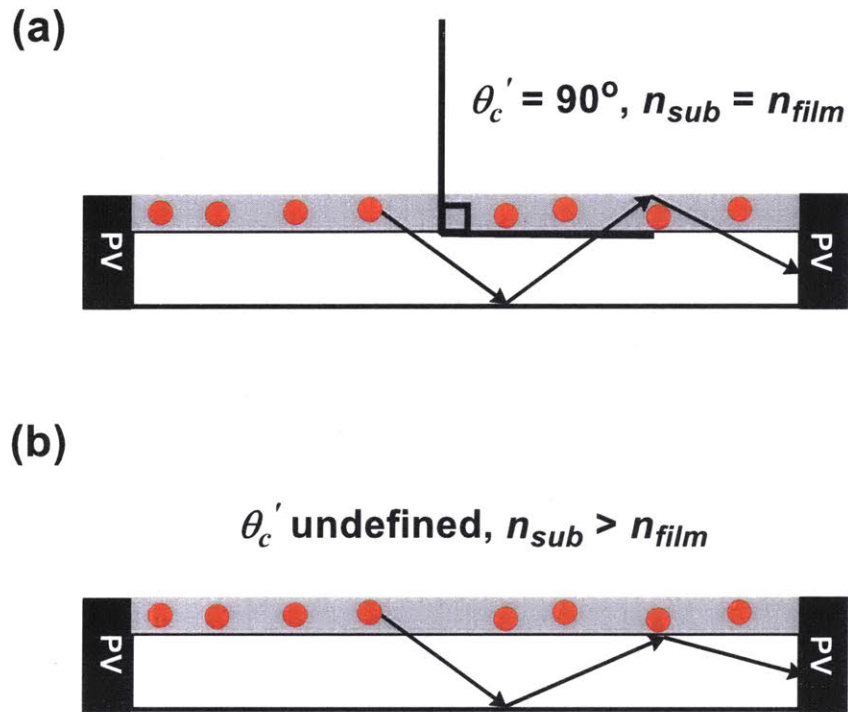


**Figure 1.7.** (a) Cross-sectional schematics of an index-matched thin-film LSC waveguiding a luminophore's emission (red). The critical angle  $\theta_c'$  that dictates the extent of waveguiding between layers is indicated. (b) A thin-film LSC in which  $\theta_c'$  is undefined.

The optical efficiency ( $\eta_{opt}$ ) of an LSC is the ratio of the amount of emitted photons that reach the edges to the amount of incident photons absorbed. As one of the most important indicators of an LSC's overall efficiency,  $\eta_{opt}$  can depend on many factors.<sup>15</sup> However, we herein approximate  $\eta_{opt}$  in the simplified manner expressed by Coropceanu and Bawendi (Equation 1.5):<sup>21</sup>

$$\eta_{opt}(\lambda) \approx \alpha(\eta_t \Phi_{PL})^{n+1}$$

**Equation 1.5**

In Equation 1.5,  $\alpha$  is the absorptance (or absorption factor), which is the fraction of photons absorbed at a given wavelength  $\lambda$  and may be calculated from the absorbance (see Chapter 3),

while  $n$  is the number of times a waveguided emitted photon is reabsorbed by the luminophore (see Figure 1.2) prior to edge concentration. Due to its presence as an exponent,  $n$  can have an immense impact on an LSC's performance. Equation 1.4 is used to estimate  $\eta_{opt}$  for larger versions of an LSC described in Chapter 3 using a Monte Carlo simulation (Section 3.4).

### 1.5 References

- (1) Harvey, E. N. *A History of Luminescence: From the Earliest Times Until 1900*; The American Philosophical Society: Philadelphia, PA, 1957.
- (2) Thomas, S. W.; Joly, G. D.; Swager, T. M. *Chem. Rev.* **2007**, *107*, 1339–1386.
- (3) (a) Lilley, D. M.; Wilson, T. J. *Curr. Opin. Chem. Bio.* **2000**, *4*, 507–517. (b) Joo, C.; Balci, H.; Ishitsuka, Y.; Buranachai, C.; Ha, T. *Ann. Rev. Biochem.* **2008**, *77*, 51–76.
- (4) Lennard, C. J.; Margot, P. A.; Stoilovic, M.; Warrenner, R. N. *J. Forensic Sci. Soc.* **1986**, *26*, 323–328.
- (5) Müllen, K.; Scherf, U. *Organic Light Emitting Devices: Synthesis, Properties, and Applications*; Wiley-VCH: Hoboken, NJ, 2006.
- (6) da Silva, L. P.; da Silva, J. C. G. E. *Chem. Phys. Chem.* **2012**, *13*, 2257–2262.
- (7) Jabłoński, A. *Nature* **1933**, *131*, 839–840.
- (8) Anslyn, E. V.; Dougherty, D. A. *Modern Physical Organic Chemistry*; University Science Books: Sausalito, CA, 2006.
- (9) Kasha, M. *Discuss. Faraday Soc.* **1950**, *9*, 14–19.
- (10) Lamansky, S.; Djurovich, P.; Murphy, D.; Abdel-Razzaq, F.; Lee, H.-E.; Adachi, C.; Burrows, P. E.; Forrest, S. R.; Thompson, M. E. *J. Am. Chem. Soc.* **2001**, *123*, 4304–4312.

- (11) Baldo, M. A.; O'Brien, D. F.; You, Y.; Shoustikov, A.; Sibley, S.; Thompson, M. E.; Forrest, S. R. *Nature*, **1998**, *395*, 151–154.
- (12) Tung, Y.-L.; Wu, P.-C.; Liu, C.-S.; Chi, Y.; Yu, J.-K.; Yu, Y.-H.; Chou, P.-T.; Peng, S.-M.; Lee, G.-H.; Tao, Y.; Carty, A. J.; Shu, C.-F.; Wu, F.-I. *Organometallics* **2004**, *23*, 3745–3748.
- (13) Förster, T. *Ann. Phys.* **1948**, *2*, 55–75.
- (14) Dexter, D. L. *J. Chem. Phys.* **1953**, *21*, 836–850.
- (15) Debije, M. G.; Verbunt, P. P. C. *Adv. Energy Mater.* **2012**, *2*, 12–35.
- (16) Slooff, L. H.; Bende, E. E.; Burgers, A. R.; Budel, T.; Pravettoni, M.; Kenny, R. P.; Dunlop, E. D.; Büchtemann, A. *Phys. Status Solidi RRL* **2008**, *2*, 257–259
- (17) Aste, N.; Tagliabue, L. C.; Del Pero, C.; Testa, D.; Fusco, R. *Renewable Energy* **2015**, *76*, 330–337.
- (18) Zhao, Y.; Meek, G. A.; Levine, B. G.; Lunt, R. R. *Adv. Opt. Mater.* **2014**, *2*, 606–611.
- (19) Mulder, C. L.; Reusswig, P. D.; Velázquez, A. M.; Kim, H.; Rotschild, C.; Baldo, M. A. *Opt. Express* **2010**, *18*, A79–A90.
- (20) Currie, M. J.; Mapel, J. K.; Heidel, T. D.; Goffri, S.; Baldo, M. A. *Science* **2008**, *321*, 226–228.
- (21) Coropceanu, I.; Bawendi, M. G. *Nano Lett.* **2014**, *14*, 4097–4101.



## Chapter 2

# Red Phosphorescence from Benzo[2,1,3]thiadiazoles at Room Temperature

Adapted from:

Gutierrez, G. D.; Sazama, G. T.; Wu, T.; Baldo, M. A. Swager, T. M. "Red Phosphorescence from Benzo[2,1,3]thiadiazoles at Room Temperature." *J. Org. Chem.*, *Submitted*.

Reproduced with permission from *The Journal of Organic Chemistry*, submitted for publication.  
Unpublished work copyright 2016 American Chemical Society.

Dr. Graham T. Sazama (Chemistry, MIT) performed computations, which were analyzed and interpreted by both Dr. Sazama and the author (hereafter G.D.G.). Tony Wu (Electrical Engineering and Computer Science, MIT) and G.D.G. collaborated on the acquisition of transient photoluminescence lifetime data.

## 2.1 Introduction

Molecules capable of phosphorescence at room temperature have been utilized in a variety of technologies, most notably in light-emitting diodes (LEDs) for next-generation electronic displays.<sup>1,2</sup> Organometallic complexes containing platinum or iridium are often bright phosphorescent emitters because spin-orbit coupling induced by these heavy metal atoms bypass the quantum mechanical restrictions that prevent intersystem crossing (ISC) from occurring.<sup>3</sup> Non-metallated organic molecules are also capable of ISC and are commonly investigated as triplet photosensitizers.<sup>4</sup> However, other classes of such materials may also produce phosphorescence at room temperature. For example, phosphorescent emission under ambient conditions has been observed from organic molecules dispersed in polymeric hosts<sup>5-9</sup>, zeolites,<sup>10</sup> and various classes of non-metallated solids, including halogenated benzophenones<sup>11</sup> and benzaldehydes,<sup>12,13</sup> carbazole-containing materials,<sup>14,15</sup> naphthalene diimides,<sup>16</sup> persulfurated aromatics,<sup>17-19</sup> and tellurophenes.<sup>20,21</sup> However, observing measurable phosphorescence from metal-free organic molecules dissolved in liquids at room temperature is often a challenging feat due to rapid non-radiative dissipation of a triplet state's energy under these conditions. As a result, few non-metallated organic molecules are known to produce significant phosphorescence in solution at room temperature.<sup>22-25</sup>

Benzo[2,1,3]thiadiazoles constitute a category of heteroaromatic molecules that are widely used in the development of fluorescent  $\pi$ -conjugated organic materials.<sup>26</sup> We herein present the room-temperature red phosphorescence exhibited by four benzo[2,1,3]thiadiazoles in cyclohexane and describe their corresponding excited-state electronic properties using computational methods.

## 2.2 *Photophysical Properties of 4,7-Dihalogenated-5,6-bis(tetradecyloxy)benzo[2,1,3]thiadiazoles in Cyclohexane*

Our study was prompted by the observation of room-temperature phosphorescence from 4,7-dibromo-5,6-bis(tetradecyloxy)benzo[2,1,3]thiadiazole (**1-Br**, Figure 2.1a) and 4,7-diiodo-5,6-bis(tetradecyloxy)benzo[2,1,3]thiadiazole (**1-I**, Figure 2.1d), both of which are heteroaromatic linkers our laboratory has used to construct fluorescent semiconducting polymers.<sup>27,28</sup> The absorption spectra of these two molecules in cyclohexane at 50  $\mu\text{M}$  are primarily confined to the ultraviolet region and under aerobic conditions these solutions exhibit extremely weak blue fluorescence when excited at  $\lambda_{\text{ex}} = 370$  nm. However, after deoxygenation with  $\text{N}_2$  gas, **1-Br** and **1-I** demonstrate profoundly red-shifted emission maxima at  $\lambda_{\text{max}} = 642$  nm and  $\lambda_{\text{max}} = 643$  nm, respectively (Figures 2.1b and 2.1e). We assigned these unexpected red emissions as phosphorescence<sup>29</sup> as a result of the large downconversions of absorbed energy that results from ISC as well as the oxygen quenching of the long-lived triplet states. The phosphorescence quantum yields ( $\Phi_P$ ) of **1-Br** and **1-I** in degassed cyclohexane are 0.55% and 0.59%, respectively. Excitation spectra monitored at  $\lambda_{\text{em}} = 575$  nm confirm that phosphorescence originates from **1-Br** and **1-I** by matching the structure of their corresponding absorption spectra (Figures 2.1c and 2.1f).

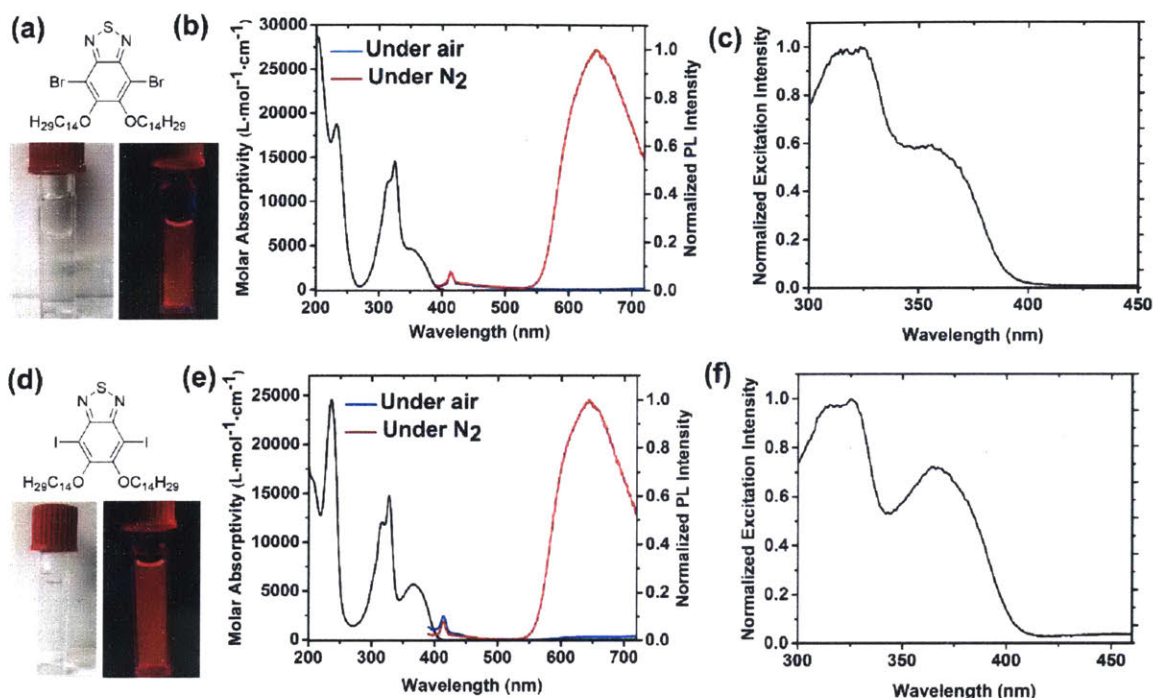


**Figure 2.1.** Photophysical properties of phosphorescent compounds **1-Br** and **1-I** in cyclohexane. (a) **1-Br** and (d) **1-I** and their appearance in degassed cyclohexane under normal and UV ( $\lambda = 365$  nm) lighting. (b) Absorption spectrum and photoluminescence spectra under air and  $\text{N}_2$  gas for **1-Br** and (e) **1-I** ( $\lambda_{\text{ex}} = 370$  nm). (c) Phosphorescence excitation spectrum of **1-Br** and (f) **1-I** ( $\lambda_{\text{em}} = 575$  nm). Photoluminescence and excitation spectra were measured for  $50 \mu\text{M}$  solutions. A small peak attributed to Raman scattering ( $\lambda_{\text{max}} = 414$  nm) of the excitation beam by the solvent overlaps with the fluorescence of all phosphorescent samples presented in this study and is not considered in our analysis.

Because phosphorescence requires molecules to undergo ISC, the resulting photoluminescence lifetimes ( $\tau_P$ ) often occur on microsecond or millisecond time scales. Time-dependent transient photoluminescence spectroscopy was employed to determine if deoxygenated solutions of **1-Br** and **1-I** in cyclohexane possess such long lifetimes. Under these conditions, the photoluminescence

of each sample exhibit delayed components on the microsecond-time scale (Figure 2.2). By fitting the intensities of these delayed responses to a first-order kinetic model with respect to time, the data reveal that **1-Br** and **1-I** possess  $\tau_P$  of 2.8  $\mu\text{s}$  and 3.6  $\mu\text{s}$ , respectively.

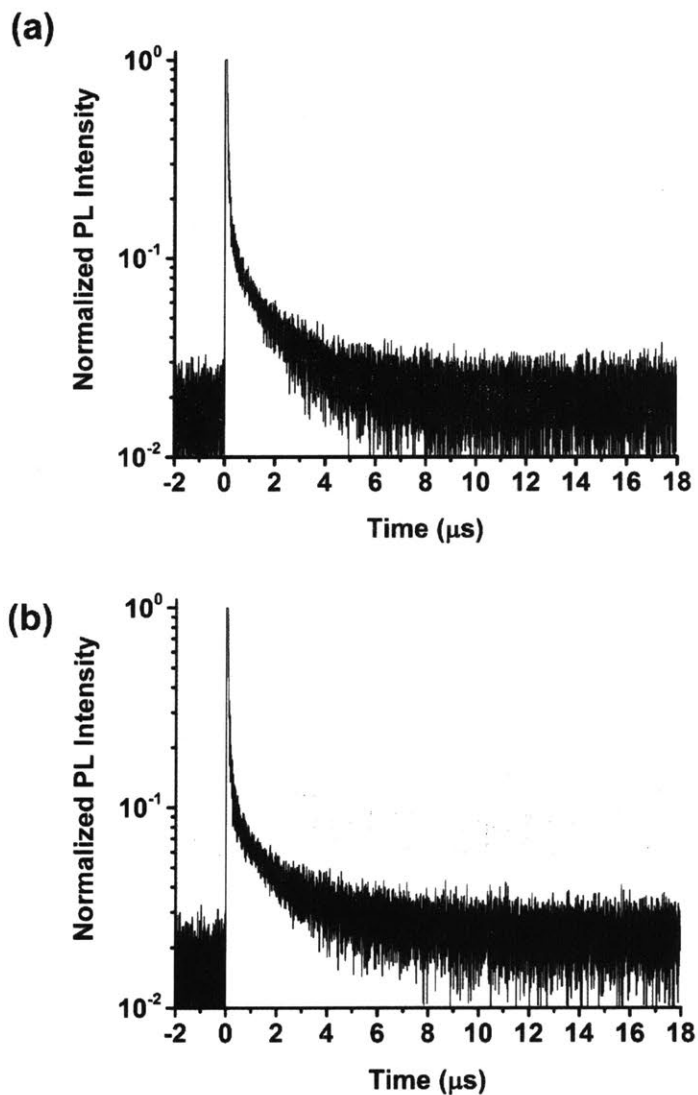
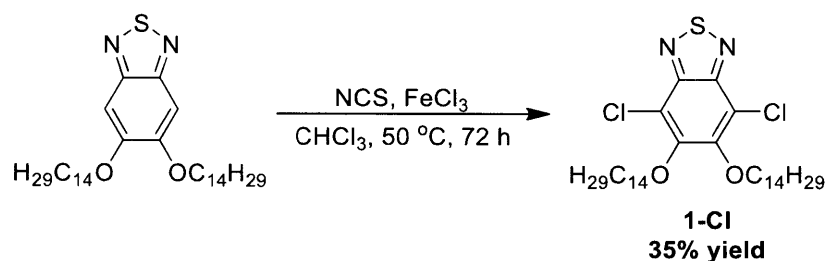


**Figure 2.2.** Time-dependent photoluminescence decays of (a) **1-Br** and (b) **1-I** in cyclohexane (50  $\mu\text{M}$ ) under inert atmosphere and at room temperature.

Following these results, we hypothesized that **1-Br** and **1-I** may be undergoing ISC and phosphorescence as a result of the influence of the heavy halides on their electronic properties. To investigate this possibility, we synthesized dichloride **1-Cl** and examined its photophysical properties in cyclohexane. **1-Cl** was accessed by reacting 5,6-bis(tetradecyloxy)benzo[2,1,3]thiadiazole with *N*-chlorosuccinimide in the presence of iron(III) chloride (Scheme 2.1). Although it possesses an absorption spectrum similar to those of **1-Br** and **1-I**, **1-Cl** primarily demonstrates blue fluorescence at  $\lambda_{\text{max}} = 424$  nm with almost no red emission under deoxygenated conditions (Figure 2.3). Our results support the possibility that phosphorescence is facilitated by a heavy atom effect induced by the bromides and iodides in **1-Br** and **1-I**, respectively (see Calculations).



**Scheme 2.1.** Synthesis of chlorinated benzo[2,1,3]thiadiazole **1-Cl**.

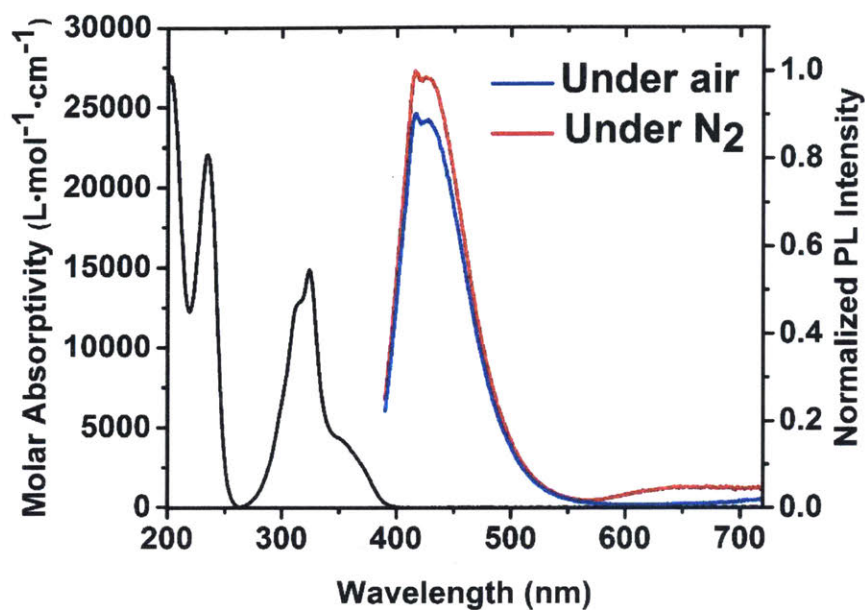
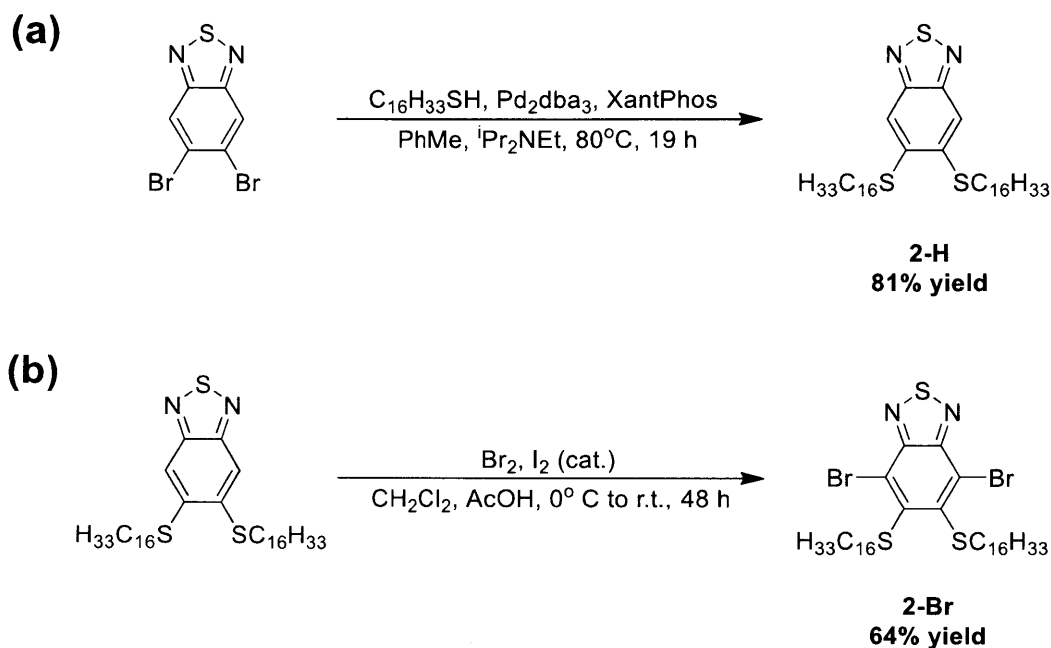


**Figure 2.3.** Absorption and emission spectra of **1-CI** in cyclohexane. Emission spectra ( $\lambda_{\text{ex}} = 370$  nm) are reported for 50  $\mu\text{M}$  samples in aerobic and deoxygenated cyclohexane.

### 2.3 Synthesis of Thioether-functionalized Benzo[2,1,3]thiadiazoles and Their Photophysical Properties in Cyclohexane

We next investigated if previously unreported benzo[2,1,3]thiadiazoles are also phosphorescent. In particular, we prepared the molecules 5,6-bis(hexadecylthio)benzo[2,1,3]thiadiazole (**2-H**)<sup>30</sup> and 4,7-dibromo-5,6-bis(hexadecylthio)benzo[2,1,3]thiadiazole (**2-Br**), the syntheses of which are presented in Scheme 2. To construct **2-H**, two equivalents of 1-hexadecanethiol were directly coupled with 5,6-dibromobenzo[2,1,3]thiadiazole using the palladium-catalyzed methodology developed by Itoh and Mase.<sup>31</sup> **2-Br** was subsequently synthesized via iodine-catalyzed bromination of **2-H**.



**Scheme 2.2.** Syntheses of thioether-functionalized benzo[2,1,3]thiadiazoles **2-H** (a) and **2-Br** (b).

The absorption and photoluminescence spectra of 50  $\mu\text{M}$  solutions of **2-H** and **2-Br** in cyclohexane are displayed in Figures 2.4b and 2.4e. The solutions of **2-H** and **2-Br** absorb only in the UV and blue regions, but produce red emissions after deoxygenation with  $\text{N}_2$  gas. **2-H** and **2-Br** thus demonstrate phosphorescence with maxima at  $\lambda_{\text{max}} = 624 \text{ nm}$  and  $\lambda_{\text{max}} = 667 \text{ nm}$ , respectively, with corresponding excitation spectra resembling their absorption profiles (Figure 2.4c and 2.4f). In the case of **2-H**, the excitation spectrum fully matches its absorption spectrum at much lower concentrations (i.e. 2.6  $\mu\text{M}$ ), an observation which is most likely the result of an inner-filter effect occurring at 50  $\mu\text{M}$ . Both molecules also possess values of  $\Phi_P$  similar to those of **1-Br** and **1-I** (0.70% for **2-H** and 0.50% for **2-Br**) in cyclohexane. Transient photoluminescence data indicate that  $\tau_P$  is 5.4  $\mu\text{s}$  for **2-H** and 3.4  $\mu\text{s}$  for **2-Br** (Figures 2.4g and 2.4h). A summary of the photophysical properties of the four phosphorescent molecules described thus far is presented in Table 2.1.



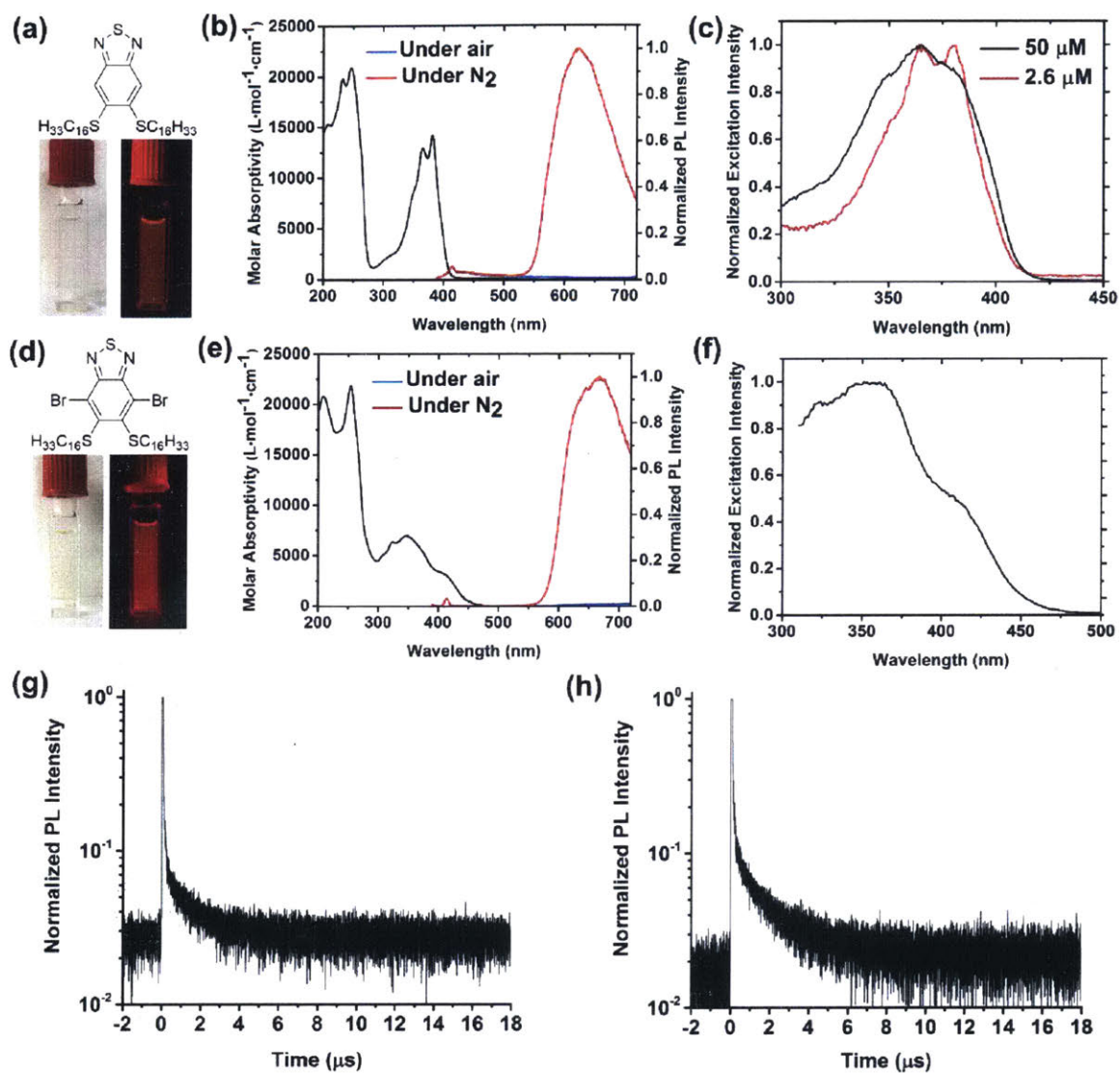


**Figure 2.4.** (a) **2-H** in cyclohexane with its (b) absorption spectrum and photoluminescence spectra under air and  $\text{N}_2$  gas and (c) phosphorescence excitation spectra at 50  $\mu\text{M}$  and 2.6  $\mu\text{M}$  ( $\lambda_{\text{em}} = 575 \text{ nm}$ ). (d-f) **2-Br** with its corresponding absorption/photoluminescence spectra ( $\lambda_{\text{ex}} = 370 \text{ nm}$ , 50  $\mu\text{M}$ ) and phosphorescence excitation spectrum ( $\lambda_{\text{em}} = 600 \text{ nm}$ , 50  $\mu\text{M}$ ). (g) Time-dependent photoluminescence decays for **2-H** and (h) **2-Br** in deoxygenated cyclohexane at 50  $\mu\text{M}$ .

Entry	$\lambda_{\text{abs.max.}}^a, \lambda_{\text{em.max}} \text{ (nm)}$	$\tau_P \text{ (\mu s)}$	$\Phi_P \text{ (\%)}^b$
<b>1-Br</b>	325, 642	2.8	0.55
<b>1-I</b>	327, 643	3.6	0.59
<b>2-H</b>	382, 624	5.4	0.70
<b>2-Br</b>	347, 667	3.4	0.50

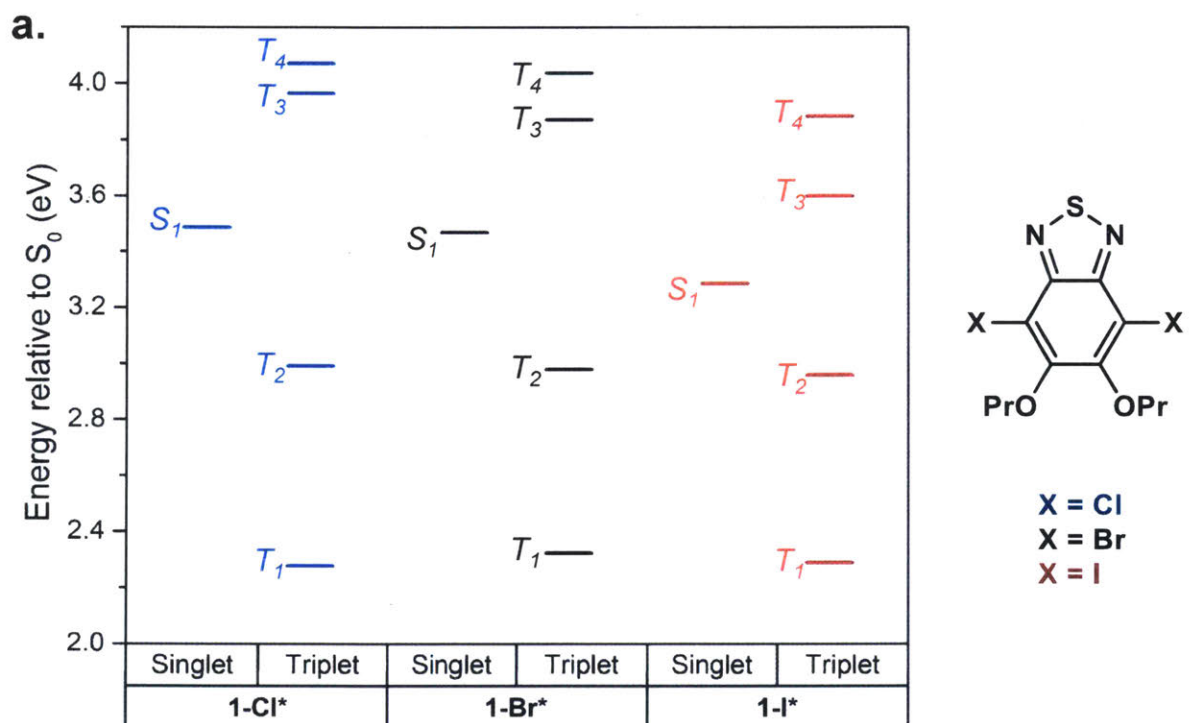
<sup>a</sup>Absorption maximum past  $\lambda = 300 \text{ nm}$ . <sup>b</sup>Measured at  $\lambda_{\text{ex}} = 370 \text{ nm}$  using 9,10-diphenylanthracene in cyclohexane under air as a standard ( $\Phi_{PL} = 77\%$ ).<sup>32</sup>

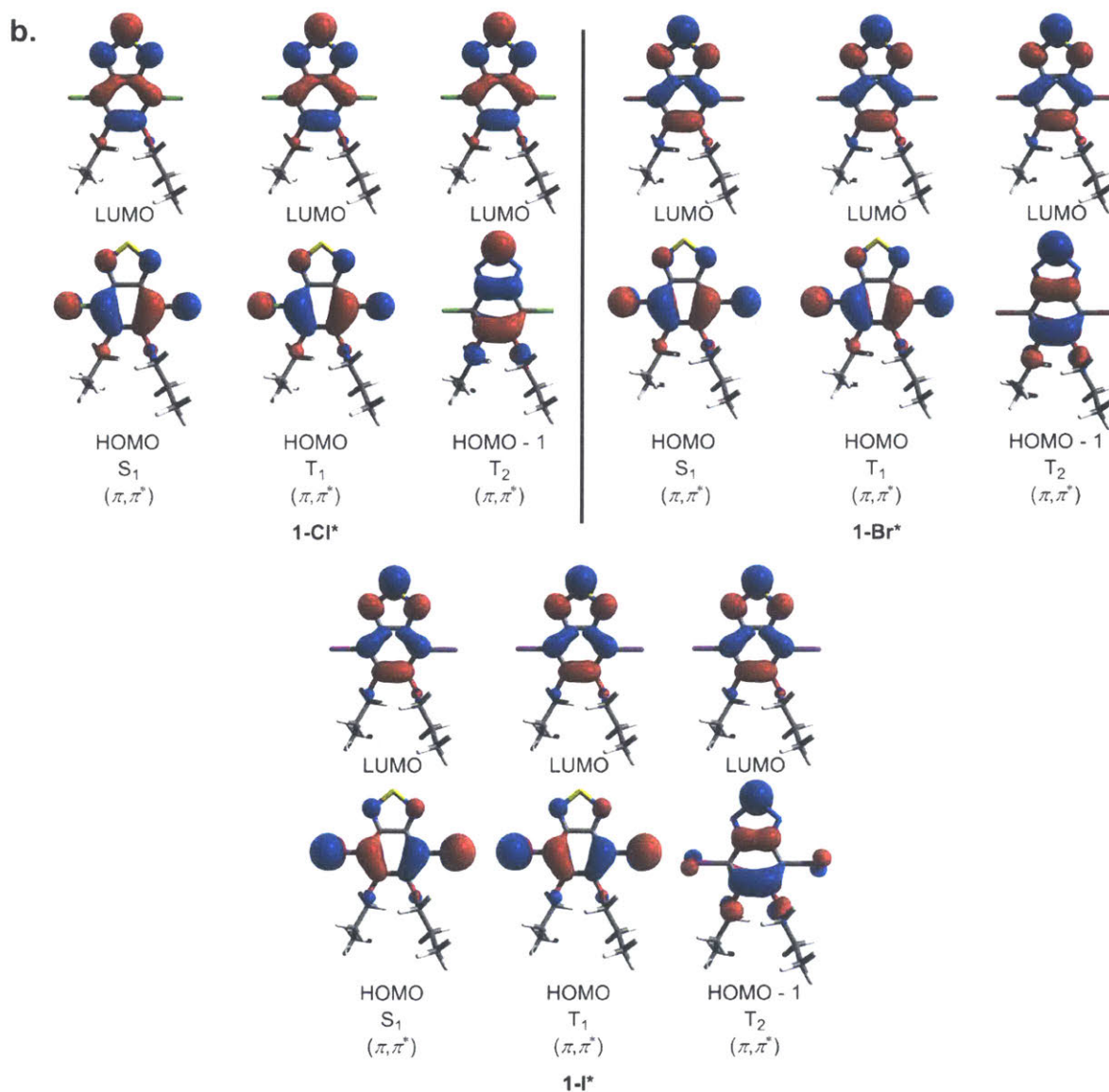
**Table 2.1.** Summary of photophysical properties of phosphorescent benzo[2,1,3]thiadiazoles in deoxygenated cyclohexane.

#### 2.4 Time-Dependent Density Functional Theory Calculations

We next performed a computational analysis of the electronic excited states of the studied benzo[2,1,3]thiadiazoles in order to determine potential phosphorescence pathways. After ground state geometry optimization of model structures **1-Cl\***, **1-Br\***, and **1-I\***, for which the large tetradecyloxy groups are replaced with propoxy substituents for computational efficiency, we carried out time-dependent density functional theory (TD-DFT) calculations to determine a mechanism for ISC. Throughout our analysis, we assume that internal conversion to  $S_1$  always occurs prior to ISC (Kasha's rule).<sup>33</sup> For each molecule, two lower-energy triplet states ( $T_1$  and  $T_2$ ) lie below  $S_1$  and thus provide thermodynamically favorable routes for ISC (Figure 2.5a). We subsequently characterized the excited states of the molecules using Kohn-Sham orbitals to depict the electronic configurational descriptions of the  $S_1$ ,  $T_1$ , and  $T_2$  states of each molecule (Figure 2.5b). We observe that, in all three molecules, the  $S_1$ ,  $T_1$ , and  $T_2$  states can all be described as symmetric  $\pi \rightarrow \pi^*$  configurations.  $S_1$  and  $T_1$  are  $\geq 88\%$  described by a HOMO  $\rightarrow$  LUMO

configuration, while  $T_2$  corresponds to a HOMO-1  $\rightarrow$  LUMO configuration ( $\geq 85\%$  character). Because the transition symmetry of  $S_1$  does not change during conversion to one of the lower-energy triplet states, ISC is most likely to be an inefficient process unless perturbations from one or more heavy atoms are introduced.<sup>34</sup> We conclude that ISC from  $S_1$  to  $T_2$  or  $T_1$  could be facilitated by the heavy bromides and iodides through second-order perturbations such as a spin-orbit-vibronic interaction.<sup>35</sup> The lighter chlorides of **1-Cl**\* likely do not carry a large enough atomic number to enable ISC in this manner, which explains why fluorescence dominates the photoluminescence spectrum of **1-Cl**.

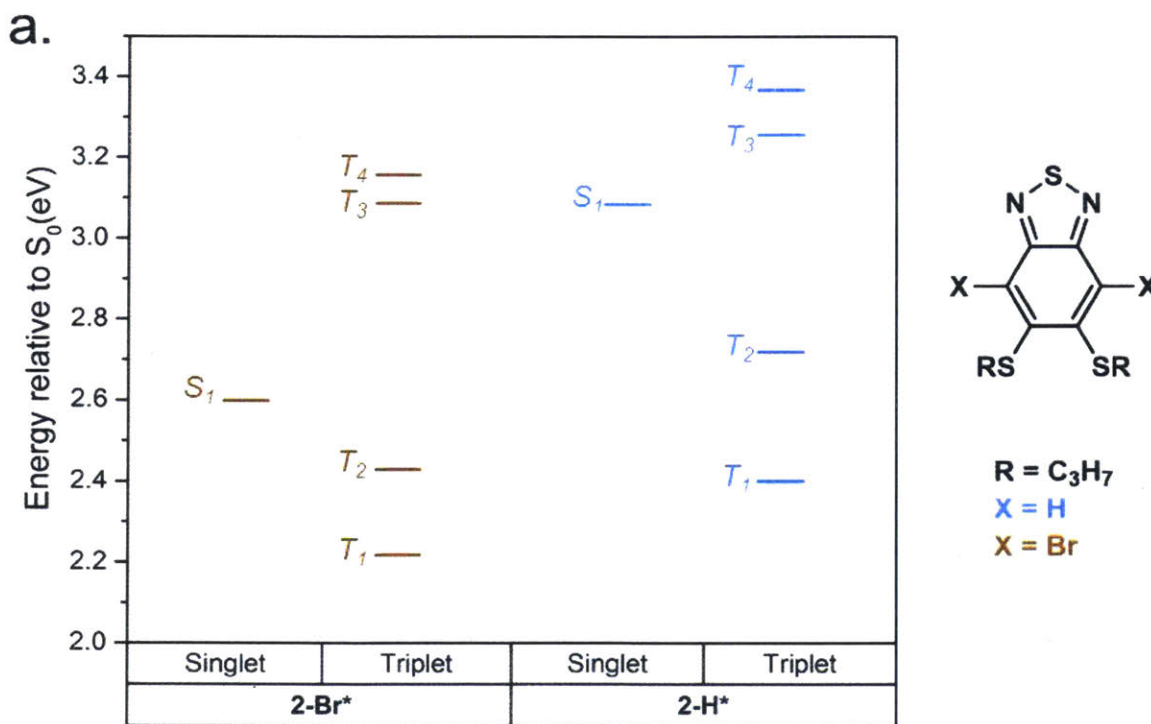




**Figure 2.5.** (a) Energy level diagrams for propoxy-functionalized derivatives **1-Cl\***, **1-Br\***, and **1-I\*** in the gas phase. (b) Kohn-Sham orbitals representing the electronic configuration descriptions of S<sub>1</sub>, T<sub>1</sub>, and T<sub>2</sub> for each calculated molecule.

Figure 6 displays the excited-state energy level diagrams for **2-H\*** and **2-Br\***, model systems where the long alkyl chains of the thioethers have been replaced with propylthio groups (Figure 2.6a).<sup>36</sup> The corresponding Kohn-Sham orbitals for S<sub>1</sub>, T<sub>1</sub>, and T<sub>2</sub> are shown in Figure 2.6b. Unlike

the other phosphors, **2-H** does not possess heavy halides that can enable ISC. However, the  $S_1$  state of **2-H\*** is distinctly an  $(n,\pi^*)$  state in which most of the orbital density is concentrated at the sulfur atoms of the alkylthio groups.  $T_1$  is best represented as a  $(\pi,\pi^*)$  state composed of a linear combination of configurations of HOMO-1  $\rightarrow$  LUMO (49% character,  $(\pi,\pi^*)$ ) and HOMO-2  $\rightarrow$  LUMO (44% character,  $(n,\pi^*)$ ).  $T_2$ , on the other hand, is a mix of mostly an  $(n,\pi^*)$  state with minority  $(\pi,\pi^*)$  character represented by two configurations: HOMO  $\rightarrow$  LUMO (81% character,  $(n,\pi^*)$ ) and HOMO-3  $\rightarrow$  LUMO (15% character,  $(\pi,\pi^*)$ ). In this case, ISC is most likely possible by coupling a change in the spin angular momentum of the excited-state electron with the difference in the transition symmetries of the  $S_1$  and  $T_1$  manifolds (El-Sayed's rule).<sup>37</sup> Similarly,  $S_1$  of **2-Br\*** is an  $(n,\pi^*)$  state,<sup>38</sup> whereas  $T_1$  is a  $(\pi,\pi^*)$  state and  $T_2$  is mostly  $(n,\pi^*)$ . Thus, we conclude that either a difference in angular orbital momentum between  $S_1$  and  $T_2$  or a heavy atom effect can lead to ISC.



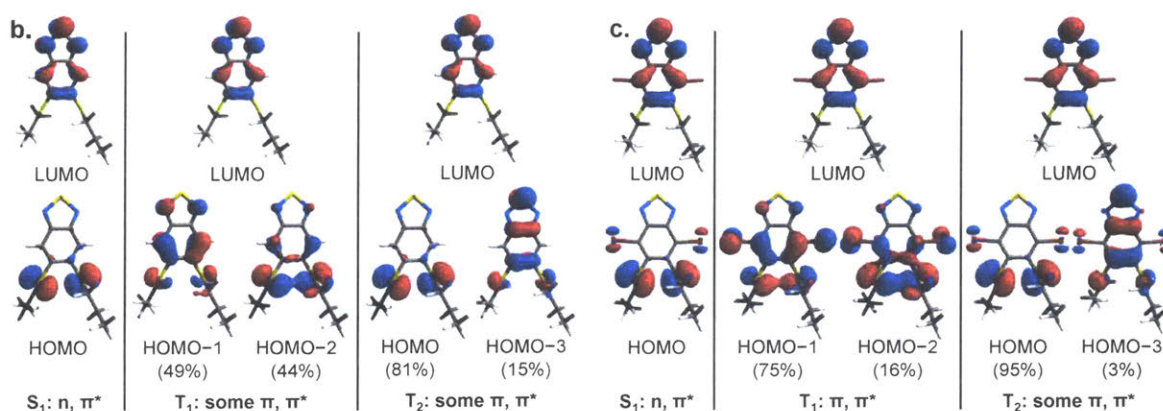


**Figure 2.6.** (a) Energy level diagrams for **2-H\*** and **2-Br\*** in the gas phase. (b) Kohn-Sham orbitals representing the electronic configuration description of S<sub>1</sub>, T<sub>1</sub>, and T<sub>2</sub> manifolds of **2-H\*** and (c) **2-Br\***. Indicated percentages describe the overall character for each displayed transition.

## 2.5 Conclusion

To conclude, we have presented a set of structurally simple benzo[2,1,3]thiadiazoles with unusual phosphorescent emissions at room temperature. The rare solution-phase photophysical properties of these species provide a new direction aimed at uncovering new classes of metal-free organic phosphorescent materials. We are currently seeking to discover new molecular motifs and realize their potential as the active components of inexpensive LEDs and other optoelectronic technologies.

## 2.6 Experimental Section

**2.6.1 Materials and Instrumentation.** Unless otherwise stated, all solvents and reagents were used as purchased. Anhydrous toluene was obtained from a solvent purification system and stored over activated 3 Å molecular sieves. HPLC-grade cyclohexane was the solvent in all photophysical studies. 5,6-dibromobenzo[2,1,3]thiadiazole was purchased from TCI Chemical Company and used without further purification. **1-I** was synthesized according to a literature procedure.<sup>28</sup>

Column chromatography was carried out using silica gel (Aldrich, 60 Å pore size, 230-400 mesh) and thin layer chromatography (TLC) was performed with silica gel TLC plates (J. T. Baker). All NMR spectra ( $^1\text{H}$ : 400 MHz,  $^{13}\text{C}$ : 101 MHz) were obtained with  $\text{CDCl}_3$  as the solvent and were referenced relative to resonances corresponding to  $\text{CDCl}_3$  ( $^1\text{H}$ :  $\delta = 7.26$  ppm;  $^{13}\text{C}$ :  $\delta = 77.16$  ppm). Peak multiplicities are designated as singlet (“s”), triplet (“t”), or multiplet (“m”). High-resolution mass spectrometry (HRMS) measurements were carried out in direct analysis in real time (DART) or with electrospray ionization (ESI) in positive mode using a Fourier transform-ion cyclotron resonance mass spectrometer.

All absorption spectra were measured with a UV/vis spectrophotometer under aerobic conditions. Photoluminescence spectra and excitation spectra were obtained with a spectrofluorometer employing a 450 W xenon short-arc lamp. Excitation and emission bandpass slits were set at 3 nm and 5 nm, respectively, and data were acquired with the excitation beam and detector oriented at a right angle. Photoluminescence spectra were corrected to account for wavelength-dependent responses by the detector, while excitation spectra were referenced relative to variations in the lamp intensity with wavelength. Phosphorescence quantum yields were measured using the relative method suggested by Brouwer<sup>39</sup> with all absorbances at the excitation wavelength maintained below 0.05 to prevent inner-filter effects from occurring. For these photoluminescence measurements, screw-top quartz cuvettes covered with a septum cap were used to hold solutions and were deoxygenated by purging them with  $\text{N}_2$  gas for about 10 minutes to induce phosphorescence. For best results, solutions analyzed by spectroscopy were not exposed to UV radiation during the deoxygenation process.

To obtain transient photoluminescence lifetime measurements, a sample was placed in a quartz tube (6-mm outer diameter, 4-mm inner diameter) and sealed with a small septum. The solution

was then deoxygenated via purging with N<sub>2</sub> gas for about 5 minutes. A 170 μJ pulsed 337 nm N<sub>2</sub> laser was used as the excitation source with photoluminescence detected using a silicon detector coupled to a 400 nm longpass optical filter. The resulting time-dependent photoluminescence data were recorded with an oscilloscope. Some residual laser signal is present as the prompt component of these decays and were not considered in our analysis. To extract the lifetime, data past this artificial prompt signal (i.e. after 1 μs) was subjected to a linear fit on the logarithmic scale.

**2.6.2 Electronic Structure Calculations.** Molecules were built and molecular mechanics were used to minimize geometries using Avogadro.<sup>40</sup> TD-DFT calculations were performed using the ORCA software package.<sup>41–43</sup> First, geometries were optimized using the AccOpt standard calculation level implemented in ORCA (BP86 functional,<sup>44</sup> ORCA default basis 4: TZVP(2d) for all non-hydrogens, and TZV(p) for hydrogens<sup>45</sup>). Numerical frequencies were then calculated to determine that geometries represented minima on the potential energy surface. Using the optimized geometries, TD-DFT calculations<sup>42</sup> were carried out using the same bases, with the PBE0 functional<sup>46</sup> and increased grid accuracy, and the resolution of identity chain-of-spheres module, RIJCOSX,<sup>43</sup> was used to reduce the computational cost of the calculations. The first 10 excited state levels and their excitation profiles were calculated for each molecule at the ground state geometry, for both singlet and triplet states, affording a first-order description of the energetic landscape. Electronic configuration descriptions of the relevant excited states (S<sub>1</sub>, T<sub>1</sub>, and T<sub>2</sub>) were visualized using Kohn-Sham orbitals depicted using the Avogadro software with extended ORCA support. All simulated molecules were treated without solvation (i.e. gas phase).

### 2.6.3 Synthetic Procedures

*4,7-Dichloro-5,6-bis(tetradecyloxy)benzo[2,1,3]thiadiazole (1-Cl)*



To an oven-dried 2-neck 100 mL round-bottom flask equipped with a magnetic stir bar and condenser were combined 5,6-bis(tetradecyloxy)benzo[2,1,3]thiadiazole<sup>27</sup> (300 mg, 0.535 mmol), *N*-chlorosuccinimide (157 mg, 1.18 mmol), and anhydrous CHCl<sub>3</sub> (30 mL). FeCl<sub>3</sub> (101 mg, 0.628 mmol) was added to the stirring solution under a stream of argon. The reaction was stirred under argon at 50 °C for 72 h. The reaction mixture was cooled to room temperature, diluted with 30 mL CHCl<sub>3</sub>, and poured into 50 mL H<sub>2</sub>O. The organic layer was washed with 100 mL NaHCO<sub>3</sub> (*aq.*) and 100 mL saturated NaCl(*aq.*), dried with MgSO<sub>4</sub>, filtered, and evaporated. The brown crude product was subjected to column chromatography (1:1 CHCl<sub>3</sub>:hexanes) to furnish **1-Cl** as a white solid (117 mg, 35% yield). *R*<sub>f</sub> = 0.38 (SiO<sub>2</sub> TLC, 1:1 CHCl<sub>3</sub>:hexanes). <sup>1</sup>H NMR (400 MHz, CDCl<sub>3</sub>): δ 4.18 (t, *J* = 6.7 Hz, 4H), 1.87 (m, 4H), 1.53 (m, 4H), 1.40-1.26 (m, 40H), 0.88 (t, *J* = 7.0 Hz, 6H). <sup>13</sup>C NMR (101 MHz, CDCl<sub>3</sub>): δ 153.3, 149.8, 116.4, 75.4, 32.1, 30.4, 29.86, 29.85, 29.84, 29.82, 29.79, 29.76, 29.6, 29.5, 26.1, 22.9, 14.3. HRMS (ESI) *m/z* calculated for C<sub>34</sub>H<sub>58</sub>Cl<sub>2</sub>N<sub>2</sub>O<sub>2</sub>S [M + H]<sup>+</sup>: 629.3669, found: 629.3687.

#### *4,7-Dibromo-5,6-bis(tetradecyloxy)benzo[2,1,3]thiadiazole (1-Br)*

Compound **1-Br** was synthesized as reported by Bouffard and Swager,<sup>27</sup> but with modified purification. To a 50 mL round-bottom flask equipped with magnetic stirbar were combined 5,6-bis(tetradecyloxy)benzo[2,1,3]thiadiazole (300 mg, 0.535 mmol), CH<sub>2</sub>Cl<sub>2</sub> (15 mL), and AcOH (7 mL). To this solution was added Br<sub>2</sub> (528 mg, 0.169 mmol, 0.17 mL) dropwise. The flask was stoppered, wrapped with aluminum foil, and contents were stirred for 2 days. The reaction mixture was then poured into 50 mL 5% w/v Na<sub>2</sub>S<sub>2</sub>O<sub>3</sub>•5H<sub>2</sub>O (*aq.*) and washed. The organic layer was then washed with 2 x 50 mL saturated NaHCO<sub>3</sub> (*aq.*) and 50 mL saturated NaCl (*aq.*), dried with MgSO<sub>4</sub>, filtered, and evaporated. The crude residue was subjected to column chromatography (3:7 CHCl<sub>3</sub>:hexanes) to yield **1-Br** as a white solid (244 mg, 64% yield). Characterization data is

consistent with those already reported.  $^1\text{H}$  NMR (400 MHz,  $\text{CDCl}_3$ ):  $\delta$  4.16 (t,  $J = 6.7$  Hz, 4H), 1.88 (m, 4H), 1.53 (m, 4H), 1.38-1.26 (m, 40H), 0.88 (t,  $J = 7.0$  Hz, 6H).

#### *5,6-Bis(hexadecylthio)benzo[2,1,3]thiadiazole (2-H)*

To a 25 mL Schlenk flask equipped with a magnetic stirbar were added 5,6-dibromobenzo[2,1,3]thiadiazole (350 mg, 1.19 mmol),  $\text{Pd}_2\text{dba}_3$  (27.3 mg, 29.8  $\mu\text{mol}$ ), and XantPhos (34.5 mg, 59.3  $\mu\text{mol}$ ). The flask was then evacuated and backfilled with argon three times before adding anhydrous toluene (6 mL), diisopropylethylamine (2 mL), and 1-hexadecanethiol (954 mg, 1.14 mL, 3.69 mmol). After purging with argon for 15 minutes at room temperature, the reaction mixture was stirred at 80  $^\circ\text{C}$  under argon for 19 h. The reaction mixture was then cooled to room temperature and filtered. Volatiles were then evaporated *in vacuo*. The crude residue was dissolved in  $\text{CH}_2\text{Cl}_2$  and combined with 3 g silica gel. After removal of the solvent, the solid mixture was dry-loaded onto a silica gel column and the product was eluted out with 1:1  $\text{CH}_2\text{Cl}_2$ :hexanes. The recovered product was lastly recrystallized from isopropanol to obtain pure **2-H** as a light yellow solid (623 mg, 81% yield).  $R_f = 0.49$  ( $\text{SiO}_2$  TLC, 1:1  $\text{CH}_2\text{Cl}_2$ :hexanes)  $^1\text{H}$  NMR (400 MHz,  $\text{CDCl}_3$ ):  $\delta$  7.68 (s, 2H), 3.04 (t,  $J = 7.4$  Hz, 4H), 1.79 (m, 4H), 1.50 (m, 4H), 1.35-1.25 (m, 48H), 0.87 (t,  $J = 7.0$  Hz, 6H).  $^{13}\text{C}$  NMR (101 MHz,  $\text{CDCl}_3$ ):  $\delta$  153.4, 142.3, 116.0, 33.6, 32.1, 29.84, 29.81, 29.78, 29.7, 29.6, 29.5, 29.33, 29.25, 28.2, 22.8, 14.3. HRMS (DART)  $m/z$  calculated for  $\text{C}_{38}\text{H}_{68}\text{N}_2\text{S}_3$   $[\text{M} + \text{H}]^+$ : 649.4617, found: 649.4617.

#### *4,7-Dibromo-5,6-bis(hexyldecylthio)benzo[2,1,3]thiadiazole (2-Br)*

In a 50 mL round-bottom flask equipped with a magnetic stirbar, **2-H** (100 mg, 0.154 mmol) was dissolved in a mixture of  $\text{CH}_2\text{Cl}_2$  (15 mL) and AcOH (4 mL) and chilled to 0  $^\circ\text{C}$ . To the stirring suspension was added  $\text{I}_2$  (1.75 mg, 7.70  $\mu\text{mol}$ ), followed by  $\text{Br}_2$  (123 mg, 0.770 mmol, 0.04 mL) dropwise. Contents were warmed to room temperature and stirred in the dark for 48 h. The reaction

mixture was then poured into 50 mL 5% w/v Na<sub>2</sub>S<sub>2</sub>O<sub>3</sub>•5H<sub>2</sub>O (aq.) and washed with 50 mL saturated NaHCO<sub>3</sub> (aq.), and 50 mL saturated NaCl (aq.). The organic layer was dried with MgSO<sub>4</sub> and filtered. Volatiles were evaporated and the crude residue was purified by column chromatography (3:7 CHCl<sub>3</sub>:hexanes) to obtain **2-Br** as a light yellow solid (79 mg, 64% yield). *R<sub>f</sub>* = 0.31 (SiO<sub>2</sub> TLC, 3:7CHCl<sub>3</sub>:hexanes). <sup>1</sup>H NMR (400 MHz, CDCl<sub>3</sub>): δ 3.08 (t, *J* = 7.4 Hz, 4H), 1.61 (m, 4H), 1.42 (m, 4H), 1.25-1.24 (m, 48H), 0.88 (t, *J* = 7.0 Hz, 6H). <sup>13</sup>C NMR (101 MHz, CDCl<sub>3</sub>): δ 153.0, 144.5, 122.6, 38.4, 32.1, 29.84, 29.82, 29.81, 29.79, 29.73, 29.65, 29.5, 29.3, 29.0, 22.8, 14.3. HRMS (DART) *m/z* calculated for C<sub>38</sub>H<sub>66</sub>Br<sub>2</sub>N<sub>2</sub>S<sub>3</sub> M<sup>+</sup>: 806.2741, found: 806.2734.

## 2.7 References

- (1) Müllen, K.; Scherf, U. *Organic Light Emitting Devices: Synthesis, Properties, and Applications*; Wiley-VCH: Hoboken, NJ, 2006.
- (2) Yersin, H. *Highly Efficient OLEDs with Phosphorescent Materials*; Wiley-VCH: Hoboken, NJ, 2008.
- (3) Evans, R. C.; Douglas, P.; Winscom, C. J. *Coord. Chem. Rev.* **2006**, *250*, 2093-2126.
- (4) (a) Yogo, T.; Urano, Y.; Ishitsuka, Y.; Maniwa, F.; Nagano, T. *J. Am. Chem. Soc.* **2013**, *127*, 12162-12163. (b) Zhang, C.; Zhao, J.; Wu, S.; Wang, Z.; Wu, W.; Ma, J.; Guo, S.; Huang, L. *J. Am. Chem. Soc.* **2013**, *135*, 10566-10578. (c) Kamkaew, A.; Lim, S. H.; Lee, H. B.; Kiew, L. V.; Chung, L. Y.; Burgess, K. *Chem. Soc. Rev.* **2013**, *42*, 77-88. (d) Zhao, J.; Wu, W.; Sun, J.; Guo, S. *Chem. Soc. Rev.* **2013**, *42*, 5323-5351.
- (5) (a) Horie, K.; Mita, I. *Chem. Phys. Lett.* **1982**, *93*, 61-65. (b) Horie, K.; Morishita, K.; Mita, I. *Macromolecules* **1984**, *17*, 1746-1750.

- (6) Lee, D.; Bolton, O.; Kim, B. C.; Youk, J. H.; Takayama, S.; Kim, J. *J. Am. Chem. Soc.* **2013**, *135*, 6325-6329.
- (7) Hirata, S.; Totani, K.; Zhang, J.; Yamashita, T.; Kaji, H.; Marder, S. R.; Watanabe, T.; Adachi, C. *Adv. Funct. Mater.* **2013**, *23*, 3386-3397.
- (8) Kwon, M. S.; Lee, D.; Seo, S.; Jung, J.; Kim, J. *Angew. Chem. Int. Ed.* **2014**, *53*, 11177-11181.
- (9) Lee, D.; Jung, J.; Bilby, D.; Kwon, M. S.; Yun, J.; Kim, J. *ACS Appl. Mater. Inter.* **2015**, *7*, 2993-2997.
- (10) Ramamurthy, V.; Caspar, J. V.; Eaton, D. F.; Kuo, E. W.; Corbin, D. R. *J. Am. Chem. Soc.* **1992**, *114*, 3882-3892.
- (11) Yuan, W. Z.; Shen, X. Y.; Zhao, H.; Lam, J. W. Y.; Tang, L.; Lu, P.; Wang, C.; Liu, Y.; Wang, Z.; Zheng, Q.; Sun, J. Z.; Ma, Y.; Tang, B. Z. *J. Phys. Chem. C* **2010**, *114*, 6090-6099.
- (12) Bolton, O.; Lee, K.; Kim, H.-J.; Lin, K. Y.; Kim, J. *Nat. Chem.* **2011**, *3*, 205-210.
- (13) Bolton, O.; Lee, D.; Jung, J.; Kim, J. *Chem. Mater.* **2014**, *26*, 6644-6649.
- (14) Gao, H. Y.; Shen, Q. J.; Zhao, X. R.; Yan, X. Q.; Pan, X.; Jin, W. J. *J. Mater. Chem.* **2012**, *22*, 5336-5343.
- (15) Yang, Z.; Mao, Z.; Zhang, X.; Ou, D.; Mu, Y.; Zhang, Y.; Zhao, C.; Liu, S.; Chi, Z.; Xu, J.; Wu, Y.-C.; Lu, P.-Y.; Lien, A.; Bryce, M. R. *Angew. Chem. Int. Ed.* **2016**, *55*, 2181-2185.
- (16) Ventura, B. Bertocco, A.; Braga, D.; Catalano, L.; d'Agostino, S.; Grepioni, F.; Taddei, P. *J. Phys. Chem. C* **2014**, *118*, 18646-18658.
- (17) Bergamini, G.; Fermi, A.; Botta, C.; Giovanella, U.; Di Motta, S.; Negri, F.; Peresutti, R.; Gingras, M.; Ceroni, P. *J. Mater. Chem. C* **2013**, *1*, 2717-2724.

- (18) Fermi, A.; Bergamini, G.; Roy, M.; Gingras, M.; Ceroni, P. *J. Am. Chem. Soc.* **2014**, *136*, 6395-6400.
- (19) Fermi, A.; Bergamini, G.; Peresutti, R.; Marchi, E.; Roy, M.; Ceroni, P.; Gingras, M. *Dyes Pigments* **2014**, *110*, 113-122.
- (20) He, G.; Torres Delgado, W.; Schatz, D. J.; Merten, C.; Mohammadpour, A.; Mayr, L.; Ferguson, M. J.; McDonald, R.; Brown, A.; Shankar, K.; Rivard, E. *Angew. Chem. Int. Ed.* **2014**, *53*, 4675-4679.
- (21) He, G.; Wiltshire, B. D.; Choi, P.; Savin, A.; Sun, S.; Mohammadpour, A.; Ferguson, M. J.; Farsinezhad, S.; Brown, A.; Shankar, K.; Rivard, E. *Chem. Commun.* **2015**, *51*, 5444-5447.
- (22) Xu, J.; Takai, A.; Kobayashi, Y.; Takeuchi, M. *Chem. Commun.* **2013**, *49*, 8447-8449.
- (23) Donkerbroek, J. J.; Elzas, J. J.; Gooijer, C.; Frei, R. W.; Velthorst, N. H. *Talanta* **1981**, *28*, 717-723.
- (24) Koch, M.; Perumal, K.; Blacque, O.; Garg, J. A.; Saiganesh, R.; Kabilan, S.; Balasubramanian, K. K.; Venkatesan, K. *Angew. Chem. Int. Ed.* **2014**, *53*, 6378-6382.
- (25) (a) Scypinski, S.; Love, L. J. *C. Anal. Chem.* **1984**, *56*, 322-327. (b) Hamai, S. *J. Chem. Soc., Chem. Commun.* **1994**, 2243-2244. (c) de la Pena, A. M.; Salinas, F.; Gomez, M. J.; Sanchez-Pena, M.; Duran-Menas, I. *Talanta*, **1993**, *40*, 1657-1664.
- (26) Neto, B. A. D.; Lapis, A. A. M.; da Silva Júnior, E. N.; Dupont, J. *Eur. J. Org. Chem.* **2013**, 228-255.
- (27) Bouffard, J.; Swager, T. M. *Macromolecules* **2008**, *45*, 5559-5562.
- (28) Gutierrez, G. D.; Coropceanu, I.; Bawendi, M. G.; Swager, T. M. *Adv. Mater.* **2016**, *28*, 497-501.

- (29) While there have been many reports on the synthesis and use of **1-Br** and its alkylated derivatives, no reports of red phosphorescence from this type of structure have previously been presented. Additionally, there are no previous reports of **1-I** or known alkylated derivatives exhibiting phosphorescence. We note that the application of column chromatography to all molecules presented in this study removes impurities that obscure clear observations of phosphorescence.
- (30) The synthesis of a benzo[2,1,3]thiadiazole functionalized with alkyl thioethers at the 4 and 7 positions has been reported. See: Liu, X.-Y.; Usui, T.; Hanna, J. *Chem Eur. J.* **2012**, *20*, 14207-14212.
- (31) Itoh, T.; Mase, T. *Org. Lett.* **2004**, *6*, 4587-4590.
- (32) Heinrich, G.; Schoof, S.; Gusten, H. *J. Photochem.* **1974**, *3*, 315-320.
- (33) Kasha, M. *Discuss. Faraday Soc.* **1950**, *9*, 14-19.
- (34) Turro, N. J.; Ramamurthy, V.; Scaiano, J. C. *Modern Molecular Photochemistry of Organic Molecules*; University Science Books: Sausalito, CA, 2010.
- (35) El-Sayed, M. A. *J. Chem. Phys.* **1965**, *43*, 2864-2872.
- (36) The alkyl chain was additionally changed to propyl to account for the very large electron density contributions from the sulfur atoms of the thioethers within the calculated occupied molecular orbitals.
- (37) (a) El-Sayed, M. A. *J. Chem. Phys.* **1962**, *36*, 573-574. (b) El-Sayed, M. A. *J. Chem. Phys.* **1963**, *38*, 2834-2838.
- (38) Because our calculations were carried out in the gas phase, the deviation of the calculated S<sub>1</sub> state (2.60 eV;  $\lambda = 477$  nm) from experimental data ( $\lambda \sim 400$ -420 nm) for **2-Br** could largely be the result of a significant hypsochromic shift commonly exhibited by  $n \rightarrow \pi^*$  transitions

upon solvation. Although smaller, such a deviation is also observed for the S<sub>1</sub> state of **2-H** (calculated wavelength for S<sub>1</sub>: 402 nm; observed: 382 nm). See: Karelson, M.; Zerner, M. C. *J. Am. Chem. Soc.* **1990**, *112*, 9405-9406.

- (39) Brouwer, A. M. *Pure Appl. Chem.* **2011**, *83*, 2213-2228.
- (40) Hanwell, M. D.; Curtis, D. E.; Lonie, D. C.; Vandermeersch, T.; Zurek, E.; Hutchison, G. R. *J. Cheminform.* **2012**, *4*, 1-17.
- (41) Neese, F. *Wiley Interdiscip. Rev. Comput. Mol. Sci.* **2012**, *2*, 73-78.
- (42) Petrenko, T.; Krylova, O.; Neese, F.; Sokolowski, M. *New J. Phys.* **2009**, *11*, 015001.
- (43) Neese, F.; Wennmohs, F.; Hansen, A.; Becker, U. *Chem. Phys.* **2009**, *356*, 98-109.
- (44) (a) Becke, A. D. *Phys. Rev. A* **1988**, *38*, 3098-3100. (b) Perdew, J. P. *Phys. Rev. B* **1986**, *33*, 8822-8824.
- (45) (a) Schäfer, A.; Horn, H.; Ahlrichs, R. *J. Chem. Phys.* **1992**, *97*, 2571-2577; (b) Weigend, F.; Ahlrichs, R. *Phys. Chem. Chem. Phys.* **2005**, *7*, 3297-3305. The Ahlrichs (2d,2p) polarization functions were obtained from the TurboMole basis set library under <ftp.chemie.uni-karlsruhe.de/pub/basen>.
- (46) Adamo, C.; Barone, V. *J. Chem. Phys.* **1999**, *110*, 6158-6169.

## **Appendix I for Chapter 2**

### **$^1\text{H}$ and $^{13}\text{C}$ NMR Spectra**

Adapted from:

Gutierrez, G. D.; Sazama, G. T.; Wu, T.; Baldo, M. A. Swager, T. M. "Red Phosphorescence from Benzo[2,1,3]thiadiazoles at Room Temperature." *J. Org. Chem.*, *Submitted*.

Reproduced with permission from *The Journal of Organic Chemistry*, submitted for publication.  
Unpublished work copyright 2016 American Chemical Society.



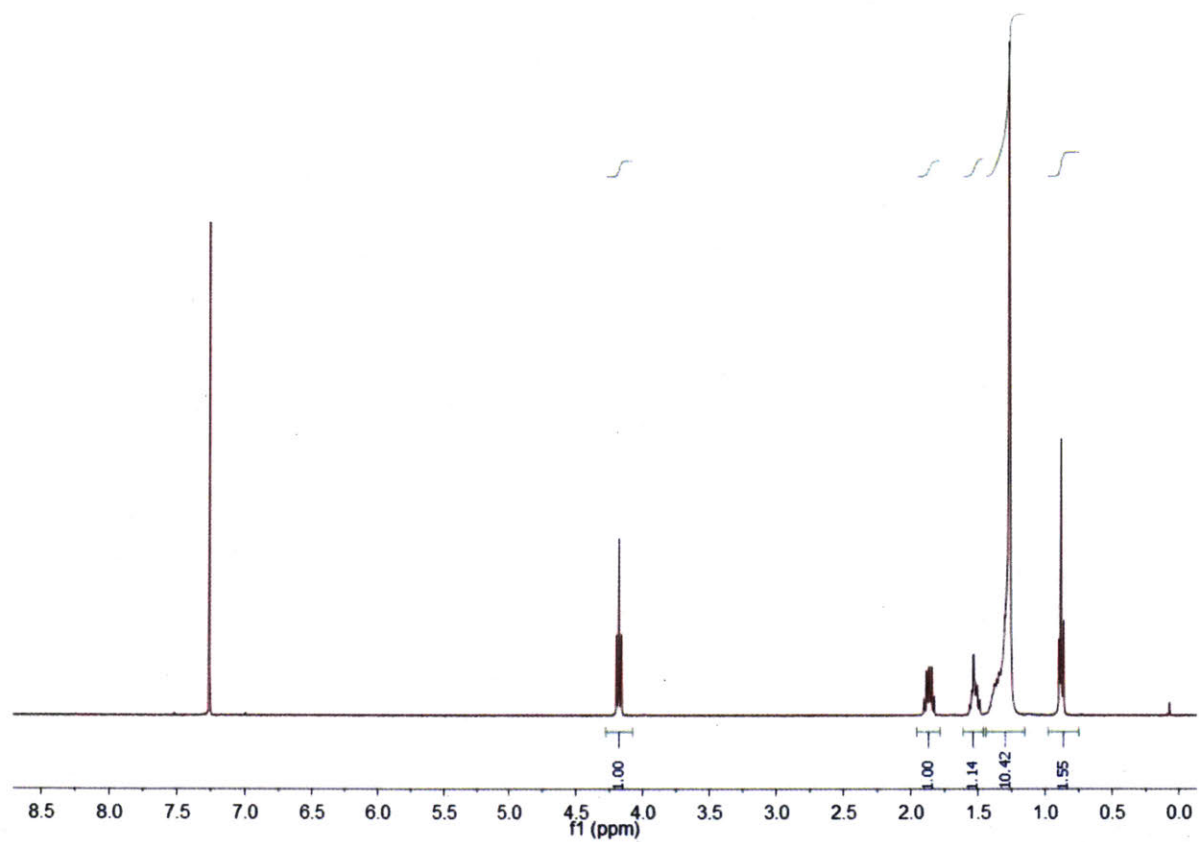


**Figure AI.2.1.**  $^1\text{H}$  NMR spectrum of 1-Cl (400 MHz,  $\text{CDCl}_3$ ).

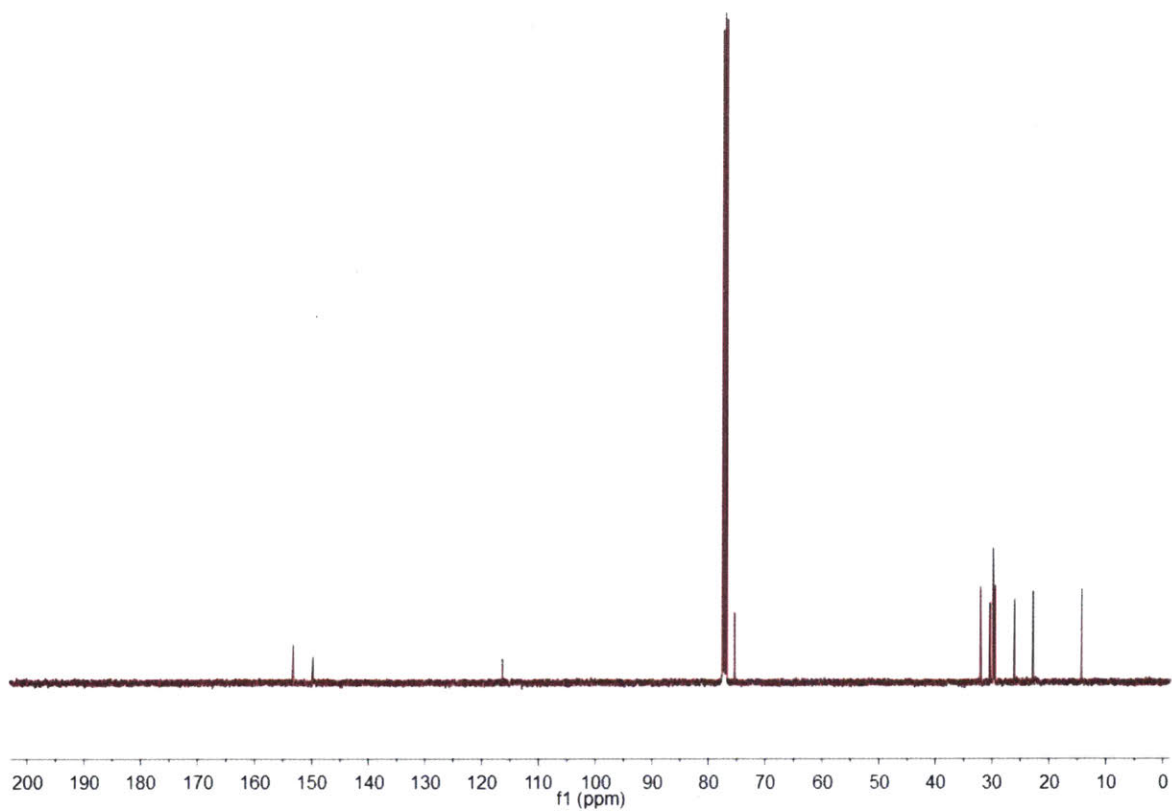


**Figure AI.2.2**  $^{13}\text{C}$  NMR spectrum of **1-Cl** (101 MHz,  $\text{CDCl}_3$ ).

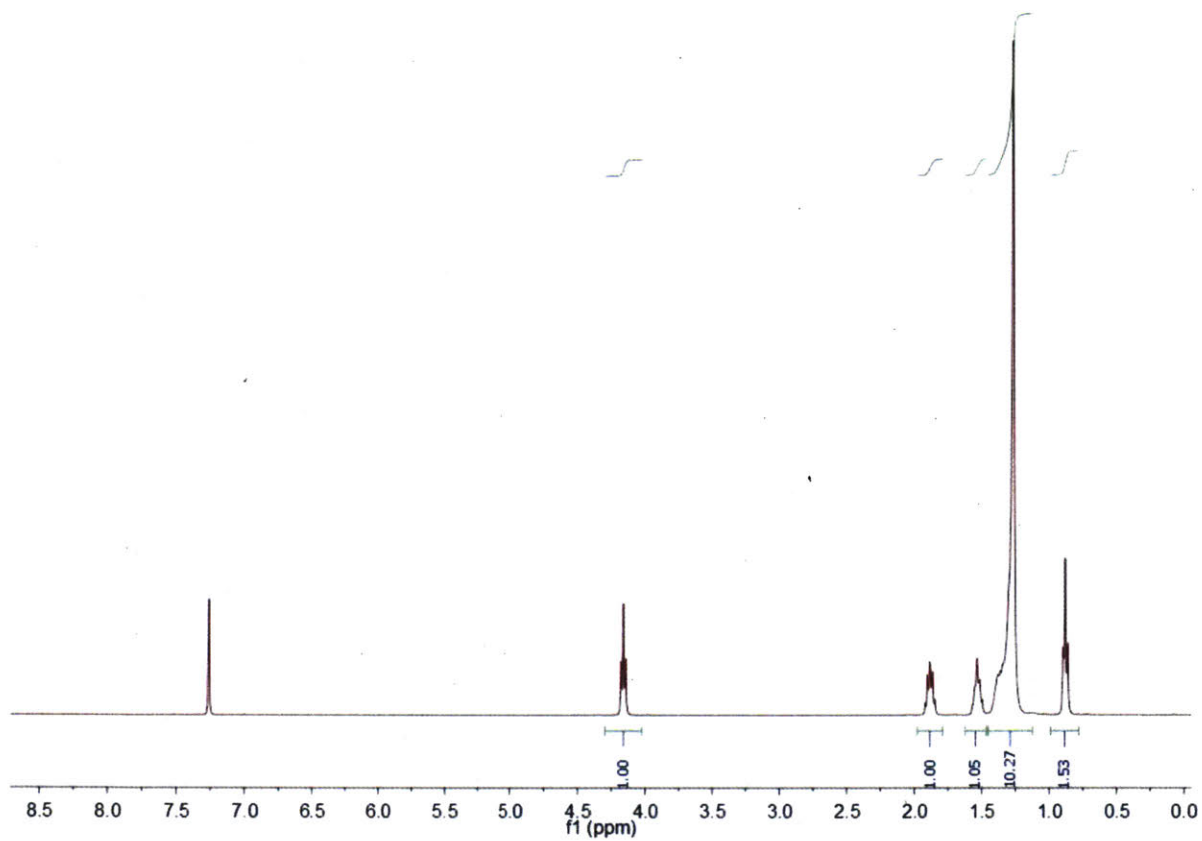


**Figure AI.2.3.**  $^1\text{H}$  NMR spectrum of **1-Br** (400 MHz,  $\text{CDCl}_3$ ).

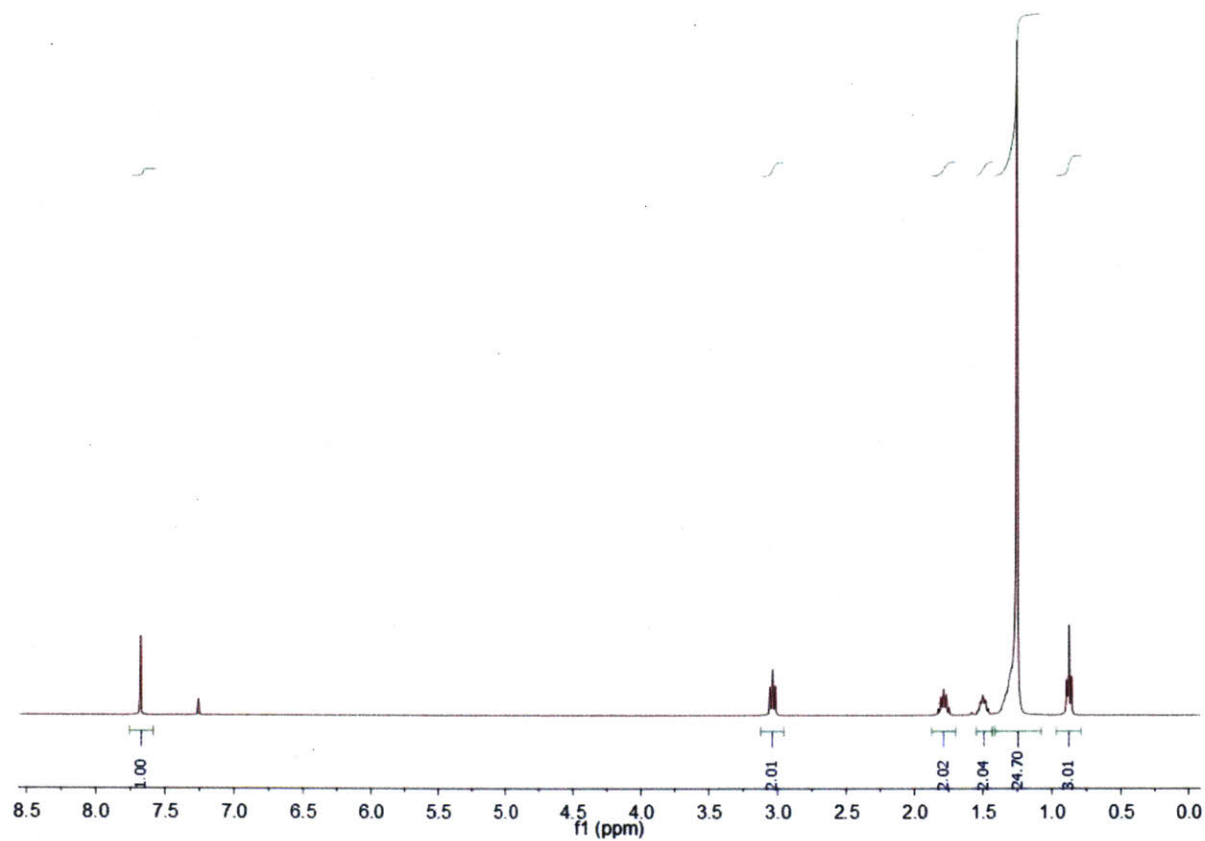


**Figure AI.2.4.** <sup>1</sup>H NMR spectrum of 2-H (400 MHz, CDCl<sub>3</sub>).

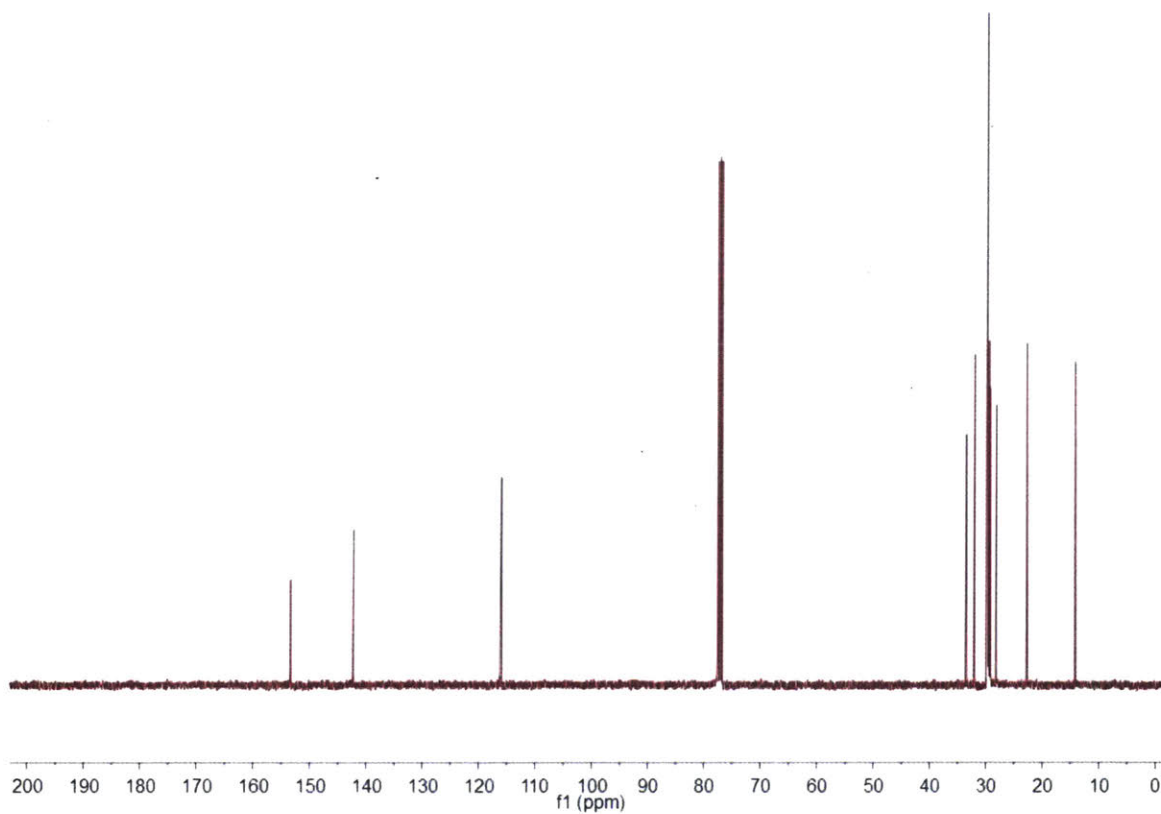


**Figure AI.2.5.**  $^{13}\text{C}$  NMR spectrum of **2-H** (101 MHz,  $\text{CDCl}_3$ ).

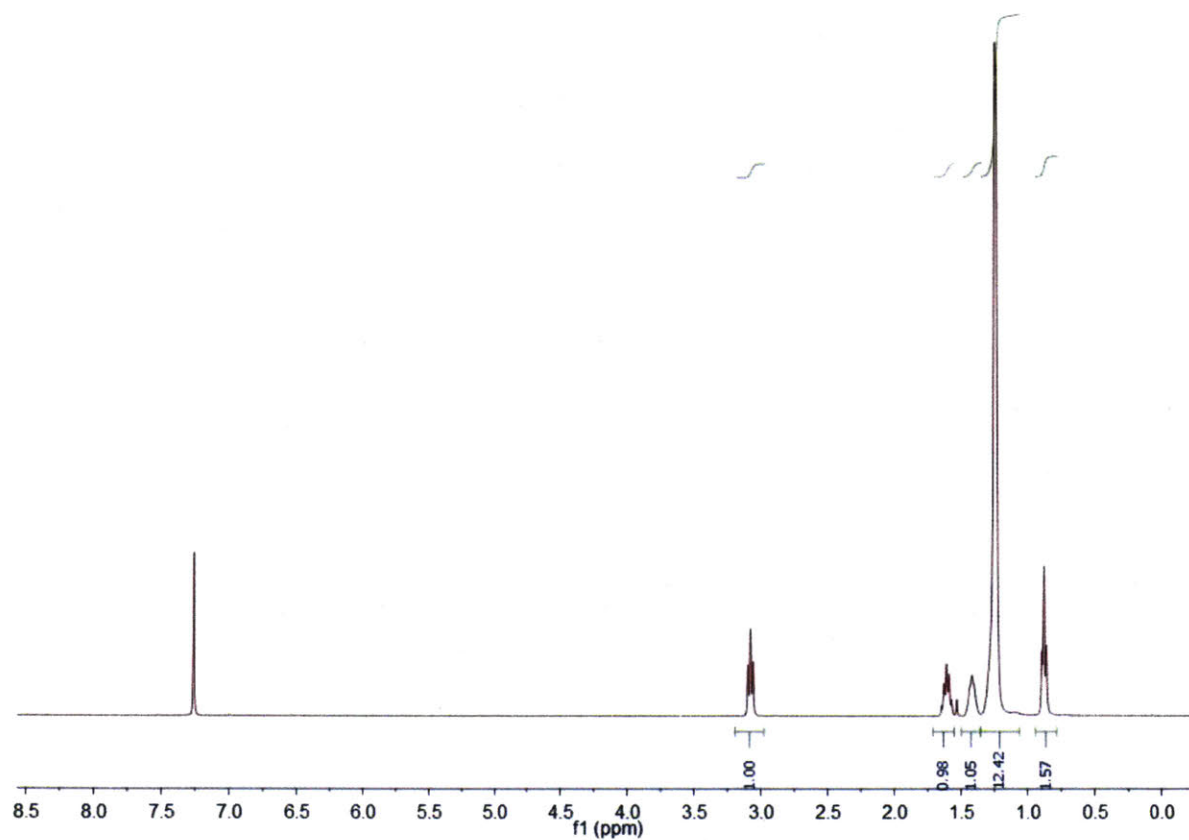


**Figure AI.2.6.**  $^1\text{H}$  NMR spectrum of 2-Br (400 MHz,  $\text{CDCl}_3$ ).

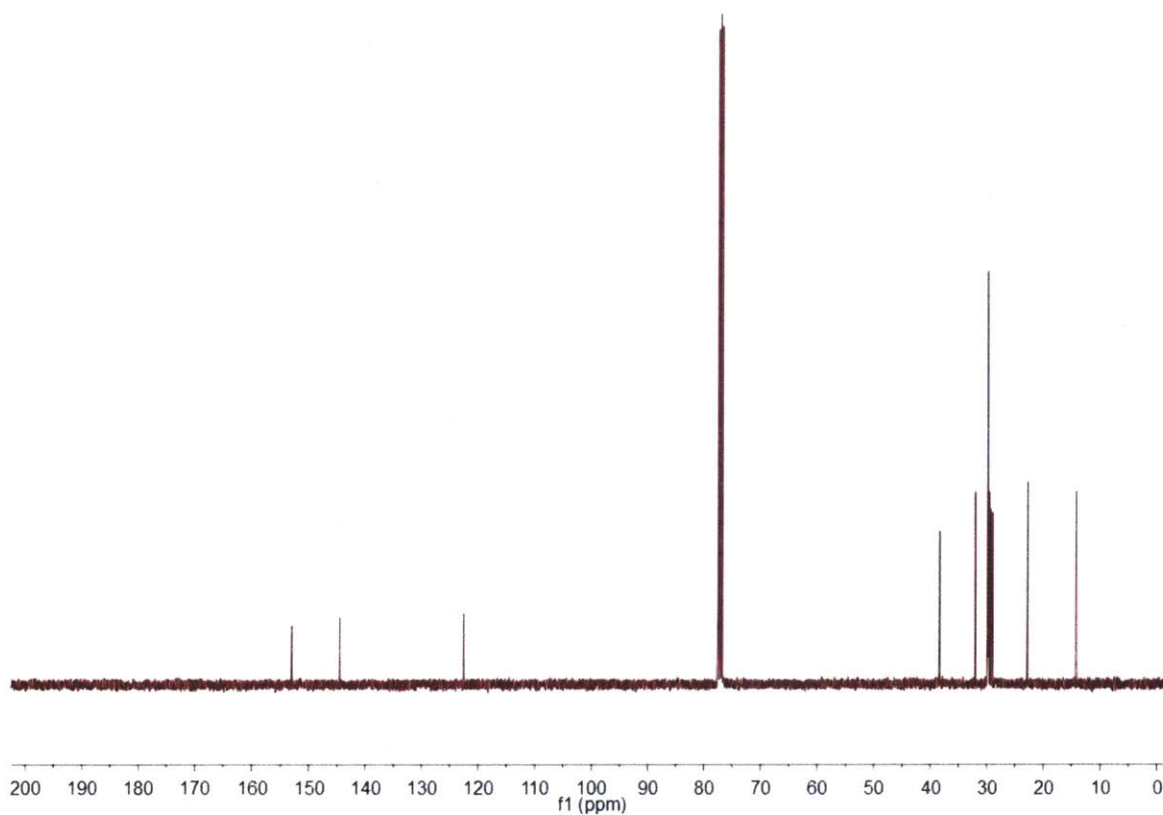


**Figure AI.2.7.**  $^{13}\text{C}$  NMR spectrum of **2-Br** (101 MHz,  $\text{CDCl}_3$ ).

## Appendix II for Chapter 2

### Computational Data

Adapted from:

Gutierrez, G. D.; Sazama, G. T.; Wu, T.; Baldo, M. A. Swager, T. M. "Red Phosphorescence from Benzo[2,1,3]thiadiazoles at Room Temperature." *J. Org. Chem.*, *Submitted*.

Reproduced with permission from *The Journal of Organic Chemistry*, submitted for publication.  
Unpublished work copyright 2016 American Chemical Society.



**1-Cl\* Optimization:**

-----  
CARTESIAN COORDINATES (ANGSTROEM)  
-----

C	1.512509	0.447541	0.731472
C	1.168399	-0.941856	0.500368
C	-0.042578	-1.290445	-0.072228
C	-0.954427	-0.262555	-0.440755
C	0.645689	1.465535	0.373479
C	-0.602064	1.133155	-0.223539
N	-2.162003	-0.435260	-1.005395
S	-2.775121	1.078252	-1.223871
O	2.740076	0.728998	1.260476
O	2.046542	-1.902301	0.915370
Cl	-0.455084	-2.958252	-0.350991
Cl	1.058814	3.133419	0.650982
N	-1.548800	1.999817	-0.622849
C	3.134772	-2.173233	-0.019376
C	2.808055	0.633151	2.715736
C	4.221110	0.985212	3.146070
H	3.708798	-1.245981	-0.179319
H	2.697322	-2.493010	-0.980538
C	4.003732	-3.267917	0.574204
C	4.376590	0.935987	4.669649
H	4.465662	1.989946	2.768605
H	4.924516	0.285126	2.668965
H	3.702502	1.650013	5.165829
H	5.403767	1.188979	4.965575

H	4.153138	-0.065893	5.065733
H	4.389183	-2.928405	1.548246
C	5.164745	-3.635114	-0.355930
H	3.376000	-4.150809	0.769795
H	5.816233	-2.769724	-0.548966
H	4.801274	-4.003446	-1.326848
H	5.785087	-4.425774	0.087600
H	2.538036	-0.391234	3.019868
H	2.076489	1.338246	3.146053

-----  
FINAL SINGLE POINT ENERGY -2044.653052379733  
-----

-----  
VIBRATIONAL FREQUENCIES  
-----

0:	0.00 cm** <sup>-1</sup>
1:	0.00 cm** <sup>-1</sup>
2:	0.00 cm** <sup>-1</sup>
3:	0.00 cm** <sup>-1</sup>
4:	0.00 cm** <sup>-1</sup>
5:	0.00 cm** <sup>-1</sup>
6:	22.14 cm** <sup>-1</sup>
7:	23.50 cm** <sup>-1</sup>
8:	34.91 cm** <sup>-1</sup>
9:	46.92 cm** <sup>-1</sup>

10: 55.78 cm<sup>\*\*</sup>-1

...

**1-CI\* TD-DFT:**

-----  
CIS/TD-DFT TOTAL ENERGY  
-----

E(SCF) = -2043.204063347 Eh

DE(CIS) = 0.128138681 Eh (Root 1)

-----  
E(tot) = -2043.075924667 Eh

-----  
FINAL SINGLE POINT ENERGY -2043.075924666806  
-----

-----  
TD-DFT/TDA EXCITED STATES (SINGLETs)  
-----

the weight of the individual excitations are printed if larger than 0.01

STATE 1: E= 0.128139 au 3.487 eV 28123.2 cm<sup>\*\*</sup>-1

75a -> 83a : 0.012201 (c= -0.11045874)

82a -> 83a : 0.935993 (c= -0.96746745)

82a -> 85a : 0.018338 (c= -0.13541960)

STATE 2: E= 0.160377 au 4.364 eV 35198.6 cm\*\*<sup>-1</sup>

81a -> 83a : 0.777782 (c= -0.88191976)

82a -> 84a : 0.173688 (c= -0.41675836)

STATE 3: E= 0.165611 au 4.507 eV 36347.4 cm\*\*<sup>-1</sup>

80a -> 83a : 0.977632 (c= 0.98875276)

80a -> 85a : 0.011038 (c= -0.10506272)

STATE 4: E= 0.167093 au 4.547 eV 36672.8 cm\*\*<sup>-1</sup>

74a -> 83a : 0.056259 (c= -0.23718977)

77a -> 83a : 0.059738 (c= 0.24441279)

78a -> 83a : 0.279305 (c= 0.52849341)

79a -> 83a : 0.583388 (c= 0.76379821)

STATE 5: E= 0.186296 au 5.069 eV 40887.3 cm\*\*<sup>-1</sup>

74a -> 83a : 0.017628 (c= 0.13277232)

77a -> 83a : 0.146136 (c= -0.38227703)

78a -> 83a : 0.421111 (c= -0.64893089)

79a -> 83a : 0.371756 (c= 0.60971795)

79a -> 85a : 0.010346 (c= -0.10171471)

82a -> 84a : 0.011699 (c= 0.10816001)

STATE 6: E= 0.193824 au 5.274 eV 42539.4 cm\*\*<sup>-1</sup>

69a -> 83a : 0.034729 (c= -0.18635759)

70a -> 83a : 0.044139 (c= -0.21009217)

72a -> 83a : 0.019947 (c= -0.14123478)

75a -> 83a : 0.021259 (c= 0.14580447)

76a -> 83a : 0.866816 (c= 0.93102964)

STATE 7: E= 0.200216 au 5.448 eV 43942.4 cm\*\*<sup>-1</sup>

74a -> 83a : 0.125591 (c= -0.35438841)

77a -> 83a : 0.562417 (c= 0.74994463)

78a -> 83a : 0.258218 (c= -0.50815159)

81a -> 85a : 0.020849 (c= -0.14439025)

STATE 8: E= 0.205255 au 5.585 eV 45048.3 cm\*\*<sup>-1</sup>

71a -> 83a : 0.013806 (c= 0.11749690)

74a -> 83a : 0.741953 (c= 0.86136671)

77a -> 83a : 0.185536 (c= 0.43073944)

79a -> 83a : 0.015900 (c= 0.12609602)

STATE 9: E= 0.208819 au 5.682 eV 45830.5 cm\*\*<sup>-1</sup>

69a -> 83a : 0.055388 (c= -0.23534616)

70a -> 83a : 0.103878 (c= -0.32230171)

72a -> 83a : 0.047847 (c= -0.21874045)

75a -> 86a : 0.011040 (c= 0.10507276)

76a -> 83a : 0.042410 (c= -0.20593697)

82a -> 86a : 0.704884 (c= -0.83957353)

82a -> 89a : 0.016630 (c= -0.12895697)

STATE 10: E= 0.209286 au 5.695 eV 45932.9 cm\*\*<sup>-1</sup>

75a -> 83a : 0.565689 (c= 0.75212306)

75a -> 85a : 0.011928 (c= -0.10921554)

76a -> 83a : 0.015140 (c= -0.12304662)

81a -> 84a : 0.051181 (c= 0.22623313)

82a -> 83a : 0.012918 (c= -0.11365923)

82a -> 85a : 0.293520 (c= 0.54177499)

-----  
TD-DFT/TDA EXCITED STATES (TRIPLETS)  
-----

the weight of the individual excitations are printed if larger than 0.01

STATE 1: E= 0.083681 au 2.277 eV 18365.8 cm\*\*<sup>-1</sup>

75a -> 83a : 0.028929 (c= 0.17008551)

82a -> 83a : 0.927455 (c= -0.96304450)

82a -> 85a : 0.011760 (c= 0.10844472)

STATE 2: E= 0.109970 au 2.992 eV 24135.6 cm\*\*<sup>-1</sup>

81a -> 83a : 0.960004 (c= -0.97979786)

STATE 3: E= 0.145695 au 3.965 eV 31976.3 cm\*\*<sup>-1</sup>

74a -> 83a : 0.127101 (c= 0.35651272)

74a -> 85a : 0.011953 (c= 0.10933122)

77a -> 83a : 0.097497 (c= -0.31224557)

78a -> 83a : 0.290148 (c= -0.53865386)

78a -> 85a : 0.015354 (c= -0.12391081)

79a -> 83a : 0.417638 (c= -0.64624919)

79a -> 85a : 0.012934 (c= -0.11372901)

STATE 4: E= 0.149624 au 4.071 eV 32838.6 cm\*\*<sup>-1</sup>

65a -> 83a : 0.039392 (c= -0.19847399)

75a -> 83a : 0.503755 (c= 0.70975712)

75a -> 85a : 0.025805 (c= 0.16063957)

76a -> 83a : 0.016798 (c= -0.12960768)

82a -> 85a : 0.372310 (c= -0.61017189)

STATE 5: E= 0.161235 au 4.387 eV 35387.0 cm\*\*<sup>-1</sup>

62a -> 83a : 0.011475 (c= 0.10711946)

68a -> 83a : 0.029983 (c= 0.17315599)

77a -> 83a : 0.172710 (c= 0.41558421)

78a -> 83a : 0.215055 (c= -0.46374016)

79a -> 83a : 0.044212 (c= 0.21026579)

81a -> 85a : 0.081272 (c= 0.28508261)

82a -> 84a : 0.418207 (c= 0.64668898)

STATE 6: E= 0.162252 au 4.415 eV 35610.2 cm\*\*<sup>-1</sup>

80a -> 83a : 0.956441 (c= -0.97797795)

80a -> 85a : 0.017098 (c= 0.13075883)

STATE 7: E= 0.177716 au 4.836 eV 39004.2 cm\*\*<sup>-1</sup>

75a -> 83a : 0.251660 (c= 0.50165680)

76a -> 83a : 0.014826 (c= -0.12176143)

81a -> 84a : 0.196380 (c= 0.44314791)

82a -> 83a : 0.054139 (c= 0.23267832)

82a -> 85a : 0.437075 (c= 0.66111621)

STATE 8: E= 0.181222 au 4.931 eV 39773.5 cm\*\*<sup>-1</sup>

78a -> 83a : 0.292813 (c= -0.54112175)

79a -> 83a : 0.275226 (c= 0.52461953)

81a -> 83a : 0.017204 (c= -0.13116415)

81a -> 85a : 0.019560 (c= 0.13985868)

82a -> 84a : 0.367393 (c= -0.60612955)

STATE 9: E= 0.183380 au 4.990 eV 40247.2 cm\*\*<sup>-1</sup>

69a -> 83a : 0.158820 (c= 0.39852259)

70a -> 83a : 0.236755 (c= 0.48657526)

70a -> 85a : 0.010845 (c= 0.10413780)

72a -> 83a : 0.098823 (c= 0.31436093)

75a -> 83a : 0.020148 (c= -0.14194336)

76a -> 83a : 0.416504 (c= -0.64537128)

STATE 10: E= 0.187350 au 5.098 eV 41118.6 cm\*\*<sup>-1</sup>

74a -> 83a : 0.015906 (c= 0.12611716)

77a -> 83a : 0.517225 (c= -0.71918333)

79a -> 83a : 0.203065 (c= 0.45062722)

79a -> 85a : 0.010745 (c= -0.10365597)

81a -> 85a : 0.052598 (c= -0.22934252)

82a -> 84a : 0.175544 (c= 0.41897961)

---

### ABSORPTION SPECTRUM VIA TRANSITION ELECTRIC DIPOLE MOMENTS

---

State	Energy (cm <sup>-1</sup> )	Wavelength (nm)	fosc (au**2)	T2 (au)	TX (au)	TY (au)	TZ (au)
1	28123.2	355.6	0.079858361	0.93483	-0.24903	-0.92715	-0.11491
2	35198.6	284.1	0.275326467	2.57512	1.40497	-0.45424	0.62837



3	36347.4	275.1	0.000906953	0.00821	0.03177	0.07834	0.03267
4	36672.8	272.7	0.001186842	0.01065	-0.09064	0.02808	-0.04063
5	40887.3	244.6	0.001437173	0.01157	-0.09450	0.02862	-0.04269
6	42539.4	235.1	0.000272117	0.00211	0.01950	0.00397	-0.04135
7	43942.4	227.6	0.010238491	0.07671	-0.24291	0.07781	-0.10792
8	45048.3	222.0	0.013538172	0.09894	-0.27602	0.08697	-0.12323
9	45830.5	218.2	0.000846712	0.00608	0.04066	-0.01004	-0.06579
10	45932.9	217.7	0.044596562	0.31963	-0.14813	-0.54427	-0.03825
11	18365.8	544.5	spin forbidden (mult=3)				
12	24135.6	414.3	spin forbidden (mult=3)				
13	31976.3	312.7	spin forbidden (mult=3)				
14	32838.6	304.5	spin forbidden (mult=3)				
15	35387.0	282.6	spin forbidden (mult=3)				
16	35610.2	280.8	spin forbidden (mult=3)				
17	39004.2	256.4	spin forbidden (mult=3)				
18	39773.5	251.4	spin forbidden (mult=3)				
19	40247.2	248.5	spin forbidden (mult=3)				
20	41118.6	243.2	spin forbidden (mult=3)				

### 1-Br\* Optimization:

-----  
 CARTESIAN COORDINATES (ANGSTROEM)  
 -----

C	1.508974	0.450981	0.724361
C	1.160674	-0.941032	0.501295
C	-0.050338	-1.288406	-0.063911
C	-0.959341	-0.263246	-0.436656
C	0.645785	1.466003	0.361995

C	-0.601990	1.135008	-0.229322
N	-2.169642	-0.434302	-0.995743
S	-2.777554	1.078789	-1.226707
O	2.739321	0.725370	1.251075
O	2.042377	-1.896172	0.921505
Br	-0.513386	-3.131505	-0.358770
Br	1.105964	3.309953	0.656325
N	-1.548544	2.000003	-0.632382
C	3.133406	-2.166479	-0.009946
C	2.810146	0.627739	2.705921
C	4.225521	0.974191	3.133123
H	3.705891	-1.238578	-0.170784
H	2.698168	-2.489790	-0.971024
C	4.002532	-3.258577	0.588123
C	4.384129	0.923552	4.656295
H	4.472595	1.978260	2.755559
H	4.925407	0.271929	2.654046
H	3.714219	1.640265	5.154226
H	5.413045	1.171857	4.950161
H	4.157059	-0.077521	5.052351
H	4.385198	-2.916737	1.562447
C	5.166166	-3.626146	-0.338509
H	3.375242	-4.141726	0.783898
H	5.816471	-2.760093	-0.532537
H	4.805380	-3.997714	-1.309179
H	5.787019	-4.414478	0.108455
H	2.536445	-0.395515	3.010158
H	2.082621	1.336295	3.137600

-----  
FINAL SINGLE POINT ENERGY -1150.527626986020  
-----

-----  
VIBRATIONAL FREQUENCIES  
-----

0: 0.00 cm\*\*<sup>-1</sup>  
1: 0.00 cm\*\*<sup>-1</sup>  
2: 0.00 cm\*\*<sup>-1</sup>  
3: 0.00 cm\*\*<sup>-1</sup>  
4: 0.00 cm\*\*<sup>-1</sup>  
5: 0.00 cm\*\*<sup>-1</sup>  
6: 22.42 cm\*\*<sup>-1</sup>  
7: 25.23 cm\*\*<sup>-1</sup>  
8: 31.37 cm\*\*<sup>-1</sup>  
9: 41.63 cm\*\*<sup>-1</sup>  
10: 55.47 cm\*\*<sup>-1</sup>

...

**1-Br\* TDDFT:**

-----  
CIS/TD-DFT TOTAL ENERGY  
-----

E(SCF) = -6270.796918070 Eh

DE(CIS) = 0.127495786 Eh (Root 1)

-----  
E(tot) = -6270.669422284 Eh

-----  
FINAL SINGLE POINT ENERGY -6270.669422284429  
-----

-----  
TD-DFT/TDA EXCITED STATES (SINGLETs)  
-----

the weight of the individual excitations are printed if larger than 0.01

STATE 1: E= 0.127496 au 3.469 eV 27982.1 cm\*\*<sup>-1</sup>

94a -> 101a : 0.012303 (c= -0.11091951)

100a -> 101a : 0.942084 (c= 0.97061005)

100a -> 105a : 0.013882 (c= -0.11782378)

STATE 2: E= 0.158215 au 4.305 eV 34724.1 cm\*\*<sup>-1</sup>

92a -> 101a : 0.090524 (c= 0.30087168)

93a -> 101a : 0.014375 (c= -0.11989438)

98a -> 101a : 0.832337 (c= 0.91232490)

99a -> 101a : 0.039084 (c= -0.19769669)

STATE 3: E= 0.160069 au 4.356 eV 35131.1 cm\*\*<sup>-1</sup>

95a -> 101a : 0.024757 (c= 0.15734321)

98a -> 101a : 0.033186 (c= -0.18217011)

99a -> 101a : 0.744915 (c= -0.86308441)

100a -> 104a : 0.145843 (c= 0.38189395)

STATE 4: E= 0.164964 au 4.489 eV 36205.4 cm<sup>\*\*</sup>-1

97a -> 101a : 0.972376 (c= -0.98609138)

97a -> 105a : 0.010967 (c= -0.10472445)

STATE 5: E= 0.173362 au 4.717 eV 38048.5 cm<sup>\*\*</sup>-1

96a -> 101a : 0.982854 (c= 0.99138984)

STATE 6: E= 0.179732 au 4.891 eV 39446.6 cm<sup>\*\*</sup>-1

92a -> 101a : 0.089728 (c= -0.29954569)

93a -> 101a : 0.070369 (c= 0.26527240)

95a -> 101a : 0.730864 (c= 0.85490606)

98a -> 101a : 0.057140 (c= 0.23903900)

100a -> 104a : 0.016597 (c= -0.12882941)

STATE 7: E= 0.182862 au 4.976 eV 40133.5 cm<sup>\*\*</sup>-1

92a -> 101a : 0.052035 (c= -0.22811101)

93a -> 101a : 0.021507 (c= 0.14665429)

95a -> 101a : 0.029651 (c= -0.17219570)

95a -> 103a : 0.013159 (c= 0.11471131)

99a -> 103a : 0.013022 (c= -0.11411440)

100a -> 102a : 0.842880 (c= 0.91808499)

STATE 8: E= 0.184096 au 5.010 eV 40404.5 cm<sup>\*\*</sup>-1

92a -> 101a : 0.415876 (c= 0.64488446)

93a -> 101a : 0.214340 (c= -0.46296841)

95a -> 101a : 0.176250 (c= 0.41982083)

98a -> 101a : 0.054775 (c= -0.23404092)

100a -> 102a : 0.105523 (c= 0.32484298)

STATE 9: E= 0.189188 au 5.148 eV 41522.0 cm<sup>\*\*</sup>-1

95a -> 102a : 0.023917 (c= 0.15465196)

99a -> 102a : 0.032216 (c= -0.17948894)

100a -> 103a : 0.911870 (c= 0.95491871)

100a -> 106a : 0.014436 (c= 0.12015092)

STATE 10: E= 0.192731 au 5.244 eV 42299.5 cm<sup>\*\*</sup>-1

92a -> 101a : 0.318438 (c= 0.56430348)

93a -> 101a : 0.635487 (c= 0.79717454)

-----  
TD-DFT/TDA EXCITED STATES (TRIPLETS)  
-----

the weight of the individual excitations are printed if larger than 0.01

STATE 1: E= 0.085352 au 2.323 eV 18732.6 cm<sup>\*\*</sup>-1

94a -> 101a : 0.046722 (c= -0.21615356)

100a -> 101a : 0.910223 (c= -0.95405593)

100a -> 105a : 0.010190 (c= -0.10094373)

STATE 2: E= 0.109460 au 2.979 eV 24023.6 cm<sup>\*\*</sup>-1

95a -> 101a : 0.018672 (c= 0.13664617)

99a -> 101a : 0.954145 (c= 0.97680370)

STATE 3: E= 0.142302 au 3.872 eV 31231.7 cm\*\*<sup>-1</sup>

92a -> 101a : 0.345359 (c= 0.58767237)

92a -> 105a : 0.028942 (c= -0.17012371)

93a -> 101a : 0.051858 (c= -0.22772433)

95a -> 101a : 0.011443 (c= -0.10697209)

98a -> 101a : 0.534851 (c= 0.73133537)

STATE 4: E= 0.148399 au 4.038 eV 32569.9 cm\*\*<sup>-1</sup>

86a -> 101a : 0.119972 (c= -0.34636975)

94a -> 101a : 0.508572 (c= -0.71314269)

94a -> 105a : 0.033932 (c= 0.18420776)

97a -> 101a : 0.016557 (c= -0.12867384)

100a -> 101a : 0.017150 (c= 0.13095870)

100a -> 105a : 0.272084 (c= 0.52161699)

STATE 5: E= 0.158127 au 4.303 eV 34704.8 cm\*\*<sup>-1</sup>

85a -> 101a : 0.052013 (c= 0.22806311)

95a -> 101a : 0.594738 (c= 0.77119291)

98a -> 101a : 0.015794 (c= 0.12567519)

99a -> 105a : 0.072625 (c= -0.26949038)

100a -> 102a : 0.011167 (c= -0.10567444)

100a -> 104a : 0.209893 (c= -0.45814075)

STATE 6: E= 0.161513 au 4.395 eV 35448.1 cm\*\*<sup>-1</sup>

97a -> 101a : 0.935608 (c= 0.96726815)

97a -> 105a : 0.017513 (c= 0.13233806)

100a -> 105a : 0.011061 (c= 0.10517276)

STATE 7: E= 0.166947 au 4.543 eV 36640.7 cm\*\*<sup>-1</sup>

95a -> 103a : 0.046569 (c= 0.21579893)

99a -> 103a : 0.020191 (c= -0.14209563)

100a -> 102a : 0.892062 (c= 0.94449024)

STATE 8: E= 0.171906 au 4.678 eV 37729.0 cm\*\*<sup>-1</sup>

91a -> 101a : 0.026540 (c= 0.16291204)

96a -> 101a : 0.912614 (c= -0.95530807)

100a -> 103a : 0.019935 (c= 0.14119068)

STATE 9: E= 0.172057 au 4.682 eV 37762.1 cm\*\*<sup>-1</sup>

95a -> 102a : 0.071170 (c= -0.26677663)

96a -> 101a : 0.021882 (c= -0.14792608)

99a -> 102a : 0.041406 (c= 0.20348370)

100a -> 103a : 0.785329 (c= -0.88618818)

100a -> 106a : 0.047293 (c= -0.21746881)

STATE 10: E= 0.174534 au 4.749 eV 38305.7 cm\*\*<sup>-1</sup>

86a -> 105a : 0.014633 (c= -0.12096803)

92a -> 101a : 0.031490 (c= 0.17745559)

94a -> 101a : 0.229336 (c= 0.47889012)

98a -> 101a : 0.038261 (c= -0.19560526)

99a -> 104a : 0.117031 (c= 0.34209786)

100a -> 101a : 0.053525 (c= -0.23135569)

100a -> 104a : 0.010440 (c= -0.10217806)

100a -> 105a : 0.456125 (c= 0.67537031)



-----  
 ABSORPTION SPECTRUM VIA TRANSITION ELECTRIC DIPOLE MOMENTS  
 -----

State	Energy (cm-1)	Wavelength (nm)	fosc (au**2)	T2 (au)	TX (au)	TY (au)	TZ	
1	27982.1	357.4	0.097105114	1.14245	-0.27561	-1.02495	-0.12635	
2	34724.1	288.0	0.011972636	0.11351	0.29513	-0.09531	0.13163	
3	35131.1	284.6	0.259554446	2.43228	1.36544	-0.44150	0.61067	
4	36205.4	276.2	0.001111547	0.01011	0.03130	0.08824	0.03661	
5	38048.5	262.8	0.000051071	0.00044	0.00412	-0.01073	-0.01760	
6	39446.6	253.5	0.019320487	0.16124	-0.35197	0.11167	-0.15777	
7	40133.5	249.2	0.000008873	0.00007	0.00770	-0.00163	0.00330	
8	40404.5	247.5	0.005873501	0.04786	-0.19165	0.06244	-0.08502	
9	41522.0	240.8	0.000062839	0.00050	0.00351	-0.00624	-0.02114	
10	42299.5	236.4	0.001775019	0.01381	0.10273	-0.03497	0.04516	
11	18732.6	533.8	spin forbidden (mult=3)					
12	24023.6	416.3	spin forbidden (mult=3)					
13	31231.7	320.2	spin forbidden (mult=3)					
14	32569.9	307.0	spin forbidden (mult=3)					
15	34704.8	288.1	spin forbidden (mult=3)					
16	35448.1	282.1	spin forbidden (mult=3)					
17	36640.7	272.9	spin forbidden (mult=3)					
18	37729.0	265.0	spin forbidden (mult=3)					
19	37762.1	264.8	spin forbidden (mult=3)					
20	38305.7	261.1	spin forbidden (mult=3)					

**1-I\* Optimization:**

-----  
CARTESIAN COORDINATES (ANGSTROEM)  
-----

C	1.498501	0.455869	0.706603
C	1.140174	-0.937762	0.503622
C	-0.079335	-1.291639	-0.041046
C	-0.979654	-0.260210	-0.424335
C	0.648120	1.476717	0.327513
C	-0.606323	1.139532	-0.250436
N	-2.196200	-0.429603	-0.969060
S	-2.792132	1.083748	-1.229186
O	2.731627	0.726494	1.232557
O	2.024068	-1.891961	0.925732
I	-0.604190	-3.304518	-0.318935
I	1.171961	3.489836	0.606423
N	-1.546703	2.003811	-0.667631
C	3.134596	-2.140357	0.010508
C	2.811333	0.602720	2.685456
C	4.229532	0.940637	3.110146
H	3.698570	-1.204699	-0.132145
H	2.718862	-2.459910	-0.960618
C	4.005526	-3.228649	0.612912
C	4.396047	0.866049	4.631549
H	4.476105	1.950058	2.746728
H	4.925917	0.244932	2.616498
H	3.729634	1.575727	5.144054
H	5.426819	1.108537	4.923813

H	4.169695	-0.140801	5.013141
H	4.370925	-2.890818	1.595290
C	5.185747	-3.578096	-0.299729
H	3.383945	-4.119135	0.793150
H	5.830501	-2.704559	-0.478232
H	4.842272	-3.945811	-1.278120
H	5.807650	-4.363882	0.150287
H	2.538081	-0.425040	2.973531
H	2.087290	1.304952	3.133430

-----  
FINAL SINGLE POINT ENERGY -1146.973728010622  
-----

-----  
VIBRATIONAL FREQUENCIES  
-----

0:	0.00 cm <sup>**</sup> -1
1:	0.00 cm <sup>**</sup> -1
2:	0.00 cm <sup>**</sup> -1
3:	0.00 cm <sup>**</sup> -1
4:	0.00 cm <sup>**</sup> -1
5:	0.00 cm <sup>**</sup> -1
6:	23.54 cm <sup>**</sup> -1
7:	26.27 cm <sup>**</sup> -1
8:	30.03 cm <sup>**</sup> -1
9:	36.26 cm <sup>**</sup> -1
10:	57.72 cm <sup>**</sup> -1

...

**1-I\* TDDFT:**

-----  
CIS/TD-DFT TOTAL ENERGY  
-----

E(SCF) = -14963.407403854 Eh

DE(CIS) = 0.120741456 Eh (Root 1)

-----  
E(tot) = -14963.286662398 Eh

-----  
FINAL SINGLE POINT ENERGY -14963.286662397926  
-----

-----  
TD-DFT/TDA EXCITED STATES (SINGLETs)  
-----

the weight of the individual excitations are printed if larger than 0.01

STATE 1: E= 0.120741 au 3.286 eV 26499.7 cm\*\*<sup>-1</sup>

112a -> 119a : 0.011045 (c= 0.10509325)

118a -> 119a : 0.953167 (c= -0.97630290)

118a -> 122a : 0.010535 (c= 0.10263787)

STATE 2: E= 0.139344 au 3.792 eV 30582.5 cm\*\*<sup>-1</sup>

110a -> 119a : 0.021320 (c= -0.14601337)

116a -> 119a : 0.943203 (c= 0.97118616)

117a -> 119a : 0.028248 (c= -0.16807170)

STATE 3: E= 0.147843 au 4.023 eV 32447.8 cm\*\*<sup>-1</sup>

115a -> 119a : 0.993771 (c= 0.99688085)

STATE 4: E= 0.154314 au 4.199 eV 33867.9 cm\*\*<sup>-1</sup>

114a -> 119a : 0.346841 (c= 0.58893197)

116a -> 119a : 0.012506 (c= -0.11183036)

117a -> 119a : 0.564410 (c= -0.75127199)

118a -> 123a : 0.046975 (c= -0.21673693)

STATE 5: E= 0.163088 au 4.438 eV 35793.7 cm\*\*<sup>-1</sup>

114a -> 119a : 0.591064 (c= -0.76880705)

116a -> 119a : 0.010682 (c= -0.10335294)

117a -> 119a : 0.206862 (c= -0.45482037)

118a -> 120a : 0.039817 (c= 0.19954260)

118a -> 123a : 0.104191 (c= -0.32278562)

STATE 6: E= 0.165098 au 4.493 eV 36234.9 cm\*\*<sup>-1</sup>

113a -> 119a : 0.963017 (c= 0.98133450)

113a -> 122a : 0.010998 (c= 0.10487157)

STATE 7: E= 0.166586 au 4.533 eV 36561.4 cm\*\*<sup>-1</sup>

114a -> 119a : 0.015870 (c= -0.12597643)

114a -> 121a : 0.020028 (c= 0.14152195)  
117a -> 119a : 0.013735 (c= -0.11719458)  
117a -> 121a : 0.023971 (c= -0.15482458)  
118a -> 120a : 0.899809 (c= -0.94858266)  
118a -> 123a : 0.012315 (c= -0.11097350)

STATE 8: E= 0.168755 au 4.592 eV 37037.5 cm\*\*<sup>-1</sup>

114a -> 120a : 0.024342 (c= 0.15601793)  
117a -> 120a : 0.033310 (c= -0.18250942)  
118a -> 121a : 0.930076 (c= -0.96440430)

STATE 9: E= 0.178664 au 4.862 eV 39212.2 cm\*\*<sup>-1</sup>

110a -> 119a : 0.846977 (c= -0.92031336)  
110a -> 122a : 0.011642 (c= 0.10789696)  
111a -> 119a : 0.096846 (c= -0.31120161)  
116a -> 119a : 0.021369 (c= -0.14618178)  
116a -> 122a : 0.011336 (c= -0.10646831)

STATE 10: E= 0.184166 au 5.011 eV 40419.8 cm\*\*<sup>-1</sup>

104a -> 119a : 0.010650 (c= -0.10319693)  
112a -> 119a : 0.894529 (c= 0.94579521)  
114a -> 123a : 0.011729 (c= -0.10830053)  
116a -> 120a : 0.012263 (c= 0.11073762)

-----  
TD-DFT/TDA EXCITED STATES (TRIPLETS)  
-----

the weight of the individual excitations are printed if larger than 0.01

STATE 1: E= 0.084067 au 2.288 eV 18450.6 cm<sup>-1</sup>

112a -> 119a : 0.074291 (c= 0.27256347)

118a -> 119a : 0.882521 (c= 0.93942605)

118a -> 122a : 0.010268 (c= 0.10132898)

STATE 2: E= 0.108655 au 2.957 eV 23847.0 cm<sup>-1</sup>

114a -> 119a : 0.090070 (c= -0.30011710)

116a -> 119a : 0.026231 (c= -0.16196078)

117a -> 119a : 0.854673 (c= -0.92448538)

STATE 3: E= 0.132229 au 3.598 eV 29021.0 cm<sup>-1</sup>

110a -> 119a : 0.165494 (c= -0.40680922)

110a -> 122a : 0.017223 (c= 0.13123538)

116a -> 119a : 0.776979 (c= 0.88146393)

117a -> 119a : 0.022050 (c= -0.14849140)

STATE 4: E= 0.142705 au 3.883 eV 31320.1 cm<sup>-1</sup>

104a -> 119a : 0.115067 (c= 0.33921597)

105a -> 119a : 0.014953 (c= -0.12228136)

112a -> 119a : 0.571222 (c= 0.75579256)

112a -> 122a : 0.032859 (c= -0.18126925)

113a -> 119a : 0.023049 (c= -0.15182046)

115a -> 119a : 0.045226 (c= -0.21266461)

118a -> 119a : 0.049926 (c= -0.22344041)

118a -> 122a : 0.120390 (c= -0.34697325)

STATE 5: E= 0.145383 au 3.956 eV 31907.8 cm\*\*<sup>-1</sup>

103a -> 119a : 0.022135 (c= 0.14877863)

114a -> 119a : 0.776223 (c= 0.88103492)

117a -> 119a : 0.076858 (c= -0.27723332)

117a -> 122a : 0.032639 (c= -0.18066301)

118a -> 120a : 0.020613 (c= -0.14357203)

118a -> 123a : 0.049082 (c= 0.22154555)

STATE 6: E= 0.147090 au 4.003 eV 32282.6 cm\*\*<sup>-1</sup>

112a -> 119a : 0.028882 (c= -0.16994766)

115a -> 119a : 0.945832 (c= -0.97253907)

STATE 7: E= 0.148941 au 4.053 eV 32688.8 cm\*\*<sup>-1</sup>

114a -> 119a : 0.017691 (c= 0.13300588)

114a -> 121a : 0.090086 (c= -0.30014266)

117a -> 121a : 0.047876 (c= 0.21880502)

118a -> 120a : 0.824404 (c= 0.90796674)

STATE 8: E= 0.149992 au 4.081 eV 32919.3 cm\*\*<sup>-1</sup>

112a -> 121a : 0.010508 (c= -0.10250951)

114a -> 120a : 0.099601 (c= -0.31559614)

117a -> 120a : 0.058726 (c= 0.24233412)

118a -> 121a : 0.819396 (c= 0.90520469)

STATE 9: E= 0.161408 au 4.392 eV 35425.1 cm\*\*<sup>-1</sup>

110a -> 119a : 0.198941 (c= 0.44602838)

111a -> 119a : 0.012363 (c= 0.11118772)

113a -> 119a : 0.655511 (c= 0.80963638)



113a -> 122a : 0.013046 (c= 0.11421917)

116a -> 119a : 0.053625 (c= 0.23156986)

118a -> 122a : 0.018049 (c= -0.13434785)

STATE 10: E= 0.161470 au 4.394 eV 35438.5 cm\*\*<sup>-1</sup>

110a -> 119a : 0.492931 (c= -0.70209041)

110a -> 122a : 0.021884 (c= 0.14793186)

111a -> 119a : 0.030496 (c= -0.17463223)

113a -> 119a : 0.265053 (c= 0.51483326)

116a -> 119a : 0.132999 (c= -0.36469061)

116a -> 122a : 0.016024 (c= -0.12658548)

---

### ABSORPTION SPECTRUM VIA TRANSITION ELECTRIC DIPOLE MOMENTS

---

State	Energy (cm <sup>-1</sup> )	Wavelength (nm)	fosc (au**2)	T2 (au)	TX (au)	TY (au)	TZ (au)
1	26499.7	377.4	0.117469629	1.45935	-0.31934	-1.15802	-0.12787
2	30582.5	327.0	0.000049470	0.00053	0.01932	-0.00933	0.00850
3	32447.8	308.2	0.000046100	0.00047	-0.00107	-0.02053	0.00673
4	33867.9	295.3	0.087813170	0.85359	0.80894	-0.26266	0.36084
5	35793.7	279.4	0.190884879	1.75566	1.16002	-0.37904	0.51609
6	36234.9	276.0	0.001913733	0.01739	-0.07501	-0.08713	-0.06456
7	36561.4	273.5	0.012753240	0.11483	0.29781	-0.09397	0.13158
8	37037.5	270.0	0.001250550	0.01112	0.03896	0.01540	-0.09675

9	39212.2	255.0	0.000125431	0.00105	-0.02857	0.00918	-0.01236
10	40419.8	247.4	0.000414431	0.00338	0.02504	0.04127	-0.03233
11	18450.6	542.0	spin forbidden (mult=3)				
12	23847.0	419.3	spin forbidden (mult=3)				
13	29021.0	344.6	spin forbidden (mult=3)				
14	31320.1	319.3	spin forbidden (mult=3)				
15	31907.8	313.4	spin forbidden (mult=3)				
16	32282.6	309.8	spin forbidden (mult=3)				
17	32688.8	305.9	spin forbidden (mult=3)				
18	32919.3	303.8	spin forbidden (mult=3)				
19	35425.1	282.3	spin forbidden (mult=3)				
20	35438.5	282.2	spin forbidden (mult=3)				

## 2-H\* Optimization:

-----  
 CARTESIAN COORDINATES (ANGSTROEM)  
 -----

C	1.422054	0.486279	0.529444
C	0.961960	-0.889961	0.572972
C	-0.311033	-1.221242	0.149155
C	-1.163499	-0.206345	-0.359365
C	0.614532	1.483471	0.016135
C	-0.687637	1.158186	-0.446237
N	-2.422287	-0.379011	-0.814088
S	-2.922629	1.115016	-1.302637
S	3.069914	0.965595	1.056476
S	1.968480	-2.218993	1.239081
H	-0.654053	-2.254646	0.183221

H	0.962275	2.515338	-0.015903
N	-1.586617	2.021403	-0.963782
C	3.238829	-2.438562	-0.092738
C	2.939456	0.818845	2.899593
C	4.293993	1.146184	3.526705
H	2.629656	-0.208070	3.135604
H	2.166017	1.522637	3.238429
H	3.744279	-1.474595	-0.239685
H	2.711825	-2.720921	-1.015187
C	4.228388	-3.523760	0.329486
C	4.240289	1.081702	5.057809
H	4.616011	2.150584	3.207528
H	5.049728	0.439185	3.149207
H	3.512702	1.800652	5.463098
H	5.221142	1.316912	5.494889
H	3.949950	0.079132	5.405317
H	4.721760	-3.221630	1.266923
C	5.282918	-3.781191	-0.753591
H	3.683291	-4.456321	0.547542
H	5.862305	-2.871638	-0.970866
H	4.817731	-4.114745	-1.693202
H	5.989589	-4.560878	-0.435592

-----  
FINAL SINGLE POINT ENERGY -1771.343656227082  
-----

-----  
VIBRATIONAL FREQUENCIES  
-----

0: 0.00 cm\*\*<sup>-1</sup>  
1: 0.00 cm\*\*<sup>-1</sup>  
2: 0.00 cm\*\*<sup>-1</sup>  
3: 0.00 cm\*\*<sup>-1</sup>  
4: 0.00 cm\*\*<sup>-1</sup>  
5: 0.00 cm\*\*<sup>-1</sup>  
6: 22.56 cm\*\*<sup>-1</sup>  
7: 27.56 cm\*\*<sup>-1</sup>  
8: 43.57 cm\*\*<sup>-1</sup>  
9: 45.21 cm\*\*<sup>-1</sup>  
10: 60.98 cm\*\*<sup>-1</sup>

...

**2-H\* TDDFT:**

-----

CIS/TD-DFT TOTAL ENERGY

-----

E(SCF) = -1770.077857018 Eh

DE(CIS) = 0.113372077 Eh (Root 1)

-----

E(tot) = -1769.964484940 Eh

-----

FINAL SINGLE POINT ENERGY -1769.964484940416

-----

-----

TD-DFT/TDA EXCITED STATES (SINGLETs)

-----

the weight of the individual excitations are printed if larger than 0.01

STATE 1: E= 0.113372 au 3.085 eV 24882.3 cm<sup>-1</sup>

71a -> 75a : 0.024071 (c= -0.15514992)

74a -> 75a : 0.955436 (c= -0.97746399)

STATE 2: E= 0.118614 au 3.228 eV 26032.7 cm<sup>-1</sup>

72a -> 75a : 0.058870 (c= 0.24263072)

73a -> 75a : 0.921818 (c= 0.96011339)

STATE 3: E= 0.146668 au 3.991 eV 32189.9 cm<sup>-1</sup>

71a -> 76a : 0.010993 (c= 0.10484838)

72a -> 75a : 0.870160 (c= 0.93282392)

73a -> 75a : 0.050986 (c= -0.22580131)

73a -> 77a : 0.010517 (c= -0.10255399)

STATE 4: E= 0.161514 au 4.395 eV 35448.2 cm<sup>-1</sup>

71a -> 75a : 0.725781 (c= -0.85192808)

72a -> 76a : 0.060282 (c= 0.24552472)

73a -> 76a : 0.155728 (c= -0.39462367)

74a -> 75a : 0.011252 (c= 0.10607648)

STATE 5: E= 0.169074 au 4.601 eV 37107.5 cm<sup>\*\*</sup>-1

74a -> 76a : 0.958386 (c= -0.97897203)

STATE 6: E= 0.170418 au 4.637 eV 37402.5 cm<sup>\*\*</sup>-1

69a -> 75a : 0.104646 (c= 0.32349106)

70a -> 75a : 0.873424 (c= 0.93457134)

70a -> 77a : 0.010876 (c= 0.10428881)

STATE 7: E= 0.178037 au 4.845 eV 39074.6 cm<sup>\*\*</sup>-1

71a -> 75a : 0.070263 (c= 0.26507106)

72a -> 76a : 0.174110 (c= -0.41726433)

73a -> 76a : 0.706953 (c= -0.84080502)

74a -> 80a : 0.013110 (c= 0.11449746)

STATE 8: E= 0.189128 au 5.146 eV 41508.9 cm<sup>\*\*</sup>-1

60a -> 75a : 0.011852 (c= 0.10886634)

63a -> 75a : 0.025270 (c= 0.15896433)

64a -> 75a : 0.010765 (c= -0.10375432)

67a -> 75a : 0.308144 (c= 0.55510702)

68a -> 75a : 0.620077 (c= 0.78744981)

STATE 9: E= 0.197321 au 5.369 eV 43306.9 cm<sup>\*\*</sup>-1

69a -> 75a : 0.073591 (c= -0.27127619)

72a -> 76a : 0.011817 (c= -0.10870782)

73a -> 76a : 0.016024 (c= 0.12658551)

74a -> 77a : 0.868377 (c= 0.93186732)

STATE 10: E= 0.204206 au 5.557 eV 44818.0 cm<sup>\*\*</sup>-1

66a -> 75a : 0.036519 (c= -0.19110011)  
69a -> 75a : 0.697779 (c= -0.83533149)  
70a -> 75a : 0.087935 (c= 0.29653848)  
72a -> 76a : 0.035346 (c= -0.18800462)  
74a -> 77a : 0.091888 (c= -0.30312975)

-----  
TD-DFT/TDA EXCITED STATES (TRIPLETS)  
-----

the weight of the individual excitations are printed if larger than 0.01

STATE 1: E= 0.088242 au 2.401 eV 19366.9 cm\*\*<sup>-1</sup>

67a -> 75a : 0.011210 (c= 0.10587866)  
72a -> 75a : 0.487265 (c= -0.69804399)  
73a -> 75a : 0.444440 (c= 0.66666319)

STATE 2: E= 0.099955 au 2.720 eV 21937.7 cm\*\*<sup>-1</sup>

71a -> 75a : 0.164144 (c= 0.40514691)  
74a -> 75a : 0.808076 (c= -0.89893034)

STATE 3: E= 0.119684 au 3.257 eV 26267.6 cm\*\*<sup>-1</sup>

72a -> 75a : 0.443971 (c= 0.66631154)  
73a -> 75a : 0.519264 (c= 0.72060006)

STATE 4: E= 0.123745 au 3.367 eV 27158.9 cm\*\*<sup>-1</sup>

69a -> 75a : 0.023659 (c= -0.15381542)  
71a -> 75a : 0.774353 (c= 0.87997304)

74a -> 75a : 0.166319 (c= 0.40782183)

STATE 5: E= 0.146909 au 3.998 eV 32242.8 cm\*\*<sup>-1</sup>

69a -> 75a : 0.101081 (c= -0.31793298)

70a -> 75a : 0.828283 (c= -0.91010034)

70a -> 77a : 0.042969 (c= -0.20728864)

STATE 6: E= 0.154378 au 4.201 eV 33882.0 cm\*\*<sup>-1</sup>

62a -> 75a : 0.039035 (c= 0.19757296)

63a -> 75a : 0.124617 (c= -0.35301182)

64a -> 75a : 0.090488 (c= 0.30081187)

67a -> 75a : 0.153279 (c= 0.39150925)

68a -> 75a : 0.043827 (c= -0.20934947)

72a -> 77a : 0.270185 (c= -0.51979348)

73a -> 77a : 0.158960 (c= 0.39869743)

74a -> 76a : 0.068077 (c= -0.26091665)

STATE 7: E= 0.159068 au 4.328 eV 34911.3 cm\*\*<sup>-1</sup>

59a -> 75a : 0.030109 (c= 0.17352070)

66a -> 75a : 0.012990 (c= -0.11397581)

69a -> 75a : 0.060800 (c= 0.24657613)

71a -> 77a : 0.016785 (c= -0.12955810)

72a -> 76a : 0.219925 (c= 0.46896147)

73a -> 76a : 0.562827 (c= -0.75021786)

74a -> 75a : 0.011730 (c= 0.10830463)

74a -> 77a : 0.016366 (c= 0.12792850)

STATE 8: E= 0.159461 au 4.339 eV 34997.7 cm\*\*<sup>-1</sup>



63a -> 75a : 0.015396 (c= -0.12407969)  
64a -> 75a : 0.010319 (c= 0.10158370)  
67a -> 75a : 0.025244 (c= 0.15888307)  
71a -> 76a : 0.010276 (c= -0.10136893)  
72a -> 77a : 0.020229 (c= -0.14222918)  
73a -> 75a : 0.014808 (c= -0.12168985)  
73a -> 80a : 0.020458 (c= -0.14303002)  
74a -> 76a : 0.821375 (c= 0.90629734)

STATE 9: E= 0.172132 au 4.684 eV 37778.6 cm\*\*<sup>-1</sup>

59a -> 75a : 0.023585 (c= 0.15357490)  
66a -> 75a : 0.014707 (c= -0.12127393)  
69a -> 75a : 0.060465 (c= 0.24589728)  
71a -> 77a : 0.022218 (c= -0.14905825)  
72a -> 76a : 0.424238 (c= 0.65133587)  
73a -> 76a : 0.304924 (c= 0.55219959)  
73a -> 79a : 0.025751 (c= -0.16047142)  
74a -> 80a : 0.059915 (c= -0.24477548)

STATE 10: E= 0.174405 au 4.746 eV 38277.5 cm\*\*<sup>-1</sup>

60a -> 75a : 0.031866 (c= -0.17850914)  
62a -> 75a : 0.015847 (c= -0.12588650)  
63a -> 75a : 0.042286 (c= -0.20563488)  
64a -> 75a : 0.016447 (c= 0.12824731)  
67a -> 75a : 0.329744 (c= -0.57423322)  
68a -> 75a : 0.501692 (c= -0.70830247)  
70a -> 76a : 0.018167 (c= -0.13478523)

-----  
 ABSORPTION SPECTRUM VIA TRANSITION ELECTRIC DIPOLE MOMENTS  
 -----

State	Energy (cm-1)	Wavelength (nm)	fosc (au**2)	T2 (au)	TX (au)	TY (au)	TZ	
1	24882.3	401.9	0.062588994	0.82810	0.79638	-0.25478	0.35912	
2	26032.7	384.1	0.000481581	0.00609	-0.03555	-0.00315	0.06940	
3	32189.9	310.7	0.035141900	0.35940	0.21733	0.55210	-0.08573	
4	35448.2	282.1	0.195009404	1.81108	-1.17767	0.37815	-0.53027	
5	37107.5	269.5	0.005425461	0.04813	-0.05655	-0.20732	-0.04423	
6	37402.5	267.4	0.000171778	0.00151	0.03415	-0.01055	0.01531	
7	39074.6	255.9	0.121053332	1.01990	0.88393	-0.28322	0.39794	
8	41508.9	240.9	0.000463805	0.00368	0.00059	0.04979	0.03463	
9	43306.9	230.9	0.020247990	0.15392	-0.34399	0.10887	-0.15407	
10	44818.0	223.1	0.000865266	0.00636	-0.06941	0.02307	-0.03171	
11	19366.9	516.3	spin forbidden (mult=3)					
12	21937.7	455.8	spin forbidden (mult=3)					
13	26267.6	380.7	spin forbidden (mult=3)					
14	27158.9	368.2	spin forbidden (mult=3)					
15	32242.8	310.1	spin forbidden (mult=3)					
16	33882.0	295.1	spin forbidden (mult=3)					
17	34911.3	286.4	spin forbidden (mult=3)					
18	34997.7	285.7	spin forbidden (mult=3)					
19	37778.6	264.7	spin forbidden (mult=3)					
20	38277.5	261.2	spin forbidden (mult=3)					

**2-Br\* Optimization:**

-----  
CARTESIAN COORDINATES (ANGSTROEM)  
-----

C	1.619143	0.425158	0.685066
C	1.187713	-0.969912	0.627663
C	-0.042594	-1.300232	0.081045
C	-0.906587	-0.271077	-0.385024
C	0.775865	1.439757	0.262223
C	-0.505129	1.117791	-0.265671
N	-2.125993	-0.438806	-0.927491
S	-2.687785	1.076006	-1.242532
S	3.236310	0.839747	1.336976
S	2.281224	-2.278068	1.180633
Br	-0.695263	-3.108111	-0.076735
Br	1.246832	3.309061	0.304993
N	-1.425023	1.990172	-0.714169
C	2.278181	-2.060266	3.017490
C	4.326566	0.336567	-0.074105
C	5.786697	0.531579	0.332494
H	4.067324	0.965339	-0.937340
H	4.115892	-0.716358	-0.305316
H	2.620141	-1.039905	3.238160
H	3.072118	-2.753558	3.337771
C	0.951045	-2.391175	3.694796
C	6.743880	0.170811	-0.809877
H	6.004582	-0.091664	1.214209
H	5.948282	1.577979	0.637391
H	6.625320	-0.879794	-1.113610

H	7.789831	0.315312	-0.504304
H	6.564498	0.798648	-1.695333
H	0.165875	-1.725518	3.303266
C	1.042728	-2.240942	5.218852
H	0.649928	-3.415967	3.430546
H	1.316423	-1.214469	5.505520
H	1.798465	-2.918994	5.643640
H	0.079811	-2.475223	5.694455

-----  
FINAL SINGLE POINT ENERGY -1796.516383463065  
-----

-----  
VIBRATIONAL FREQUENCIES  
-----

0:	0.00 cm** <sup>-1</sup>
1:	0.00 cm** <sup>-1</sup>
2:	0.00 cm** <sup>-1</sup>
3:	0.00 cm** <sup>-1</sup>
4:	0.00 cm** <sup>-1</sup>
5:	0.00 cm** <sup>-1</sup>
6:	19.08 cm** <sup>-1</sup>
7:	23.30 cm** <sup>-1</sup>
8:	31.92 cm** <sup>-1</sup>
9:	38.64 cm** <sup>-1</sup>
10:	47.00 cm** <sup>-1</sup>

...

**2-Br\* TDDFT:**

-----  
CIS/TD-DFT TOTAL ENERGY  
-----

E(SCF) = -6916.582664275 Eh

DE(CIS) = 0.097574337 Eh (Root 1)

-----  
E(tot) = -6916.485089938 Eh

-----  
FINAL SINGLE POINT ENERGY -6916.485089938187  
-----

-----  
TD-DFT/TDA EXCITED STATES (SINGLETs)  
-----

the weight of the individual excitations are printed if larger than 0.01

STATE 1: E= 0.097574 au 2.655 eV 21415.1 cm\*\*<sup>-1</sup>

105a -> 109a : 0.012336 (c= 0.11106915)

108a -> 109a : 0.968026 (c= -0.98388294)

STATE 2: E= 0.112644 au 3.065 eV 24722.5 cm\*\*<sup>-1</sup>

106a -> 109a : 0.153293 (c= -0.39152684)

107a -> 109a : 0.816530 (c= 0.90362029)

STATE 3: E= 0.126793 au 3.450 eV 27827.8 cm\*\*<sup>-1</sup>

106a -> 109a : 0.804217 (c= -0.89678156)

107a -> 109a : 0.142675 (c= -0.37772299)

107a -> 112a : 0.010643 (c= -0.10316306)

STATE 4: E= 0.149662 au 4.073 eV 32847.0 cm\*\*<sup>-1</sup>

98a -> 109a : 0.012794 (c= -0.11310873)

100a -> 109a : 0.013928 (c= 0.11801643)

102a -> 109a : 0.018806 (c= 0.13713460)

104a -> 109a : 0.281427 (c= 0.53049652)

105a -> 109a : 0.538717 (c= -0.73397357)

107a -> 110a : 0.061636 (c= 0.24826519)

108a -> 110a : 0.029729 (c= 0.17242100)

STATE 5: E= 0.151891 au 4.133 eV 33336.3 cm\*\*<sup>-1</sup>

104a -> 109a : 0.013500 (c= -0.11618844)

105a -> 109a : 0.010547 (c= 0.10269966)

108a -> 110a : 0.925413 (c= 0.96198392)

108a -> 111a : 0.011415 (c= -0.10683989)

STATE 6: E= 0.159259 au 4.334 eV 34953.4 cm\*\*<sup>-1</sup>

98a -> 109a : 0.015379 (c= -0.12401262)

99a -> 109a : 0.010096 (c= 0.10047829)

100a -> 109a : 0.060166 (c= 0.24528758)

102a -> 109a : 0.100664 (c= 0.31727665)

103a -> 109a : 0.013163 (c= 0.11472849)

104a -> 109a : 0.375492 (c= 0.61277373)

105a -> 109a : 0.159588 (c= 0.39948499)

107a -> 110a : 0.230445 (c= -0.48004705)

STATE 7: E= 0.163902 au 4.460 eV 35972.4 cm\*\*<sup>-1</sup>

103a -> 109a : 0.957571 (c= 0.97855578)

STATE 8: E= 0.167434 au 4.556 eV 36747.6 cm\*\*<sup>-1</sup>

107a -> 113a : 0.025445 (c= -0.15951403)

108a -> 110a : 0.014816 (c= -0.12172108)

108a -> 111a : 0.916114 (c= -0.95713833)

STATE 9: E= 0.170223 au 4.632 eV 37359.7 cm\*\*<sup>-1</sup>

102a -> 109a : 0.110559 (c= 0.33250427)

105a -> 109a : 0.051823 (c= 0.22764705)

106a -> 110a : 0.299057 (c= -0.54686105)

107a -> 110a : 0.334873 (c= 0.57868255)

107a -> 111a : 0.107998 (c= -0.32862997)

108a -> 112a : 0.028024 (c= -0.16740488)

STATE 10: E= 0.172455 au 4.693 eV 37849.4 cm\*\*<sup>-1</sup>

102a -> 109a : 0.684536 (c= -0.82736665)

104a -> 109a : 0.167365 (c= 0.40910296)

106a -> 110a : 0.071643 (c= -0.26766287)

108a -> 112a : 0.031142 (c= -0.17647105)

-----  
TD-DFT/TDA EXCITED STATES (TRIPLETS)  
-----

the weight of the individual excitations are printed if larger than 0.01

STATE 1: E= 0.082232 au 2.238 eV 18047.8 cm\*\*<sup>-1</sup>

101a -> 109a : 0.037865 (c= 0.19459039)

106a -> 109a : 0.182542 (c= -0.42724888)

107a -> 109a : 0.688337 (c= -0.82966050)

108a -> 109a : 0.036759 (c= -0.19172511)

STATE 2: E= 0.090011 au 2.449 eV 19755.1 cm\*\*<sup>-1</sup>

105a -> 109a : 0.034091 (c= 0.18463819)

106a -> 109a : 0.010508 (c= -0.10250926)

107a -> 109a : 0.025671 (c= -0.16022119)

108a -> 109a : 0.897508 (c= 0.94736877)

STATE 3: E= 0.113337 au 3.084 eV 24874.6 cm\*\*<sup>-1</sup>

105a -> 109a : 0.087243 (c= -0.29536874)

106a -> 109a : 0.656443 (c= 0.81021198)

107a -> 109a : 0.197419 (c= -0.44431852)

108a -> 110a : 0.016523 (c= -0.12854240)

STATE 4: E= 0.117952 au 3.210 eV 25887.5 cm\*\*<sup>-1</sup>

100a -> 109a : 0.028953 (c= -0.17015531)

102a -> 109a : 0.012747 (c= -0.11290403)

104a -> 109a : 0.038084 (c= 0.19515208)

105a -> 109a : 0.750470 (c= 0.86629685)

106a -> 109a : 0.082130 (c= 0.28658390)

107a -> 109a : 0.019635 (c= -0.14012442)

108a -> 109a : 0.033984 (c= -0.18434692)

STATE 5: E= 0.138335 au 3.764 eV 30361.1 cm\*\*<sup>-1</sup>



98a -> 109a : 0.116304 (c= 0.34103315)  
99a -> 109a : 0.053623 (c= -0.23156552)  
100a -> 109a : 0.123565 (c= -0.35151797)  
102a -> 109a : 0.024030 (c= -0.15501582)  
104a -> 109a : 0.574347 (c= -0.75785676)  
105a -> 109a : 0.010282 (c= 0.10140092)  
107a -> 110a : 0.019045 (c= 0.13800195)  
108a -> 112a : 0.010528 (c= -0.10260744)

STATE 6: E= 0.143913 au 3.916 eV 31585.3 cm\*\*-1

91a -> 109a : 0.082666 (c= 0.28751619)  
98a -> 109a : 0.011733 (c= 0.10831915)  
99a -> 109a : 0.055916 (c= 0.23646621)  
101a -> 109a : 0.526624 (c= -0.72568876)  
101a -> 112a : 0.025976 (c= -0.16117191)  
103a -> 109a : 0.010294 (c= 0.10145815)  
106a -> 109a : 0.014664 (c= -0.12109440)  
106a -> 112a : 0.047115 (c= 0.21705976)  
107a -> 109a : 0.014135 (c= -0.11888967)  
107a -> 112a : 0.098817 (c= 0.31435209)  
107a -> 113a : 0.013580 (c= -0.11653271)  
108a -> 110a : 0.015311 (c= 0.12373859)

STATE 7: E= 0.144657 au 3.936 eV 31748.5 cm\*\*-1

102a -> 109a : 0.039887 (c= -0.19971698)  
106a -> 110a : 0.018541 (c= -0.13616582)  
107a -> 109a : 0.015470 (c= 0.12437757)  
107a -> 110a : 0.076447 (c= -0.27649008)

107a -> 112a : 0.016697 (c= 0.12921552)  
108a -> 110a : 0.737642 (c= -0.85886102)  
108a -> 111a : 0.012918 (c= 0.11365735)

STATE 8: E= 0.146211 au 3.979 eV 32089.5 cm\*\*<sup>-1</sup>

89a -> 109a : 0.014358 (c= 0.11982408)  
100a -> 109a : 0.026042 (c= -0.16137486)  
102a -> 109a : 0.184909 (c= -0.43001084)  
105a -> 112a : 0.013529 (c= 0.11631567)  
106a -> 110a : 0.095946 (c= -0.30975098)  
107a -> 110a : 0.438864 (c= -0.66246831)  
108a -> 110a : 0.139814 (c= 0.37391757)

STATE 9: E= 0.155227 au 4.224 eV 34068.4 cm\*\*<sup>-1</sup>

107a -> 113a : 0.052091 (c= -0.22823475)  
108a -> 110a : 0.024563 (c= -0.15672656)  
108a -> 111a : 0.828464 (c= -0.91020010)

STATE 10: E= 0.160398 au 4.365 eV 35203.2 cm\*\*<sup>-1</sup>

102a -> 109a : 0.240029 (c= 0.48992759)  
103a -> 109a : 0.021475 (c= 0.14654263)  
104a -> 109a : 0.068849 (c= -0.26239118)  
105a -> 109a : 0.019320 (c= 0.13899804)  
106a -> 110a : 0.086035 (c= 0.29331777)  
107a -> 110a : 0.312336 (c= -0.55887028)  
107a -> 111a : 0.124656 (c= 0.35306673)  
108a -> 112a : 0.020285 (c= 0.14242543)  
108a -> 113a : 0.018026 (c= 0.13426046)

108a -> 115a : 0.021392 (c= -0.14625946)

---

ABSORPTION SPECTRUM VIA TRANSITION ELECTRIC DIPOLE MOMENTS

---

State	Energy (cm-1)	Wavelength (nm)	fosc (au**2)	T2 (au)	TX (au)	TY (au)	TZ	
1	20950.7	477.3	0.027509051	0.43227	-0.57528	0.18571	-0.25851	
2	24785.4	403.5	0.009533919	0.12663	0.14369	0.31575	-0.07930	
3	27384.2	365.2	0.085516545	1.02808	-0.34448	-0.94933	0.09050	
4	32939.8	303.6	0.000087525	0.00087	0.01605	0.00974	0.02285	
5	33088.8	302.2	0.081879128	0.81464	0.78961	-0.25530	0.35494	
6	34816.3	287.2	0.047863993	0.45259	-0.58890	0.18903	-0.26466	
7	36015.2	277.7	0.000532904	0.00487	-0.00347	-0.05888	-0.03732	
8	37286.1	268.2	0.061781528	0.54549	0.64600	-0.20895	0.29071	
9	37595.0	266.0	0.000692196	0.00606	0.00617	0.07384	0.02390	
10	38032.8	262.9	0.010376810	0.08982	0.26217	-0.08509	0.11767	
11	17881.3	559.2	spin forbidden (mult=3)					
12	19592.7	510.4	spin forbidden (mult=3)					
13	24893.9	401.7	spin forbidden (mult=3)					
14	25463.2	392.7	spin forbidden (mult=3)					
15	30413.3	328.8	spin forbidden (mult=3)					
16	31497.6	317.5	spin forbidden (mult=3)					
17	31558.2	316.9	spin forbidden (mult=3)					
18	31865.2	313.8	spin forbidden (mult=3)					
19	34858.7	286.9	spin forbidden (mult=3)					
20	35297.2	283.3	spin forbidden (mult=3)					

## Chapter 3

# $\pi$ -Conjugated Polymers as Surrogate Absorbers for Minority Emitters in Low-Reabsorbing Luminescent Solar Concentrators

Part of this chapter were adapted and reprinted with permission from:

Gutierrez, G. D.; Coropceanu, I.; Bawendi, M. G.; Swager, T. M. "A Low Reabsorbing Luminescent Solar Concentrator Employing  $\pi$ -Conjugated Polymers." *Adv. Mater.* **2016**, *28*, 497–501.

Copyright 2015 Wiley-VCH Verlag GmbH & Co. KGaA

The research presented herein was completed in collaboration with Igor Coropceanu (Chemistry, MIT), who designed the integrating sphere setup presented and performed the Monte Carlo simulation. G.D.G. thanks Lionel Moh for helpful discussions on spectroscopic ellipsometry and Phil Reusswig and Tony Wu for preliminary integrating sphere assistance.

### 3.1 Introduction

To increase the viability of solar radiation as a widespread and accessible class of renewable energy, researchers are actively developing solutions to lower the cost of deploying highly efficient photovoltaic (PV) devices. One widely investigated approach is to use a platform capable of focusing solar energy onto a set of small, but efficient PV cells. The most convenient example of this approach is the luminescent solar concentrator (LSC), which has the advantage that it is compatible with typical infrastructures.<sup>1-4</sup> LSCs consist of transparent plastic or glass waveguides that channel luminophore photoemission from the absorption of sunlight to much smaller PV cells attached at their edges.<sup>5</sup>

### 3.2 Addressing the Reabsorption Problem with Amplifying $\pi$ -Conjugated Polymers

Although a promising architecture as a result of the ability to effectively collect sunlight without tracking the sun, conventional LSCs are often plagued by a multitude of unfavorable processes that curb their ability to deliver light to PV cells.<sup>3</sup> Of these limitations, non-radiative reabsorption by the luminophores is regarded as one of the most severe problems and results from significant overlap of the molecule's absorption and emission spectra (see Figure 1.2).<sup>6</sup> Thus, although luminophores with high photoluminescence quantum yields ( $\Phi_{PL}$ ) such as perylene bisimides are desired,<sup>7,8</sup> their performance in LSCs will suffer if they possess small Stokes shifts.

A general approach to reducing reabsorption by molecules with narrow Stokes shifts, such as a perylene bisimide, is to employ minimal concentrations of luminophore such that its probability of encountering an emitted photon en route to the edges of the LSC is low.<sup>9</sup> This tactic, however, comes at the cost of poor light harvesting by the emitter. To overcome this drawback and power the coupled PV cells, one or more strongly absorbing luminescent species can be added to the LSC to enhance the minority perylene bisimide's emission through energy transfer processes. Materials

that have been recently investigated in an analogous manner are semiconducting heterostructured quantum dots<sup>10-12</sup> and rods<sup>13</sup> wherein the excitons of a higher gap CdS shell are efficiently shuttled to a highly luminescent lower gap CdSe core with a much smaller absorption cross-section, resulting in a separated absorption spectrum primarily resembling that of the shell and an emission entirely attributed to the core. Although organic luminophore-based LSCs that exploit energy transfer schemes are also well documented,<sup>14-18</sup> those aimed at specifically reducing reabsorption through the use of minority emitters have relied on a limited set of dyes<sup>19,20</sup> and biological motifs.<sup>21</sup> The extension of this strategy to discover the untapped potential of any powerful organic emitter with a very small Stokes shift, especially one as prized as a perylene bisimide, remains as a challenge.

As highly delocalized semiconducting macromolecular wires,  $\pi$ -conjugated polymers accommodate fast exciton migration along their backbones that may be easily disrupted by smaller quantities of lower gap emitters.<sup>22</sup> Such energy transfer may be accomplished through dipole-dipole coupling mechanisms (i.e. Förster resonance energy transfer, or FRET) between a luminescent polymer and a minority emitter with significant spectral overlap between the emission of the donor and absorption of the acceptor.<sup>23</sup> However, our laboratory has demonstrated that thin films of poly(arylene ethynylene)s (PAEs) may participate in electron exchange energy transfer processes (i.e. the Dexter mechanism) that circumvent this requirement and amplify the emission of spectrally mismatched fluorescent far red dyes.<sup>24</sup> We hypothesized that a combination of two luminescent PAEs of different optical bandgaps ( $E_g$ ) may cooperate in an excitonic relay with a red-emitting perylene bisimide through both FRET and electron exchange processes (Figure 3.1, a, b). Furthermore, through bandgap tuning of the polymers and judicious selection of the minority

red emitter, the absorption spectra of both polymers can be decoupled from the emission of the terminal species while still exhibiting significant absorption within the visible spectrum.

To demonstrate the promise of this proposed down-conversion, this chapter begins by describing a highly emissive, low reabsorbing thin film LSC that makes use of a migratory excitonic cascade from PAEs **P1** ( $E_g \approx 2.7$  eV) and **P2** ( $E_g \approx 2.3$  eV) to minority perylene bisimide Lumogen F Red 305 (**Red 305**,  $E_g \approx 2.0$  eV), the structures of which are displayed in Figure 3.1c. As the efficiencies of both FRET and electron exchange highly depend on the distance between donor and acceptor,<sup>25</sup> a core requirement necessary to effectively activate all modes of energy transfer in this ternary scheme is to keep all participants in the cascade proximate to each other. An ideal configuration involves hosting the minority emitter in a layer of **P1** and **P2**. To accomplish this we needed to address the tendency of  $\pi$ -conjugated polymers to undergo aggregation-induced luminescence quenching that impedes energy transfer to the high  $\Phi_{PL}$  minority luminophore.<sup>26</sup> To overcome this problem, we utilized bulky *tert*-butylated pentiptycene units to render the polymers' backbones incapable of simple and direct  $\pi$ - $\pi$  stacking. **P1**<sup>27</sup> and **P2**<sup>28</sup> are structurally modified derivatives of PAEs previously studied by our laboratory and were synthesized via the Sonogashira cross coupling reaction (see Section 3.7). As a result of their inability to undergo interchain  $\pi$ - $\pi$  stacking and alkyl substituents in their repeat units, these PAEs have high solubility for mixing with other polymers and casting into thin films. The *tert*-butylated pentiptycene repeat units were also used to result in highly amorphous and thus morphologically stable<sup>29</sup> films to maintain efficient energy transfer between **P1**, **P2**, and **Red305** over time. The absorption and emission spectra of thin films of **Red 305** in poly(methyl methacrylate) (PMMA) and the individual PAEs are displayed in Figure 3.1d. Although both **P1** and **P2** possess small Stokes shifts, there is no overlap between their absorption and the emission of **Red 305**, thereby supporting the directed energy transfer cascade.

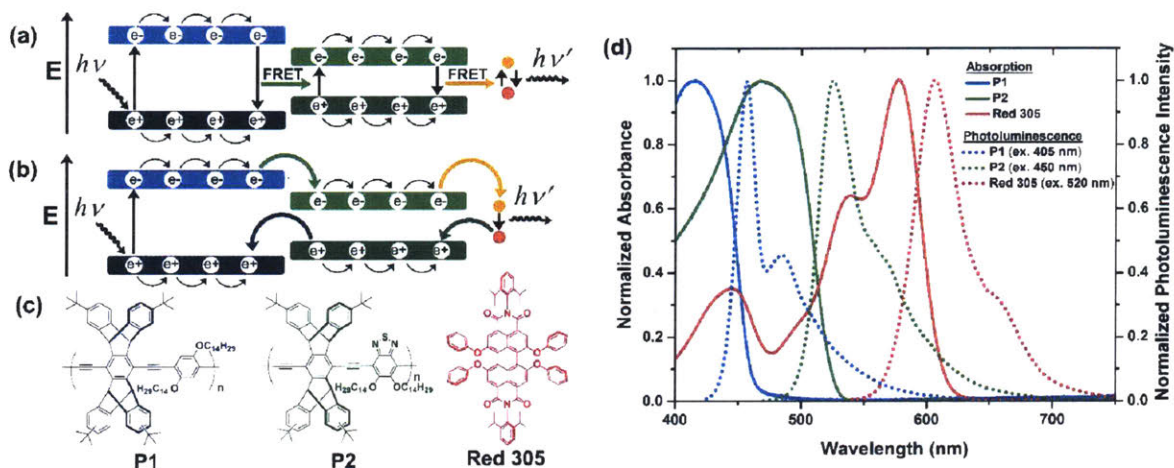


**Figure 3.1.** Photoinduced migratory cascade of excitons in thin films of two  $\pi$ -conjugated polymers, **P1** (blue) and **P2** (green), to minority fluorophore **Red 305** (red) via (a) FRET and (b) electron exchange (Dexter) energy transfer. (c) Structures of **P1**, **P2**, and **Red 305**. (d) Absorption (solid) and emission (dashed) spectra of thin films of **P1** (blue) and **P2** (green) and a sample of 0.5 wt% **Red 305** in PMMA (red). Optical bandgaps were estimated from absorption onsets.

### 3.3 Properties of a Prototype of the Designed LSC

The schematic of the LSC is illustrated in Figure 3.2a. The device is a 50/50 blend of **P1** and **P2** that functions as the host matrix for small amounts of **Red 305** as the terminal isotropic emitter. The resulting thin film composite lies on a thick transparent square substrate that acts as the primary waveguiding medium. The latter feature is best realized with a host layer refractive index that is nearly equal to or lower than the substrate at the relevant emission wavelengths (see Section 1.4).<sup>21</sup> Consequently, the corresponding light guided to the edges of the LSC will be primarily confined to the substrate, thereby avoiding reabsorption. To obtain the refractive index  $n$  as a function of wavelength (Figure 3.2b), we applied spectroscopic ellipsometry to model the dielectric function of a host layer consisting of 1:1 (by weight) **P1**:**P2** (see Section 3.7). The



wavelength profile of  $n$  exhibits wide dispersion that is typical of thin films of semiconducting  $\pi$ -conjugated polymers:<sup>30</sup>  $n$  ranges as low as 1.58 in the absorptive regime and as high as about 1.70 in the emissive region of the blend. Within the photoluminescence of **Red 305** ( $\lambda = 545$  nm to  $\lambda = 800$  nm),  $n$  ranges from 1.65 to 1.61. Guided by this data, we used N-SF10 glass ( $n \approx 1.7$ ) as a compatible substrate, although polycarbonate is also a potential candidate ( $n \approx 1.6$ ). It is worth noting that the refractive indices of  $\pi$ -conjugated polymer films often depend on the thickness and processing conditions of the film.<sup>31</sup> Thus, the data in Figure 3.3b is best translated to the LSC if similar processing conditions are observed. Nonetheless, by design  $n$  is relatively low for  $\pi$ -conjugated polymer films containing highly polarizable benzo[2,1,3]thiadiazoles as repeat units<sup>32</sup> and this is the result of the large internal free volume provided by the *tert*-butylated pentiptycene scaffold.<sup>33</sup>

**LSC1** was constructed by spin casting a blend of 1:1 (by weight) **P1:P2** containing 1.5 wt% **Red 305** on top of a square piece of N-SF10 glass with dimensions 17.5 mm x 17.5 mm x 1.5 mm (**Figure 3**). We found the resulting layer to be optically clear and observed no evidence of large aggregates of **Red305** via polarized optical microscopy. The geometric gain ( $G$ ), or the ratio of the area of a single face of the LSC to the total area of edges coupled to a PV device, represents the concentrating capability of the LSC. Assuming all four edges will be completely covered by PV cells, the value of  $G$  for **LSC1** is approximately 3. The measured film thickness of **LSC1** (186.2 nm) is close to that of the ellipsometry sample and thus correlates with the data in Figure 3.2b. As a result of its small amount, **Red 305** was assumed to not affect  $n$ .

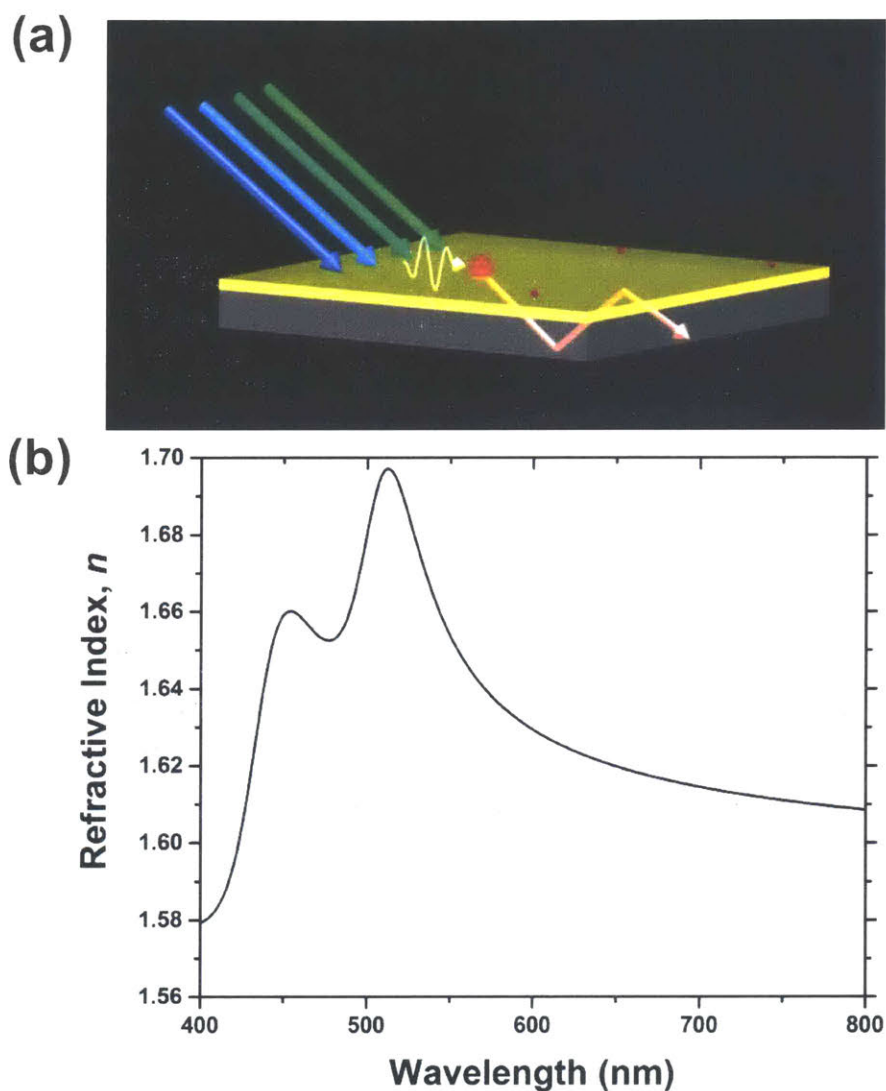


**Figure 3.2.** (a) Schematic of the designed LSC (yellow layer: blend of **P1** and **P2**; red: molecule of Red 305) illustrating exciton diffusion from **P1** and **P2** to **Red 305**. (b) Refractive index ( $n$ ) of a film of 1:1 (by weight) **P1:P2** (thickness = 188.3 nm).

The absorption and photoluminescence spectra of **LSC1** is displayed in Figure 3.3a.<sup>34</sup> The two major bands that span  $\lambda = 400$  nm to  $\lambda = 540$  nm are attributed to **P1** and **P2**, whereas the much smaller peak centered at  $\lambda = 564$  nm is assigned to the minority **Red 305** present. To directly quantify the amount of light absorbed at a given wavelength, the absorption spectrum is displayed

in the form of its absorbance, which corresponds to the fraction of incident light absorbed after correcting for reflection (i.e. absorbance =  $1 - 10^{-A}$ , where  $A$  is the measured absorbance). **LSC1** absorbs approximately 70% of light at its absorption maximum ( $\lambda_{\text{max}} = 422$  nm) and as much as 40% around  $\lambda = 500$  nm. In contrast to these larger magnitudes, the peak absorption of **Red 305** is only about 2%. However, upon excitation of **LSC1** in a regime where absorption is mainly attributed to **P1** (i.e.  $\lambda_{\text{ex}} = 405$  nm), the photoluminescence spectrum almost completely resembles that of **Red 305** with minor residual emission from **P2** present.

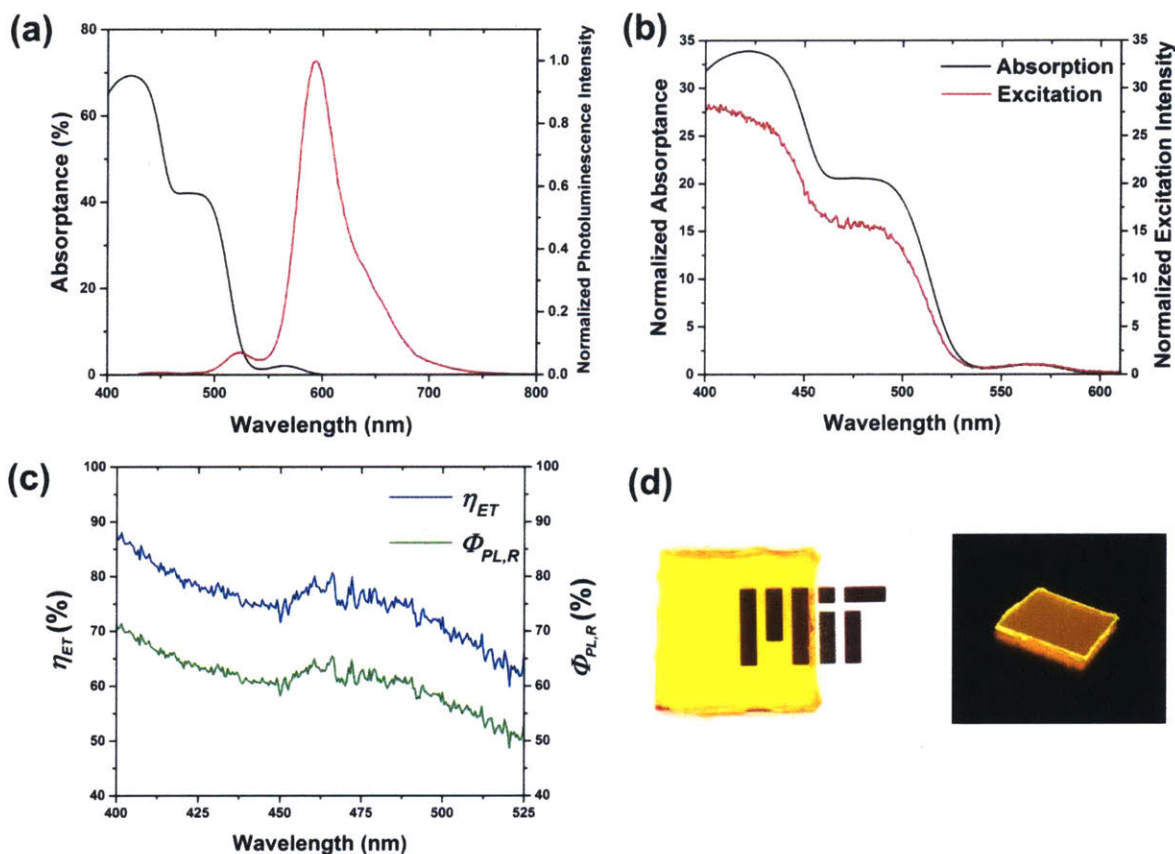


**Figure 3.3.** (a) Absorption and emission ( $\lambda_{\text{ex}} = 405$  nm) spectra of **LSC1** with absorption in terms of its absorbance. (b) Absorption and excitation spectra ( $\lambda_{\text{em}} = 630$  nm) of **LSC1** normalized at  $\lambda = 564$  nm. (c) Plots of the energy transfer efficiency ( $\eta_{ET}$ ) from **P1** and **P2** to **Red 305** and estimated

photoluminescence quantum yield of **Red 305** ( $\Phi_{PL,R}$ ) in LSC1 with respect to wavelength. (d) **LSC1** under normal lighting (left) and UV radiation at  $\lambda = 365$  nm to illustrate light concentration at the edges (right).

The total  $\Phi_{PL}$  of **LSC1** was evaluated with an integrating sphere and measured with an excitation wavelength of  $\lambda_{ex} = 405$  nm, which is close to the absorption maximum. For **LSC1**,  $\Phi_{PL}$  was determined to be 79%, among the highest values observed for  $\pi$ -conjugated polymer thin films.<sup>35</sup> Following precedent for other systems,<sup>15,20</sup> a portrait of the efficiency of energy transfer ( $\eta_{ET}$ ) from the PAEs to **Red 305** was then determined. An excitation spectrum was acquired via monitoring an emission wavelength of  $\lambda_{em} = 630$  nm, which should be effectively attributed to **Red 305** (Figure 3.3b). From this data,  $\eta_{ET}$  from **P1** and **P2** to **Red 305** per wavelength was calculated as the ratio of the normalized excitation intensity to the normalized absorbance (Figure 3.3c). The spectra are normalized at the absorption maximum of the minority **Red 305** to assign a default  $\eta_{ET}$  of 100%. Within the higher-energy band ( $\lambda = 400$  nm to  $\lambda = 460$  nm),  $\eta_{ET}$  maintains values between 88% and 80%, while efficiencies for the second band ( $\lambda = 460$  nm through  $\lambda = 525$  nm) vary from 80% to 62%. By invoking the Kasha-Vavilov rule for **LSC1**,  $\Phi_{PL}$  from **Red 305** ( $\Phi_{PL,R}$ ) as a function of excitation wavelength may then be estimated with Equation 3.4,

$$\Phi_{PL,R}(\lambda) = \Phi_{PL}^{\circ} \left( \frac{F_R}{F_{total}} \right) \left( \frac{\eta_{ET}(\lambda)}{\eta_{ET}^{\circ}} \right)$$

**Equation 3.1**

where  $\Phi_{PL}^{\circ}$  and  $\eta_{ET}^{\circ}$  are the total quantum yield and energy transfer efficiency at  $\lambda_{ex} = 405$  nm, respectively.  $F_R/F_{total}$  is the fraction of the area under the emission spectrum (Figure 3.3a) that is assigned to **Red 305** (i.e. between  $\lambda = 545$  nm and  $\lambda = 800$  nm) due to the very small contribution from **P2**. This ratio indicates that, with  $\lambda_{ex} = 405$  nm, this region is responsible for about 88% of the observed photoluminescence. Through Equation 1, the plot of  $\Phi_{PL,R}$  with excitation wavelength

indicates that **Red 305** maintains quantum yields near or above 50% at all wavelengths via energy transfer by **P1** and **P2** (Figure 3.3c).

### 3.4 Monte Carlo Simulation of LSC1

The key metric of an LSC's performance is its optical efficiency ( $\eta_{opt}$ ), defined as the fraction of incident photons emanating from the edges of the device. As a key goal of LSC research is to scale developed prototypes to commercially relevant sizes, we applied a Monte Carlo simulation to assess the promise of larger versions of our designed LSC by calculating  $\eta_{opt}$  as a function of  $G$  through an analysis of unproductive loss channels. Figure 4 summarizes these results using the photophysical data in Figure 3a, the total  $\Phi_{PL}$ , and an assumed refractive index of 1.7 across all emission wavelengths as inputted parameters for **LSC1**. For **LSC1**,  $\eta_{opt}$  was calculated as approximately 40%. A plot of  $\eta_{opt}$  versus  $G$  (Figure 3.4a) exhibits a slow and steady decrease as  $G$  increases, an expected trend due to non-radiative reabsorption by the trace absorption of **Red 305**. Despite this drop, scaled versions of **LSC1** are projected to maintain high  $\eta_{opt}$  at large  $G$  and is well above 20% even at  $G = 400$ , on par with predictions for high-performing nanocrystal LSCs.<sup>36</sup> The concentration factor, or the product of  $G$  and  $\eta_{opt}$ , is also plotted as a function of  $G$  and represents the actual magnitude of photon concentration by the LSC and rises in a nearly linear fashion as  $G$  increases. For example, at  $G = 400$ , a 90-fold concentration of photons toward PV cells at the edges is expected.

Figure 3.4b summarizes the simulation's calculated impact of the possible loss mechanisms on the performance of **LSC1** at  $G = 200$  and a single excitation wavelength ( $\lambda_{ex} = 405$  nm). The displayed chart tabulates the fates of incident photons that strike the face of the scaled LSC. Prior to absorption, the fixed Fresnel coefficient for the inputted refractive index directly contributes to a 7% loss of photons via reflection off the surface of the LSC. By taking into account that some

incident photons are lost due to incomplete absorption by the LSC after this reflection occurs (“Not Absorbed,” 31%), the simulation predicts non-radiative events (“Not Reemitted”) to result in a modest 21% loss in which minor reabsorption processes play a large role. Additionally, a leakage of emitted photons through the waveguide’s escape cone (“Facial Loss”) is projected to result in a 15% overall loss. The remaining 27% of incident photons, albeit down-converted by **Red 305** (“Collected”), represents  $\eta_{opt}$ .

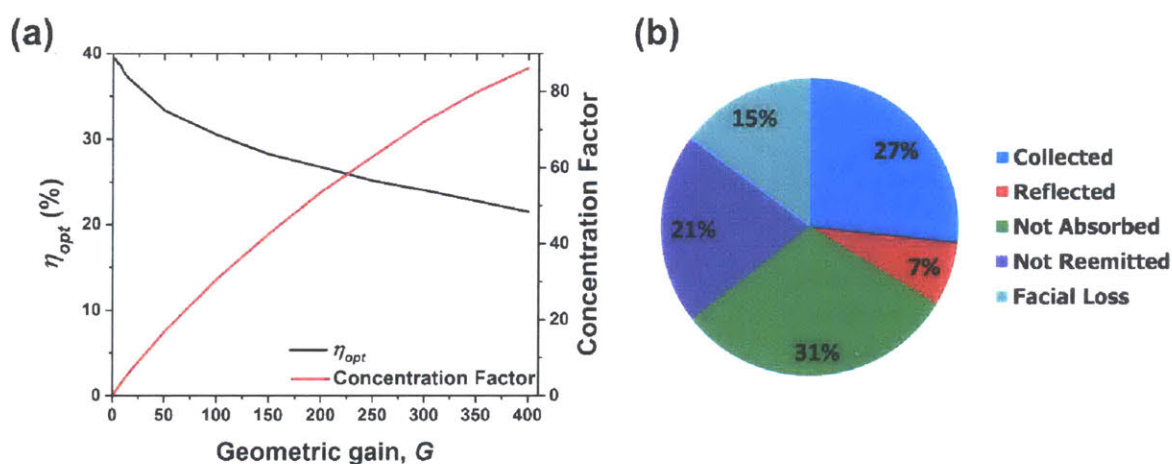


**Figure 3.4.** (a) Projected optical efficiency ( $\eta_{opt}$ ) and concentration factor with increasing geometric gain ( $G$ ) for **LSC1**. (b) Calculated loss channels (rounded) for  $G = 200$  ( $\lambda_{ex} = 405$  nm).

### 3.5 LSCs Utilizing Conjugated Polymers in PMMA

To further increase the promise of the use of  $\pi$ -conjugated polymers in commercially viable LSCs, we sought to reduce the amount of polymers used in the devices while retaining efficient energy transfer to minority emitters. Specifically, we postulated whether efficient near-field energy transfer can occur in PMMA, a popular LSC host material. In general, polymers of different compositions tend to resist mixing and tend to phase separate. Blends of  $\pi$ -conjugated polymers are capable of phase separating in PMMA.<sup>37</sup> We hypothesized whether near-field energy transfer

is possible through a three-polymer cascade from **P1** and **P2** to minority amounts of a third red-emitting polymer **P3** (Figure 3.5). Under these conditions, the *tert*-butylated pentiptycene repeat units would also prevent any luminescence quenching from occurring.

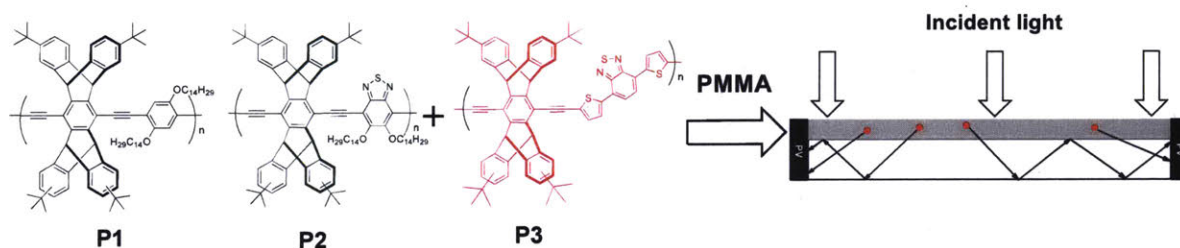


**Figure 3.5.** Schematic for LSC exploiting the phase-separating tendency of different polymers to enable an energy transfer cascade from **P1** and **P2** to a minority emitter **P3**. The red circles represent phase-separated microdomains of three  $\pi$ -conjugated polymers.

As with **P1** and **P2**, **P3** was synthesized using the Sonogashira cross coupling reaction (see Section 3.6.3). The photophysical properties of a thin film of **P3** is presented in Figure 3.6a, with  $\lambda_{\text{max}} = 501$  nm for visible absorption and  $\lambda_{\text{max}} = 660$  nm for emission.  $E_g$  for **P3** as a thin film was estimated as 1.97 eV and is therefore suitable as a terminal emitter in the proposed cascade. A PMMA film doped 5:2:1 **P1**:**P2**:**P3** (8 wt% total) was spin-casted onto a PMMA substrate using chloroform as the solvent. The absorption and emission spectra of the resulting model LSC (**LSC2**) is shown in Figure 3.6b and shows wide spectral separation between the absorption and emission maxima. When excited at  $\lambda_{\text{max}} = 405$  nm, **LSC2** demonstrates an emission spectrum primarily due to **P3** with some residual emission from **P1** and **P2**.  $\Phi_{PL}$  was estimated as 20% at  $\lambda_{\text{max}} = 405$  nm (relative to perylene in PMMA as a standard,  $\Phi_{PL} = 87\%^{38}$ ).

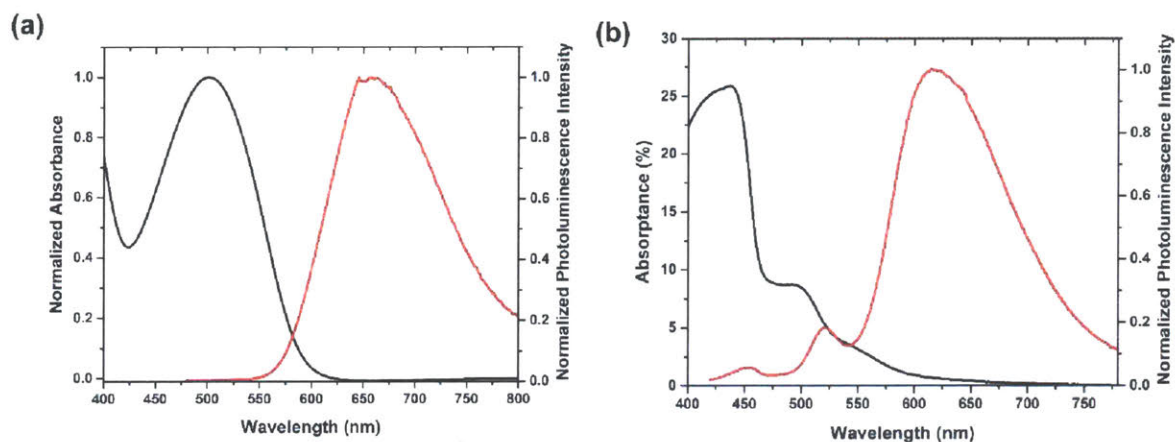


**Figure 3.6.** Photophysical properties of (a) **P3** as a thin film and (b) **LSC2**.

### 3.6 Conclusion

To summarize, we have demonstrated a blend of  $\pi$ -conjugated polymers as amplifying antennae for a minority emitter to create low reabsorbing thin film LSCs with significant absorption in the visible spectrum and, in one case, performance similar to state-of-the-art analogs. The participants of the described cascade all possess solubilities that allow for facile and low-cost solution processing of amorphous, highly luminescent thin films. Through the development of even lower gap luminescent  $\pi$ -conjugated polymers, we envision creating additional high-performance LSCs capable of more complete absorption of the visible spectrum with efficient energy transfer directed toward spectrally separated minority terminal luminophores that emit in the far red or near-infrared for improved spectral matching with silicon PV cells.

### 3.7 Experimental Section

**3.7.1 Materials and Instrumentation.** Prior to use, *N,N*-diisopropylamine was distilled over KOH and sparged under argon for 1 hour. Toluene was passed through a solvent purification system (SPS) via columns of activated alumina, stored over 3 Å molecular sieves, and sparged under argon for 1 hour. Anhydrous THF was also obtained from the same SPS and used



immediately. Unless otherwise indicated, all other purchased solvents and reagents were used without additional purification. Lumogen F Red 305 was obtained from BASF and also used without further purification. Column chromatography was implemented with silica gel (60 Å pore size, 230 – 400 mesh, Sigma-Aldrich) as the solid phase. Thin layer chromatography (TLC) was carried out with Baker-flex silica gel IB-F plates (J. T. Baker). N-SF10 glass samples (Schott) were obtained as circular blank plates (25 mm diameter, 1.5 mm thickness) from UQG Optics (Cambridge, UK) and manually cut to specification with a diamond cutter. The glass was cleaned with acetone and chloroform, followed by a stream of N<sub>2</sub> gas, before use.

<sup>1</sup>H NMR (400 MHz) and <sup>13</sup>C NMR (101 MHz, proton-decoupled) spectra were acquired using a Bruker Avance III HD NMR spectrometer. The multiplicities and/or shape of all indicated resonances are labeled with the following key: singlet (“s”), doublet (“d”), doublet of doublets (“dd”), triplet (“t”), multiplet (“m”), and broad (“br.”). All spectra were obtained with CDCl<sub>3</sub> as the solvent and reported chemical shifts are referenced with respect to solvent peaks ( $\delta = 7.26$  ppm for <sup>1</sup>H and  $\delta = 77.16$  ppm for <sup>13</sup>C). NMR data for  $\pi$ -conjugated polymers are reported in the context of a single repeat unit. Gel permeation chromatography (GPC) measurements were carried out using an Agilent 1260 Infinity gel permeation chromatograph with UV/vis and refractive index detectors calibrated against polystyrene standards and THF as the eluent. The injection concentration of the prepared GPC samples was 0.5 mg/mL. High resolution mass spectrometry (HRMS) data were obtained via direct analysis in real time (DART) with positive ionization at the MIT Department of Chemistry Instrumentation Facility with a Bruker Daltronics APEXIV 4.7 Tesla FT-ICR mass spectrometer. Mass spectrometry (MS) via matrix assisted laser desorption/ionization-time of flight (MALDI-TOF) was performed at the MIT Biopolymers Laboratory using 2,5-dihydroxybenzoic acid as the matrix. Melting point determination was

carried out with a MelTemp II melting point apparatus (Laboratory Devices Inc, USA). Spin coated samples were created using a Model WS-400 Spin Processor (Laurel Technologies Corporation) coupled to a vacuum line. Film thicknesses were measured using a Dektak 6M profilometer. Ellipsometry measurements were carried out using a J. A. Woollam Co., Inc. M-2000D variable angle spectroscopic ellipsometer and the V.A.S.E. 32 software package.

Photophysical spectra were obtained with thin films facing the source lamps. Absorption spectra were obtained using an Agilent Cary 4000 UV/vis spectrophotometer. Photoluminescence and excitation spectra were acquired on a HORIBA Jobin Yvon Fluorolog-3 spectrofluorometer (model FL-321) equipped with a 450 W xenon lamp as the excitation source. Front-face detection was used to observe photoluminescence near excitation.

Quantum yield measurements for LSC1 were taken using an integrating sphere (Labsphere RTC-060-SF). The experimental set-up that was used is shown schematically in Figure 3.7 below. The sample was illuminated using a 405 nm diode laser with an excitation power of 5mW that was chopped at 210 Hz. The output was collected using a calibrated germanium detector (Newport: 818-UV) through a Stanford Research Systems lock-in amplifying system. The integrating sphere included two baffles, one which lay immediately beneath the sample holder to prevent direct emission into the detector as well as a baffle on a side, which could be used to ensure that reflected light from the initial beam could only reach the detector after multiple reflection events.

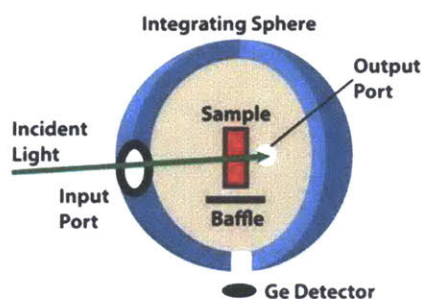


**Figure 3.7.** The configuration used to measure the absolute quantum yield of LSC1.

Two measurements were then taken using this system: 1) Laser Intensity (LI), where the laser was directed behind one of the baffles with the sample outside of the sphere; 2) Sample Fluorescence (SF) where the excitation beam was passed through the sample and out through an exit port and the reflection was allowed to exit through the side port. From these two measurements and the absorbance of the sample, it was possible to extract the photoluminescence quantum yield ( $\Phi_{PL}$ ) of LSC1 by calculating the number of photons absorbed and the number of photons emitted (Equation 3.2):

$$\Phi_{PL} = \frac{\frac{SF}{EQE(S)} / \frac{LI}{EQE(L)}}{Abs(L)}$$

**Equation 3.2**

In Equation 3.2, EQE(S) and EQE(L) refer to the external quantum efficiency of the detector at the wavelength of the sample emission and of the excitation wavelength, respectively, and Abs(L) is the absorbance of the sample at the excitation wavelength.

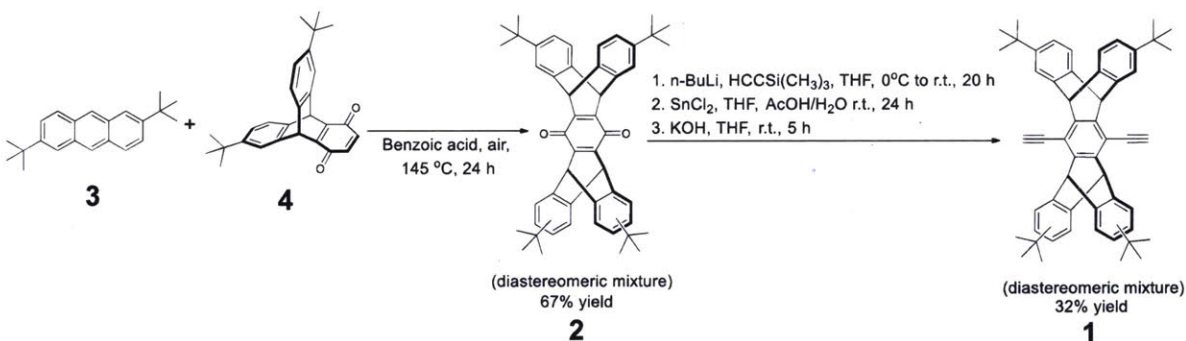
**3.7.2 Thin films of P1, P2, P3, Red 305 in PMMA and LSCs.** Thin films of P1 and P2 were spin casted onto soda-lime glass substrates from 20 mg/mL chloroform solutions at 2000 rpm for 45 seconds. A thin film of 0.5 wt% Red 305 in PMMA was made by drop casting a chloroform solution containing 100 mg/mL PMMA and 0.5 mg/mL Red 305 onto a soda-lime glass substrate.

The thin film of **P3** was processed in the same way as those of **P1** and **P2**.

**LSC1:** 0.2 mL of a 0.375 mg/mL solution of **Red 305** in chloroform was added to a vial containing 2.50 mg **P1** and 2.50 mg **P2**. After dissolution of the polymers, 0.1 mL of the resulting solution was drawn into a syringe and quickly added on top of a blank plate of N-SF10 glass spinning at 2000 rpm. Upon completion of the injection, the sample was spun at the same speed for 45 seconds.

**LSC2:** 5 mg **P1**, 2 mg **P2**, 1 mg **P3**, and 100 mg PMMA ( $M_w \sim 15,000$ ) were dissolved in 1 mL  $\text{CHCl}_3$  and spin-casted onto a PMMA substrate (cm x cm x 0.6 cm) at 4500 rpm for 45 seconds.

**3.7.3 Synthetic procedures.** 2,6-di-*tert*-butylantracene (**3**),<sup>39</sup> 6,10-di(*tert*-butyl)tritycene-1,4-quinone (**4**),<sup>33</sup> 1,4-bis(tetradecyloxy)benzene (**6**),<sup>22</sup> and 5,6-bis(tetradecyloxy)benzo[2,1,3]thiadiazole (**8**)<sup>28</sup> were synthesized following published procedures.



**Scheme 3.1.** Synthesis of *tert*-butylated pentiptycene dialkyne **1**.

#### *tert*-Butylated pentiptycene quinone **2**

The following synthesis is a modified preparation of **2** described in Nesterov et al.<sup>38</sup> in which benzoic acid is employed as the solvent. To a 50 mL round bottom flask containing a magnetic stir bar, **3** (1.10 g, 3.79 mmol), **4** (1.88 g, 4.73 mmol), and benzoic acid (5.55 g, 45.5 mmol) were added and mechanically blended with a spatula. The flask was submerged in an oil bath heated to

145°C, a temperature at which benzoic melts, covered, and stirred under aerobic conditions. After 15 h, the reaction was quickly aerated and resealed with stirring proceeding for another 9 h. The reaction mixture was cooled to room temperature and the resulting solid slab was triturated into 2 x 30 mL CHCl<sub>3</sub>. The fractions were combined and washed 2 x 100 mL saturated NaHCO<sub>3</sub> (aq.) solution, followed by 100 mL saturated NaCl (aq.) solution. The organic layer was dried with MgSO<sub>4</sub> and filtered. 15 g silica gel was added to the organic layer and volatiles were evaporated. The residue was dry-loaded at the top of a column of silica gel and purified using 100% hexanes as eluent to remove excess 2,6-di-*tert*-butylanthracene (**3**), followed by 1:1 CHCl<sub>3</sub>:hexanes to obtain **2** as an orange solid and set of inseparable diastereomers (1.74 g, 67% yield). <sup>1</sup>H NMR (400 MHz, CDCl<sub>3</sub>): δ (ppm) = 7.40 (d, 4H, *J* = 1.8 Hz, 4H), 7.28 (d, 4H, *J* = 7.8 Hz, 4H), 6.98 (dd, 4H, *J*<sub>1</sub> = 1.8 Hz, *J*<sub>2</sub> = 7.8 Hz, 4H), 5.70 (s, 4H), 1.22 (s, 36 H). <sup>13</sup>C NMR (101 MHz, CDCl<sub>3</sub>): δ (ppm) = 180.5, 151.4, 148.8, 144.0, 141.0, 123.7, 122.0, 121.8, 47.4, 34.7, 31.6.

#### *tert*-Butylated pentiptycene dialkyne **1**

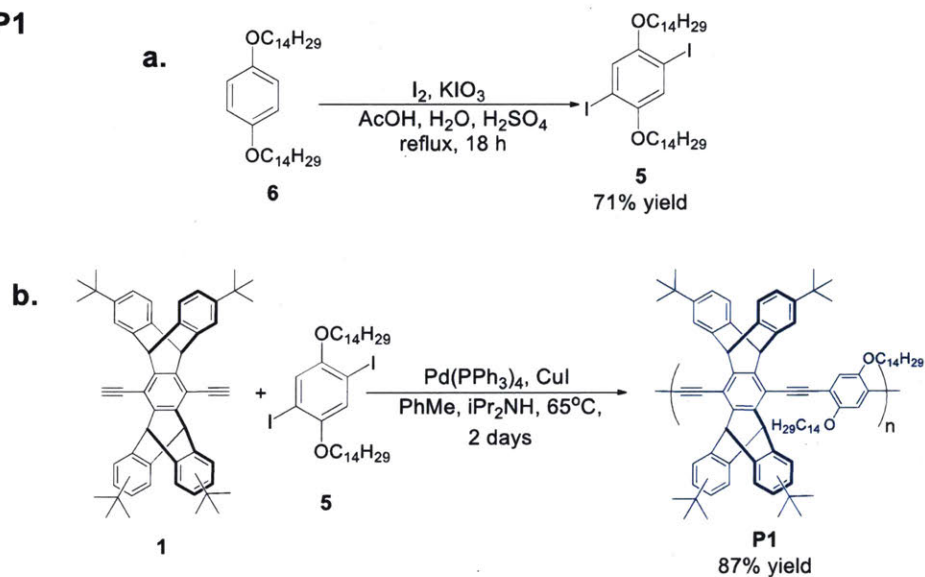
This procedure was performed with some modifications to the preparation of **1** described by Nesterov et al.<sup>40</sup> To a solution of trimethylsilylacetylene (1.00 g, 10.22 mmol, 1.44 mL) in 30 mL anhydrous THF at 0 °C were added *n*-BuLi (1.60 M in hexanes, 8.76 mmol, 5.47 mL) dropwise. The mixture was stirred at 0 °C under argon for 30 minutes and then cannula-transferred into a 500 mL 3-neck round bottom flask containing **2** (2.00 g, 2.92 mmol) in 200 mL anhydrous THF at 0 °C. The reaction was stirred at 0 °C for 1 h and then at room temperature for 18 h, all of which was under argon. The mixture was then poured into 100 mL 10% w/v NH<sub>4</sub>Cl (aq.). 250 mL Et<sub>2</sub>O was added and the biphasic mixture was partitioned. The organic layer was washed with 100 mL H<sub>2</sub>O, then 100 mL saturated NaCl (aq.), dried with MgSO<sub>4</sub>, and concentrated *in vacuo*. The crude residue was passed through a plug of silica gel using 1:1 CHCl<sub>3</sub>:hexanes as the eluent. The crude

mixture of diols was isolated as a beige solid and immediately dissolved in 50 mL THF (de-inhibited by distillation). The solution was sparged with argon for 25 minutes. A degassed solution of  $\text{SnCl}_2 \cdot 2\text{H}_2\text{O}$  (1.65 g, 7.30 mmol) in 5 mL  $\text{H}_2\text{O}$  and 5 mL AcOH was cannula-transferred into the mixture and then stirred at room temperature under argon for 24 h. 20 mL of saturated  $\text{NaHCO}_3$ (aq.) solution was carefully added to neutralize the AcOH, followed by 25 mL  $\text{H}_2\text{O}$ . The resulting precipitate was filtered and washed with 10 mL saturated  $\text{NaHCO}_3$ (aq.) solution and 10 mL  $\text{H}_2\text{O}$ . 100 mL  $\text{CHCl}_3$  was added to the solid to dissolve any organic species with any remaining insoluble precipitates filtered off. The remaining solid was treated with another 100 mL  $\text{CHCl}_3$ , then filtered off. Both  $\text{CHCl}_3$  fractions were combined and evaporated. The resulting crude material was subjected to column chromatography (3:7  $\text{CHCl}_3$ :hexanes) to isolate 823 mg of a mixture of TMS-protected intermediates immediately carried over to the next step. ( $R_f = 0.41, 0.50$  ( $\text{SiO}_2$  TLC, 1:9  $\text{CHCl}_3$ :hexanes)). The resulting solid was dissolved in 25 mL de-inhibited THF, to which a solution of KOH (106 mg, 1.89 mmol) in 10 mL MeOH was added. After stirring the reaction at room temperature for 3 h, the mixture was poured into 50 mL  $\text{Et}_2\text{O}$ , washed with 150 mL saturated NaCl (aq.), 100 mL  $\text{H}_2\text{O}$ , and another 150 mL saturated NaCl (aq.) solution. The organic layer was dried with  $\text{MgSO}_4$ . To the filtered solution was added 5 g silica gel with volatiles then evaporated. The sample was dry-loaded onto a column of silica gel and chromatographed using a 1:9  $\text{CHCl}_3$ :hexanes/1:1  $\text{CHCl}_3$ :hexanes gradient to furnish 658 mg **1** as an off-white solid and mixture of diastereomers (32% overall yield).  $R_f = 0.34$  ( $\text{SiO}_2$  TLC, 1:9  $\text{CHCl}_3$ :hexanes).  $^1\text{H}$  NMR (400 MHz,  $\text{CDCl}_3$ ):  $\delta$  (ppm) = 7.39 (d,  $J = 1.8$  Hz, 4H), 7.30-7.27 (2 d,  $J = 7.8$  Hz, 4H), 6.97 (dd, 4H,  $J_1 = 1.8$  Hz,  $J_2 = 7.8$  Hz, 4H), 5.78 (s, 4H), 3.71-3.70 (2 s, 2H), 1.23 (s, 36H).  $^{13}\text{C}$  NMR (101 MHz,  $\text{CDCl}_3$ ):  $\delta$  (ppm) = 148.4, 145.0, 142.20, 142.15, 123.3, 123.2, 121.96, 121.92, 121.3,

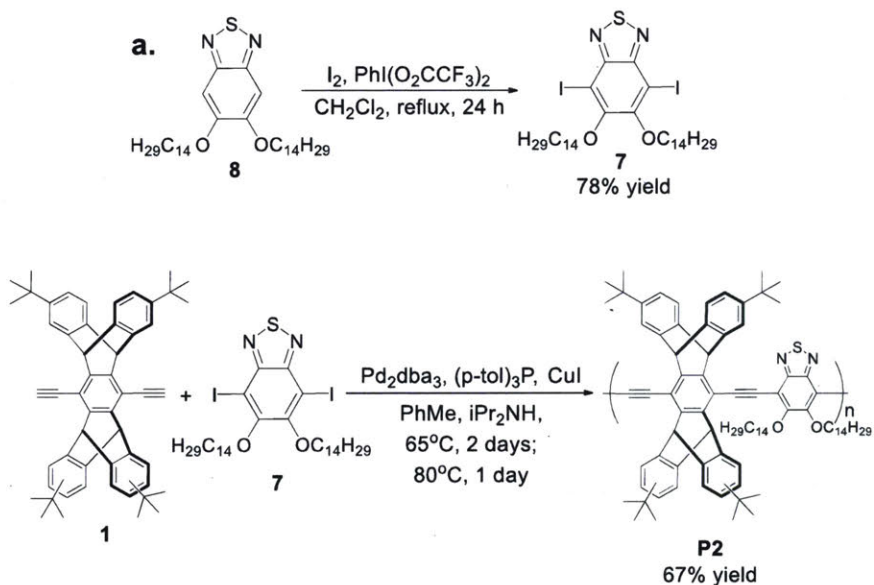
121.2, 114.01, 113.97, 84.43, 84.38, 79.60, 79.58, 52.0, 34.7, 31.6. MS (MALDI-TOF, m/z)

calculated for  $C_{54}H_{54}$ ,  $M^+$ : 702.423, found: 702.465.<sup>41</sup>

i. P1



ii. P2



**Scheme 3.2.** Synthesis of  $\pi$ -conjugated polymers **P1** and **P2** from **1** and their respective bandgap-limiting co-monomers **5** and **7**.

#### *2,5-diiodo-1,4-bis(tetradecyloxy)benzene (5)*

Compound **5** was prepared with some modification to a general procedure offered for the synthesis of 2,5-diiodo-1,4-bis(alkoxy)benzenes.<sup>22</sup> **6** (1.50 g, 2.98 mmol), I<sub>2</sub> (757 mg, 2.98 mmol), KIO<sub>3</sub> (319 mg 1.49 mmol), 30 mL AcOH, 3 mL H<sub>2</sub>O, and 0.3 mL H<sub>2</sub>SO<sub>4</sub> were added to a 100 mL round-bottom flask containing a magnetic stirbar and reflux condenser. The reaction was stirred at reflux for 18 h. 20 mL 10% Na<sub>2</sub>S<sub>2</sub>O<sub>3</sub>·5H<sub>2</sub>O (*aq.*) solution was then added to the flask. The mixture was added to 200 mL CH<sub>2</sub>Cl<sub>2</sub> to dissolve the crude product and 100 mL H<sub>2</sub>O. The organic layer was partitioned and then washed with 100 mL saturated NaHCO<sub>3</sub> (*aq.*) solution and 100 mL saturated NaCl (*aq.*) solution. The organic layer was dried with MgSO<sub>4</sub>, filtered, and evaporated. The resulting residue was recrystallized from isopropanol twice to obtain **5** as a white solid (1.59 g, 71% yield). <sup>1</sup>H NMR (400 MHz, CDCl<sub>3</sub>): δ (ppm) = 7.17 (s, 2H) 3.92 (t, *J* = 6.5 Hz, 4H), 1.80 (m, 4H), 1.49 (m, 4H), 1.26 (br. m, 40H) 0.88 (t, *J* = 7.1 Hz, 6H). <sup>13</sup>C NMR (101 MHz, CDCl<sub>3</sub>): δ (ppm) = 153.0, 122.9, 86.5, 70.5, 32.1, 30.5, 29.9, 29.8, 29.7, 29.7, 26.1, 22.8, 14.3. HRMS (DART, *m/z*) calculated for C<sub>34</sub>H<sub>58</sub>I<sub>2</sub>N<sub>2</sub>O<sub>2</sub>S, M<sup>+</sup>: 754.2677, found: 754.2676.

#### *4,7-Diiodo-5,6-bis(tetradecyloxy)benzo[2,1,3]thiadiazole (7)*

The preparation of **7** is based on a procedure for the production of 4,7-diiodo-5,6-bis(octyloxy)benzo[2,1,3]thiadiazole reported by Nagarjuna et al.<sup>42</sup> To a 300 mL round-bottom flask equipped with a magnetic stirbar were added **8** (2.50 g, 4.46 mmol), iodine (1.36 g, 5.35 mmol), [bis(trifluoroacetoxy)iodo]benzene (2.30 g, 5.35 mmol), and 150 mL CH<sub>2</sub>Cl<sub>2</sub>. A reflux condenser was attached to the flask and contents were heated to reflux and stirred for 24 hours. The reaction mixture was cooled to room temperature and washed with 2 x 100 mL 20% Na<sub>2</sub>S<sub>2</sub>O<sub>3</sub> (*aq.*) solution, 2 x 100 mL 20% NaHCO<sub>3</sub> (*aq.*) solution and 2 x 100 mL saturated NaCl (*aq.*) solution. The organic layer was dried with anhydrous MgSO<sub>4</sub> and filtered through a short plug of



silica gel with CH<sub>2</sub>Cl<sub>2</sub> as the eluent. The solvent was evaporated under reduced pressure and the resulting residue was recrystallized from isopropanol. The material was lastly subject to column chromatography using 1:1 CHCl<sub>3</sub>:hexanes as the eluent to furnish **7** as a white solid (2.83 g, 78% yield). R<sub>f</sub> = 0.46 (SiO<sub>2</sub> TLC, 1:1 CHCl<sub>3</sub>:hexanes). m.p. 81 °C – 82 °C. <sup>1</sup>H NMR (400 MHz, CDCl<sub>3</sub>): δ (ppm) = 4.12 (t, *J* = 6.7 Hz, 4H), 1.91 (m, 4H), 1.54 (m, 4H), 1.26 (br. m, 40H) 0.88 (t, *J* = 7.1 Hz, 6H). <sup>13</sup>C NMR (101 MHz, CDCl<sub>3</sub>): δ (ppm) = 157.2, 151.9, 82.8, 75.1, 32.1, 30.5, 29.9-29.8, 29.6, 29.5, 26.3, 22.8, 14.3. HRMS (DART, *m/z*) calculated for C<sub>34</sub>H<sub>58</sub>I<sub>2</sub>N<sub>2</sub>O<sub>2</sub>S, [M + H]<sup>+</sup>: 813.2381, found: 813.2367.

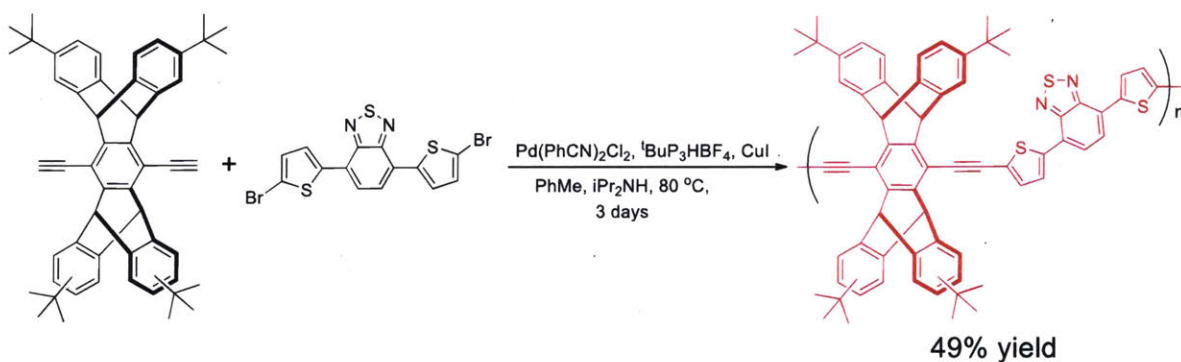
#### *π-Conjugated polymer P1*

To a 25 mL Schlenk flask equipped with a magnetic stirbar were added **1** (300 mg, 0.427 mmol), **5** (349 mg, 0.469 mmol), Pd(PPh<sub>3</sub>)<sub>4</sub> (24.66 mg, 21.34 μmol), and CuI (4.06 mg, 21.34 μmol). After degassing the flask with 3 vacuum-argon backfill cycles, 7 mL of degassed toluene and 3 mL of degassed *N,N*-diisopropylamine were added. The reaction mixture was stirred under argon at 65 °C for 2 days, which was then cooled to room temperature. The viscous mixture was then added dropwise to the vortex of 200 mL of rapidly stirring methanol. The resulting precipitate was filtered and washed with 50 mL methanol. After dissolving in chloroform, and passed through a short plug of silica gel using chloroform as the eluent. The collected fraction was concentrated *in vacuo* to approximately 10-15 mL and the polymer was precipitated in 200 mL stirring acetone. The polymer was filtered, washed with 50 mL acetone, and dried to yield **P1** as a brilliant yellow solid (459 mg, 87% yield). <sup>1</sup>H NMR (400 MHz, CDCl<sub>3</sub>): δ (ppm) = 7.51 (br. s., 6H), 7.43 (br. s., 4H), 7.07 (br. s., 4H), 6.05 (br. s., 4H), 4.51 (br. s., 4H), 2.26 (br. s., 4H), 1.75 (br. s., 4H), 1.48 (br. s., 4H), 1.33-1.18 (br. m, 76H), 0.90 (br. t., *J* = 6.9 Hz, 6H). <sup>13</sup>C NMR (101 MHz, CDCl<sub>3</sub>): δ (ppm)

= 154.0, 148.3, 145.4, 144.5, 142.5, 123.4, 121.9, 121.3, 118.0, 115.1, 93.6, 91.5, 70.4, 52.4, 34.8, 32.1, 31.8, 30.1, 29.8, 29.5, 26.5, 22.9, 14.3. GPC (THF):  $M_n = 46$  kDa,  $\bar{D} = 2.1$ .

### $\pi$ -Conjugated polymer **P2**

To a 25 mL Schlenk flask equipped with a magnetic stirbar were added **1** (170 mg, 0.242 mmol), **7** (197 mg, 0.242 mmol),  $\text{Pd}_2(\text{dba})_3$  (5.65 mg, 17.8  $\mu\text{mol}$ ), (*p*-tol) $_3\text{P}$  (7.40 mg, 71.1  $\mu\text{mol}$ ), and  $\text{CuI}$  (2.33 mg, 35.6  $\mu\text{mol}$ ). Following 3 vacuum-argon backfill cycles, 7 mL anhydrous degassed toluene and 3 mL anhydrous degassed *N,N*-diisopropylamine were added and contents were stirred under argon at room temperature for 20 minutes and then at 65 °C for 2 days. Subsequently, the reaction mixture was stirred at 80 °C for 1 day. The reaction was worked up in the same way as that of **P1** to furnish **P2** as a brilliant orange solid (209 mg, 67% yield).  $^1\text{H}$  NMR (400 MHz,  $\text{CDCl}_3$ ):  $\delta$  (ppm) = 7.64 (br. s., 4H), 7.50 (br. d.,  $J = 7.8$  Hz, 4H), 7.08 (br. d.,  $J = 7.8$  Hz, 4H), 6.36 (br. s., 4H), 4.94 (br. s., 4H), 2.37 (br. s., 4H), 1.85 (br. s., 4H), 1.52 (br. s., 4H), 1.38-1.24 (br. m., 76H), 0.89 (br. t.,  $J = 6.6$  Hz, 6H).  $^{13}\text{C}$  NMR (101 MHz,  $\text{CDCl}_3$ ):  $\delta$  (ppm) = 157.2, 153.3, 148.4, 146.4, 145.4, 145.2, 142.6, 123.5, 122.0, 121.5, 115.3, 108.6, 98.3, 90.4, 75.6, 52.3, 34.8, 32.1, 31.8, 31.4, 30.1-29.9 (br.), 29.6, 26.8, 22.9, 14.3. GPC (THF):  $M_n = 24$  kDa,  $\bar{D} = 1.7$ .



**Scheme 3.3.** Synthesis of **P3**.

### *Conjugated Polymer P3*

To a 25 mL Schlenk flask with stirbar was combined **1** (75.0 mg, 0.107 mmol), 4,7-bis(2-bromo-5-thienyl)-2,1,3-benzothiadiazole (48.8 mg, 0.107 mmol), Pd(PhCN)<sub>2</sub>Cl<sub>2</sub> (2.05 mg, 5.33 μmol), P(<sup>t</sup>Bu)<sub>3</sub>HBF<sub>4</sub> (3.10 mg, 10.7 μmol), CuI (1.02 mg, 5.33 μmol), anhydrous toluene (5 mL) and anhydrous diisopropylamine (2 mL). The suspension was stirred while degassed with argon at room temperature for 10 minutes. The reaction mixture was then stirred under argon atmosphere at 80° C for 3 days. The mixture was cooled to room temperature, and added to stirring methanol to precipitate the polymer. After centrifugation to retrieve the solid, the polymer was then passed through a plug of silica gel with CHCl<sub>3</sub> as solvent, concentrated, then precipitated from acetone. The polymer was again dissolved in CHCl<sub>3</sub> and precipitated from 50 mL stirring hexanes to obtain **P3** as a red solid (52 mg, 49% yield). <sup>1</sup>H NMR (400 MHz, CDCl<sub>3</sub>): δ (ppm) = 8.27 (br. s, 2H), 8.13 (br. d., 2H), 7.70 (br. s, 2H), 7.48 (br. s., 4H), 7.39 (br. m, 4H), 7.02 (br. m, 4H), 5.86 (br. s, 4H), 1.28 (br. s, 36H). GPC (THF): M<sub>n</sub> = 12 kDa, Đ = 3.1.

**3.7.4 Spectroscopic Ellipsometry.** Ellipsometry data were acquired at a single incident angle of 70° and with a scan range of λ = 192 nm through λ = 994 nm. Samples were coated on a square silicon substrate with facial dimensions 9.9 mm x 9.9 mm and a thickness of 0.525 mm. Before coating, the substrate was initially cleaned with a stream of N<sub>2</sub> gas. A native SiO<sub>2</sub> layer with thickness 6.946 nm was initially determined by the ellipsometer. The analyzed sample consisted of a composite blend of **P1** and **P2** prepared under the same processing conditions as **LSC1**, but with **Red 305** absent. 2.50 mg of **P1** and 2.50 mg of **P2** were dissolved in 0.2 mL of chloroform. 0.1 mL of the resulting solution was spin-casted onto a silicon substrate at 2000 rpm for 45 seconds.

The model used to fit the data to yield the refractive index  $n$  describes the dielectric constant  $\varepsilon$  as a function of photon energy  $E$  and employs a series of harmonic oscillators (Equation 3.3). This treatment follows the guidance of Compoy-Quiles et al. in their analysis of polyfluorenes and assumes the casted film to be an isotropic layer.<sup>31</sup>

$$\varepsilon(E) = K + \sum_{j=1}^N A_j e^{i\phi_j} \left[ (E + E_{c_j} + i\Gamma_j)^{-1} - (E - E_{c_j} + i\Gamma_j)^{-1} \right]$$

**Equation 3.3**

Here,  $N$  is the number of oscillators that obey the model and, for this study,  $N = 7$ . This value of  $N$  is the sum of oscillators used to analyze individual polyfluorene-based analogs for **P1** (PFO) and **P2** (F8BT) by Compoy-Quiles et al.<sup>31</sup>  $A_j$  is the amplitude of an oscillator,  $\phi_j$  is the exciton phase,  $E_{c_j}$  is the corresponding center energy, and  $\Gamma_j$  represents the broadening. A constant  $K$  accounts for additional transitions in the ultraviolet region. The form of the dielectric function indicated by Equation 3.6<sup>43</sup> was used to fit the experimental data (Figures 3.8 and 3.9) by employing a Levenberg-Marquardt minimization algorithm. The fit additionally uses the film thickness of the blend measured via profilometry (i.e. 188.3 nm), which was kept fixed and not fitted by the algorithm. In the region of interest (i.e.  $\lambda = 400 - 800$  nm), the model (solid line) closely fits the experimental data (dashed line). The mean squared error of the fit is 11.54.

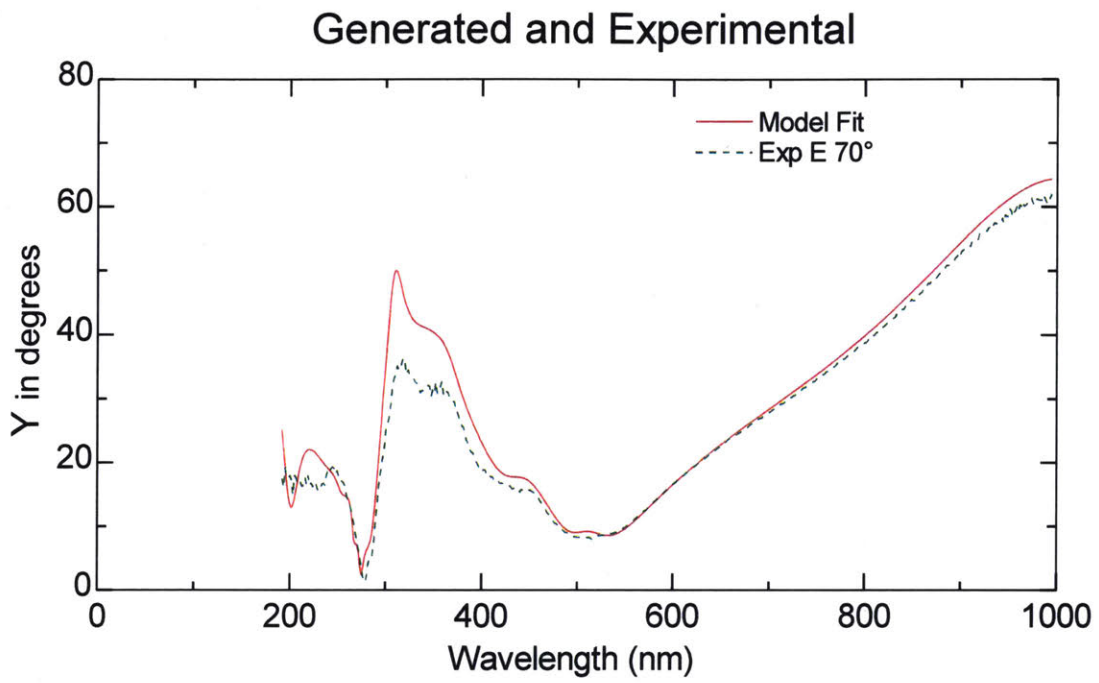


**Figure 3.8.** Ellipsometry data for the amplitude ratio  $\Psi$  (“Y”) and its model fit.

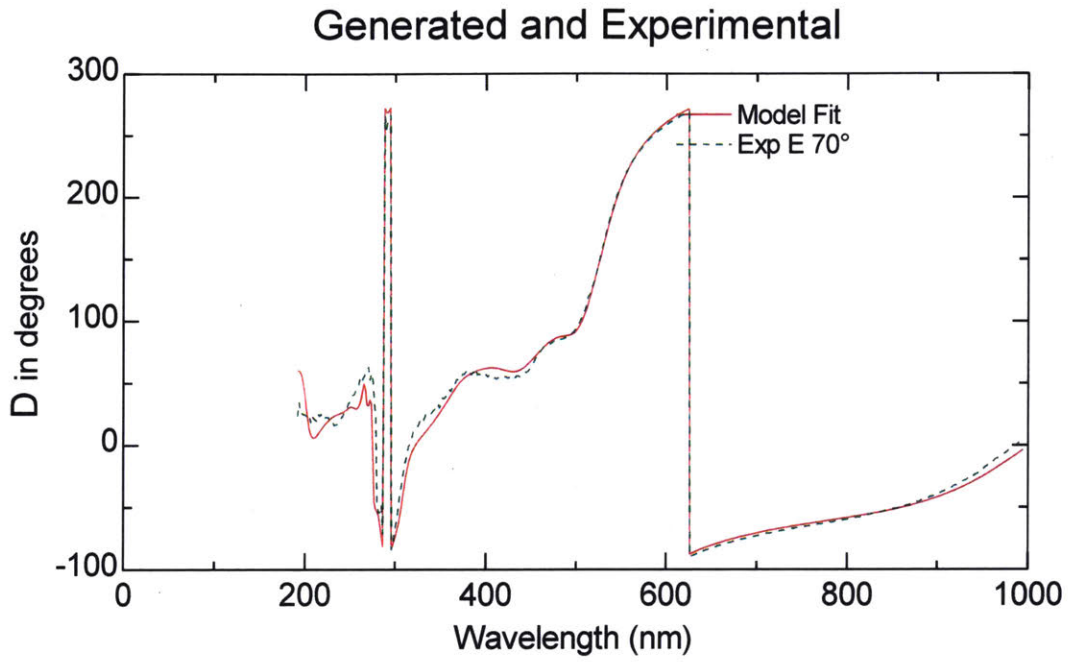


**Figure 3.9.** Ellipsometry data for the phase shift  $\Delta$  (“D”) and its model fit.

Parameter	Fitted Value
$K$	$2.2512 \pm 0.0264$
$\phi_1$	$5.3288 \pm 0.147$
$A_1$	$0.052294 \pm 0.00642$
$E_{c1}$	$2.4452 \pm 0.0115$
$\Gamma_1$	$0.21759 \pm 0.0209$
$\phi_2$	$-10.117 \pm 0.0164$
$A_2$	$3.6084 \pm 0.976$

$E_{c2}$	4.6051±0.00489
$\Gamma_2$	0.42278±0.135
$\phi_3$	-0.5264±0.239
$A_3$	0.091561±0.0219
$E_{c3}$	2.8239±0.035
$\Gamma_3$	0.34234±0.0708
$\phi_4$	-19.139±0.459
$A_4$	1.5969±0.752
$E_{c4}$	5.1561±0.221
$\Gamma_4$	1.2041±0.375
$\phi_5$	2.7043±0.858
$A_5$	0.40926±0.389
$E_{c5}$	4.1308±0.115
$\Gamma_5$	0.628±0.27
$\phi_6$	-0.59275±0.596
$A_6$	3.5452±1.92
$E_{c6}$	4.6408±0.0142
$\Gamma_6$	0.40098±0.154

$\phi_7$	-4.9983±2.61
$A_7$	0.33321±1.78
$Ec_7$	4.6212±0.0492
$\Gamma_7$	0.222±0.249

**Table 3.1.** Fitted parameters obtained for Equation 3.3 ( $N = 7$ ).

In addition to a plot of  $n$  with wavelength, the extinction coefficient  $k$ , the imaginary component of the complex refractive index  $\tilde{n}$  (i.e.  $\tilde{n}(\lambda) = n(\lambda) + ik(\lambda)$ ), was also obtained in the fitting process (Figure 3.10). The extinction coefficient  $k$  is an indication of the extent of absorption by the **P1:P2** layer per wavelength and thus bears resemblance to the absorption attributed to **P1** and **P2** in Figure 3.4a.



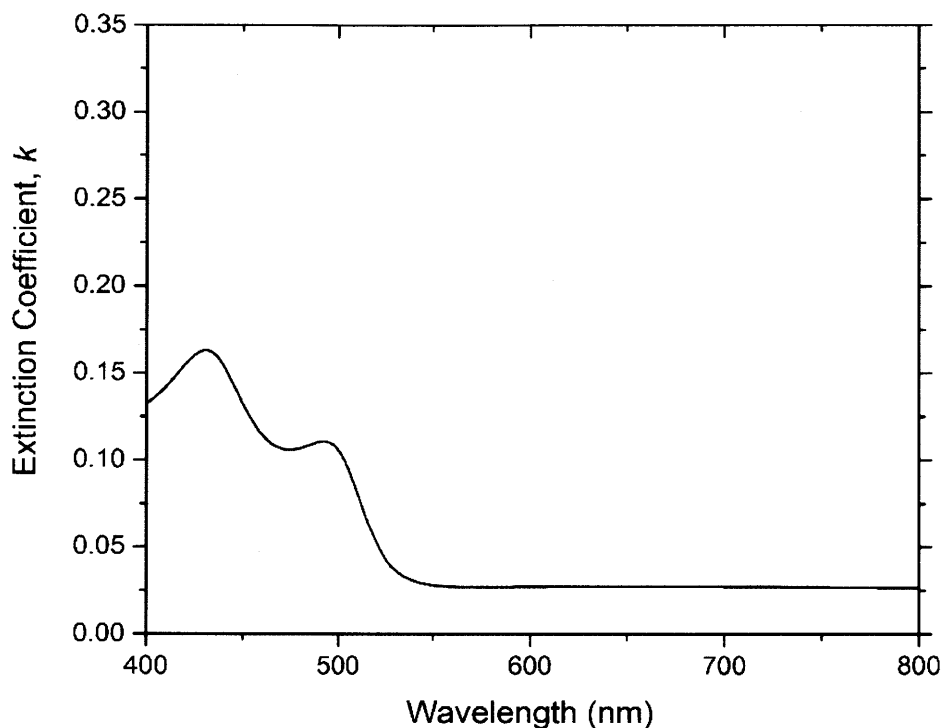


**Figure 3.10.** Profile of the extinction coefficient  $k$  of the analyzed blend composed of **P1** and **P2**.

**3.7.5 Details for Monte Carlo Simulation.** The Monte Carlo simulation was carried out using an implementation fully described in the supplementary information of a previous report.<sup>10</sup> Briefly, a photon with a specified wavelength was released into the LSC from the top and it was determined whether the photon was reflected and then whether it was absorbed. If it was absorbed, it was then determined whether the photon was re-emitted, and if so, it was given a wavelength sampled (from the photoluminescence spectrum) and a propagation length and direction. The photon was then allowed to propagate through the device until it was collected or lost. As inputs the program used the absorption and emission spectra of the composite and the refractive index, which, from the ellipsometry data, was approximated to be 1.7 for all wavelengths to simplify the analysis of the LSC by treating it as a symmetric slab waveguide. The slight refractive index difference between

the luminescent film and N-SF10 glass was assumed to not influence refractive-index dependent parameters, namely the Fresnel reflection coefficient and trapping efficiency.

To better assess the low reabsorption of the LSC, the absorption spectrum (Figure 3.3a) used was cut off and corrected at  $\lambda = 650$  nm due to a slight sinusoidal baseline drift between  $\lambda = 650$  nm to  $\lambda = 800$  nm that was attributed to thin film interference effects.<sup>44,45</sup> Past  $\lambda = 650$  nm, all absorbance values were manually set to  $1 \times 10^{-4}$ . This phenomenon manifests in a regime where no absorption by the LSC is expected and is post-reflection event that should have little to no relevance to the performance analysis.

Once the absorption spectrum was corrected, the photophysical spectra were plotted on a logarithmic scale to clearly view the low extent of reabsorption by the minority **Red 305** (Figure 3.11).

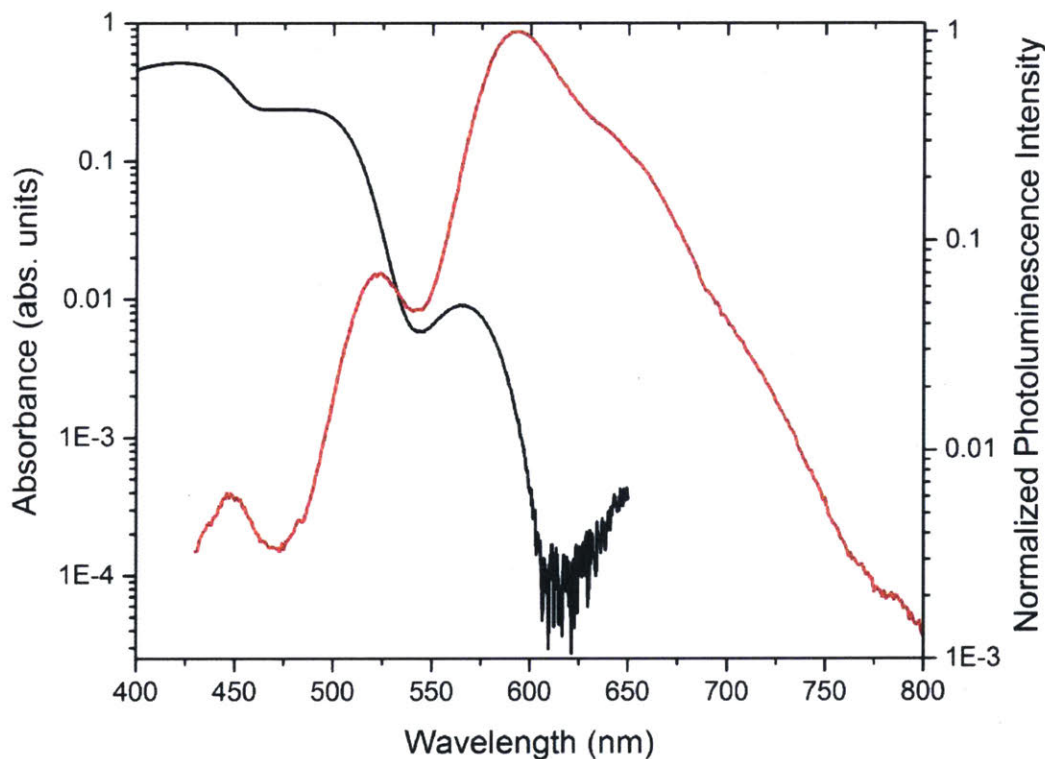


**Figure 3.11.** Absorption and emission spectra (logarithmic) of LSC1 after the specified baseline correction.

### 3.8 References

- (1) Rowan, B. C.; Wilson, L. R.; Richards, B. S. *IEEE J. Sel. Top. Quantum Electron.* **2008**, *14*, 1312–1322.
- (2) van Sark, W. G. J. H. M.; Barnham, K. W. J.; Slooff, L. H.; Chatten, A. J.; Büchtemann, A.; Meyer, A.; McCormack, S. J.; Koole, R.; Farrell, D. J.; Bose, R.; Bende, E. E.; Burgers, A. R.; Budel, T.; Quilitz, J.; Kennedy, M.; Meyer, T.; Donegá, C. D. M.; Meijerink, A.; Vanmaekelbergh, D. *Opt. Express* **2008**, *16*, 21773–21792.
- (3) Debije, M. G.; Verbunt, P. P. C. *Adv. Energy Mater.* **2012**, *2*, 12–35.
- (4) Selected examples of architectures: a) Batchelder, J. S.; Zewail, A. H.; Cole, T. *Appl. Opt.* **1981**, *20*, 3733–3754.; b) Sholin, V.; Olson, J. D.; Carter, S. A. *J. Appl. Phys.* **2007**, *101*, 123114; c) Slooff, L. H.; Bende, E. E.; Burgers, A. R.; Budel, T.; Pravettoni, M.; Kenny, R. P.; Dunlop, E. D.; Büchtemann, A. *Phys. Status Solidi RRL* **2008**, *2*, 257–259; d) Giebink, N. C.; Wiederrecht, G. P.; Wasielewski, M. R. *Nat. Photonics* **2011**, *5*, 694–701.
- (5) For an alternative approach, see: Yoon, J.; Li, L.; Semichaevsky, A. V.; Ryu, J. H.; Johnson, H. T.; Nuzzo, R. G.; Rogers, J. A. *Nat. Commun.* **2011**, *2*, 343.
- (6) ten Kate, O. M.; Hooning, K. M.; van der Kolk, E. *Appl. Opt.* **2014**, *53*, 5238–5245.
- (7) Würthner, F. *Chem. Commun.* **2004**, 1564–1579.
- (8) Benjamin, W. E.; Veit, D. R.; Perkins, M. J.; Bain, E.; Scharnhorst, K.; McDowall, S.; Patrick, D. L.; Gilbertson, J. D. *Chem. Mater.* **2014**, *26*, 1291–1293.

- (9) Wilson, L. R.; Rowan, B. C.; Robertson, N.; Moudam, O.; Jones, A. C.; Richards, B. S. *Appl. Opt.* **2010**, *49*, 1651–1661.
- (10) Coropceanu, I.; Bawendi, M. G. *Nano Lett.* **2014**, *14*, 4097–4101.
- (11) Meinardi, F.; Colombo, A.; Velizhanin, K. A.; Simonutti, R.; Lorenzon, M.; Beverina, L.; Viswanatha, R.; Klimov, V. I.; Brovelli, S. *Nat. Photonics* **2014**, *8*, 392–399.
- (12) Bradshaw, L. R.; Knowles, K. E.; McDowall, S.; Gamelin, D. R. *Nano Lett.* **2015**, *15*, 1315–1323.
- (13) Bronstein, N. D.; Li, L.; Xu, L.; Yao, Y.; Ferry, V. E.; Alivisatos, A. P.; Nuzzo, R. G. *ACS Nano* **2014**, *8*, 44–53.
- (14) Swartz, B. A.; Cole, T.; Zewail, A. H. *Opt. Lett.* **1977**, *1*, 73–75.
- (15) Bailey, S. T.; Lokey, G. E.; Hanes, M. S.; Shearer, J. D. M.; McLafferty, J. B.; Beaumont, G. T.; Baseler, T. T.; Layhue, J. M.; Broussard, D. R.; Zhang, Y.-Z.; B. P. Wittmershaus, B. P. *Sol. Energy Mater. Sol. Cells* **2007**, *91*, 67–75.
- (16) Bozdemir, O. A.; Erbas-Cakmak, S.; Ekiz, O. O.; Dana, A.; Akkaya, E. U. *Angew. Chem. Int. Ed.* **2011**, *50*, 10907–10912.
- (17) ter Schiphorst, J.; Kendhale, A. M.; Debije, M. G.; Menelaou, C.; Herz, L. M.; Schenning, A. P. J. *Chem. Mater.* **2014**, *26*, 3876–3878.
- (18) Tummeltshammer, C.; Taylor, A.; Kenyon, A. J.; Papakonstantinou, I. *J. Appl. Phys.* **2014**, *116*, 173103.
- (19) Currie, M. J.; Mapel, J. K.; Heidel, T. D.; Goffri, S.; Baldo, M. A. *Science* **2008**, *321*, 226–228.
- (20) Banal, J. L.; Ghiggino, K. P.; Wong, W. W. H. *Phys. Chem. Chem. Phys.* **2014**, *16*, 25358–25363.

- (21) Mulder, C. L.; Theogarajan, L.; Currie, M.; Mapel, J. K.; Baldo, M. A.; Vaughn, M.; Willard, P.; Bruce, B. D.; Moss, M. W.; McLain, C. E.; Morseman, J. P. *Adv. Mater.* **2009**, *21*, 3181–3185.
- (22) Swager, T. M.; Gil, C. J.; Wrighton, M. S. *J. Phys. Chem.* **1995**, *99*, 4886–4893.
- (23) Tian, Z.; Yu, J.; Wu, C.; Szymanski, C.; McNeill, J. *Nanoscale* **2010**, *2*, 1999–2011.
- (24) Levine, M.; Song, I.; Andrew, T. L.; Kooi, S. E.; Swager, T. M. *J. Polym. Sci., Part A: Polym. Chem.* **2010**, *48*, 3382–3391.
- (25) Anslyn, E. V.; Dougherty, D. A. *Modern Physical Organic Chemistry*; University Science Books: Sausalito, CA, 2006.
- (26) Jenekhe, S. A.; Osaheni, J. A. *Science* **1994**, *265*, 765–768.
- (27) Yang, J.-S.; Swager, T. M. *J. Am. Chem. Soc.* **1998**, *120*, 11864–11873.
- (28) Bouffard, J.; Swager, T. M. *Macromolecules* **2008**, *41*, 5559–5562.
- (29) Zhang, Y.; Yip, H.-L.; Acton, O.; Hau, S. K.; Huang, F.; Jen, A. K.-Y. *Chem. Mater.* **2009**, *21*, 2598–2600.
- (30) Ramsdale, C. M.; Greenham, N. C. *Adv. Mater.* **2002**, *14*, 212–215.
- (31) Campoy-Quiles, M.; Heliotis, G.; Xia, R.; Ariu, M.; Pintani, M.; Etchegoin, P.; Bradley, D. D. C. *Adv. Funct. Mater.* **2005**, *15*, 925–933.
- (32) Ramsdale, C. M.; Greenham, N. C. *J. Phys. D: Appl. Phys.* **2003**, *36*, L29–L34.
- (33) Long, T. M.; Swager, T. M. *J. Am. Chem. Soc.* **2003**, *125*, 14113–14119.
- (34) The absorption spectrum was corrected for minor thin film interference effects in the transparent region by correcting the baseline at  $\lambda = 650$  nm. Through this correction, a logarithmic view of the photophysical spectra reveals the measured absorbance at the

emission maximum ( $\lambda_{\text{ex}} = 594 \text{ nm}$ ) to be approximately 500 times smaller than that at the absorption maximum (Figure 3.9).

- (35) (a) Hsieh, B. R.; Yu, Y.; Forsythe, E. W.; Schaaf, G. M.; Field, W. A. *J. Am. Chem. Soc.* **1998**, *120*, 231–232. (b) Ego, C.; Marsitzky, D.; Becker, S.; Zhang, J.; Grimsdale, A. C.; Müllen, K.; MacKenzie, J. D.; Silva, C.; Friend, R. H. *J. Am. Chem. Soc.* **2003**, *125*, 437–443. (c) Kim, J.-S.; Friend, R. H.; Grizzi, I.; Burroughes, J. H. *Appl. Phys. Lett.* **2005**, *87*, 023506. (d) Cadby, A. J.; Dean, R.; Elliott, C.; Jones, R. A. L.; Fox, A. M.; Lidzey, D. G. *Adv. Mater.* **2007**, *19*, 107–111. e) Giovanella, U.; Botta, C.; Galeotti, F.; Vercelli, B.; Battiato, S.; Pasini, M. *J. Mater. Chem. C* **2013**, *1*, 5322–5329.
- (36) Erickson, C. S.; Bradshaw, L. R.; McDowall, S.; Gilbertson, J. D.; Gamelin, D. R.; Patrick, D. L. *ACS Nano* **2014**, *8*, 3461–3467.
- (37) (a) Chappell, J.; Lidzey, D. J. *J. Microsc.* **2003**, *209*, 188–193. (b) Chou, H.-L.; Hsu, S.-Y.; Wei, P.-K. *Polymer* **2005**, *46*, 4967–4970.
- (38) Melhuish, W. H. *J. Opt. Soc. Am.* **1964**, *52*, 183–186.
- (39) Fu, P. P.; Harvey, R. G. *J. Org. Chem.* **1977**, *42*, 2407–2410.
- (40) Nesterov, E. E.; Zhu, Z.; Swager, T. M. *J. Am. Chem. Soc.* **2005**, *127*, 10083–10088.
- (41) A slight, but noticeable downfield offset in the chemical shifts was observed in the  $^1\text{H}$  NMR spectrum with increasing concentration of **1**. Both  $^1\text{H}$  and  $^{13}\text{C}$  NMR spectra are reported for a 20 mg/mL of **1** solution in  $\text{CDCl}_3$ .
- (42) Nagarjuna, G.; Kokil, A.; Kumar, J.; Venkataraman, D. *J. Mater. Chem.* **2012**, *22*, 16091–16094.
- (43) Terry, F. L. *J. Appl. Phys.* **1991**, *70*, 409–417.
- (44) Burns, S. E.; Greenham, N. C.; Friend, R. H. *Synth. Met.* **1996**, *76*, 205–208.

(45) Wan, W. M. V.; Friend, R. H.; Greenham, N. C.; *Thin Solid Films* **2000**, *363*, 310–313.

## Appendix for Chapter 3

### $^1\text{H}$ and $^{13}\text{C}$ NMR Spectra

Partially adapted from:

Gutierrez, G. D.; Coropceanu, I.; Bawendi, M. G.; Swager, T. M. "A Low Reabsorbing Luminescent Solar Concentrator Employing  $\pi$ -Conjugated Polymers." *Adv. Mater.* **2016**, 28,497–501.

Reproduced with permission. Copyright 2015 Wiley-VCH Verlag GmbH & Co. KGaA



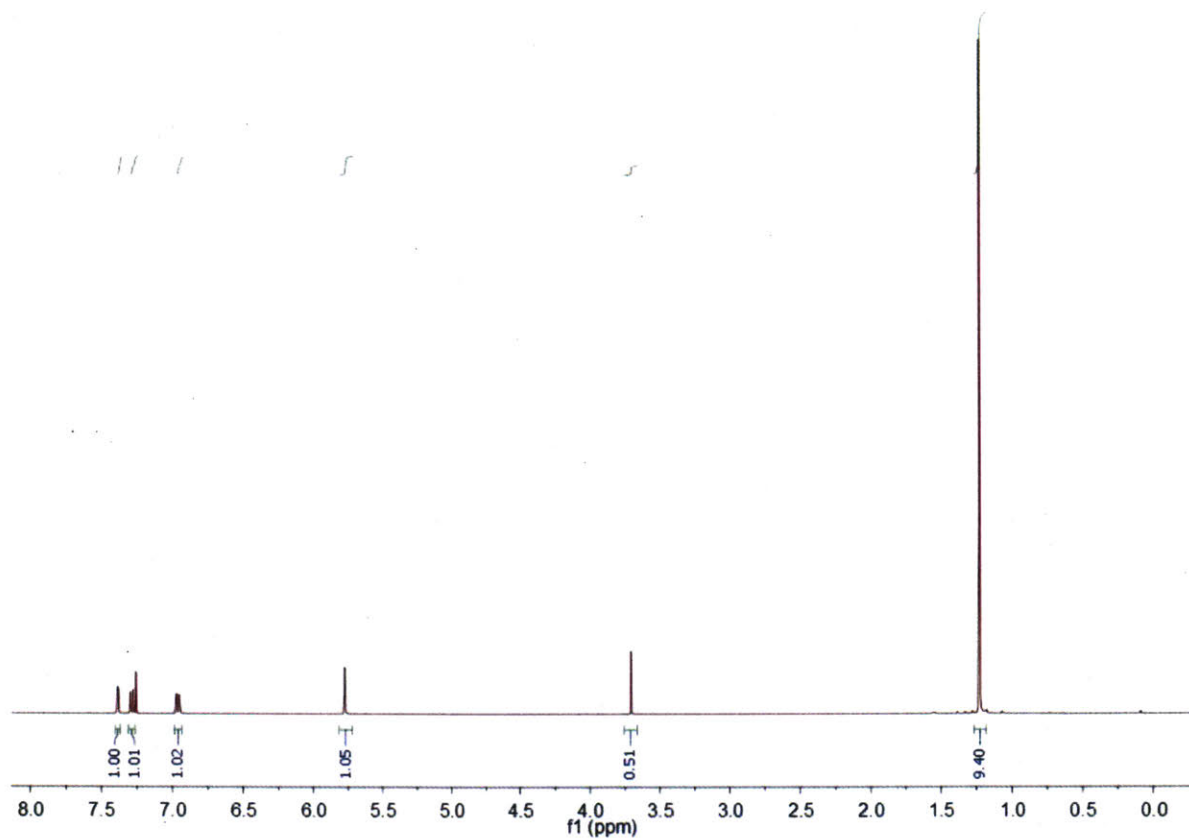


**Figure A.3.1.**  $^1\text{H}$  NMR spectrum of **1** (400 MHz,  $\text{CDCl}_3$ ).

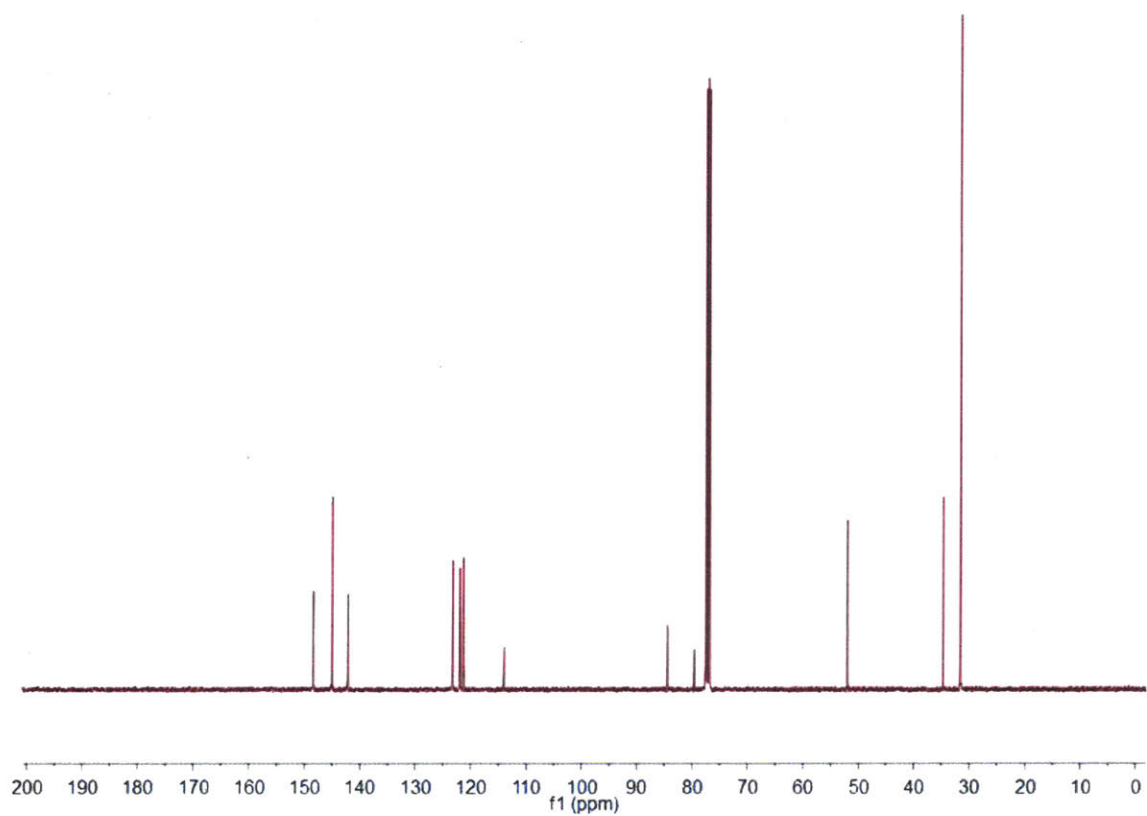


**Figure A.3.2.**  $^{13}\text{C}$  NMR spectrum of **1** (101 MHz,  $\text{CDCl}_3$ ).

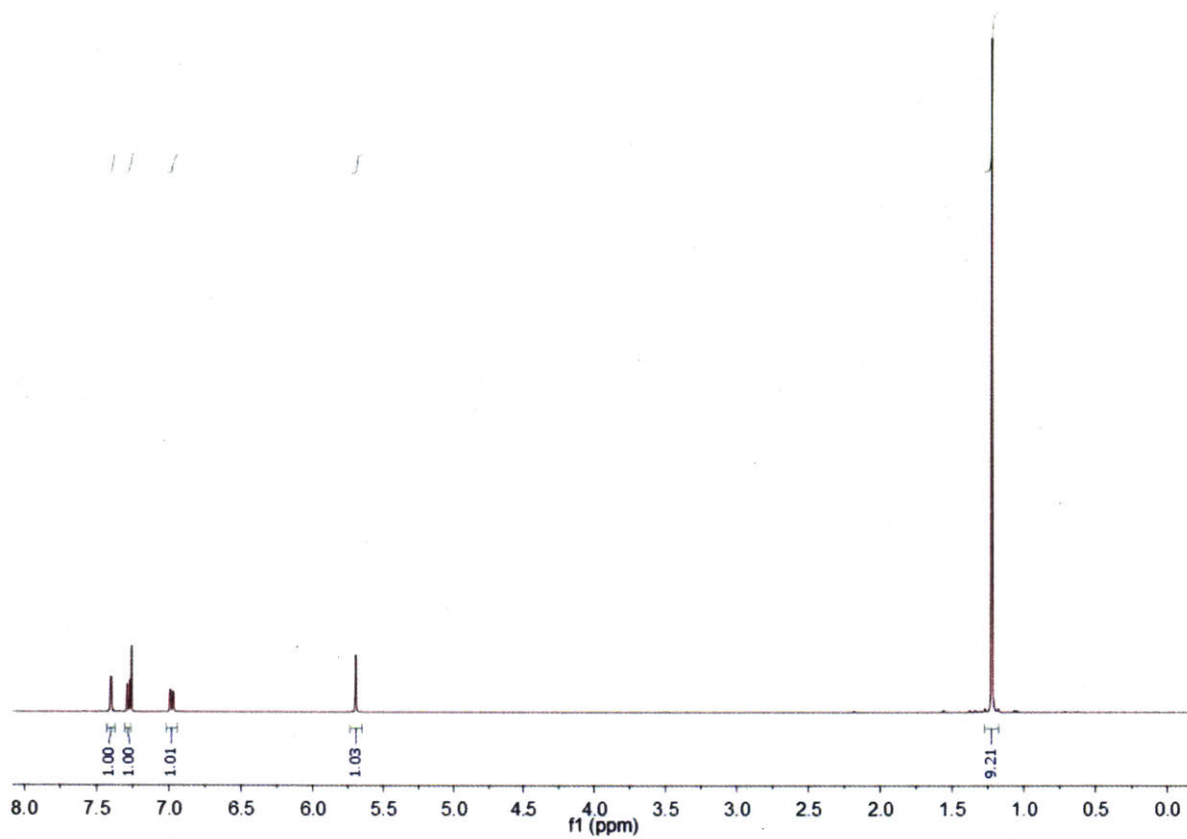


**Figure A.3.3.**  $^1\text{H}$  NMR spectrum of **2** (400 MHz,  $\text{CDCl}_3$ ).

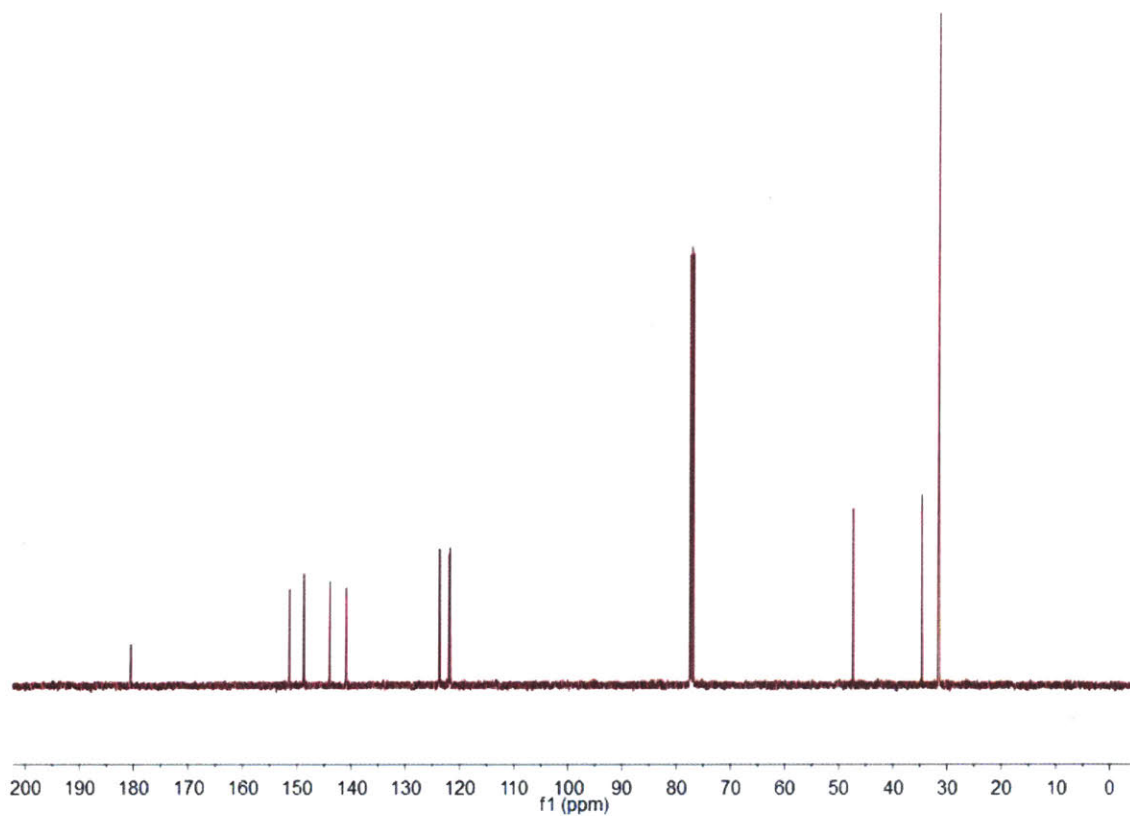


**Figure A.3.4.**  $^{13}\text{C}$  NMR spectrum of **2** (101 MHz,  $\text{CDCl}_3$ ).

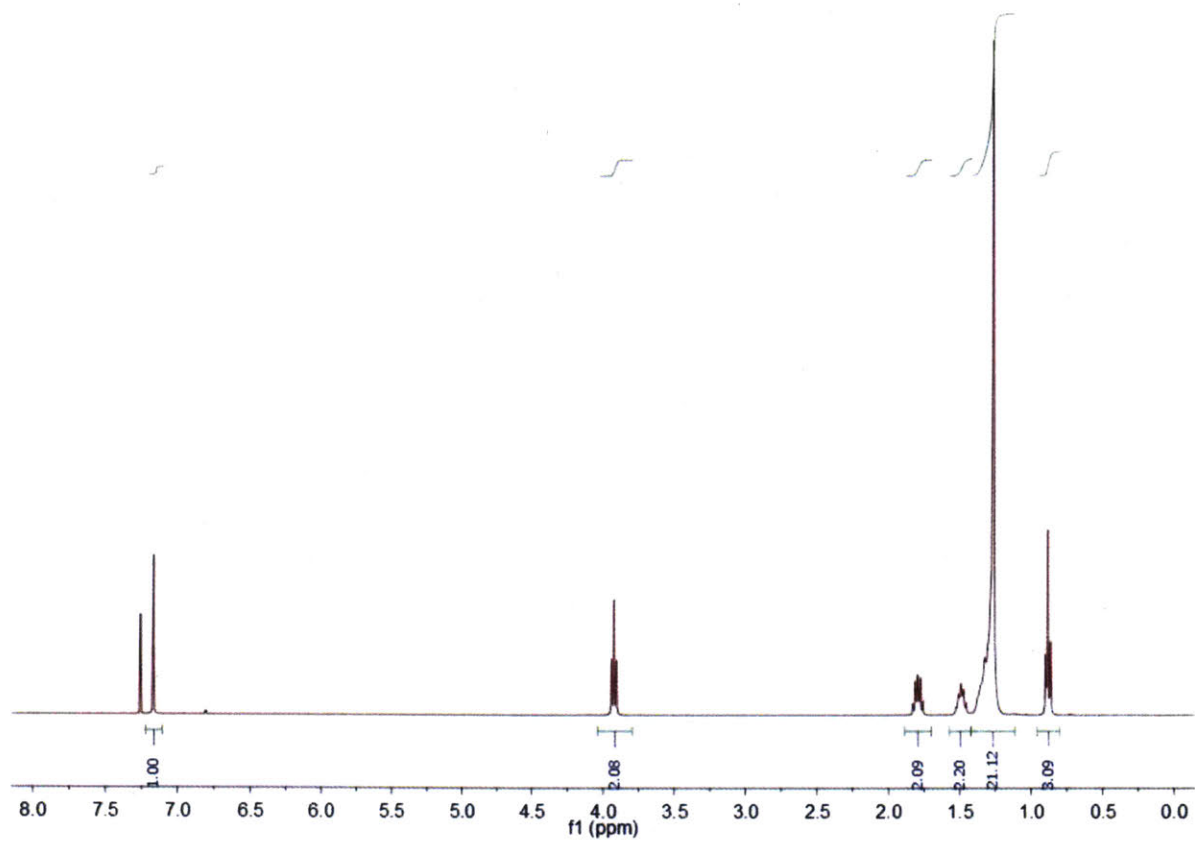
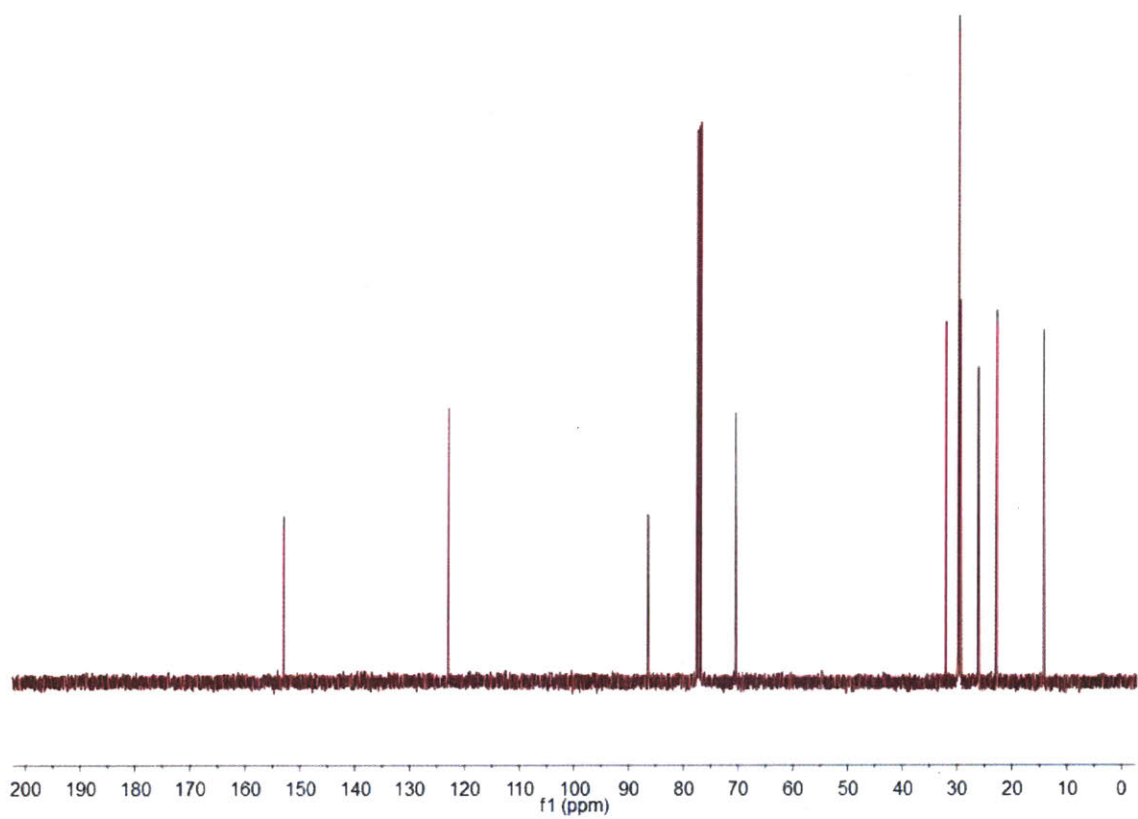
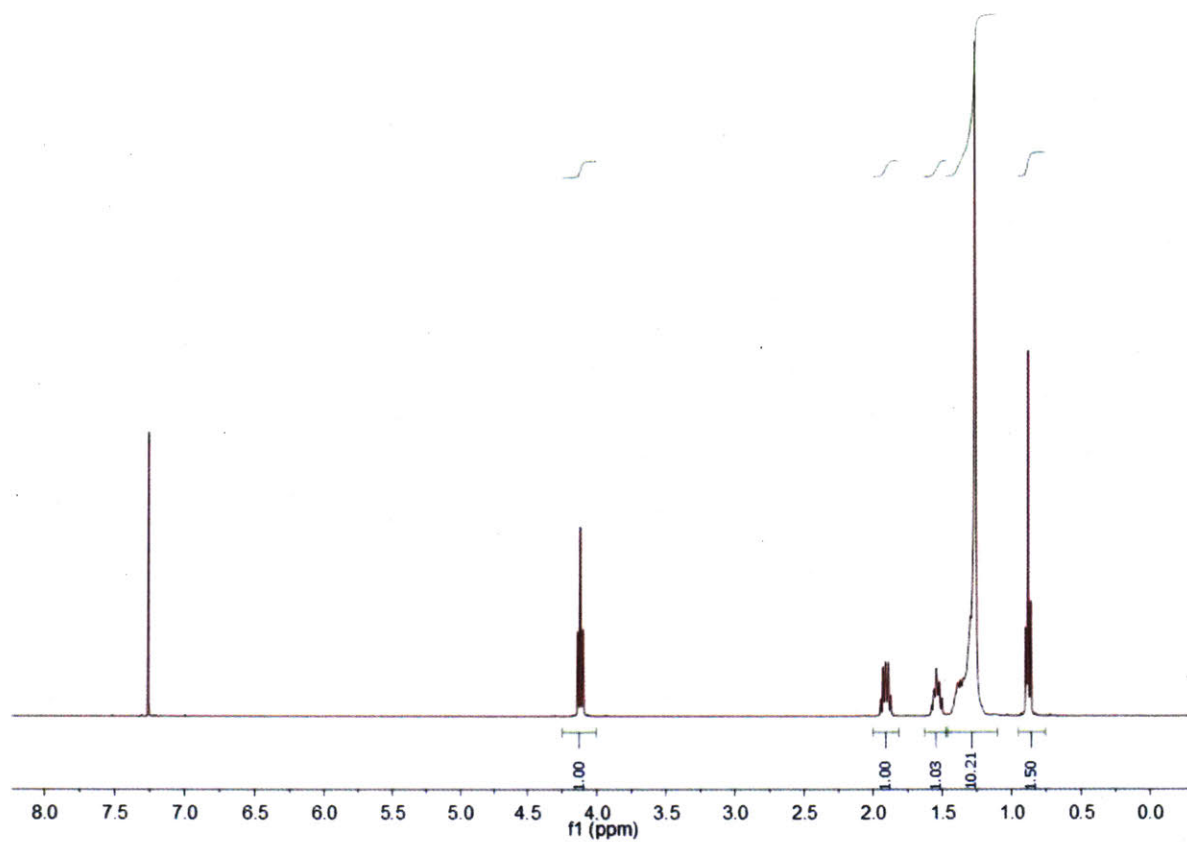


Figure A.3.5.  $^1\text{H}$  NMR spectrum of **5** (400 MHz,  $\text{CDCl}_3$ ).



**Figure A.3.6.**  $^{13}\text{C}$  NMR spectrum of **5** (101 MHz,  $\text{CDCl}_3$ ).



**Figure A.3.7.**  $^1\text{H}$  NMR spectrum of **7** (400 MHz,  $\text{CDCl}_3$ ).

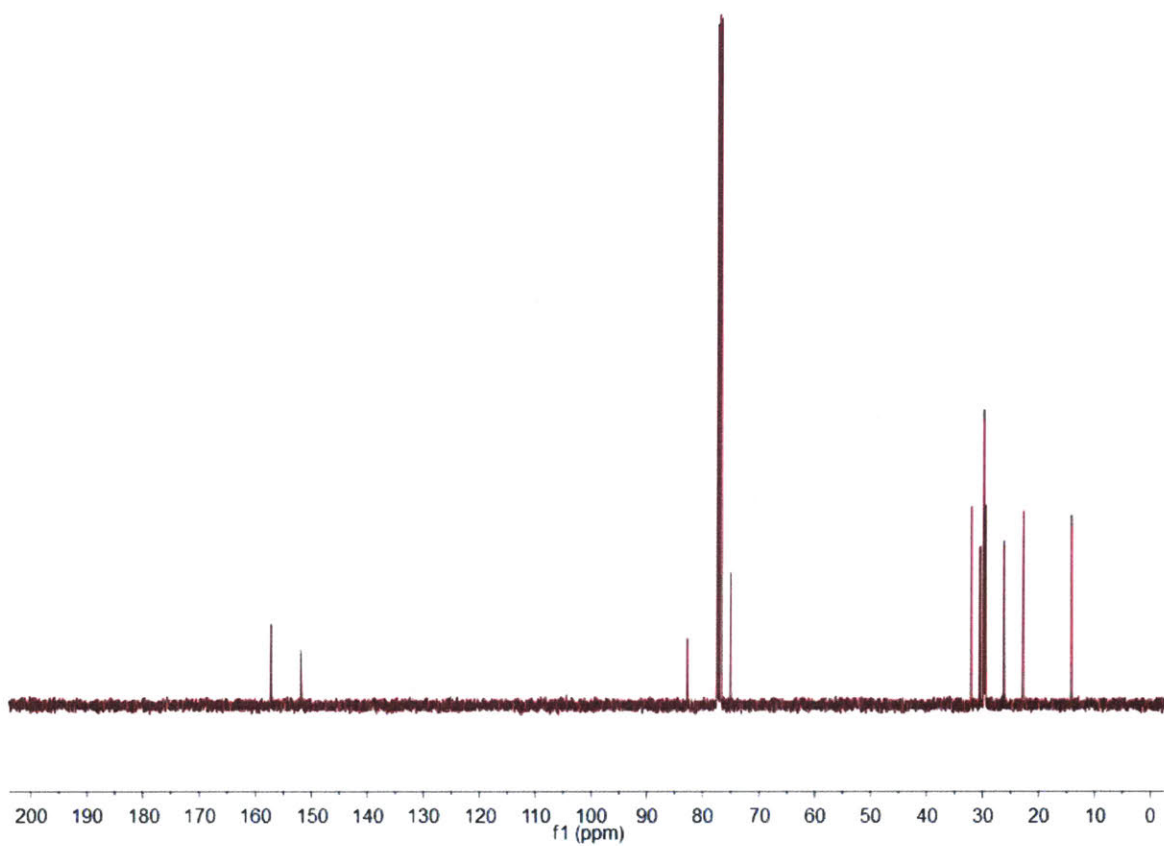


**Figure A.3.8.**  $^{13}\text{C}$  NMR spectrum of **7** (101 MHz,  $\text{CDCl}_3$ ).



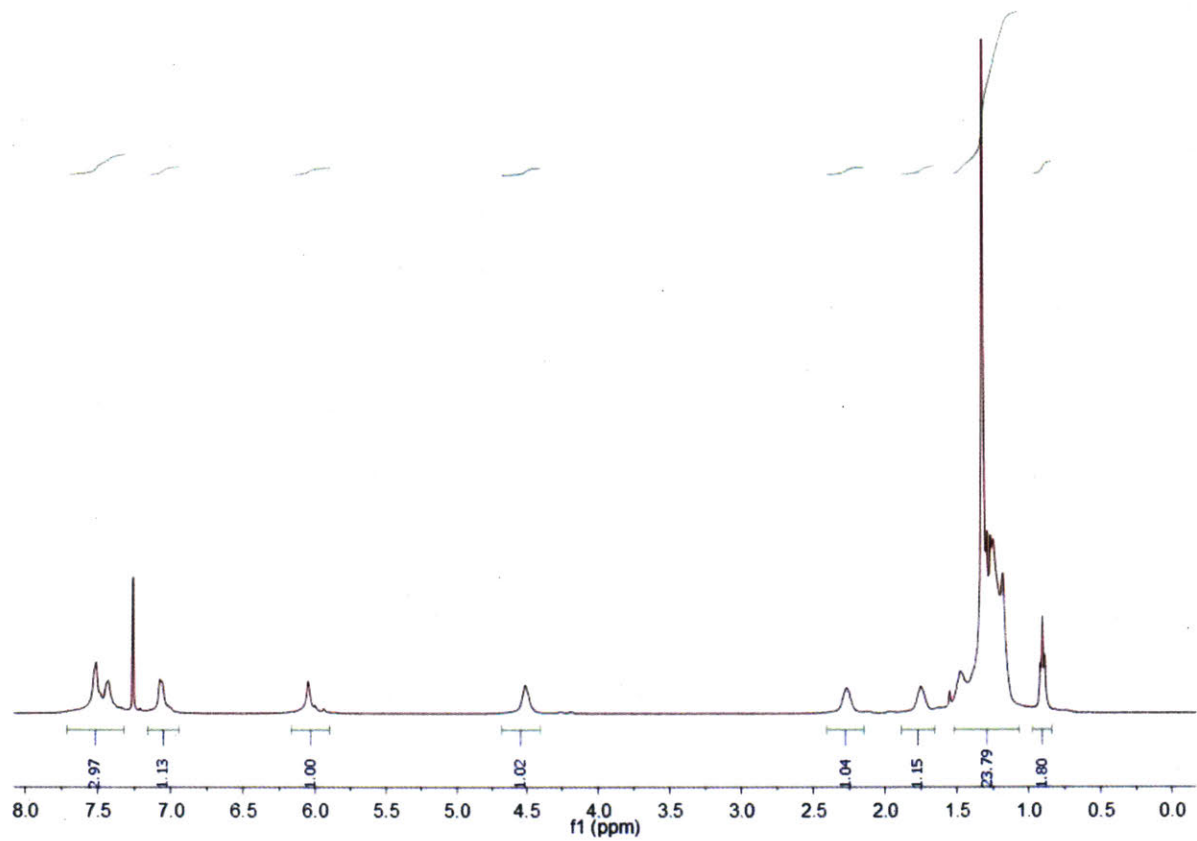


**Figure A.3.9.**  $^1\text{H}$  NMR spectrum of P1 (400 MHz,  $\text{CDCl}_3$ ).

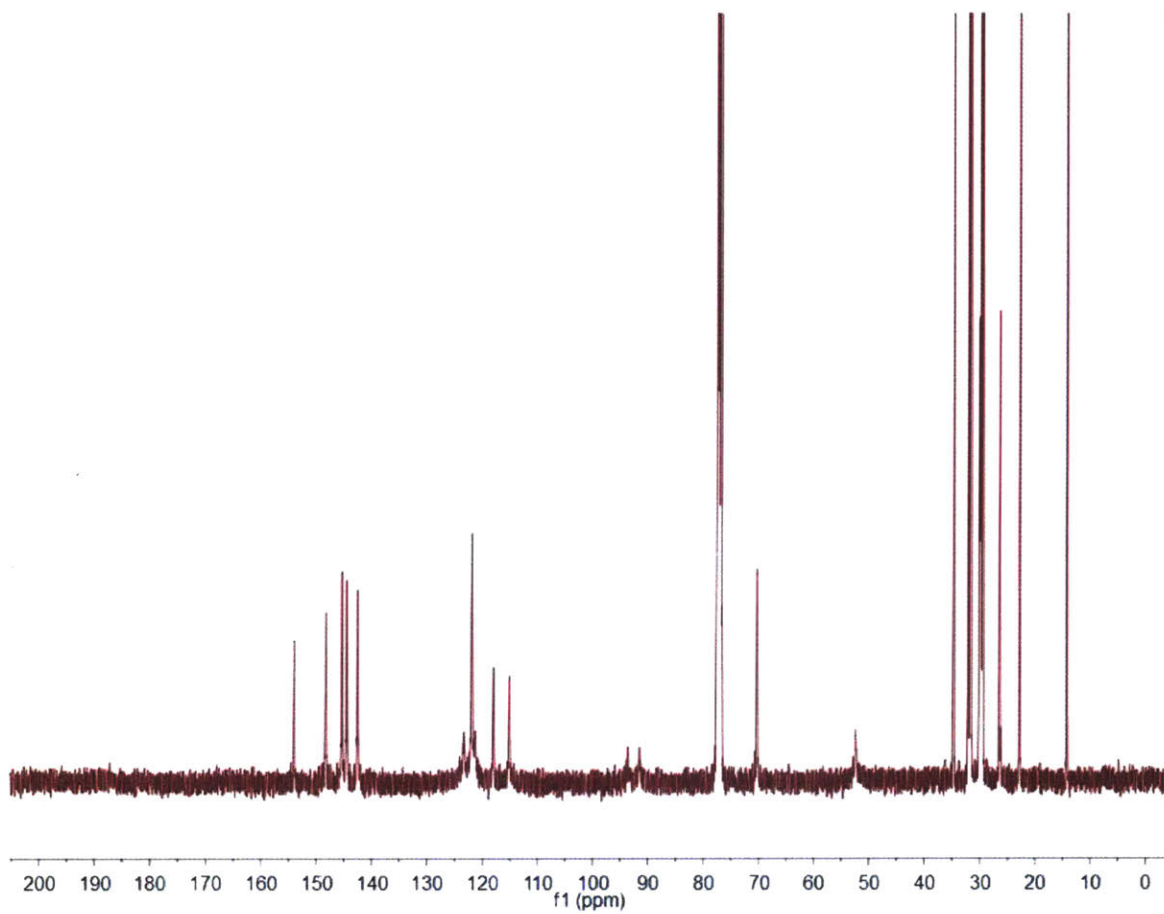


**Figure A.3.10.**  $^{13}\text{C}$  NMR spectrum of **P1** (101 MHz,  $\text{CDCl}_3$ ).

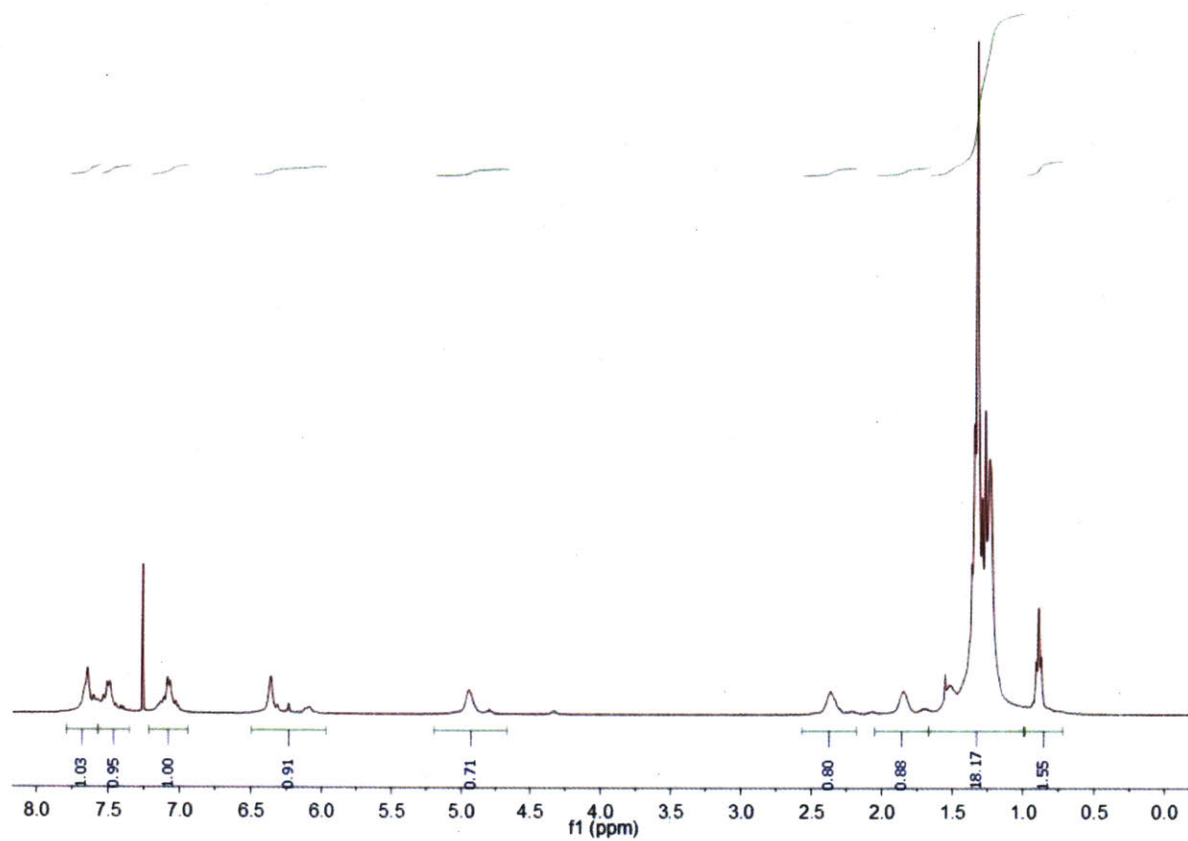


**Figure A.3.11.**  $^1\text{H}$  NMR spectrum of P2 (400 MHz,  $\text{CDCl}_3$ ).

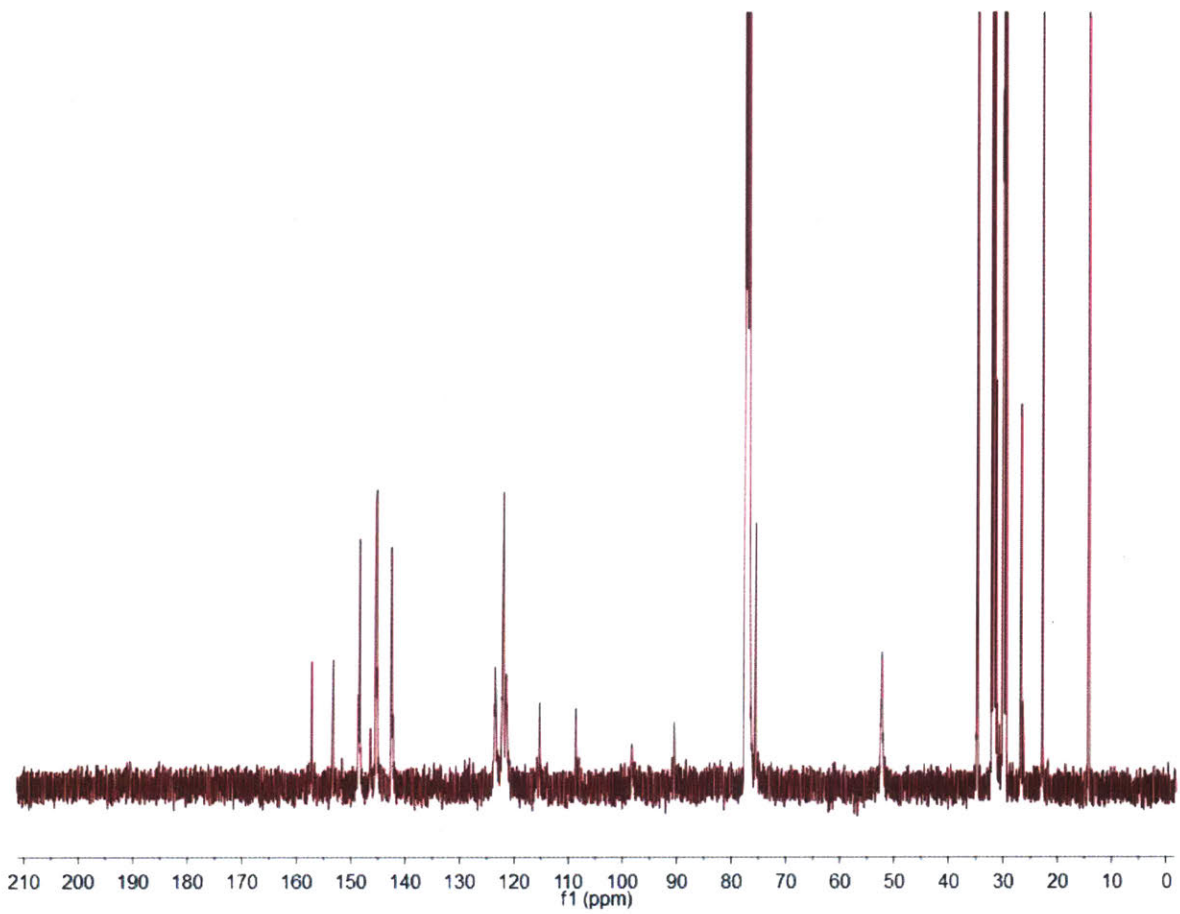


**Figure A.3.12.**  $^{13}\text{C}$  NMR spectrum of **P2** (101 MHz,  $\text{CDCl}_3$ ).

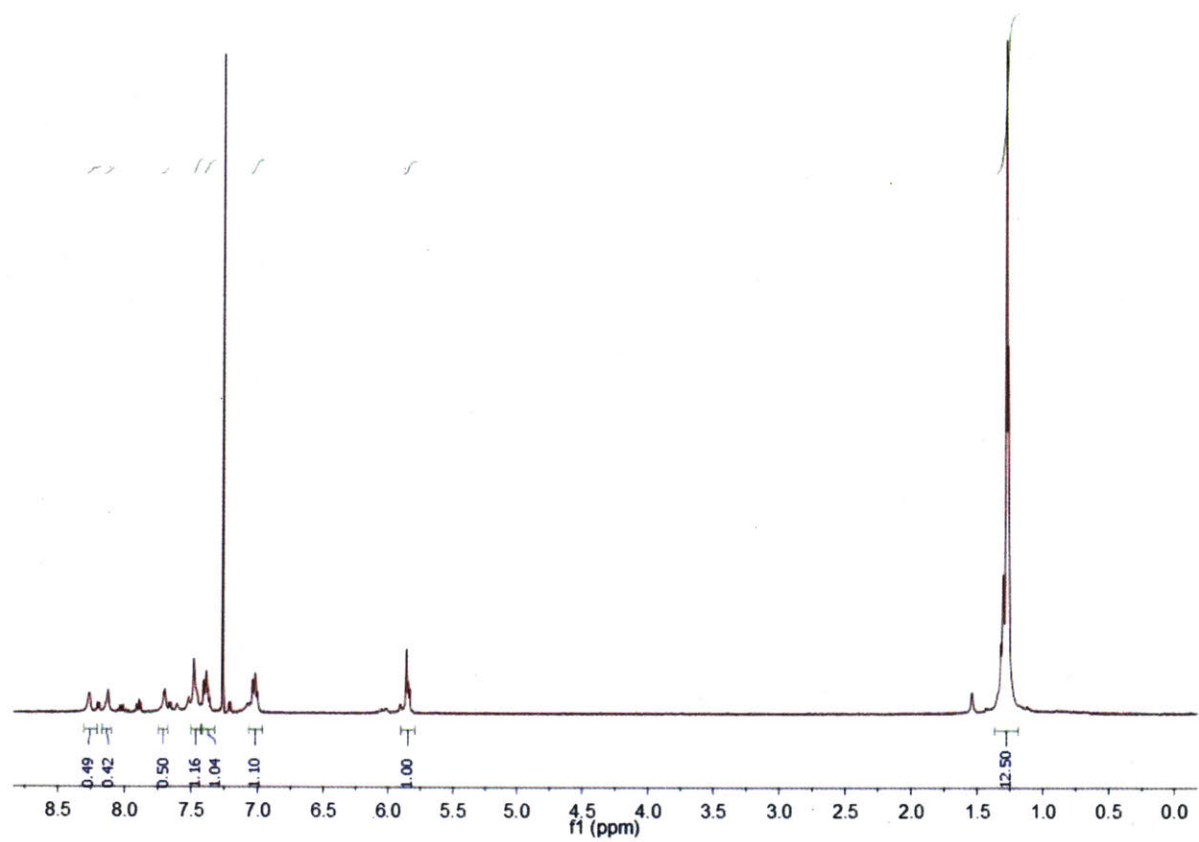


**Figure A.3.13.**  $^1\text{H}$  NMR spectrum of P3 (400 MHz,  $\text{CDCl}_3$ ).

## **Chapter 4**

# **The Fluorofluorescent Solar Concentrator**

This work was performed in collaboration with Dr. Joseph J. Walsh (Chemistry, MIT: assistance with solar concentrator construction) and Dr. Graham T. Sazama (Chemistry, MIT: computations).

#### 4.1 Introduction

In Chapters 1 and 3, we discussed the luminescent solar concentrator (LSC) as a promising technology capable of expanding the options by which solar cells can be incorporated into buildings at low costs. The LSC generally consists of an inexpensive transparent plastic or glass slab containing small amounts of one or more photoluminescent species.<sup>1</sup> Sunlight absorbed by the luminophores is converted to photoluminescence that is subsequently concentrated toward much smaller photovoltaic (PV) cells attached at the edges of the LSC through total internal reflection. As a transparent waveguide, an LSC can act as a functional window capable of facilitating the self-sustainability of an edifice, residence, or public structure. However, in the event the photoluminescent system degrades due to constant exposure to sunlight, the entire LSC must be removed and replaced, causing inconvenient and costly disruption to infrastructure. One way to construct an LSC that permits facile removal of photobleached luminophores is to dissolve them within an optically clear liquid solution that is encapsulated between two blank plastic or glass slabs. In this configuration, the solution can be readily drained out of the LSC and replaced at any time. Additionally, any solvent can be recovered via distillation for future use, thus minimizing waste. Despite the promise of this architecture, few examples of such an LSC employing replaceable media such as organic solvents<sup>2</sup> or liquid polymers<sup>3,4</sup> are reported.

We envisioned using liquid perfluorocarbons (PFCs) as an alternative and advantageous type of solvent within this proposed LSC. PFCs are commercially available materials that usually exhibit no odor, flammability, nor toxicity<sup>5</sup> and therefore suitable for widespread use. Furthermore, due to the low polarizability of fluorine, PFCs often possess low refractive indices that will permit efficient coupling of the luminophore's emission into the higher-index outer slabs. In such a case, the critical angle for total internal reflection  $\theta_c$  (Equation 4.1, cf. Equation 1.4) is undefined since

the refractive index of the outer slabs ( $n_{slab}$ ) is greater than that of the encapsulated solvent ( $n_{solv}$ ), causing all waveguided light to become quickly trapped in the slabs.

$$\theta_c = \sin^{-1} \left( \frac{n_{slab}}{n_{solv}} \right)$$

#### Equation 4.1

We hypothesized that this mismatch in refractive indices will subsequently prevent the waveguided emission from reentering the solution, thus circumventing any non-radiative reabsorption that will severely undermine the LSC's ability to concentrate light on larger scales (Figure 4.1).<sup>6</sup> While the use of a lower-index solid-state host for coupling luminophore emission into relatively expensive higher-index substrates is reported,<sup>7,8</sup> the concept has not yet been extended to low-index liquid solutions using conventional and inexpensive plastics, such as poly(methyl methacrylate) (PMMA), as the primary waveguide.

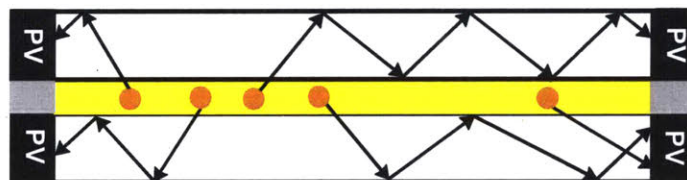


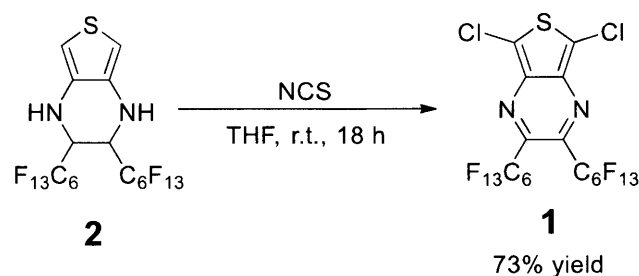
**Figure 4.1.** Cross-sectional illustration of an LSC utilizing the emission of a luminophore (orange dots) dissolved in a liquid PFC (yellow layer) to power PV devices at the edges of two transparent plastic or glass sheets.

Following the schematic in Figure 4.1, we herein describe the fluorofluorescent solar concentrator (FSC), an LSC utilizing an encapsulated solution of a highly emissive organic luminophore dissolved in Fluorinert FC-770, a commercially available liquid PFC with a refractive index of 1.27.<sup>9</sup>



## 4.2 Synthesis of a Highly Emissive Perfluoroalkylated Organic Dye

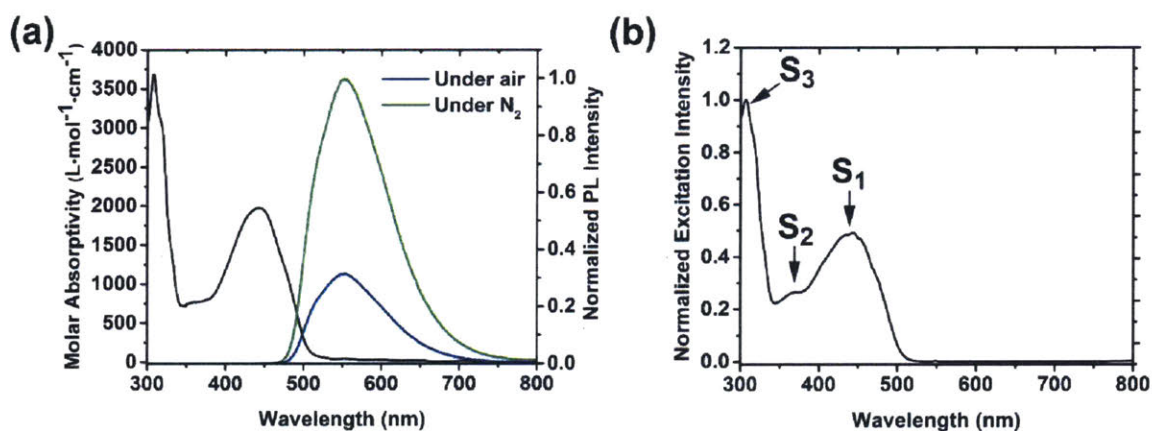
To account for the tendency of PFCs to resist mixing with non-fluorinated materials (the “fluorous effect”),<sup>10</sup> any luminophores applied in the FSC should possess significant fluorine content to be fully dissolved in FC-770. Our laboratory<sup>11,12</sup> and others<sup>13</sup> have demonstrated that organic molecules can be solubilized in PFCs by functionalizing them with perfluorinated alkyl chains. We particularly focused our attention on perfluoroalkylated thieno[3,4-*b*]pyrazine **1** (Scheme 4.1). **1** was synthesized via oxidative aromatization of a bis(perfluorohexyl)tetrahydrothieno[3,4-*b*]pyrazine **2** with *N*-chlorosuccinimide (NCS) in THF. The reaction results in good yield (73%) and is readily performed on gram-scales.



**Scheme 4.1.** Synthesis of perfluoroalkylated thieno[3,4-*b*]pyrazine **1**.

Compound **1** is a fluorescent dye that demonstrates excellent solubility in FC-770. The photophysical properties of **1** in FC-770 at room temperature are shown in Figure 4.2. Within the visible spectrum, the dye absorbs with  $\lambda_{\text{max}} = 442$  nm and produces yellow-green photoluminescence centered at  $\lambda_{\text{max}} = 550$  nm (Figure 4.2a). The corresponding fluorescence quantum yield ( $\Phi_F$ ) of under aerobic conditions is 30%. Surprisingly, however,  $\Phi_F$  approximately triples to 91% when the solution is deoxygenated with  $\text{N}_2$  gas. We found the fluorescence lifetime ( $\tau_F$ ) of **1** in FC-770 under air to be 30 ns via frequency modulation of the molecule’s photoluminescence against a standard. When the solution is deoxygenated with  $\text{N}_2$  gas,  $\tau_F$  changes

to 93 ns and consistently matches the same three-fold increase in  $\Phi_F$ , thus suggesting that photoluminescence quenching by oxygen is occurring. Time-dependent density functional theory (TD-DFT) calculations were employed to better understand the electronic excited states of the dye. Computations (see Appendix II for Chapter 4) performed on the simpler trifluoromethylated analog of **1** (“**1-CF<sub>3</sub>**”) suggest that the first three excited singlet states ( $S_1$ ,  $S_2$ , and  $S_3$ ) correspond to the bands labeled in the excitation spectrum of **1** shown in Figure 4.2b. Assuming Kasha’s rule applies, these calculations also suggest that the observed lifetimes are relatively long due to the position of the transition dipole moment associated with  $S_1$  (Figure 4.2c). With this transition dipole lying along the short axis of the molecule,  $S_1$  inherently possesses a relatively low oscillator strength ( $f_{osc} \approx 0.07$ ), which often corresponds to a larger fluorescence lifetime.<sup>14</sup> The low oscillator strength is also evident from the low extinction coefficients associated with the  $S_1$  transition (i.e. across  $\lambda \sim 400$  nm–525 nm).



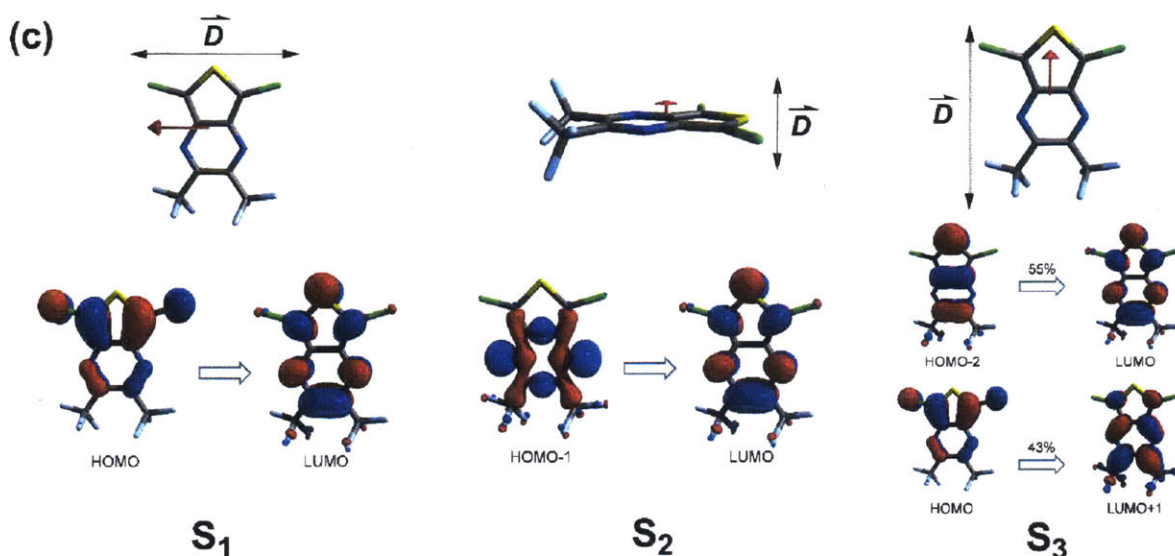


**Figure 4.2.** Photophysical spectra and computations for compound **1**. (a) Absorption spectrum and photoluminescence spectra under air and nitrogen ( $\lambda_{\text{ex}} = 420$  nm). (b) Excitation spectrum of **1** (monitored  $\lambda_{\text{em}} = 550$  nm) with corresponding electronic transitions as suggested by TD-DFT calculations from trifluoromethylated derivative **1-CF<sub>3</sub>**. (c) Transition dipole moments ( $\vec{D}$ ) and Kohn-Sham molecular orbitals for  $S_1$ ,  $S_2$ , and  $S_3$ .

#### 4.3 Construction and Characterization of the Fluorofluorescent Solar Concentrator

To construct the FSC, which is hereafter named **FSC1** (Figure 4.3), a PMMA frame (outer dimensions: 3 cm x 24 cm x 0.5 cm, inner dimensions: 1 cm x 22 cm x 0.2 cm) was glued between two blank sheets of PMMA (3 cm x 12 cm x 0.6 cm) with acrylic cement. One of the outer sheets contains a 0.6 cm hole surrounded by a small gasket to allow for loading of the luminescent solution into the confined frame. A deoxygenated solution of **1** in FC-770 was subsequently added to the enclosure and sealed with a rubber septum in a  $\text{N}_2$ -filled glovebox. The concentration of dye employed (1.7 mM) corresponds to an optical density of 1 at  $\lambda_{\text{max}} = 442$  nm. PMMA was also found to be resistant to any dissolution by FC-770.

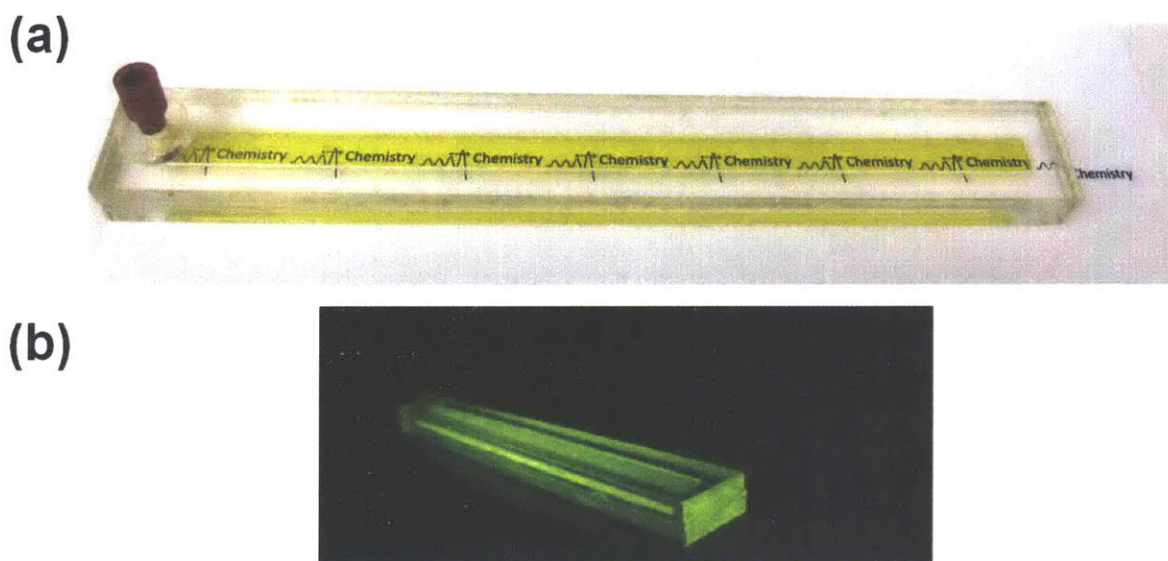


**Figure 4.3.** FSC1 under (a) ambient and (b) ultraviolet ( $\lambda = 365$  nm) lighting.

We next evaluated the performance of FSC1 by moving an excitation source across one of its faces and concurrently monitoring the photoluminescence that reaches one of the short edges with a fiber optic probe coupled to a spectrofluorometer. Through these measurements, we aimed to obtain a portrait of how non-radiative reabsorption affects photoluminescence that waveguides into the outer PMMA edges as the distance between the excitation source and edge ( $d$ ) changes. We first monitored the edge emission that arises only from the center of the edge (i.e. the edge of the enclosed frame containing the luminescent solution) by placing the probe directly in front of this region and blocking the outer edges with electrical tape. We hypothesized that the output that escapes through this portion of the edge is primarily composed of any emission that did not waveguide into the edges and instead travels directly through the PFC solution and thus subject to reabsorption. (Figure 4.4a). Upon monitoring the edge output with excitation distance, we observe not only a decrease in the overall emission intensity (Figure 4.4b) as well as gradual narrowing of

the emission band of **1** (Figure 4.4c) with increasing  $d$ , both of which are characteristic indications of non-radiative reabsorption.

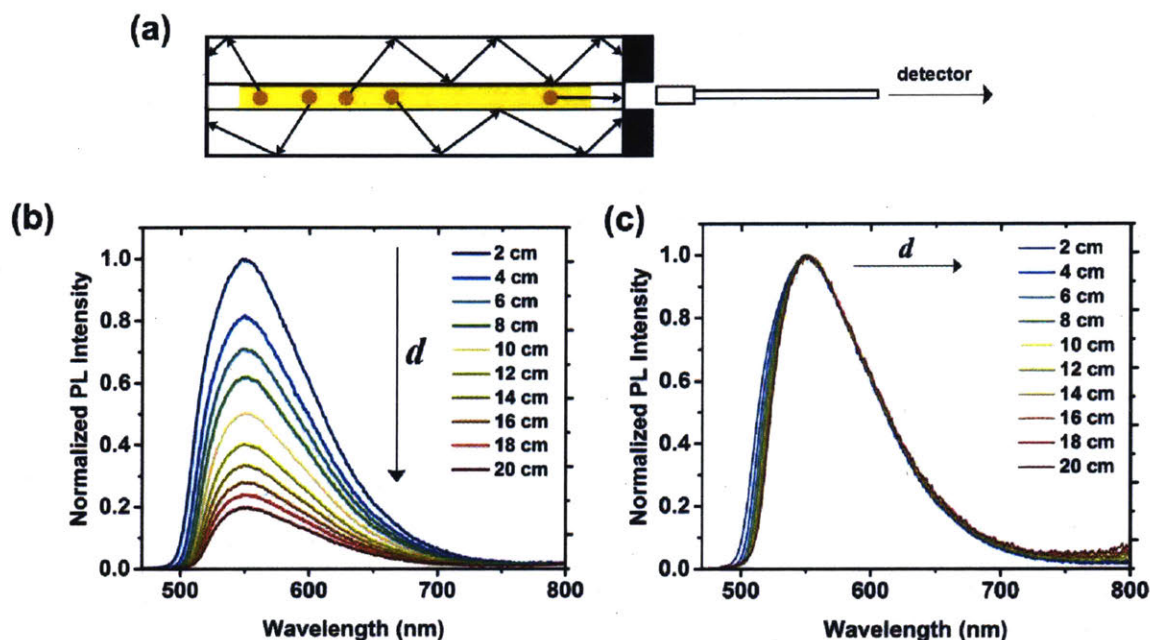


**Figure 4.4.** Distant-dependent excitation studies of FSC1. (a) Illustration of detection method from edge of central frame. (b) Photoluminescence output as a function of the excitation distance  $d$ . (c) The same outputs presented in Figure 4.4b, but each normalized to their own data sets to depict how the emission is affected by non-radiative reabsorption by traveling directly through the luminescent solution.

However, when the photoluminescence output of an outer edge is exclusively examined (Figure 4.5a), there is no indication of band narrowing (Figure 4.5c) as the excitation source moves farther from the edge, which supports our primary hypothesis that any photoluminescence that refracts into the PMMA sheets is trapped in the outer PMMA sheets and consequently circumvents any non-radiative reabsorption that is only possible in the fluorocarbon solution. Interestingly, we also observe an increase in the emission intensity from the outer edge as  $d$  increases, which is

likely due to the ability of the luminophore's emission to “spread out” into the PMMA layers rather than travel through the luminescent solution to the center edge (Figure 4.5b).

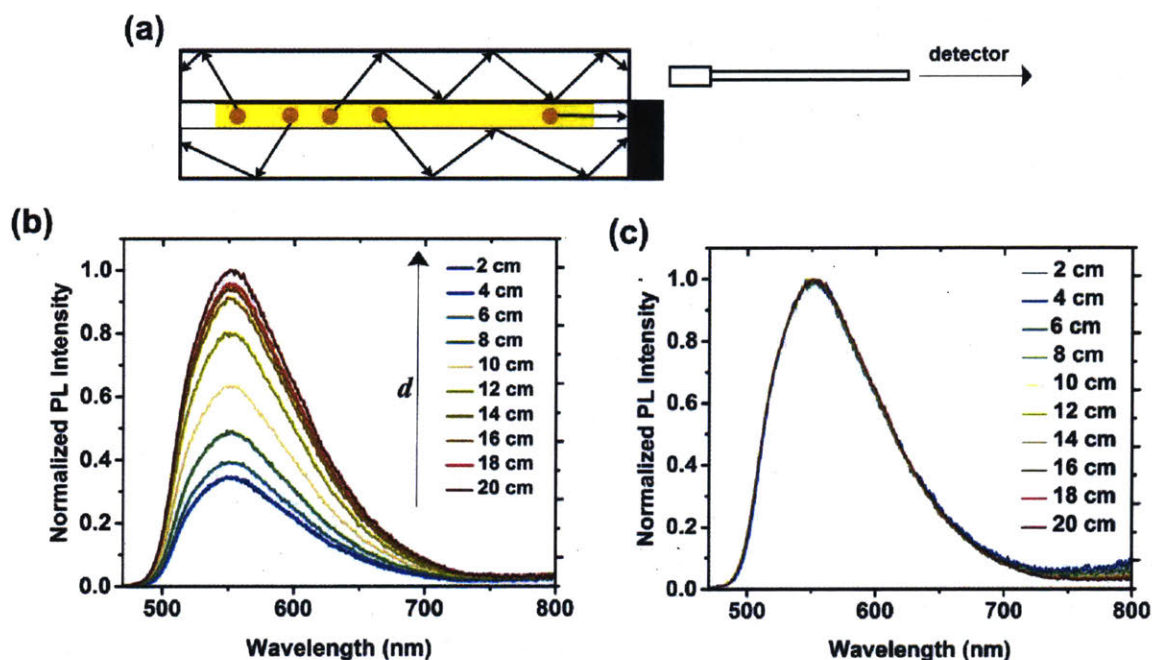


**Figure 4.5.** Relative edge emission output of FSC1 from the upper PMMA slabs. (a) Method of detection, as similar to Figure 4.4a. (b) Relative photoluminescence output as a function of  $d$ . (c) Photoluminescence outputs each normalized to their own maximum to illustrate that the observed edge emission is not affected by reabsorption effects with increasing  $d$ .

#### 4.4 Conclusion

In summary, we have demonstrated the potential of a photoluminescent fluorocarbon solution as the emissive layer in LSCs. We have obtained initial evidence that photoluminescence guided by the PMMA slabs enclosing the solution shield this emission from non-radiative reabsorption processes while traveling to the edges of the LSC. We next seek to better quantify this unaffected

emission using a calibrated solar light source and consequently assess the promise of our designed LSC for testing on large scales.

#### 4.5 Experimental Section

**4.5.1 Materials and Instrumentation.** THF was passed through a short plug of activated basic alumina just before use. *N*-chlorosuccinimide was purchased from TCI Chemical Company and used without further purification. Compound **2** was prepared as indicated by Takeda et al.<sup>11</sup> Cast PMMA and glass slabs were purchased from McMaster Carr. <sup>13</sup>C (101 MHz) and <sup>19</sup>F (376 MHz) NMR data were acquired with a Bruker Avance III HD NMR spectrometer with resonances identified as singlets (“s”), triplets (“t”), or multiplets (“m”). <sup>1</sup>H and <sup>13</sup>C NMR spectra were referenced relative to the solvent (CDCl<sub>3</sub>, <sup>1</sup>H: 7.26 ppm; <sup>13</sup>C: 77.16 ppm).  $\alpha,\alpha,\alpha$ -trifluorotoluene was used as an internal standard for <sup>19</sup>F NMR data ( $\delta = -63.72$  ppm). IR data were obtained using a Thermo Scientific Nicolet 6700 FT-IR spectrometer in attenuated total reflectance mode (Ge crystal) and with data corrected for atmospheric background. High-resolution mass spectrometry (HRMS) data was obtained using a Bruker Daltonics APEXIV 4.7 Tesla FT-ICR mass spectrometer at the MIT Department of Chemistry Instrumentation Facility.

Absorption spectra were obtained with an Agilent Cary 4000 UV/Vis spectrophotometer under air. Photoluminescence spectra were obtained with a HORIBA Jobin Yvon Fluorolog- $\tau$ 3 spectrofluorometer (model FL3-21) in which the excitation source (450 W Xe lamp). Solutions measurements were configured such that the detector and excitation beam oriented at a right angle. Fluorescence quantum yields were measured using Courmarin 6 in ethanol as a standard ( $\Phi_F = 78\%$ ). Fluorescence lifetimes were obtained via frequency domain measurements with a HORIBA Jobin Yvon MF<sup>2</sup> Multi-Frequency Fluorometer in which the excitation source was a 365 nm laser diode. 1,4-Bis(5-phenyl-2-oxazolyl)benzene (POPOP) in aerobic cyclohexane ( $\tau_F = 1.12$  ns) was

used as a standard.<sup>17</sup> The data was subjected to a least-squares regression algorithm to extract the fluorescence lifetime. Data for both aerobic and degassed solutions of **1** were best fit to single-component exponential decays (see Appendix I for Chapter 4).

Distance-dependent LSC reabsorption and scattering measurements were obtained using the Fluorolog- $\tau$ 3 spectrofluorometer coupled to an FL-3000 Fiber-Optics Adapter (HORIBA Jobin Yvon) in which a fiber optic probe directs the LSC's edge emission to the detector. An LSC was placed on a flat opaque surface and the probe faced the edge farthest from the injection gasket. The excitation beam used was an elliptical 4.5 mW laser diode module (CPS450, Thorlabs) with constant power maintained by a 5 V wall unit (LDS5, Thorlabs). These measurements were performed in the dark. The xenon lamp and excitation channel were shut off during the experiments.

**4.5.2 Electronic Structure Calculations.** Electronic structure calculations were performed using the same procedure presented in Chapter 2. The computational data for molecule **1-CF<sub>3</sub>** was obtained under gas-phase conditions. The transition dipole moments were calculated by ORCA and visualized with Avogadro.

**4.5.3 FSC preparation.** The solid PMMA components of **FSC1** were cut from a cast PMMA sheet with a Universal Laser Systems CO<sub>2</sub> laser at the MIT Laboratory of Engineering Materials. Edges to be examined by spectroscopy were solvent-polished with dichloromethane. The components were glued together with a non-fluorescent acrylic cement (Weld-On).

#### **4.5.4 Synthetic Procedures**

*5,7-Dichloro-2,3-bis(perfluorohexyl)thieno[3,4-*b*]pyrazine (1)*



To a solution of compound **2**<sup>11</sup> (2.500 g, 3.22 mmol) in 120 mL THF in a 300 mL round-bottom flask was slowly added *N*-chlorosuccinimide (2.580 g, 19.32 mmol). The mixture was stirred at room temperature for 18 h. The reaction mixture was concentrated *in vacuo* and hexanes was then added to the crude residue. The resulting suspension was filtered and the filtrate was concentrated. The crude residue was subjected to silica gel column chromatography twice: once with 100% hexanes as eluent, followed by 4:1 hexanes:CHCl<sub>3</sub>. The product was dissolved in 10 mL perfluorohexanes and passed through a 0.45 μM nylon syringe filter to additional organic impurities. Evaporation of the solvent resulted in an orange oil that was allowed to solidify under vacuum. Compound **1** was thus obtained as a bright orange, waxy solid (1.99 g, 73% yield). <sup>13</sup>C NMR (101 MHz, CDCl<sub>3</sub>): δ 141.4 (t), 134.0 (s), 124.6 (s), 121.7 (m), 118.9 (m), 116.0 (m), 113.6 (m), 111.4 (m), 106.2 (m). <sup>19</sup>F NMR (376 MHz, CDCl<sub>3</sub>): δ -126.9 (m, 4F), -123.6 (s, 4F), -120.9 (s, 4F), -118.7 (s, 4F), -107.0 (s, 4F), -85.8 (m, 6F). FTIR (ATR, Ge crystal): ν (cm<sup>-1</sup>) 1511, 1364, 1317, 1227, 1192, 1143, 1128, 1087, 1050, 1021, 967, 892, 816, 784, 763, 742, 707, 665, 648. HRMS (DART, *m/z*) calculated for C<sub>18</sub>Cl<sub>2</sub>F<sub>26</sub>N<sub>2</sub>S, [M + H]<sup>+</sup>: 840.8817, found: 840.8817.

#### 4.6 References

- (1) Debjie, M. G.; Verbunt, P. P. C. *Adv. Energy Mater.* **2012**, *2*, 12–35.
- (2) Sholin, V.; Olson, J. D.; Carter, S. A. *J. Appl. Phys.* **2007**, *101*, 123114.
- (3) Kondepuni, R.; Srinivasan, S. *Solar Energy Mater.* **1990**, *20*, 257–263.
- (4) Mansour, A. F. *Polym. Test.* **1998**, *17*, 153–162.
- (5) (a) Zhu, D.-W. *Macromolecules* **1996**, *29*, 2813–2817. (b) Tsai, W.-T.; Chen, H.-P.; Hsien, W.-Y. *J. Loss Prevent. Proc.* **2002**, *15*, 55–65.
- (6) Wilson, L. R.; Rowan, B. C.; Robertson, N.; Moudam, O.; Jones, A. C.; Richards, B. S. *Appl. Opt.* **2010**, *49*, 1651–1661.

- (7) Currie, M. J.; Mapel, J. K.; Heidel, T. D.; Goffri, S.; Baldo, M. A. *Science* **2008**, *321*, 226–228.
- (8) Gutierrez, G. D.; Coropceanu, I.; Bawendi, M. G.; Swager, T. M. *Adv. Mater.* **2016**, *28*, 497–501.
- (9) *Fluorinert Electronic Liquid FC-770*; MSDS; 3M: St. Paul, MN, 2007.
- (10) Cametti, M.; Crousse, B.; Metrangolo, P.; Milani, R.; Resnati, G. *Chem. Soc. Rev.* **2012**, *41*, 31–42.
- (11) Takeda, Y.; Andrew, T. L.; Lobez, J. M.; Mork, A. J.; Swager, T. M. *Angew. Chem. Int. Ed.* **2012**, *51*, 9042–9046.
- (12) Sletten, E. M.; Swager, T. M. *J. Am. Chem. Soc.* **2014**, *136*, 13574–13577.
- (13) Sun, H.; Putta, A.; Kloster, J. P.; Tottempudi, U. K. *Chem. Commun.* **2012**, *48*, 12085–12087.
- (14) Strickler, S. J.; Berg, R. A. *J. Chem. Phys.* **1963**, *37*, 814–822.
- (15) Würthner, F. *Chem. Commun.* **2004**, 1564–1579.
- (16) Brouwer, A. M. *Pure Appl. Chem.* **2011**, *83*, 2213–2228.
- (17) Boens, N.; Qin, W.; Basarić, N.; Hofkens, J.; Ameloot, M.; Pouget, J.; Lefèvre, J.-P.; Valeur, B.; Gratton, E.; vandeVen, M.; Silva, N. D.; Engelborghs, Y.; Willaert, K.; Sillen, A.; Rumbles, G.; Phillips, D.; Visser, A. J. W. G.; van Hoek, A.; Lakowicz, J. R.; Malak, H.; Gryczynski, I.; Szabo, A. G.; Krajcarski, D. T.; Tamai, N.; Miura, M. *Anal. Chem.* **2007**, *79*, 2137–2149.

**Appendix I for Chapter 4**  
 **$^{13}\text{C}$  and  $^{19}\text{F}$  NMR Spectra and Photoluminescence Lifetime**  
**Data**

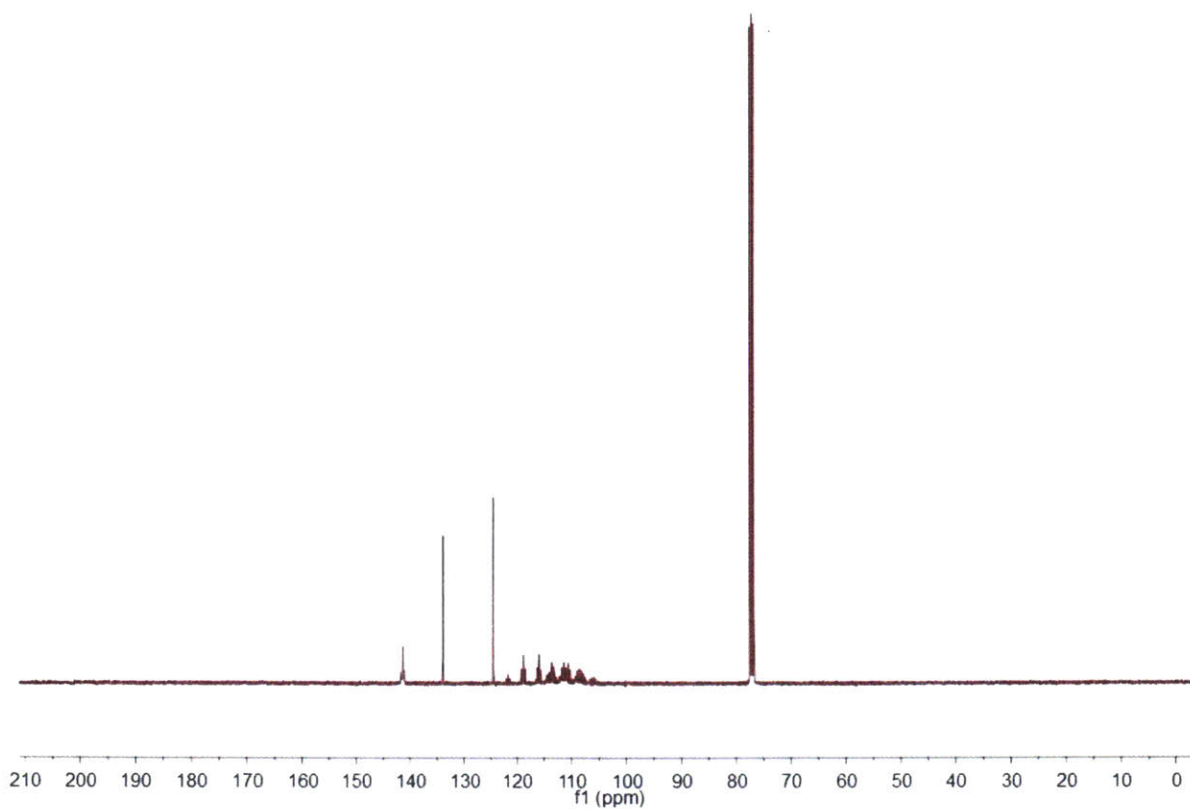


**Figure AI.4.1.**  $^{13}\text{C}$  NMR spectrum of **1** (101 MHz,  $\text{CDCl}_3$ ).

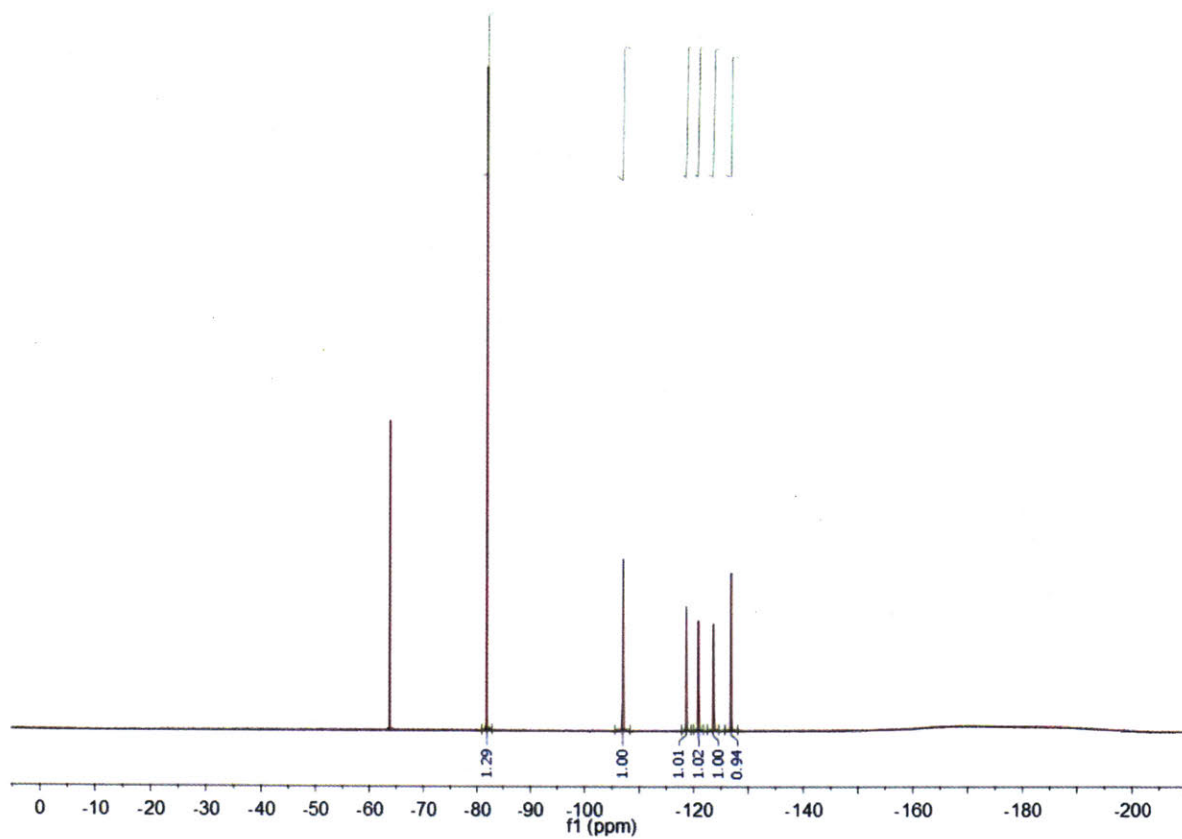


**Figure AI.4.2.**  $^{19}\text{F}$  NMR spectrum of **1** (376 MHz,  $\text{CDCl}_3$ ,  $\alpha,\alpha,\alpha$ -trifluorotoluene as internal standard).

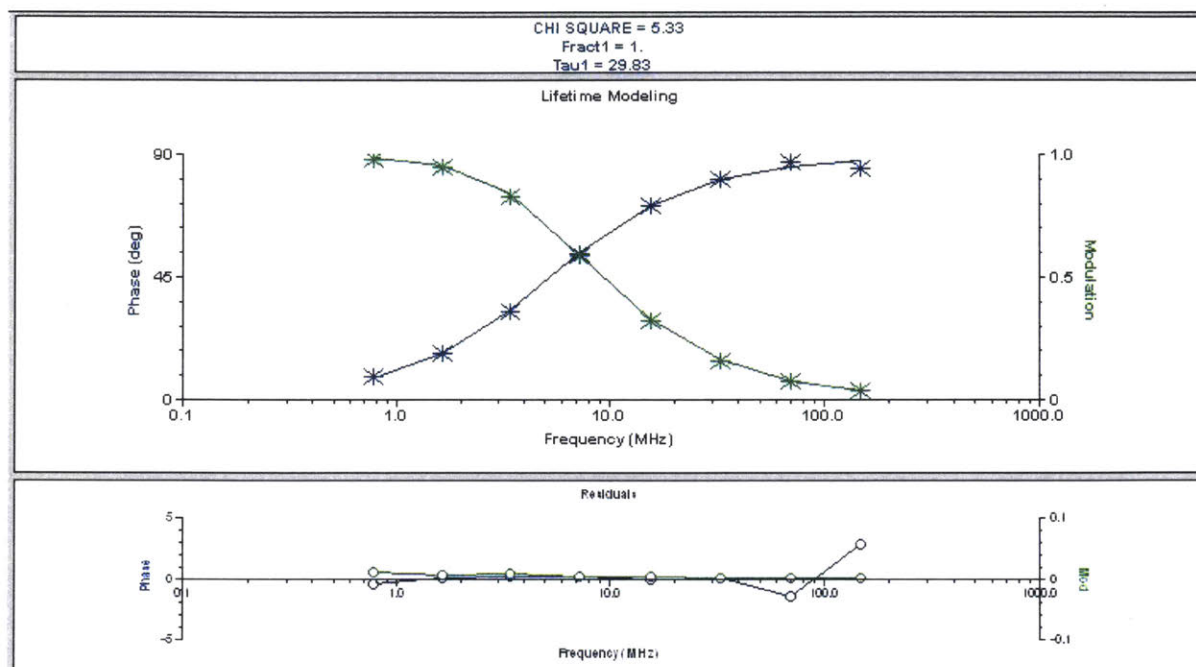


**Figure AI.4.3.** Photoluminescence lifetime data and modeling ( $\tau_F = 29.8$  ns,  $\chi^2 = 5.33$ ) for 1 in aerobic FC-770.

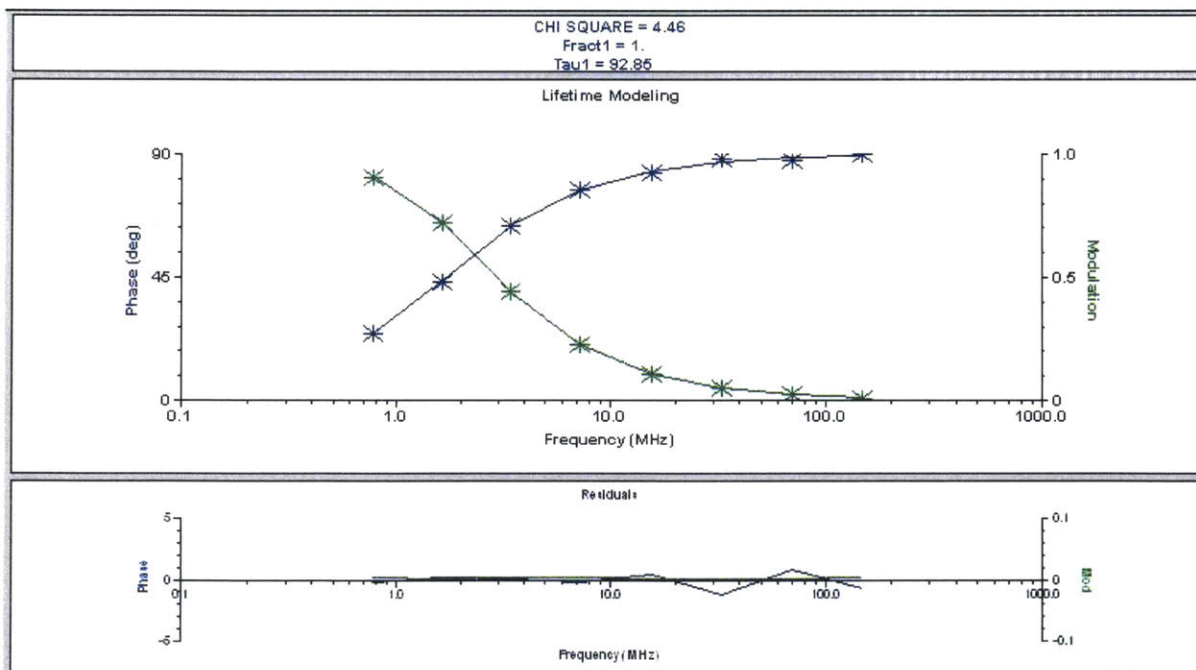


**Figure AI.4.4.** Photoluminescence lifetime data and modeling ( $\tau_F = 92.9$  ns,  $\chi^2 = 4.46$ ) for 1 in deoxygenated FC-770.

**Appendix II for Chapter 4**  
**Computational Data**

## 1-CF<sub>3</sub> Calculations

Geometry Optimization:

-----

CARTESIAN COORDINATES (ANGSTROEM)

-----

C	2.225722	0.083802	-0.264577
C	1.698177	-1.275662	-0.206403
N	0.410357	-1.514972	-0.130991
C	-0.423301	-0.444911	-0.117866
N	1.437124	1.132397	-0.259343
C	0.101198	0.907918	-0.188187
C	-1.810480	-0.479125	-0.044880
S	-2.466424	1.129977	-0.063363
C	-0.898813	1.872471	-0.168911
C	2.571182	-2.539969	-0.193476
F	3.577672	-2.464112	-1.101430
F	1.846683	-3.637685	-0.481842
F	3.127550	-2.726381	1.034830
C	3.720099	0.425457	-0.369235
F	4.468443	-0.334102	0.471183
F	3.949513	1.716240	-0.062102
F	4.172141	0.218427	-1.636444
Cl	-0.731454	3.579389	-0.233198
Cl	-2.836900	-1.851280	0.051684

-----

TOTAL SCF ENERGY

-----



Total Energy : -2332.56730779 Eh -63472.38332 eV

-----  
VIBRATIONAL FREQUENCIES  
-----

0: 0.00 cm\*\*<sup>-1</sup>  
1: 0.00 cm\*\*<sup>-1</sup>  
2: 0.00 cm\*\*<sup>-1</sup>  
3: 0.00 cm\*\*<sup>-1</sup>  
4: 0.00 cm\*\*<sup>-1</sup>  
5: 0.00 cm\*\*<sup>-1</sup>  
6: 26.13 cm\*\*<sup>-1</sup>  
7: 45.57 cm\*\*<sup>-1</sup>  
8: 69.48 cm\*\*<sup>-1</sup>  
9: 86.81 cm\*\*<sup>-1</sup>  
10: 99.04 cm\*\*<sup>-1</sup>

TD-DFT Calculation:

-----  
CIS/TD-DFT TOTAL ENERGY  
-----

E(SCF) = -2330.934762857 Eh

DE(CIS) = 0.106102654 Eh (Root 1)

-----  
E(tot) = -2330.828660203 Eh

-----  
FINAL SINGLE POINT ENERGY -2330.828660203070  
-----

-----  
TD-DFT/TDA EXCITED STATES (SINGLETs)  
-----

the weight of the individual excitations are printed if larger than 0.01

STATE 1: E= 0.106103 au 2.887 eV 23286.8 cm<sup>-1</sup>

82a -> 83a : 0.934057 (c= 0.96646627)

82a -> 85a : 0.034861 (c= -0.18671057)

STATE 2: E= 0.126645 au 3.446 eV 27795.4 cm<sup>-1</sup>

81a -> 83a : 0.985204 (c= -0.99257467)

STATE 3: E= 0.157805 au 4.294 eV 34634.2 cm<sup>-1</sup>

80a -> 83a : 0.545417 (c= 0.73852331)

82a -> 84a : 0.426425 (c= -0.65301194)

STATE 4: E= 0.178064 au 4.845 eV 39080.4 cm<sup>-1</sup>

76a -> 83a : 0.299202 (c= 0.54699320)

79a -> 83a : 0.588032 (c= -0.76683270)

81a -> 84a : 0.096448 (c= -0.31056018)

STATE 5: E= 0.185365 au 5.044 eV 40683.0 cm\*\*<sup>-1</sup>

82a -> 86a : 0.988425 (c= 0.99419549)

STATE 6: E= 0.189374 au 5.153 eV 41562.9 cm\*\*<sup>-1</sup>

76a -> 83a : 0.016237 (c= -0.12742421)

79a -> 83a : 0.027611 (c= -0.16616595)

82a -> 87a : 0.933613 (c= -0.96623671)

STATE 7: E= 0.190580 au 5.186 eV 41827.5 cm\*\*<sup>-1</sup>

76a -> 83a : 0.370110 (c= -0.60836700)

79a -> 83a : 0.369113 (c= -0.60754648)

81a -> 84a : 0.193550 (c= 0.43994295)

82a -> 87a : 0.052485 (c= 0.22909600)

STATE 8: E= 0.198689 au 5.407 eV 43607.1 cm\*\*<sup>-1</sup>

77a -> 83a : 0.978913 (c= -0.98940020)

STATE 9: E= 0.201044 au 5.471 eV 44124.1 cm\*\*<sup>-1</sup>

76a -> 83a : 0.283934 (c= -0.53285443)

78a -> 83a : 0.016932 (c= 0.13012348)

81a -> 84a : 0.683562 (c= -0.82677829)

STATE 10: E= 0.201716 au 5.489 eV 44271.6 cm\*\*<sup>-1</sup>

78a -> 83a : 0.864841 (c= -0.92996843)

80a -> 83a : 0.061134 (c= 0.24725229)

81a -> 84a : 0.011327 (c= -0.10643007)

82a -> 84a : 0.024163 (c= 0.15544510)

### Oscillator strength ( $f_{osc}$ ) and transition dipole moment data

#### ABSORPTION SPECTRUM VIA TRANSITION ELECTRIC DIPOLE MOMENTS

State	Energy (cm-1)	Wavelength (nm)	$f_{osc}$	T2 (au**2)	TX (au)	TY (au)	TZ (au)	
1	23286.8	429.4	0.067651365	0.95640	-0.35265	-0.91097	0.04670	
2	27795.4	359.8	0.002623991	0.03108	0.00665	0.00067	0.17617	
3	34634.2	288.7	0.040595886	0.38588	-0.57837	0.22553	0.02249	
4	39080.4	255.9	0.000143731	0.00121	0.03241	-0.01261	-0.00122	
5	40683.0	245.8	0.000016827	0.00014	-0.00137	0.00273	-0.01126	
6	41562.9	240.6	0.000038816	0.00031	-0.01699	0.00426	0.00086	
7	41827.5	239.1	0.000328182	0.00258	-0.04710	0.01900	0.00190	
8	43607.1	229.3	0.001447344	0.01093	0.00316	-0.00233	0.10446	
9	44124.1	226.6	0.001820353	0.01358	0.10890	-0.04130	-0.00420	
10	44271.6	225.9	0.029938140	0.22263	-0.43610	0.17933	0.01675	
11	13956.5	716.5	spin forbidden (mult=3)					
12	23295.0	429.3	spin forbidden (mult=3)					
13	26442.3	378.2	spin forbidden (mult=3)					
14	31192.4	320.6	spin forbidden (mult=3)					
15	32416.9	308.5	spin forbidden (mult=3)					
16	33539.5	298.2	spin forbidden (mult=3)					
17	37158.0	269.1	spin forbidden (mult=3)					
18	38324.8	260.9	spin forbidden (mult=3)					
19	38770.5	257.9	spin forbidden (mult=3)					
20	39729.6	251.7	spin forbidden (mult=3)					

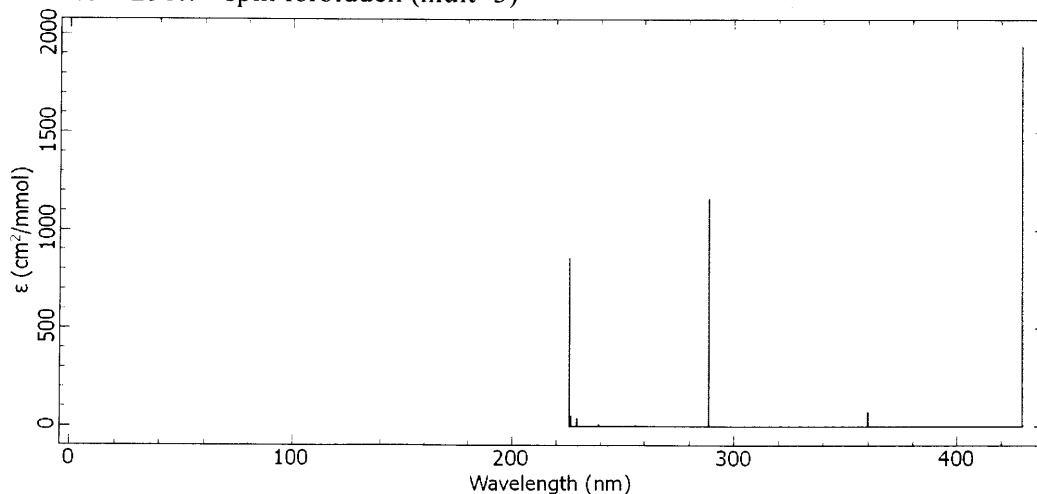


Figure AII.4.1. Computed absorption spectrum for 1-CF<sub>3</sub>.

## **Chapter 5**

# **Towards Naphthazarin Iptycenes as a New Scaffold for Solid-State Luminescent and Novel Redox-Active Metallopolymers**

This chapter only contains results independently obtained by G.D.G. Continued investigation of this project is currently being performed by Dr. Cagatay Dengiz, G.D.G. thanks Dr. Dengiz for helpful discussions.

## 5.1 Introduction

A major goal of modern organic materials research concerns the development of novel polymers that possess unique functions as a result of the spatial arrangement of repeating structural motifs attached to their backbones. To this end, this chapter discusses the initial efforts toward ligands iptycene-containing main-chain metallopolymers as tunable solid-state luminescent or redox-active materials.

## 5.2 Iptycene-Functionalized Naphthazarin Metallopolymers

The synthesis and application of main-chain organometallic polymers, or those in which repeat units are held together by a coordinating metal, is a widely investigated field of research. Examples include ferrocene containing main-chain polymers,<sup>1</sup> those employing terpyridines<sup>2</sup> or N-heterocyclic carbenes,<sup>2,3</sup> as well as transition metal-complexed polyynes.<sup>4</sup> Quinizarin (1,4-dihydroxy-9,10-anthraquinone) is also an example of a ligand notably used in the synthesis of organometallic complexes (Figure 5.1a).<sup>5</sup> Metals such as copper<sup>6</sup>, rhenium<sup>7</sup>, and Group III metals<sup>8</sup> have resulted luminescent species when complexed to quinizarin in solution. Additionally, there have been previous reports of metallopolymers of naphthazarin (1,4-dihydroxy-5,8-naphthaquinone) complexed with transition metals such as cobalt and nickel (Figure 5.1b).<sup>8</sup>

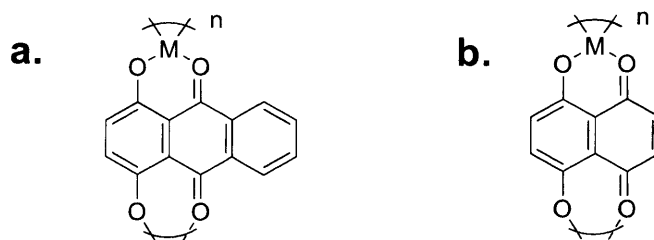


**Figure 5.1.** (a) Main-chain polymeric quinizarins and (b) naphthazarin metallopolymers.

After demonstrating that alkylated iptycenes yield solid-state materials with very high photoluminescence quantum yields in Chapter 3, we hypothesized that iptycenes functionalized at the naphthazarin core could yield metallopolymers with strong solid-state photoluminescence and consequently demonstrate promise as materials for use in luminescent solar concentrators (Figure 5.2).

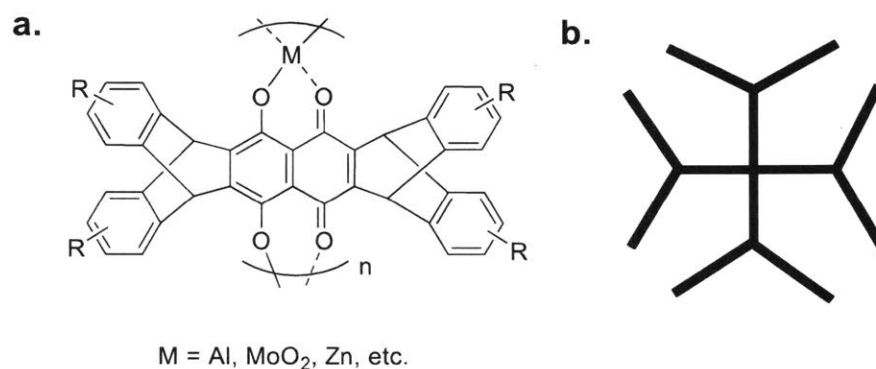
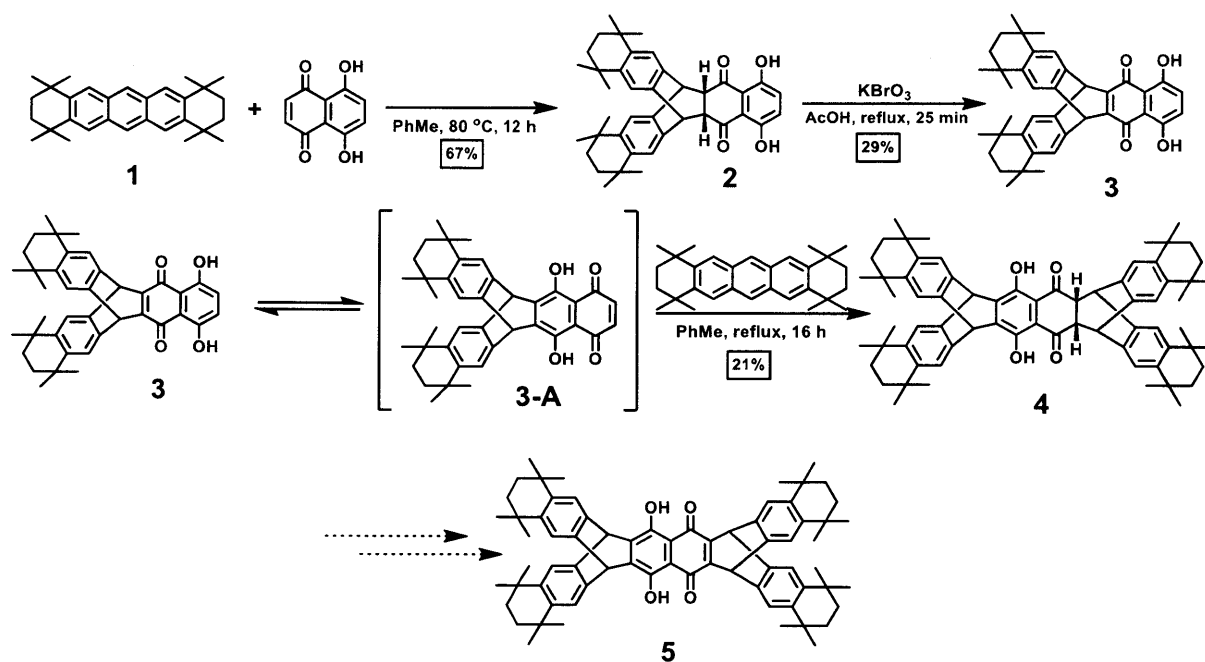


**Figure 5.2.** (a) Naphthazarin-based iptycene metallopolymers with suggested metals for complexation. (b) Predicted orientation of iptycene wings that could preclude luminescence quenching interactions in the solid state.

Additionally, through-space homoconjugation between the iptycenes<sup>9</sup> and chelating backbone could possibly be exploited to tune the electronic properties of the polymer backbone. Through these interactions, we also aim to pursue novel redox-active materials that may be used as tunable sensors or electrochromic switches. This work herein describes the synthesis of iptycene-based naphthazarins as an initial effort toward novel main-chain metallopolymers. To our knowledge, the structures described herein are unreported.

### 5.3 Synthetic Progress and Outlook

The key reaction used to access the naphthazarin iptycenes in Figure 5.2 is the Diels-Alder ([4+2]) cycloaddition, one of the most versatile and atom-economical methods for forming carbon-carbon bonds. Beginning with Scheme 5.1, naphthazarin was reacted with alkylated anthracene **1** to produce cycloadduct **2** in good yield (67%). Enolization and oxidation of **2** with AcOH/KBrO<sub>3</sub> produced naphthazarin triptycene **3** in 29% yield. Naphthazarin-based cycloadducts are known to tautomerize to expose the quinone-based dienophile for reaction with another diene to furnish a second cycloaddition.<sup>10</sup> A second equivalent of **1** underwent successful cycloaddition with tautomer **3-A** to yield cycloadduct **4** in 21% yield. Compound **4** is the precursor of naphthazarin pentiptycene **5**, a key ligand to be used in the proposed metallopolymer syntheses.

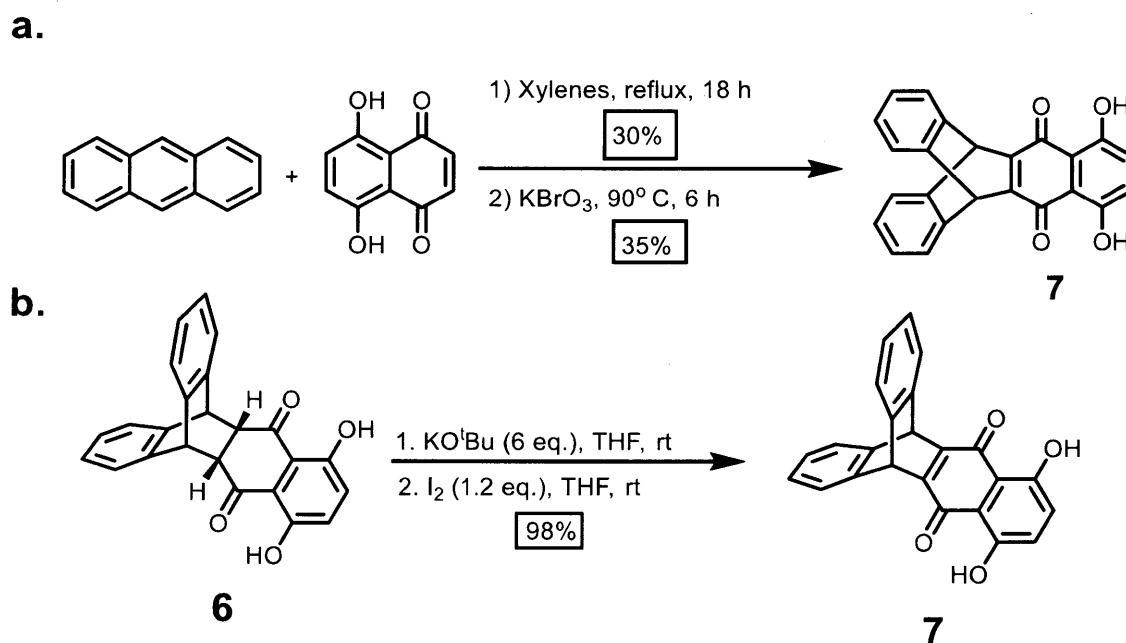


**Scheme 5.1.** Synthesis toward naphthazarin pentiptycene **5**.

We next postulated whether the oxidation required to restore  $\pi$ -conjugation of the naphthazarin core could be improved by utilizing milder conditions. As shown in Scheme 5.2a, We found that KO<sup>t</sup>Bu enolizes cycloadduct **6** and, in the presence of iodine, transforms into **7** in



excellent yield (98%). We envision using this milder method to access a portfolio of functionalized naphthazarin pentiptycenes with varying degrees of internal free volume or tuned electronic properties based on what substituents are attached to the iptycene wings. These structures represent an unexplored class of organic materials whose properties and incorporation into devices are currently under investigation.



**Scheme 5.2.** (a) Synthesis of **6** with oxidation occurring under acidic conditions. (b) Synthesis of naphthazarin triptycene **6** under mild oxidation with KO<sup>t</sup>Bu/I<sub>2</sub> from Diel-Alder cycloadduct **7**.

#### 5.4 Experimental Section

**5.4.1 Materials and Instrumentation.** Naphthazarin was purchased from Alfa Aesar and used without further purification. Anthracene was recrystallized from ethanol/toluene prior to use. Compound **1** was synthesized as specified by Bouffard et al.<sup>11</sup> NMR spectra were acquired with a Bruker Avance III HD NMR spectrometer (<sup>1</sup>H: 400 MHz, <sup>13</sup>C: 101 MHz). Resonances were

labeled as singlet (“s”), doublet of doublets (“dd”), pseudo-triplet ( $\psi$ t), or multiplet (“m”). High-resolution mass spectrometry was performed with a Bruker Daltonics APEXIV 4.7 Tesla FT-ICR mass spectrometer in direct analysis in real time (DART, positive mode).

#### 5.4.2 Synthetic Procedures

##### *Compound 2*

Naphthazarin (250 mg, 1.31 mmol) and compound **1** (730 mg, 1.98 mmol) were mixed with toluene (20 mL) in a round-bottom flask equipped with stirbar and condenser. The reaction was stirred under reflux for 12 h. Silica gel column chromatography (1:1 CH<sub>2</sub>Cl<sub>2</sub>:hexanes) yields pure **2** as a yellow solid (500 mg, 68%). <sup>1</sup>H NMR (400 MHz, CDCl<sub>3</sub>):  $\delta$  12.14 (s, 2H), 7.34 (s, 2H), 7.02 (s, 2H), 6.99 (s, 2H), 4.77 (s, 2H), 3.28 ( $\psi$ t, 2H), 1.66 (m, 4H), 1.44 (m, 4H), 1.33 (s, 6H), 1.22 (s, 6H), 1.11 (s, 6H), 0.96 (s, 6H). <sup>13</sup>C NMR (101 MHz, CDCl<sub>3</sub>):  $\delta$  203.5, 154.9, 143.34, 143.27, 138.3, 136.4, 127.9, 122.0, 114.6, 50.9, 50.4, 35.3, 35.0, 34.5, 34.1, 32.18, 32.15, 31.8, 31.6. HRMS (DART, m/z) calculated for C<sub>34</sub>H<sub>58</sub>I<sub>2</sub>N<sub>2</sub>O<sub>2</sub>S, M<sup>+</sup>: 754.2677, found: 754.2676. HRMS (DART, m/z) calculated for C<sub>40</sub>H<sub>44</sub>O<sub>4</sub>, [M-H]<sup>-</sup>: 587.3167, found: 587.3167.

##### *Compound 3*

**2** (100 mg, 0.17 mmol), KBrO<sub>3</sub> (28 mg, 0.17 mmol), and AcOH (5 mL) were combined in a round-bottom flask. Contents were stirred and refluxed for 25 minutes. Silica gel column chromatography using 1:1 CH<sub>2</sub>Cl<sub>2</sub> yields pure **3** as a red solid (29 mg, 29% yield). <sup>1</sup>H NMR (400 MHz, CDCl<sub>3</sub>):  $\delta$  12.63 (s, 2H), 7.37 (s, 4H), 7.10 (s, 2H), 5.86 (s, 2H), 1.62 (s, 8H), 1.23 (s, 24H). <sup>13</sup>C NMR (101 MHz, CDCl<sub>3</sub>):  $\delta$  177.9, 164.6, 154.1, 142.2, 140.6, 131.9, 122.7, 111.6, 47.1, 35.2, 34.5, 32.1, 31.9. HRMS (DART, m/z) calculated for C<sub>40</sub>H<sub>42</sub>O<sub>4</sub>, [M+H]<sup>+</sup>: 587.3156, found: 587.3155.

##### *Compound 4*

Compound **3** (29 mg, 0.049 mmol) and **1** (38 mg, 0.10 mmol) were combined with 5 mL toluene in a 50 mL round-bottom flask and stirred and refluxed for 16 h. The resulting precipitate was filtered and washed with hexanes to obtain **4** (10 mg, 21% yield).  $^1\text{H}$  NMR (400 MHz,  $\text{CDCl}_3$ ):  $\delta$  12.41 (s, 2H), 7.30 (s, 4H), 7.25 (s, 2H), 6.80 (s, 2H), 5.76 (s, 2H), 4.71 (s, 2H), 3.17 (s, 2H), 1.62 (s, 8H), 1.56 (s, 4H), 1.30 (s, 6H), 1.27 (s, 6H), 1.23 (s, 6H), 1.19 (s, 12H), 1.16 (s, 6H), 0.73 (m, 2H), 0.99 (s, 6H), 0.61 (s, 6H).  $^{13}\text{C}$  NMR (101 MHz,  $\text{CDCl}_3$ ):  $\delta$  203.6, 150.1, 145.5, 143.2, 143.0, 141.7, 141.6, 140.6, 138.2, 136.2, 122.5, 122.4, 122.1, 122.0, 113.0, 51.1, 50.4, 47.0, 35.4, 35.3, 34.6, 34.5, 34.44, 34.40, 33.9, 32.5, 32.1, 31.9, 31.5. HRMS (DART,  $m/z$ ) calculated for  $\text{C}_{70}\text{H}_{80}\text{O}_4$ ,  $[\text{M}+\text{H}]^+$ : 985.6129, found: 985.6132.

#### *Compound 6*

Anthracene (974 mg, 5.26 mmol), naphthazarin (1.00 g, 5.26 mmol), and xylenes (10 mL) were combined in a 50 mL round-bottom flask equipped with a condenser and stirred under reflux for 18 h. The solvent was then evaporated and the crude residue was subjected to silica gel column chromatography (100%  $\text{CHCl}_3$ ), followed by recrystallization from toluene to obtain **6** as a yellow solid (586 mg, 30% yield).  $^1\text{H}$  NMR (400 MHz,  $\text{CDCl}_3$ ):  $\delta$  12.43 (s, 2H), 7.46 (dd, 2H), 7.22 (dd, 2H), 7.14 (dd, 2H), 7.09 (s, 2H), 6.96 (s, 2H), 5.04 (s, 2H), 3.35 ( $\psi$ t, 2H).  $^{13}\text{C}$  NMR (101 MHz,  $\text{CDCl}_3$ ):  $\delta$  202.2, 155.9, 141.9, 139.8, 128.7, 126.7, 124.6, 124.1, 114.2, 49.7, 49.6.

#### *Compound 7*

##### **A. Oxidation under acidic conditions**

**6** (400 mg, 1.10 mmol),  $\text{KBrO}_3$  (180 mg, 1.10 mmol), and AcOH were placed in a 50 mL round-bottom flask with condenser and heated to  $90^\circ\text{C}$  for 6 h. After cooling to room temperature, the reaction mixture was poured into 100 mL  $\text{H}_2\text{O}$  and washed with 2 x 20 mL hot  $\text{H}_2\text{O}$ , followed by

10 mL methanol. Silica gel column chromatography (1:1 CH<sub>2</sub>Cl<sub>2</sub>:hexanes) was then applied to furnish pure **7** (140 mg, 35 % yield). <sup>1</sup>H NMR (400 MHz, CDCl<sub>3</sub>): δ 12.61 (s, 2H), 7.48 (dd, 4H), 7.10 (s, 2H), 7.06 (dd, 4H), 6.03 (s, 2H). <sup>13</sup>C NMR (101 MHz, CDCl<sub>3</sub>): δ 175.2, 167.0, 152.9, 143.6, 132.7, 125.9, 124.6, 111.4, 47.6.

### B. Oxidation under basic conditions

To an oven-dried 50 mL round-bottom flask was added **6** (100 mg, 0.270 mmol) and KO<sup>t</sup>Bu (180 mg, 1.63 mmol). After cycling the flask with vacuum and argon twice, 15 mL THF was added to the flask. After stirring under argon for 1 h, I<sub>2</sub> (82 mg, 0.33 mmol) was added to the flask. The blue reaction mixture was stirred for 19 h before quenching with 10 mL 10% HCl. The product was extracted with CHCl<sub>3</sub> and washed with saturated Na<sub>2</sub>S<sub>2</sub>O<sub>3</sub> (aq.), followed by saturated NaCl (aq.). The organic layer was dried with MgSO<sub>4</sub>, filtered and evaporated to yield **7** as a red solid (97 mg, 98% yield). <sup>1</sup>H NMR (400 MHz, CDCl<sub>3</sub>): δ 12.60 (s, 2H), 7.48 (dd, 4H), 7.10 (s, 2H), 7.06 (dd, 4H), 6.03 (s, 2H).

### 5.5 References

- (1) (a) Nguyen, P.; Gómez-Elipe, P.; Manners, I. *Chem. Rev.* **1999**, *99*, 1515–1548. (b) Abd-El-Aziz, A. S. *Macromolecular Rapid Commun.* **2002**, *17*, 995–1031.
- (2) Williams, K. A.; Boydston, A. J.; Bielawski, C. W. *Chem. Soc. Rev.* **2007**, *36*, 729–744.
- (3) Boydston, A. J.; Williams, K. A.; Bielawski, C. W. *J. Am. Chem. Soc.* **2005**, *127*, 12496–12497.
- (4) Kingsborough, R. P.; Swager, T. M. Transition Metals in Polymeric π-Conjugated Organic Frameworks. In *Progress in Inorganic Chemistry*; Karlin, K. D., Ed.; John Wiley & Sons, Inc.: Hoboken, NJ, 1999; Vol. 48, pp 123–231.

- (5) Selected examples: (a) Bakola-Christianopoulou, M. N.; Akrivos, P. D.; Baumgarten, M. *Can. J. Chem.* **1987**, *65*, 1485–1490. (b) Ishikawi, T.; Inoue, H.; Makishima, A. *J. Mater. Sci.* **2000**, *35*, 1669–1674.
- (6) Wang, Y.; Sun, H.; Hou, L.; Shang, Z.; Dong, Z.; Jin, W. *Anal. Methods* **2013**, *5*, 5493–5500.
- (7) Sathiyendiran, M.; Liao, R.-T.; Thanasekaran, P.; Luo, T.-T.; Venkataramanan, N. S.; Lee, G.-H.; Peng, S.-M.; Lu, K.-L. *Inorg. Chem.* **2006**, *45*, 10052–10054.
- (8) (a) Quinti, L.; Allen, N. S.; Edge, M.; Murphy, B. P.; Perotti, A. *J. Photochem. Photobio. A: Chem.* **2003**, *155*, 79–91. (b) Quinti, L.; Allen, N. S.; Edge, M.; Murphy, B. P.; Perotti, A. *J. Photochem. Photobio. A: Chem.* **2003**, *155*, 93–106.
- (9) Selected examples: (a) Bottei, R. S.; Gerace, P. L. *J. Inorg. Nucl. Chem.* **1961**, *23*, 245–251. (b) Papageorgiou, V. P.; Christianopoulou, M. M.; Boutis, L. L.; Papageorgiou, A.; Tsipis, C. A. *Inorg. Chem. Acta* **1986**, *124*, 203–206. (c) Rao, T. R.; Rao, P. R.; Lingaiah, P.; Deshmukh, L. S. *Angew. Makromol. Chem.* **1991**, *191*, 177–189. (d) Papageorgiou, V. P.; Christianopoulou, M. M.; Boutis, L. L.; Papageorgiou, A.; Tsipis, C. A. *Inorg. Chem. Acta* **1986**, *124*, 203–206.
- (10) Kawasumi, K.; Wu, T.; Zhu, T.; Chae, H. S.; Van Voorhis, T.; Baldo, M. A.; Swager, T. M. *J. Am. Chem. Soc.* **2015**, *137*, 11908–11911.
- (11) (a) Kelly, T. R.; Ananthasubramanian, L.; Borah, K.; Gillard, J. W.; Goerner, R. N.; King, P. F.; Lyding, J. M.; Tsang, W.-G.; Vaya, J. *Tetrahedron* **1984**, *40*, 4569–4577. (b) Carreño, M. C.; Ruano, J. L. G.; Urbano, A. *J. Org. Chem.* **1996**, *61*, 6136–6138.
- (12) Bouffard, J.; Eaton, R. F.; Müller, P.; Swager, T. M. *J. Org. Chem.* **2007**, *72*, 10166–10180.

**Appendix for Chapter 5**  
 **$^1\text{H}$  and  $^{13}\text{C}$  NMR Spectra**

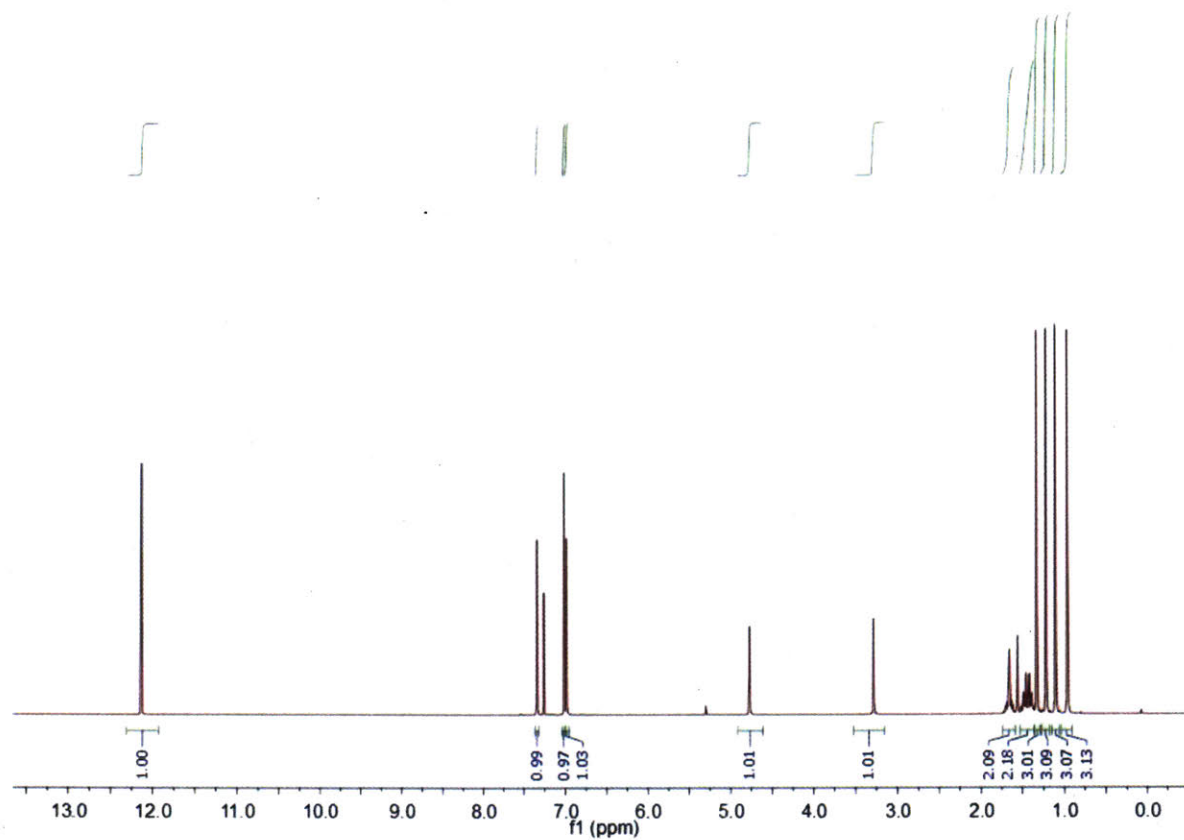


**Figure A.5.1.**  $^1\text{H}$  NMR spectrum of **2** (400 MHz,  $\text{CDCl}_3$ ).

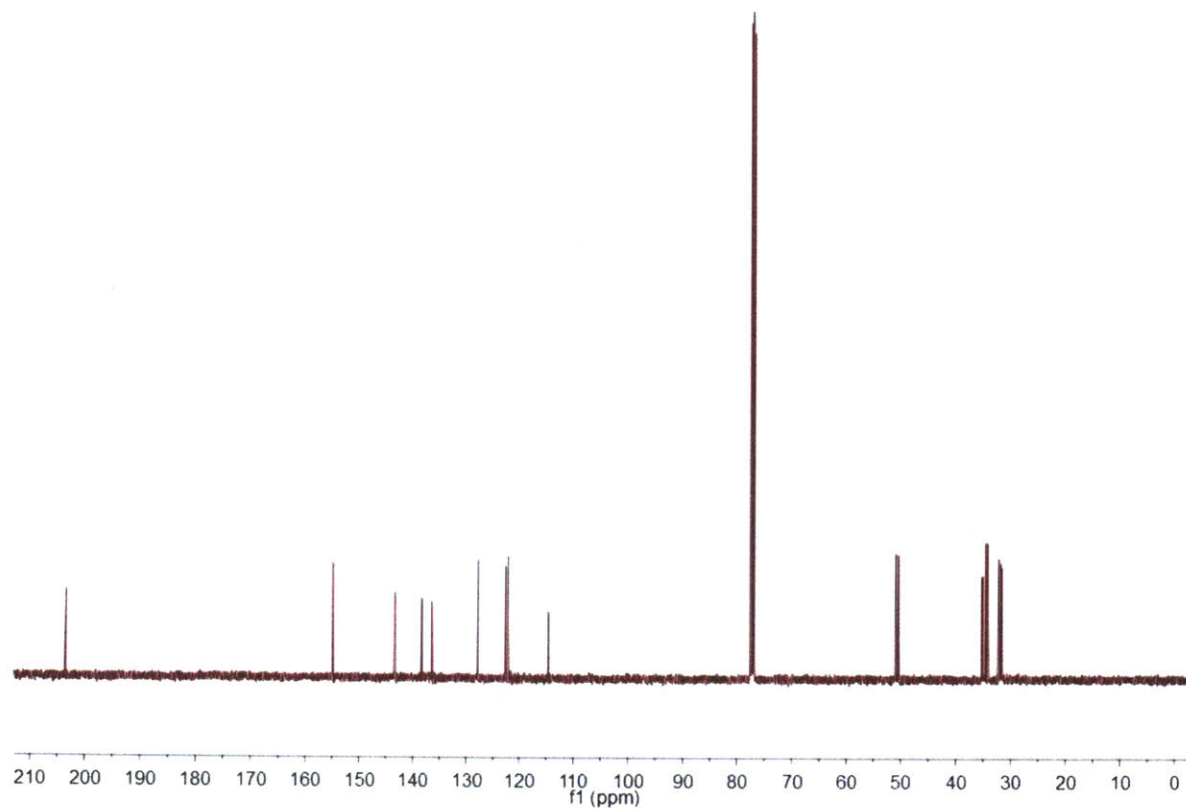


**Figure A.5.2.**  $^{13}\text{C}$  NMR spectrum of **2** (101 MHz,  $\text{CDCl}_3$ ).



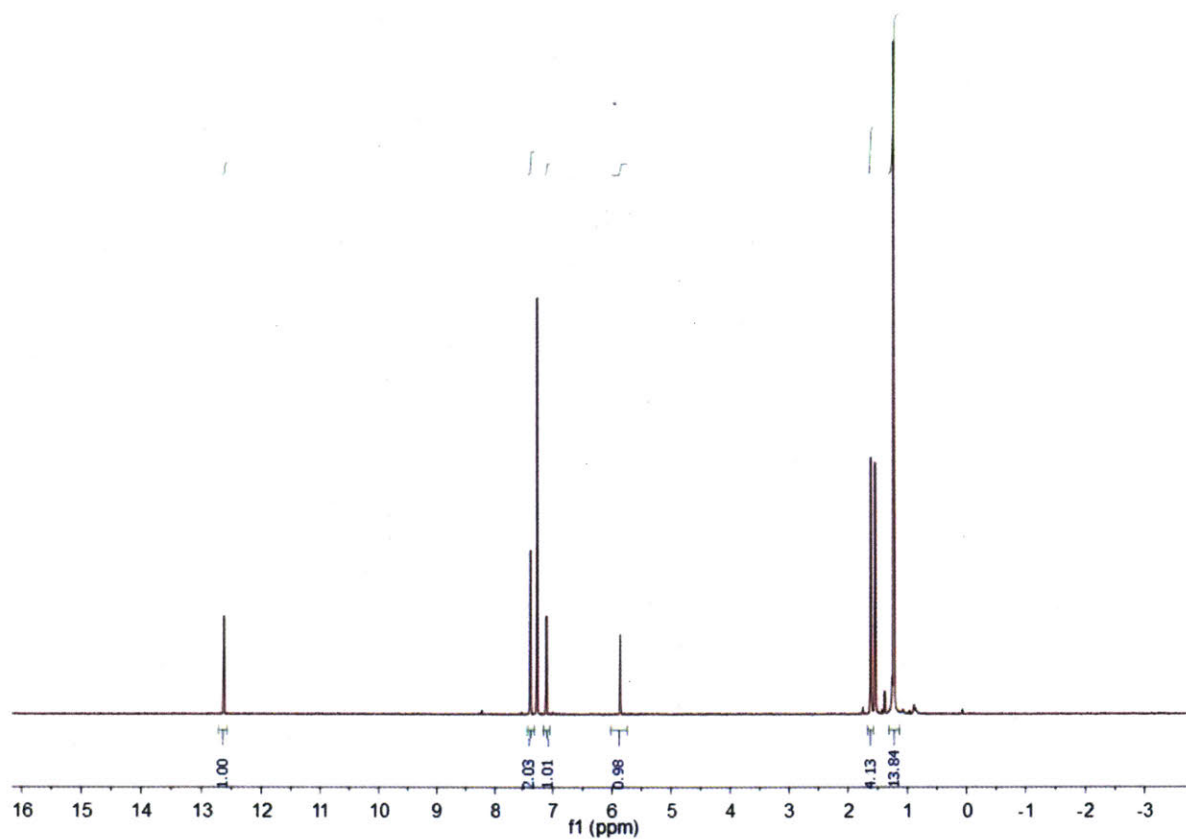


**Figure A.5.1.**  $^1\text{H}$  NMR spectrum of **3** (400 MHz,  $\text{CDCl}_3$ ).

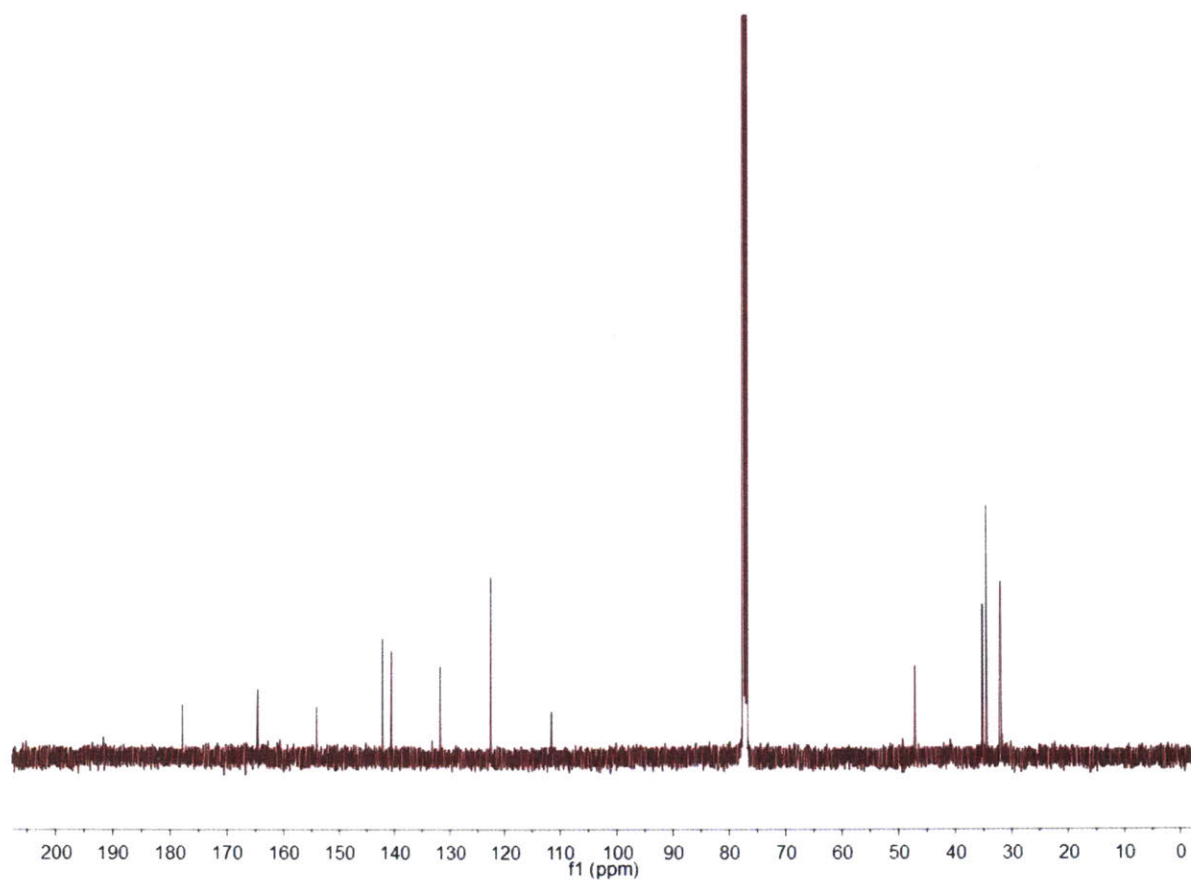


**Figure A.5.1.**  $^{13}\text{C}$  NMR spectrum of **3** (101 MHz,  $\text{CDCl}_3$ ).

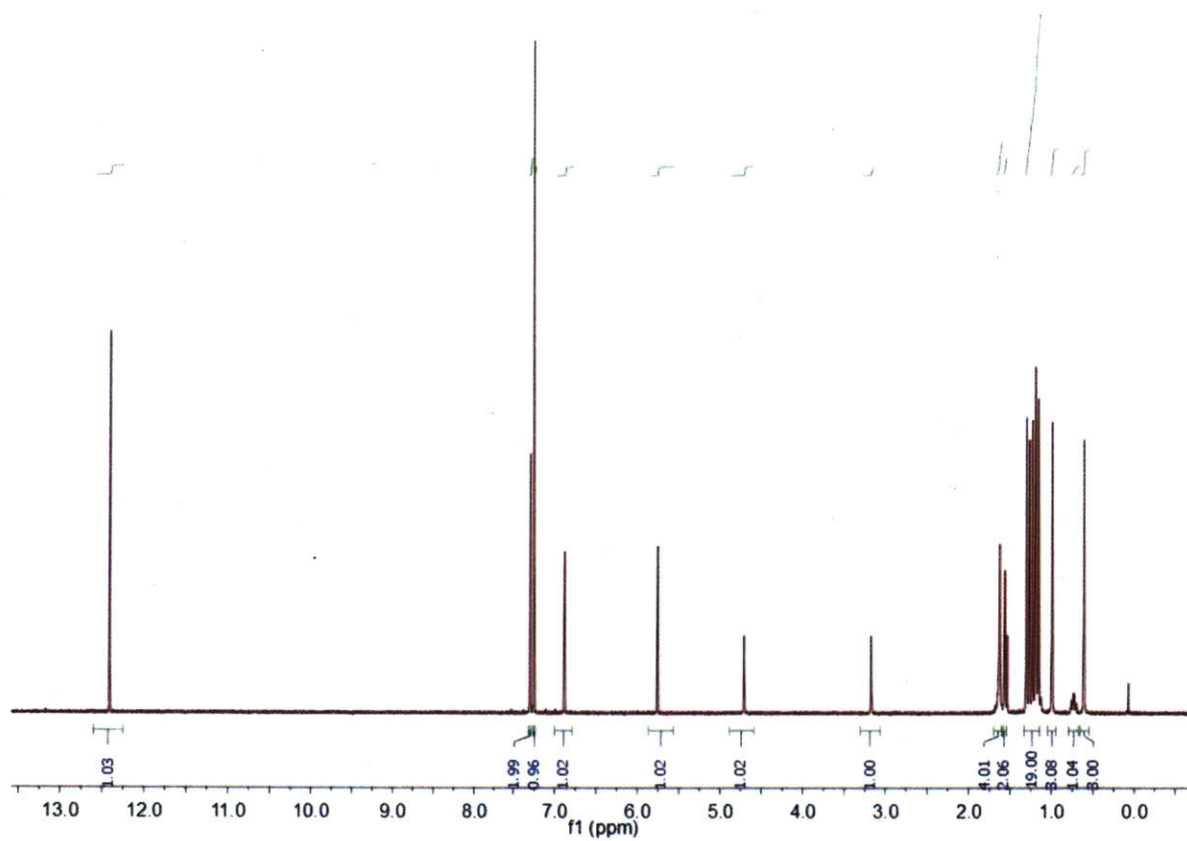
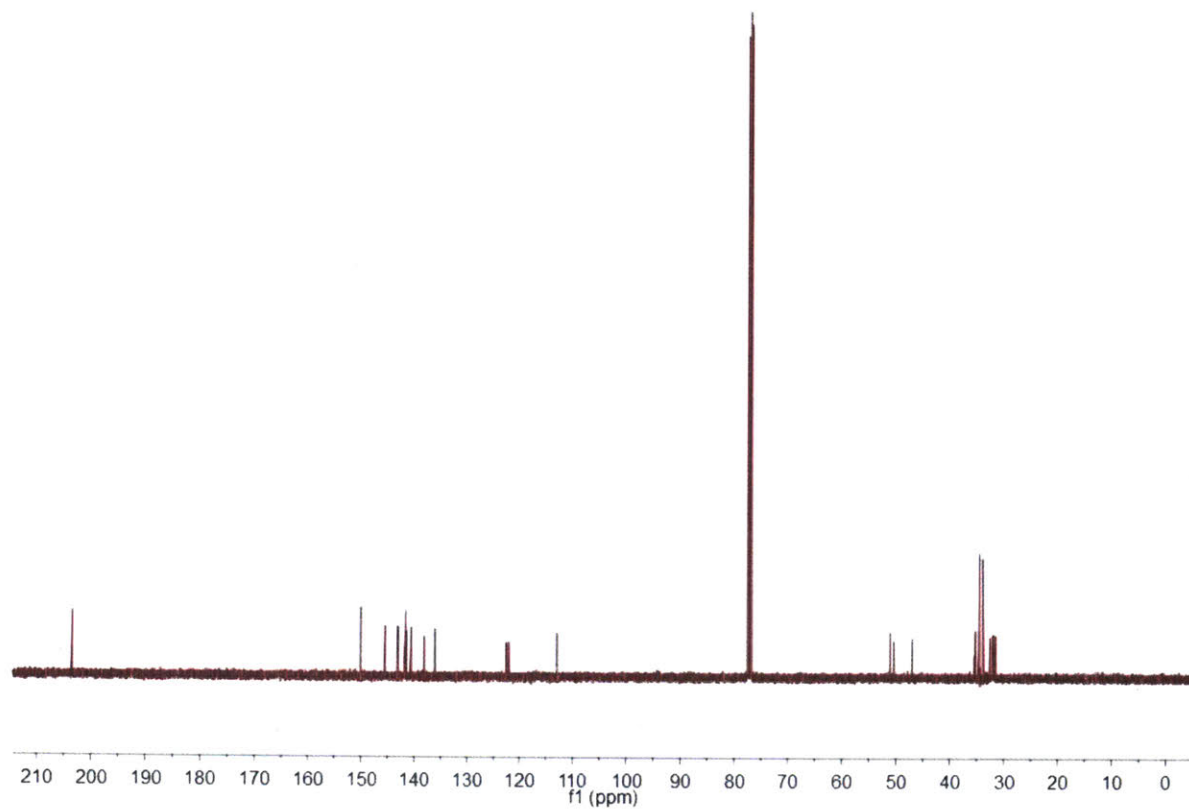
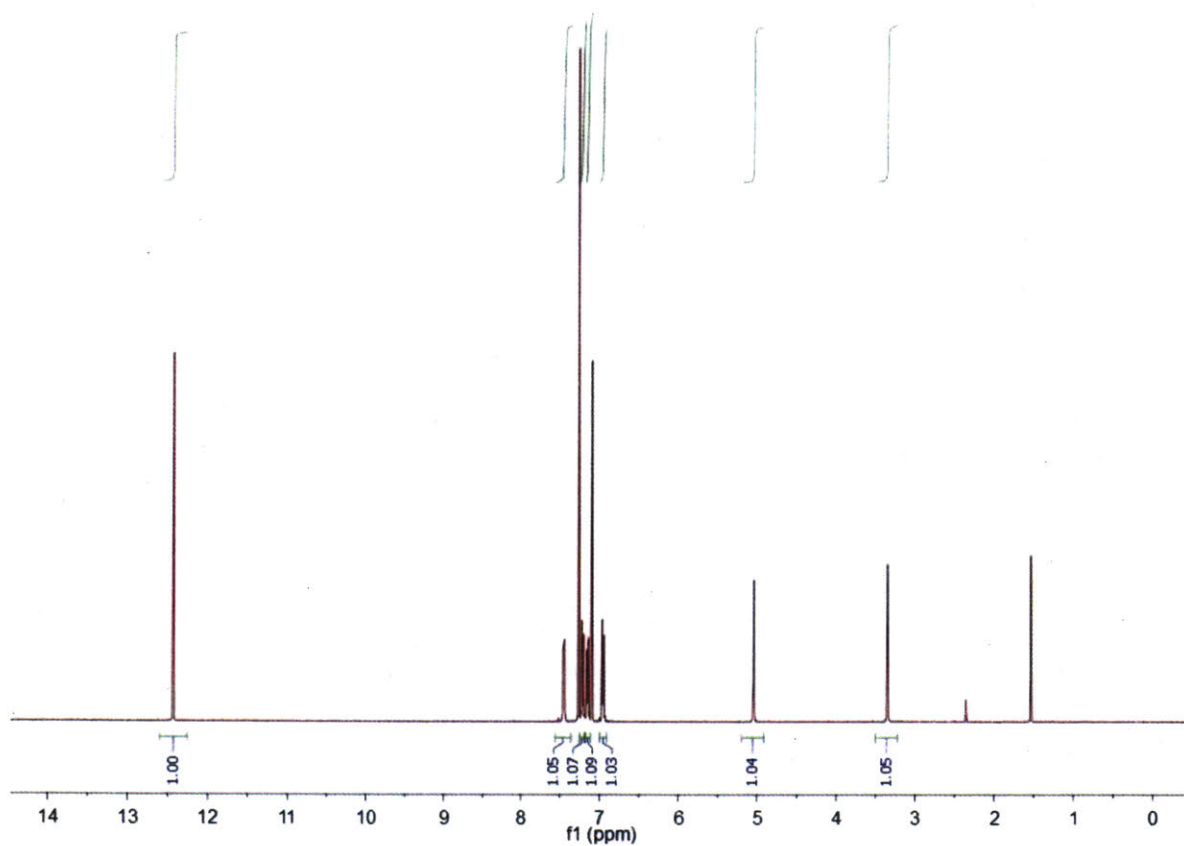


Figure A.5.5.  $^1\text{H}$  NMR spectrum of **4** (400 MHz,  $\text{CDCl}_3$ ).



**Figure A.5.6.**  $^{13}\text{C}$  NMR spectrum of **4** (101 MHz,  $\text{CDCl}_3$ ).



**Figure A.5.7.**  $^1\text{H}$  NMR spectrum of **6** (400 MHz,  $\text{CDCl}_3$ ).

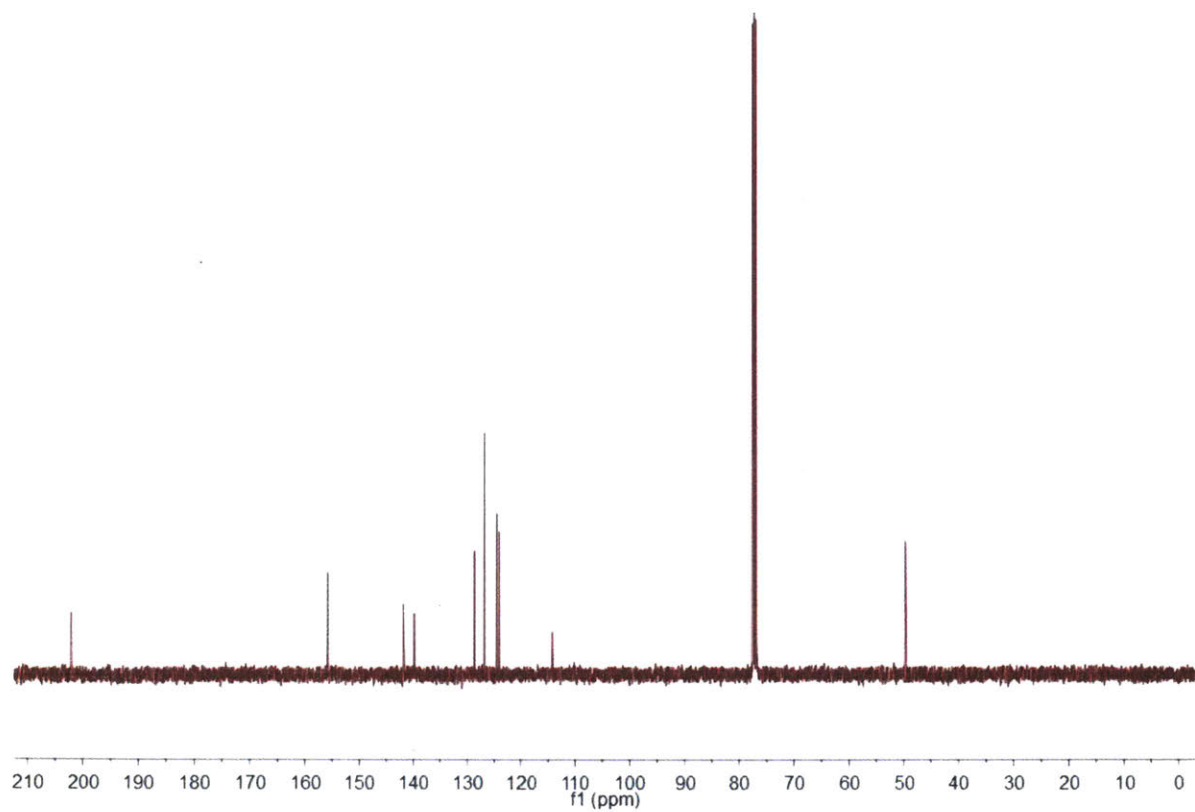


**Figure A.5.8.**  $^{13}\text{C}$  NMR spectrum of **6** (101 MHz,  $\text{CDCl}_3$ ).

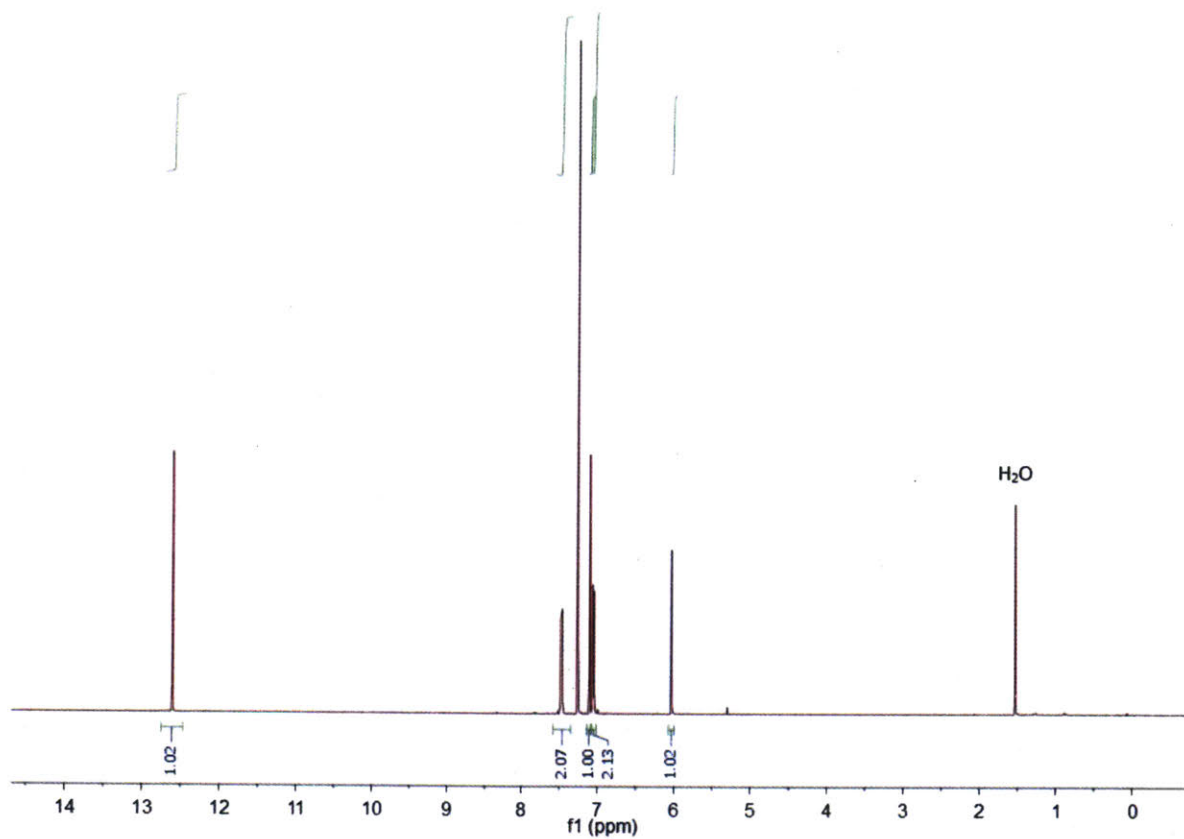


**Figure A.5.9.**  $^1\text{H}$  NMR spectrum of 7 (400 MHz,  $\text{CDCl}_3$ ).

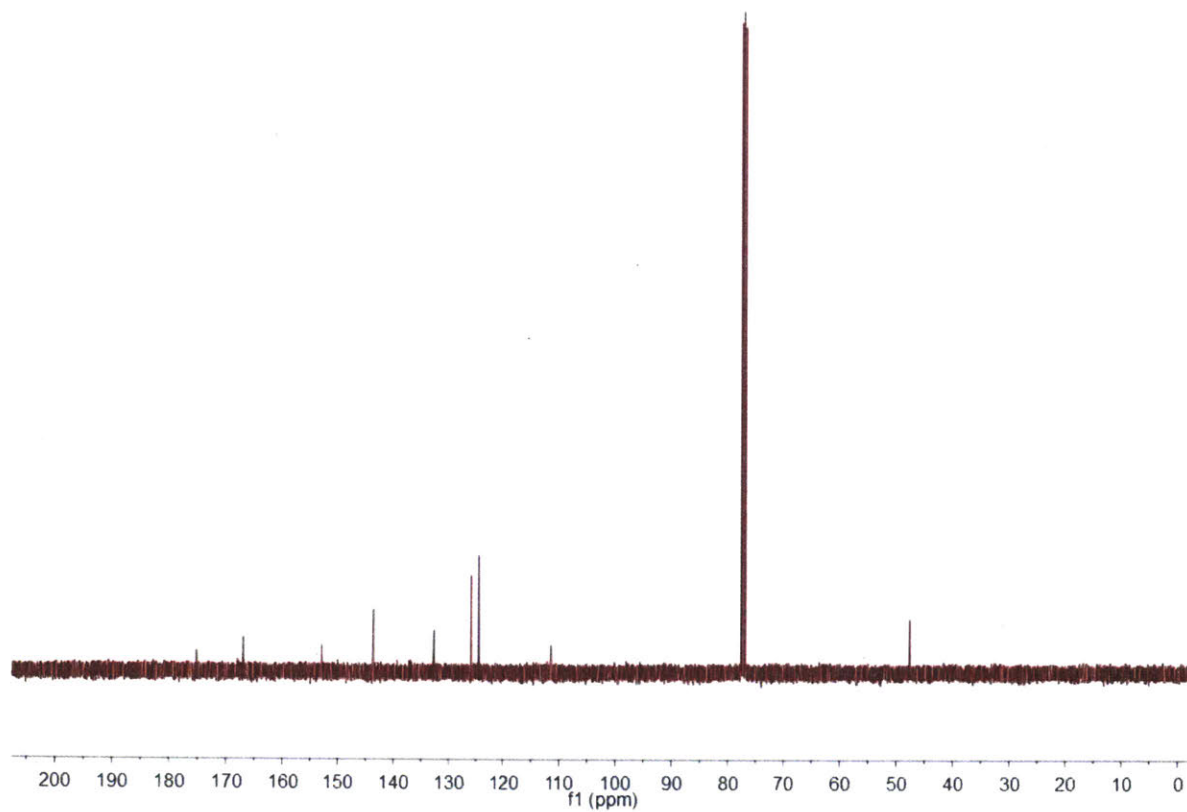


**Figure A.5.10.**  $^{13}\text{C}$  NMR spectrum of **7** (101 MHz, CDCl<sub>3</sub>).



# Gregory D. Gutierrez

---

## Curriculum Vitae

### Education

---

**Massachusetts Institute of Technology (MIT), Cambridge, MA** **September 2011-June 2016**  
Doctor of Philosophy in Organic Chemistry  
Dissertation title: Luminescent Organic Materials and Their Application in Solar Technologies

**Cornell University, Ithaca, NY** **August 2007-May 2011**  
College of Arts and Sciences  
Bachelor of Arts in Chemistry, *magna cum laude* with distinction in all subjects

### Research Experience

---

**Ph.D. Candidate** **November 2011-Present**  
Department of Chemistry, Massachusetts Institute of Technology, Cambridge, MA  
Doctoral Advisor: Prof. Timothy M. Swager

Investigated new paradigms in photoluminescent organic materials and their application in luminescent solar concentrators for the strategic and cost-effective integration of photovoltaics into existing infrastructures.

**Undergraduate Researcher** **June 2009-May 2011**  
Department of Chemistry and Chemical Biology, Cornell University, Ithaca, NY  
Research Advisor: Prof. William R. Dichtel

Studied the synthesis and properties of two-dimensional organoboron covalent organic frameworks for the non-covalent functionalization of graphene as a platform for structurally precise materials in organic electronics.

### Teaching Experience

---

**Laboratory Teaching Assistant** **September 2011-May 2012**

Department of Chemistry, Massachusetts Institute of Technology, Cambridge, MA  
Course: 5.310, Laboratory Chemistry (Fall 2011 & Spring 2012)

## Undergraduate Laboratory Assistant

August 2010-December 2010

Department of Chemistry and Chemical Biology, Cornell University, Ithaca, NY

Course: Chemistry 3020, Honors Experimental Chemistry II (Instrumental Methods of Analysis)

## Awards

---

- National Science Foundation Graduate Research Fellowship, 2013 – 2016
- MIT Department of Chemistry Award for Outstanding Teaching, 2012

## Publications

---

1. **G. D. Gutierrez**, G. T. Sazama, T. Wu, M. A. Baldo, T. M. Swager “Red Phosphorescence from Benzo[2,1,3]thiadiazoles at Room Temperature,” *Submitted*.
2. **G. D. Gutierrez**, I. Coropceanu, M. G. Bawendi, T. M. Swager, “A Low Reabsorbing Luminescent Solar Concentrator Employing  $\pi$ -Conjugated Polymers,” *Adv. Mater.* **2016**, *28*, 497-501.
3. E. L. Spitler, B. T. Koo, J. L. Novotney, J. W. Colson, F. J. Uribe-Romo, **G. D. Gutierrez**, P. Clancy, W. R. Dichtel, “A 2D Covalent Organic Framework with 4.7-nm Pores and Insight into its Interlayer Stacking,” *J. Am. Chem. Soc.* **2011**, *133*, 19416-19421.

## Patents

---

1. T. M. Swager, **G. D. Gutierrez**, Compositions, Articles, and Methods for Down-Converting Light and Other Applications. U.S. Patent Application No. 14/952,199 (Filed November 25, 2015).

## Presentations

---

1. **G. D. Gutierrez**, “Luminescent Organic Materials and Their Applications in Solar Technologies.” MIT Chemistry Student Seminar Series, Cambridge, MA, USA, January 29, 2016, Oral Presentation.
2. **G. D. Gutierrez**, I. Coropceanu, M. G. Bawendi, T. M. Swager, “A Low Reabsorbing Luminescent Solar Concentrator Employing  $\pi$ -Conjugated Polymers.” MIT Materials Processing Center Materials Day, Cambridge, MA, USA, October 14, 2015, Poster Presentation.
3. **G. D. Gutierrez**, I. Coropceanu, M. G. Bawendi, T. M. Swager, “A Luminescent Solar Concentrator Employing  $\pi$ -Conjugated Polymers.” MIT Energy Initiative Solar Day, Cambridge, MA, USA, September 10, 2015, Poster Presentation.
4. **G. D. Gutierrez**, G. T. Sazama, T. M. Swager, “Room-Temperature Red Phosphorescence of Benzo[2,1,3]thiadiazoles.” Meeting of the American Chemical Society, Boston, MA, USA, August 19, 2015, Oral Presentation.

5. **G. D. Gutierrez**, T. M. Swager, "Design and Evaluation of a Conjugated Polymer Amplifying Luminescent Solar Concentrator." MIT Polymer Day, Cambridge, MA, USA, March 11, 2015, Poster Presentation.
6. **G. D. Gutierrez**, T. M. Swager, "Design and Evaluation of a Conjugated Polymer Amplifying Luminescent Solar Concentrator." Meeting of the Materials Research Society, Boston, MA, USA, December 4, 2014, Poster Presentation.

## Activities and Service

---

### **Career Panel Organizer**

**January 2014 & January 2015**

Department of Chemistry, Massachusetts Institute of Technology, Cambridge, MA

- Invited professionals from the Greater Boston Area to speak with graduate students and postdoctoral fellows about careers possible with a doctoral degree in chemistry.
- Organized startups panel (2014) and co-organized intellectual property law panel (2015).

### **Contributor for *SYNFACTS***

**Fall 2012 & Fall 2013**

Publisher: Georg Thieme Verlag KG, Stuttgart, Germany

- Contributed 24 highlights on recent research publications on the synthesis of organic materials and unnatural products.

### **Member, Organic Chemistry Graduate Seminar Committee**

**Academic Year 2012-2013**

Department of Chemistry, Massachusetts Institute of Technology, Cambridge, MA

- Worked with faculty to select and host speakers for the MIT organic chemistry seminar series.

## Acknowledgements

I must begin by thanking my research advisor, Professor Tim Swager, for his support and guidance over the past several years. In addition to his never-ending flow of ideas, Tim's commitment to my projects and keeping the group well-funded has been immensely motivating throughout my time at MIT. However, I am also extremely thankful that he allowed me the intellectual independence to pursue my research in the way I found most meaningful. Much of this thesis would not have been possible otherwise. For these reasons and more, I am proud of the work I have accomplished as a member of his group. I would also like to thank Professor Jeremiah Johnson for serving as my thesis committee chairman and meeting with me to discuss my research and degree progress throughout my graduate career. I am grateful to both him and Professor Mo Movassaghi for taking the time to evaluate and provide feedback on my fourth-year original research proposal and this thesis.

One of the best things about my experience at MIT was the opportunity to meet so many bright and diligent researchers that I am grateful to call both colleagues and friends. These people have graced the lab with their insight, passion for science, and, above all, consistent willingness to help. Joe Azzarelli and Markrete Krikorian, and Lionel Moh have been with me since the beginning and I very much look forward to their post-graduate school adventures. Working in the lab with some great officemates and baymates made lab life all the more interesting and fun. Baltasar Bonillo and Sébastien Rochat were among my first baymates at my main lab location and were excellent resources and teachers. Kat Mirica, it was great meeting you and I'm looking forward to hearing about your next big discoveries and inventions. Georgios Markopoulos always kept the office, bay, and entire lab lively. Toward the later half of my Ph.D. studies, I have have been fortunate to work alongside Myles Herbert and Sibon Lin. And Sarah Luppino! Your focus on work-life balance is a contagious perspective that I want to adopt as I move on forward. Good luck in your final year.

Grace Han and Tran Truong were my fellow solar researchers and I learned much about OPVs and many elements of modern solar research through their work. Silvia Rocha and Derik Frantz, I'm visiting Switzerland and SLO (respectively) sooner than you know it. Thanks to both of you for not only always inviting me over for dinner/drinks/video games/whatever at your place, but for also providing advice on my research. Jan Schnorr, I'm looking forward to the best days ahead for C2Sense. I am also grateful to have learned much from other fantastic scientists throughout the years: Katsuaki "Kawa" Kawasumi, Eilaf Ahmed, Kazuhiro Nakabayashi, Christian Belger, Bora Yoon, Ellen Sletten, Maggie He, Sophie Liu, Cagatay Dengiz, Pan Wang, Jens Engelhart, Jon Weis, Carlos Zuniga, Joe Walish, Derek Schipper, Duncan den Boer, Joel Batson, Yoshihiro Inamoto, Kelvin Frazier, and John Goods. I also wish the best of luck to Kathleen White, Vera Shroeder, Wen Jie Ong, Byungjin Koo, John Fennell, Intak Jeon, Frank He, Qifan Zhang, and Constantin Voll with their remaining time in the group.

It's also a privilege to close out my graduate experience with soon-to-be Professors Julia Kalow, Graham Sazama, Lauren Zarzar, and Liz Sterner. Quite the clean sweep with academic hires this year. I especially have to give a shout out to Graham for being willing to fulfil my every request on the TD-DFT calculations in this thesis, especially within the last couple of months. I couldn't

have put together Chapters 2 and 4 without you. I would also like to thank Julia for taking the time to provide feedback on Chapter 1.

In addition to our stellar graduate students and postdocs, the Swager Group is extremely fortunate to have had key people that strive to make it the great academic organization it is. Caitlin McDowell was the first person to help me get settled into lab. Brian Pretti has done an excellent job keeping the lab in good shape and well-stocked, as well as just being awesome in general. I also have to thank Kathy Sweeney for always being so helpful with administrative requests.

Saving the most important set of people for last, I'd like to finish this (life) chapter by thanking my family – my mother, father, and my sister Julie – for always, and I mean always, believing that this Ph.D. was possible. They never failed to frequently check up on me to ask how I'm doing, even as I was fully absorbed and lost in my work. I cannot possibly ever thank them enough for their support and faith in me. And lastly, I want to thank Serena for her steadfast support along this journey. With all the encouragement and support, this was totally worth it.